



The
University
Of
Sheffield.

Access to Electronic Thesis

Author: Sarah Elizabeth Tomlinson

Thesis title: Understanding the friction between human fingers and contacting surfaces

Qualification: PhD

Date awarded: 11 November 2009

This electronic thesis is protected by the Copyright, Designs and Patents Act 1988. No reproduction is permitted without consent of the author. It is also protected by the Creative Commons Licence allowing Attributions-Non-commercial-No derivatives.

This thesis was embargoed until

If this electronic thesis has been edited by the author it will be indicated as such on the title page and in the text.



Department of Mechanical Engineering

Understanding the friction between
human fingers and contacting surfaces

Sarah Elizabeth Tomlinson

*Submitted for the degree
of
Doctor of Philosophy*

August 2009

Department of Mechanical Engineering

Understanding the friction between human fingers and contacting surfaces

Sarah Elizabeth Tomlinson

Submitted for the degree of Doctor of Philosophy
August 2009

Friction tests were carried out to assess the friction between a human finger and contacting surface, in different conditions. Tests examined the effect of normal force, the area of contact, the effect of triangular and rectangular cross-section ridges and the effect of moisture.

The tests found that when a finger is contacting a nominally flat surface, the friction force increases with normal force, following a two part linear relationship. This is associated with a large initial deformation of the finger, followed by a smaller scale deformation, after a certain load.

The introduction of water to the contact results in an initial increase, which is followed by a decrease, in friction. There are two principal mechanisms responsible for this increase; water absorption to the stratum corneum, and capillary adhesion. These mechanisms increase friction by increasing the area of contact, and therefore the amount of adhesion.

When the finger is contacting a ridged surface, triangular ridges display a higher friction force than rectangular ridges. This is thought to be due to the larger penetration depth that is possible with triangular ridges. The main mechanisms of friction for the triangular ridges are adhesion and interlocking friction. The main mechanisms of friction for the larger, rectangular ridged surfaces are adhesion, ploughing friction and a reduction in friction force due to an energy return from the finger forming back to its original shape. These

tests showed that for a large friction force, surfaces should have high, narrow and widely spaced ridges. This, however, is at the expense of consistent friction across the surface.

The understanding gained was then applied to the area of rugby ball design. Tests showed that the existing rugby ball surface designs with the highest friction were ones with pyramid pimples. However, rounded pimples surfaces performed more consistently across all test conditions.

Keywords: Grip, friction, skin, human finger

Acknowledgements

I would like to thank my supervisors Dr Matt Carré and Dr Roger Lewis, for their support throughout the past three years. I would also like to thank Philips Applied Technologies for kindly letting me visit and use their facilities. Also, thanks to Gilbert rugby for the supply of rugby ball samples.

I would also like to thank the many people who have given me support and advice during my PhD, including; Bo Persson for the capillary adhesion calculations; Chris Grigson and Julian Klepacki for help with equipment design; the Electrical Engineering Department for support with electrical issues and fingerprint information; Nicolas Martin from dentistry; summer placement students Xiaoxiao Liu and Caroline Texier for helping with experiments; Ben Vaughan for help with CAD drawings; the Technicians in the Department of Mechanical Engineering for the manufacture of test samples; PhD students and RA's within the Department of Mechanical Engineering who have helped me with the operation of new equipment and some computer programming issues. Finally, I would like to thank all those who volunteered to help with testing.

Contents

1	Introduction	1
1.1	Importance of Study	1
1.2	Aims and Objectives	2
1.3	Structure of Thesis	3
2	Literature Review	4
2.1	Introduction to Human Skin Friction	4
2.1.1	Gripping an Object	4
2.2	Properties and Friction of Rubber	8
2.2.1	General Structure of Rubber	8
2.2.2	Modelling Rubber	8
2.2.3	Laws of Friction	9
2.2.4	Mechanisms of Friction in Rubber Contacts	9
2.2.5	Static Coefficient of Friction of Rubber	11
2.2.6	Variation of Coefficient of Friction with Normal Force	12
2.2.7	Coefficient of Friction Variation with Speed and Temperature	13
2.2.8	Flash Temperature	13
2.2.9	Stick-Slip	14
2.3	Friction Mechanisms and Skin Structure	14
2.4	Techniques for Measuring Skin Friction	19
2.5	Parameters Influencing Friction	21
2.5.1	Normal Force Applied in the Contact	22
2.5.2	Contact Parameters	26
2.5.3	Direction of Motion	27
2.5.4	Sliding Speed	27
2.5.5	Hydration	28
2.5.6	Deformation of the Finger When Contacting a Surface	29
2.5.7	Modelling the Contact of a Finger with a Surface	30
2.6	Discussion	33
2.6.1	Normal Force	33
2.6.2	Contact Parameters	34
2.6.3	Hydration	35
2.7	Conclusions	36

3	Equipment and Testing Procedure.....	38
3.1	Original Rig (A) Design	38
3.2	Modifications to Rig A	39
3.3	Rig B – Test Equipment used at Philips Applied Technologies.....	40
3.4	Testing Procedure	41
3.5	Moisture Measurement	44
3.6	Roughness Measurements	48
3.7	Finger Properties.....	49
4	Relationship Between Friction Force and Normal Force	50
4.1	Test Method	50
4.2	Results	52
4.2.1	Results from the Experiments Involving Thirty Two Volunteers .	52
4.2.2	Results from Tests Involving One Finger at Larger Loads	55
4.2.3	Results from Low Load Tests.....	61
4.3	Discussion	64
4.3.1	Variation of Friction Force with Normal Force.....	64
4.3.2	The Variation in Coefficient of Friction Between the Materials Tested	68
4.3.3	Variation in Friction Between People	74
4.3.4	Errors in the Results.....	75
4.4	Conclusions.....	76
5	Area of Contact in Finger Friction Tests.....	77
5.1	Methods for Measuring the Area of Contact and Deformation of the Finger.....	77
5.1.1	High Speed Video Camera Analysis.....	77
5.1.2	Finger Print Ink.....	79
5.1.3	Electrical Resistance.....	80
5.2	Results from Area Tests.....	81
5.2.1	High Speed Video Camera Results	81
5.2.2	Electrical Resistance Results.....	87
5.2.3	Finger Print Results.....	89
5.3	Comparison of the Effectiveness of Each Method.....	90
5.4	Area of Contact	93
5.4.1	Hertzian Contact.....	93

5.4.2	JKR Theory	96
5.4.3	Contact for Rough Spheres.....	97
5.5	Relationship Between Friction Force and Normal Force	99
5.5.1	Friction due to Bulk Deformation of the Finger	99
5.5.2	Friction due to Deformation of the Ridges	101
5.5.3	Friction due to Adhesion	102
5.6	Conclusions.....	104
6	Effect of Moisture on the Measured Friction.....	105
6.1	Survey of Moisture Variation Between People and During Different Activities	105
6.2	Friction Tests at Varying Levels of Finger Moisture.....	109
6.2.1	Results from Friction Tests	111
6.3	Discussion of Moisture Test Results.....	113
6.3.1	Absorption of Moisture Causing a Change in the Young's Modulus of the Skin.....	114
6.3.2	Viscous shear in liquid bridges.....	117
6.3.3	Capillary Adhesion	121
6.3.4	Capillary Adhesion, Viscous Shearing and Water Absorption..	127
6.3.5	Overall Mechanism of Increased Friction.....	129
6.4	Conclusions from Moisture Tests.....	131
7	Influence of Surface Roughness and Fine Ridges on Friction	132
7.1	Current Textures used to Enhance Grip	132
7.2	Procedure for Friction Tests on Different Surface Roughness and Fine Ridges	134
7.3	Results from Roughness and Fine Ridge Friction Tests	135
7.3.1	Results from Surface Roughness Friction Tests	135
7.3.2	Results from the Fine Ridge Tests.....	136
7.4	Discussion of Results from Roughness and Fine Ridge Friction Tests	136
7.4.1	Discussion of Roughness Friction Tests.....	136
7.4.2	Discussion of the Fine Ridge Friction Tests.....	137
7.4.3	Friction Mechanisms for a Finger Moving Over Fine Ridges....	140
7.4.4	Hysteresis Friction.....	1401

7.4.5	Adhesive Friction.....	146
7.4.6	Interlocking Friction	148
7.4.7	Comparison of Predicted Friction to Measured Friction.....	149
7.5	Conclusions.....	151
8	Finger Friction when Contacting Large Rectangular Ridges	153
8.1	Method	154
8.2	Results	156
8.3	Discussion	163
8.3.1	Friction Mechanisms	163
8.3.2	Friction Prediction.....	169
8.3.3	Influence of Ridge Dimensions on Friction Measurements	171
8.3.4	Affect of Increased Humidity on Friction	175
8.4	Conclusions.....	177
9	Relating Finger Friction to Rugby	179
9.1	Introduction to Rugby and the Need for Friction Tests	179
9.2	Method of Testing Rugby Balls	181
9.2.1	Ball Surfaces Tested	181
9.2.2	Friction Tests.....	182
9.2.3	Accuracy Tests.....	183
9.2.4	High Speed Video Filming.....	184
9.3	Results from Rugby Ball Testing.....	185
9.4	Discussion of the Results from Rugby Ball Tests	191
9.4.1	Mechanism for Catching a Ball	191
9.4.2	Handling a Ball with Dry Hands.....	192
9.4.3	Handling a Ball with a Small Amount of Moisture on the Fingers	193
9.4.4	Handling a Ball with Wet Fingers	196
9.4.5	Handling a Wet Ball.....	196
9.4.6	Handling a Ball in a Game, Compared to in the Laboratory	197
9.5	Conclusions from the Rugby Ball Tests	198
10	Conclusions and Future Work	200
10.1	Conclusions.....	200
10.2	Future Work.....	206
10.2.1	Area of contact	206

10.2.2 Moisture Tests.....	207
10.2.3 Pressure Distribution of Contact	207
10.2.4 Deformation of the finger	207
10.2.5 Rugby balls.....	207
Appendix 1 – Publications	218
Appendix 2 – Grip Classifications	219
Appendix 3– Cutometer Measurements for Elasticity and Viscoelasticity with Respect to Immediate Distension.....	221
Appendix 4– Hand Washing Procedure	222
Appendix 5– Matlab® Program for Calculating Average Friction and Normal Force.....	223
Appendix 6– Results from tests with 32 volunteers examining the effect of normal force on friction force	227
Appendix 7 - Sample calculation of the adhesive friction, for brass.....	229
Appendix 8 – Summary of surveyed textures.....	230
Appendix 9 – Spring Constant of an Uncompressed Finger	254
Appendix 10 – Tracking of Finger, Video Output	255
Appendix 11 – The Equations for the Lines of Best Fit Relating the Normal Force to the Maximum and Minimum Friction Force.....	256
Appendix 12 - Positioning of the Finger at Maximum and Minimum Points of Friction, During the Same Slide.....	257
Appendix 13 – Derivation of Hysteresis Friction, for Pyramid Pimples.....	259

Nomenclature

A	real area of contact
A_0	nominal area of contact
A_s	area of sensor
a	radius of contact area
a'	modified radius of contact
b	width of contact
c	constant
d	distance
dl	length of contact
E	Young's modulus
E^*	reduced Young's modulus
F	friction force
F_a	adhesive friction
F_D	deformation force
F_d	deformation friction
F_e	friction reduction due to energy return
F_h	hysteresis friction
F_i	interlocking friction
F_p	ploughing friction
F_r	friction from deformation/movement of ridges
F_t	tangential force
F_T	total friction
F_v	friction from viscous effects
H	horizontal force
h	penetration depth
h_r	ridge height
h_{max}	maximum deflection depth
K	Boltzman's constant
k	spring constant
L	length of contact
m	constant
N	normal force
N'	equivalent load
n	number of pimples/ridges
p	contact pressure
R	electrical resistance, when referring to area contact circuit
R	radius of finger/sphere, when referring to a dimension
r	radius of circle
r'	modified radius of circle
R^2	squared Pearson correlation coefficient
R_a	average roughness
R_g	gas constant

R_p	Pearson correlation coefficient
R_q	root mean square roughness
s	ridge spacing
SC	stratum corneum
T	temperature
t_s	time
t	distance from centre line to ridge edge
U	work done or strain energy or activation energy
u	velocity
V	molar volume or volume
V_0	molecular constant
v_s	sliding velocity
W	resultant force
w_a	adhesion energy
w	width of ridge
x	distance travelled
y	distance between finger and surface
y and x	on graphs, indicate vertical and horizontal axes
α	contact specific constant
β	loss fraction
γ	surface energy
ΔH_v	molar heat of vaporisation
δ	deflection
δ_s	solubility parameter
ε	dielectric constant
ζ	molecular constant
η	dynamic viscosity
θ	angle of ridge to vertical
λ	peak to peak distance of ridges
μ	coefficient of friction
ν	Poisson's ratio
τ	shear stress
τ_0	contact specific constant
ψ	proportionality constant

1 Introduction

This thesis describes a three year study examining the friction between a human finger and a contacting surface. The texture and material of the contacting surface was varied, and tested in both wet and dry conditions.

1.1 Importance of Study

Objects are gripped and manipulated on a daily basis. The optimisation of the friction between the hand and the gripped object can improve comfort, safety, performance and usability. There are several main areas of application for this work.

The sports industry has a keen interest in improving grip on items such as rugby balls, tennis rackets and hockey sticks. Currently in rugby, pimple patterns are used on the ball surface to optimise grip, however, the optimum shape, size or distribution of the pimples is unknown. The main objective for improved grip in sport is to enhance equipment performance, resulting in an improved game for players and spectators. An improved product will ultimately have an economic impact.

Grip of objects such as kitchen utensils, tools and hand rails is an area where there is a need for safety improvements. In 2007/2008 there were 43 518 reported accidents at work due to handling, lifting or carrying [1]. One of the problems with such objects is the need for safe handling in wet and also oily conditions. The surfaces generally need texture to deal with the variety of contaminants. However, the optimum texture for these applications is currently unknown.

Finally, improved grip of products is important for inclusive design; design for use by everyone. An example of this is a bottle screw top. Bottle tops often have a series of ridges to aid grip and therefore the application of torque for their removal. Many elderly people have difficulties in opening bottles and jars. There is the opportunity to optimise the texture of bottle tops and jars, to make them easier to open. This research work can be directly applied to this application and improve the independence and therefore quality of life for a vast number of people.

1.2 Aims and Objectives

The aim of this study was to improve the understanding of the friction mechanisms when a finger contacts a surface. In particular, the effects of normal force, moisture and surface texture.

The objectives of this study were to:

1. Develop a method for measuring finger friction
2. Determine the relationship between friction and normal force for a finger contacting a flat surface, of differing materials
3. Develop a method for measuring area of contact
4. Determine the effect of moisture on human finger friction
5. Determine the effect of roughness and surface texture on the friction between the finger and the surface

These results can be applied to form the basis of future research with an application of surface texture design. Full understanding of friction mechanisms needs to be developed to avoid textures being designed using trial and error. The simplest case is that of the finger contacting a flat surface, which will be investigated in the normal force and area tests. Since objects are often gripped with wet hands, the moisture work will further the understanding of friction between the finger and a flat surface. Finally, tests

on textures will provide information that can directly form the initial basis of grip design.

1.3 Structure of Thesis

The thesis commences with a review of previous work in this field of research. It then addresses all objectives, with at least one chapter dedicated to each objective. The structure consists of the following:

Literature Review – a review of work done in the fields of skin and elastomer friction.

Relationship Between Friction Force and Normal Force – a description of tests to analyse how the friction force varies with normal force, when the finger is contacting a flat surface

Area of Contact in Finger Friction Tests – the development of a method to measure the area of contact in friction tests. The results are then used to explain the relationship between the friction force and normal force.

Effect of Moisture on Finger Friction – a description of tests to measure the effect of small amounts of water added to the finger contact. The results are then explained using previous work and analytical models.

Influence on Surface Roughness and Fine Ridges – a survey was done of how texture is currently added to surfaces to improve grip. The change in friction with surface roughness and small, triangular cross-section ridges was assessed.

Finger Friction when Contacting Large Rectangular Ridges – seventeen different rectangular ridge patterns were tested to investigate how they affect friction, at two different humidity levels (45 % and 90 %).

Relating Finger Friction to Rugby – a case study on the application of the results and the method of friction measurements to the game of rugby; illustrating the industrial application of this work.

2 Literature Review

2.1 Introduction to Human Skin Friction

When attempting to lift or move an object, perception of the frictional properties of the finger-surface contact is achieved using receptors in the fingertips, and this information is then fed to the brain [2]. Understanding the friction involved in an interaction is important for the ergonomic design of objects to improve the efficiency of lifting. The friction at the fingertips is not only important for lifting and manipulating, but also for surface perception (personal feelings about a product/object based on the characteristics of the surface) [3]. Everyday tasks, such as typing, turning of door handles and switching on of lights can be made easier by altering the materials and texture of objects to improve the contact, whilst also considering any contaminants present.

The first step in understanding the frictional relationship between the skin of the hand and an object is to identify how objects are gripped. This includes looking at the effect the grip has on the friction force and how the frictional properties influence the way an object is gripped. There has been a large amount of work carried out on the frictional properties of the skin [4], using various different methods, testing different areas of the skin and also investigating various parameters, such as moisture and normal force.

2.1.1 *Gripping an Object*

Grips can be classified in many different ways due to the positioning of the fingers or the forces applied by them. In total, eight standard grips (Appendix 2) have been specified, five of which are general grips, one is applied to carrying something such as a light suitcase and two are specific to packaging [5]. These, however, can be more generally categorised as either the precision or the power grip [6]. The precision grip is a pinching action

between the fingers and the opposing thumb. The power grip includes the palm in the grip, with the object being held between the fingers and the palm, and counter pressure being applied by the thumb, as illustrated in Figure 2.1. The choice of grip is not solely dependent on the shape and size of the object, but also the purpose of use.

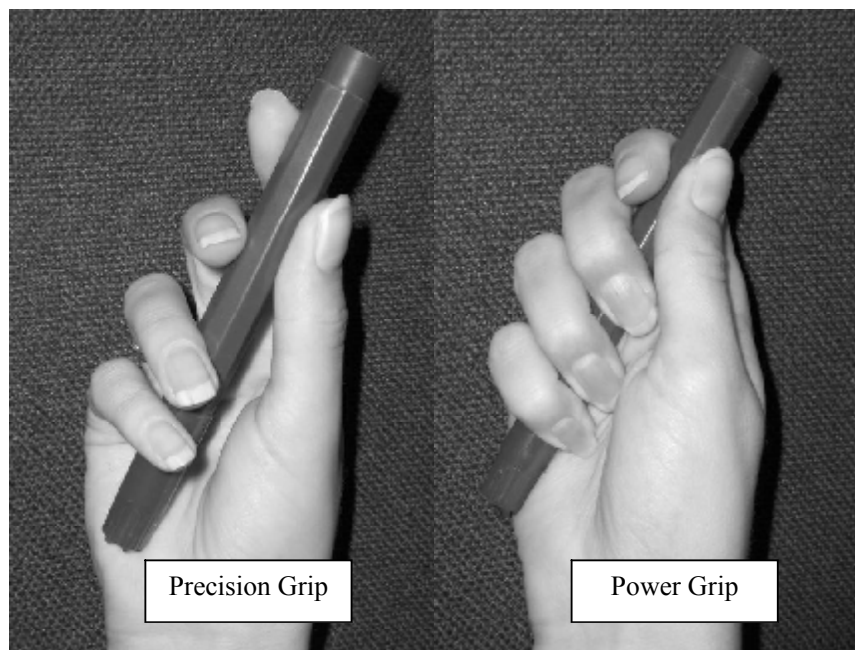


Figure 2.1 – Examples of the precision and power grip

The actual normal force applied when lifting an object depends on the object's weight, shape, and the frictional properties of the surface. For other actions, it depends upon the application, for example whether a person is simply holding a bottle, or squeezing it to release the contents. It has been shown that friction is used to optimise grip regardless of whether it is due to the surface structure or the material type [7]. Burstedt *et al.* [8] investigated this using a mass with attached contact discs. The surface of these discs could be altered to have different frictional properties. The normal force, lateral and tangential forces were then measured using 3-directional force transducers attached to the contact discs. The results showed that the

fingers adjust the normal force at the digits to the local frictional properties of the contact to achieve grasp stability. When lifting an object, a preload (normal force) is applied before applying a lifting force; this is to perceive the properties of the object to be lifted. The normal force at the digit is then altered for both tangential force and frictional properties of the grip, by the use of controlled 'frictional slips' [8]. This total force is then distributed between the digits in a way that reduces the overall normal force, to ensure that the ratio between normal force and the total load is similar across all digits. In a separate study by Flanagan *et al.* [9] it was found that for multi-digit manipulation (3 fingers) the time taken for all digits to be in contact with the surface was 96 ms from the first digit to the final one, this compares to only 26 ms for 2 digit lifting, illustrating the added complexity of multi-digit operations. This is due to additional processing requirements of the information from the extra digits, and then the process of distributing the pressure between a larger number of digits to secure the object with the minimum applied load.

As regards the shape of the manipulated object, the angle relative to the perpendicular of the lifting direction, in most cases not the curvature, effects the normal force applied. As the angle increases, the normal force also rises [10]. The curvature, however, only affects the grip force when considering torsional loads and is used to select the grasp points when the person cannot see the object [11]. This increase in normal force with angle could be to do with the grip that needs to be employed, within either the power or precision grip classification. Work carried out by McDonnell *et al.* [12] showed that the force applied in excess of that required, depended on the grip type and this was due to the difference in contact area of the finger with the object; increasing contact area increases the coefficient of friction.

The normal force applied is also affected by the age of the person carrying out the manipulative task. The applied normal force is increased for both

children and old people compared to that of younger adults [13]. This is for two different reasons; the difference in properties of the skin and the development stage of the brain and receptors. Forssberg *et al.* [13] showed that children display an immaturity in storing and processing frictional information. This is thought to be a learnt process, mainly developing after the age of two; however, it is present to an extent in younger children. The child is therefore unable to react effectively to sudden events such as slipping, so they apply a larger than needed normal force to prevent slippage from occurring.

Older people apply a greater normal force than required for accurate lifting; twice that of the younger groups, due to a reduction in ability to detect the frictional properties of a contacting surface [14]. There are mixed reviews about the effect of age on the friction of skin contacts; however, a decrease in coefficient of friction would mean that a greater normal force is needed to prevent slippage, thus providing another reason why older people may apply larger normal forces than younger age groups. The change, with age, in the frictional force between the finger and contacting material is dependent upon the roughness of the material. For example, Cole [14] found that the change in the coefficient of friction for acetate occurred at an earlier age than for sandpaper. This is thought to be because the roughness of the sandpaper dominates the frictional properties of the interaction. Although these changes with age are present, they were not seen until the age of 50 years for the acetate and 70 years for the sandpaper [14]. Other work assessing the effect of age [15, 16], have found age not to change the measured friction; however, these tests were done against a smooth material (Teflon and steel, respectively). Other work showing age to affect friction [17] is inconclusive due to a small sample size (3 volunteers).

The reduction in detection of frictional properties with age has been assigned to two mechanisms. Firstly, the skin is less hydrated, reducing roughness

perception. Secondly, the force amplitude and direction applied to/by the fingers is detected by the receptors found in the papillae dermis [18] (area of loose connective tissue in the dermis which extends up to the epidermis, illustrated in Figure 2.5), these are part of a feedback and feedforward mechanism of signal processing and detection between the finger and the brain [19]. With age, these sensing nerves deteriorate, so older people are less receptive to the properties of the object being lifted, and therefore apply a larger than needed force to compensate [14].

2.2 Properties and Friction of Rubber

Fingers behave in a similar manner to viscoelastic materials such as rubber [20]. The behaviour of rubber has been researched to a greater extent than human fingers. To begin to understand finger friction, it is first useful to examine previous work on rubber friction.

2.2.1 General Structure of Rubber

Rubber is made up of disordered polymeric chains of molecules. When a force is applied, the chains start to straighten and align themselves. This straightening of chains gives rise to a non-linear section on the stress-strain curve. Once the chains are aligned, the stress-strain relationship is linear [21].

2.2.2 Modelling Rubber

There are many different models which can be used to represent the stress-strain behaviour of viscoelastic materials. The one most suitable for rubber is the Zener Model [22], illustrated in Figure 2.2. However, Boyer *et al.* [20] suggest that skin is best modelled using the Kelvin-Voigt model, also illustrated in Figure 2.2. Both these models have spring and viscous damper components. A viscoelastic material is one that exhibits both viscous and

elastic characteristics, during deformation. The spring component of the model represents the elastic behaviour of the material and the viscous damper represents the viscous behaviour of the material.

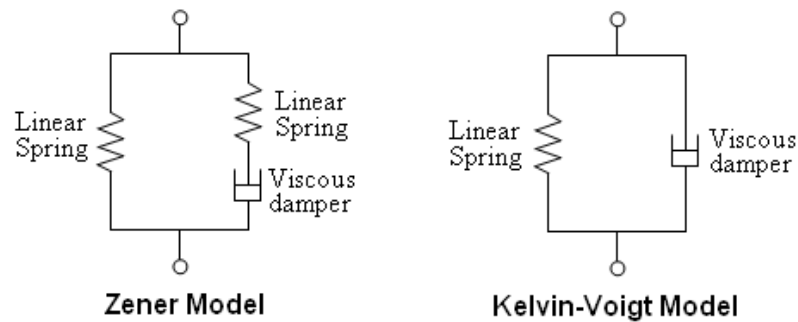


Figure 2.2 – Zener model and Kelvin-Voigt models of viscoelastic materials

2.2.3 Laws of Friction

The three accepted laws of friction formed by Da Vinci, Amonton and Coulomb are stated below; but viscoelastic materials generally do not obey these laws:

- Frictional force is proportional to normal force [23]
- Frictional force is independent of area [23]
- Coefficient of friction is independent of the velocity between the two surfaces provided that the velocity is not zero [23]

2.2.4 Mechanisms of Friction in Rubber Contacts

There are two mechanisms concerned with friction in viscoelastic materials; adhesion and hysteresis. Adhesion is more prevalent when a smooth surface is traversed over the rubber [25] and depends significantly on the roughness of the component the rubber is sliding on [26]. Adhesion is the

process of bonds forming between the contacting surfaces and the friction force is the force required to shear these bonds [27].

Hysteresis friction is a predominantly plastic mechanism. It is the process of deforming the rubber, which requires an energy input. Some of this energy is then dissipated due to the properties of the rubber; i.e. hysteresis. Figure 2.3 illustrates the two mechanisms acting when an elastomer moves over a rigid body.

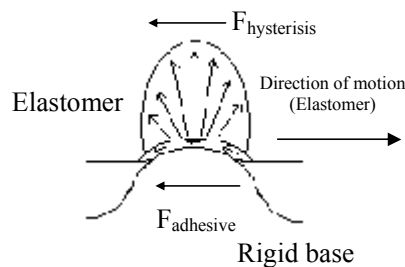


Figure 2.3 – Adhesive and hysteresis friction mechanisms, modified from [25]

In some sliding conditions Schallamach waves can be seen. Williams [25] explains this clearly using the four stages that are reproduced in the drawings of Figure 2.4. These waves have the function of stabilising the system, in turn reducing the coefficient of friction and reducing the effects of temperature, sliding speed and load [28]. These waves are seen when the sliding velocity exceeds a critical velocity. This critical velocity is dependent upon geometry and normal force. Barquins [28] found that the critical velocity decreased as the diameter of the hemisphere, contacting the smooth elastomer, and the normal force was increased.

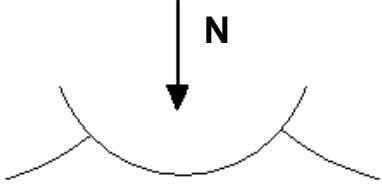
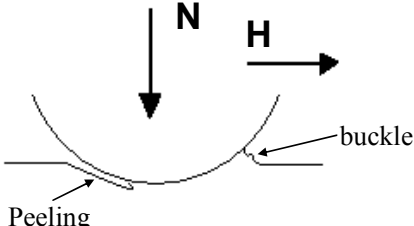
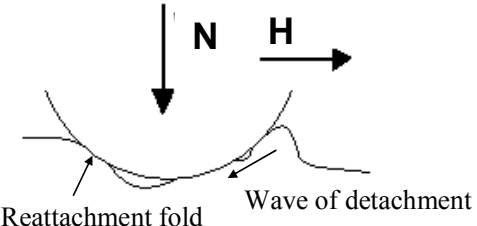
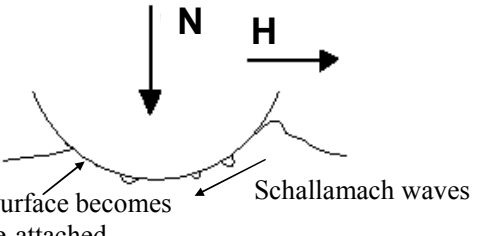
<p>Smooth rigid cylinder in contact with the rubber surface.</p> <p>N is the applied normal force, H is the horizontal force to move the object</p>	
<p>Front buckles and back peels away from the object surface.</p>	
<p>Local recovery and slip causes the rubber and object to reattach to the back part of the contact.</p>	
<p>This then reaches a position where the process can start again.</p>	

Figure 2.4 – Waves of detachment when a rigid cylinder moves along a rubber surface, modified from [25]

2.2.5 Static Coefficient of Friction of Rubber

Moore [23] states that the static coefficient of friction of viscoelastic materials is not always greater than kinetic coefficient of friction. Persson [24] explains that it is situation dependent, due to the nature of the slide affecting the results. This means that if there is a long dwell time before motion, and a

low-frequency relaxation process in the rubber, a traditionally recognised static coefficient of friction (peak at the start of the motion) may be seen. However, if the motion starts very slowly, this will not be seen. This dependence upon velocity makes it a difficult parameter to measure [29]. Rubber molecules will arrange themselves in a way that most strongly bonds to the contacting surfaces [24], which is why the static coefficient of friction is dependent upon dwell time and contact geometry [24, 28]. When the rubber is contacting with another rubber, chain inter-diffusion will occur, further contributing to both the static and dynamic coefficient of friction [24]. The rubber modulus also affects the static coefficient of friction. This is most easily understood by considering a rubber block on a surface (the illustration also used in [24]), if a force is applied to the top of the block, the block will initially deform and not actually move, once this force is great enough it will start to move, the extent of this deformation is due to the rubber modulus.

2.2.6 Variation of Coefficient of Friction with Normal Force

The work done [23] examining the variation of coefficient of friction with normal force, for a rigid sphere contacting and flat, smooth elastomer, is based on the assumption made by Schallamach [29] that the friction force is proportional to the contact area. The relationship of contact radius (a) to applied load (N) can be described by Equation 2.1 [27-29], which can be modified to Equation 2.2. However, in reality the power can be greater than $2/3$ due to a small amount of plastic flow [27]. This relationship holds well for both smooth sliding and in the presence of Schallamach waves [28]. However, the area of contact must reach a plateau (with applied normal load) and this results in a limit to the friction force [29].

$$a \propto N^{\frac{1}{3}} \quad 2.1$$

$$F = c \cdot N^{\frac{2}{3}} \quad 2.2$$

where F is the friction force and c is a constant

2.2.7 Coefficient of Friction Variation with Speed and Temperature

Unlike non-viscoelastic materials the frictional properties of the contact rely on the speed of the sliding motion, unless this is extremely low $<10^{-10}\text{ms}^{-1}$ [30]. At a velocity below 0.1 mms^{-1} the area of contact will decrease with increased velocity. This is due to the frequency of the deformations increasing. At velocities above 10^{-3}ms^{-1} the area of contact increases with increasing velocity. This increase in area is due to an increase in contact temperature (Equation 2.3 [29]). The increase in temperature causes the rubber to become elastically softer [30], this means the rubber can more easily deform to that of the contacting surface, hence a larger contact area. The friction force for an elastomer can be described using Equation 2.4 [31], valid for temperatures less than the glass transition temperature and low velocities. This equation illustrates clearly that an increase in temperature will increase the friction force.

$$v_s = A \cdot \exp\left(\frac{-E}{K \cdot T}\right) \quad 2.3$$

$$F = \frac{U}{\zeta} + \frac{K \cdot T}{\zeta} \ln \frac{V}{V_0} \quad 2.4$$

where, v_s is sliding velocity, K is Boltzman's constant, T is temperature, E is Young's modulus, F is Friction Force, U is Activation energy, ζ and V_0 are molecular constants, and V is the molar volume.

2.2.8 Flash Temperature

An increase in temperature due to flash temperature does not increase the friction, as would be predicted by Equation 2.4, but reduces it. Flash temperature refers to the sharp and local increase in temperature occurring in the rubber and counter-face contact at the asperity contact region during slip [30]. To have a build up of flash temperature the rubber must slide the distance of the largest asperity of the non rubber contact [30], this distance

refers to the length measurement along the surface of the largest protrusion (asperity).

2.2.9 Stick-Slip

Stick-slip occurs in many situations, for example creaking door and violin string [32], and it is also a phenomenon seen with rubbers in contact. The traditional model of stick-slip is that of a block moving on a surface, with a spring attached to it. Tension is applied to the spring, but the block will not move because the static coefficient of friction is too high. Once this is overcome the block will move. The velocity of the block will be greater than that of the spring, so it will once again come to rest and the process start again [32], i.e. the force builds up until the static coefficient of friction is overcome and the two surfaces move again [33]. There are many theories for the mechanisms of stick-slip. Berman *et al.* [32] mention three; surface topography model, distance-dependent model and rate and state model (applicable when lubricant is present). In non-viscoelastic materials stick-slip is dependent upon inertia stiffness, mass of moving parts, molecular/asperity size, sliding velocity, relaxation time and previous history [32]. This is not to say that these do not also affect stick-slip of viscoelastic materials, however, due to their low elastic modulus and high internal friction, there could also be other factors at work. One of the explanations for stick-slip in viscoelastic materials is that a reduction in the dynamic coefficient of friction causes stick-slip, this reduction can be due to flash temperature [30].

2.3 Friction Mechanisms and Skin Structure

The basic structure of human skin consists of the epidermis as the surface layer. Beneath this there is the dermis, followed by the subcutaneous tissue, as shown in Figure 2.5 [34]. The dermis contributes to the load carrying and elastic properties of the skin. Collagen fibres make up 77% of the dermis, and these bio-viscoelastic solids are the main load carrying elements.

Elastins account for 4% of the content of the dermis and contribute highly to the elastic properties of the skin [34].

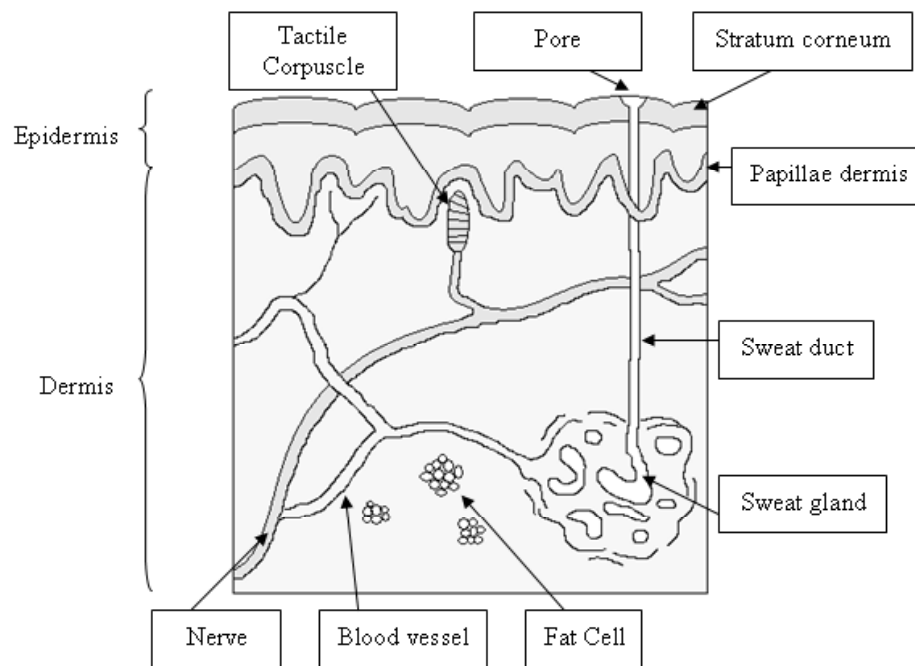


Figure 2.5 - Skin structure. Adapted from [35]

As with elastomers, the principal mechanisms of human skin friction are adhesion and hysteresis. For human skin friction, the magnitude of adhesive friction is determined by two main factors [36]. Firstly, the type of adhesive bonds, for example van der Waals forces, electrostatic forces or hydrogen bonds. Secondly, the area of contact over which the adhesive bonds are formed [36]. Comaish and Bottoms [37] state that the skin does not follow Amonton's Law; so the friction force is not proportional to the normal force and is dependent on the area of contact.

The skin is a viscoelastic material with varying properties depending on the age of a person. There is an increase in the Young's Modulus at the age of 30 [38], but the friction properties are not found to change until later than this.

Table 2.1 shows the in-vivo properties for the skin, found in the literature. The Poisson's ratio has been measured in-vitro and for a cows teat it was found to be 0.5-1.3 [39], depending on direction. However, for many experiments with human skin it is often assumed to have a Poisson's ratio of 0.5 [40, 41]. Due to the mechanisms of friction, it is not only the surface layer of the skin that affects the coefficient of friction, but the whole structure. The properties of the different layers are shown in Table 2.1. The location of the skin is also specified in some instances, because there are no unique values for the properties of the skin [23]. The properties vary depending on location, age, gender and factors such as sun exposure [42, 43]. The properties biological elasticity and viscoelastic properties with respect to immediate distension, were measured using a Cutometer SEM 474 [43]. The Cutometer is a skin suction device, which applies suction to the skin and measures the skins deformation whilst doing so. The biological elasticity refers to the skins ability to recover to its original state after deformation, and the results shown are for tests at 500 mbar pressure. It is measured using a ratio of the immediate retraction (after the application of pressure) and the final deformation (the deformation just before the pressure is removed). The viscoelastic properties with respect to immediate distension, is a ratio of the delayed distension and the immediate distension (after 0.48 s) (Appendix 3 shows a diagram illustrating these values).

Table 2.1 – Properties of the whole skin, epidermis and dermis.

	Skin	Epidermis	Dermis
Thickness (mm)	1.11 - 1.28 [42] (Neck)	0.06-0.8 [34] 1.5 [44] (palm)	3-5 [34] 1.1-1.8 [42] (arm) 1.1 [45]
Young's modulus (Nm⁻²)	4.2 x 10 ⁵ to 8.5 x 10 ⁵ [38] 2 x 10 ⁴ to 10 ⁵ [40] (Forearm)	2.1e10 ⁶ [38] (SC) (back)	E = 2.1 x 10 ⁹ [46]
Density (kgm⁻³)		1110 – 1190 [47] 1500 (SC) [47]	1116 [47]
Ultimate Tensile Strength (Nm⁻²)	7.3 [47] (hand) 9.5 [47] (arm)	SC is Stratum Corneum (see Figure 2.5) Young: 26.2 ± 3.4 years Old: 74.5 ± 5.7 years	
Biological Elasticity	Young 0.66±0.33 [43] (palm) Old 0.53±0.02 [43] (palm)		
Viscoelastic properties wrt immediate distension	Young 0.49±0.05 [43] (palm) Old 0.53±0.04 [43] (palm)		

The skin on the fingertips has ridges on the surface, which are traditionally thought to aid grip. There are five main ridge patterns, and these can be seen in Figure 2.6. The pattern determines the quantity of ridges [48]. The way in which the ridges are counted is to draw a line from the centre of the pattern to the point known as the Triradius (the point at which three differently orientated ridges meet). This is illustrated in Figure 2.7.

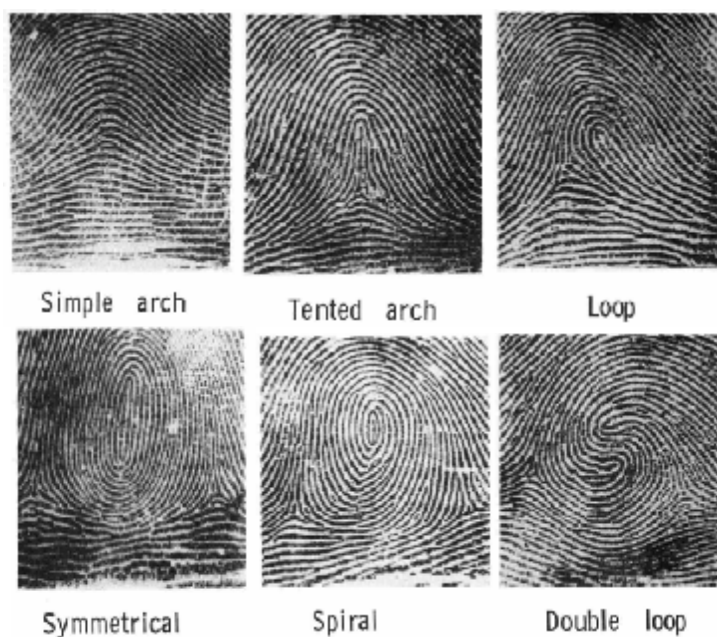


Figure 2.6 – Different finger patterns. Reprinted by permission from Macmillian Publishers Ltd: The Journal of Investigative Dermatology [49], copyright 1970

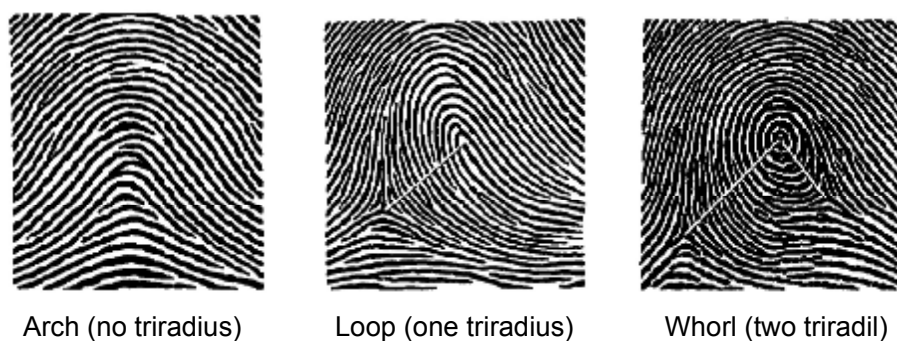


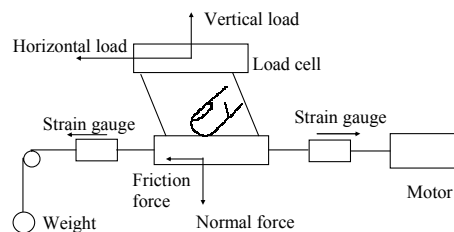
Figure 2.7 – Method for counting finger ridges. Holt SB, Quantitative genetics of finger-print patterns, The British Medical Bulletin, 1970; 54 (4), 247 – 250, by permission of Oxford University Press [48].

The studies of the finger ridge patterns found that men tend to have more ridges than women. Holt [48] carried out studies on 825 men and 825 women, finding that men have on average 145 ridges, with a standard deviation of 51, whereas women only had on average 127 ridges, with a standard deviation of 53. The ridge density determines the ridge width, so women have finer ridges than men. The height of the ridges is $59 \pm 19.2 \mu\text{m}$ [50]. Some people also have inter-papillary ridges, which can change with

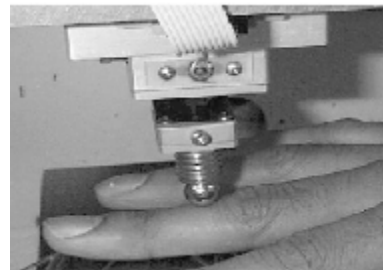
age, however, these are much smaller; with a ridge height of $24.9 \pm 10 \mu\text{m}$ [50].

2.4 Techniques for Measuring Skin Friction

Many of the tests carried out on skin, especially the earlier ones, tested the forearm or calf skin rather than the hand, due to the test results being more consistent in these areas. The most widely used, and earliest design of skin friction testing rig, consists of a probe running along the skin under a constant applied normal force [37, 51]. This probe moves with either a linear or rotational motion. In these designs the applied normal force is usually regulated using either static weights [37], a spring load [52], balanced beams [51] or in the more modern of equipment computer controlled servo feedback [53], shown in Figure 2.8.



Surface moving along the finger. Modified from Han [54] ©1996 IEEE



UMT probe, reproduced with permission, from Sivamani [53]

Figure 2.8 – Different designs for skin friction measurements

The advantage of the probe method is that the normal force and speed of the probe can be controlled. However, the curvature of the probe significantly affects the results due to the deformation of the skin [55]. When considering the fingers, this type of deformation is not seen in a wide range of tasks, which is a disadvantage of the method.

An increasingly popular design of rig, which is a more finger-specific test, is one where the finger is moved along, whilst in contact with, some sort of stationary measuring device. The normal and friction forces are then measured using strain gauges [56], piezoelectric material [57], leaf springs [58], potentiometers [59] or load cells, or a combination of these. An example of this design is shown in Figure 2.9 [60].

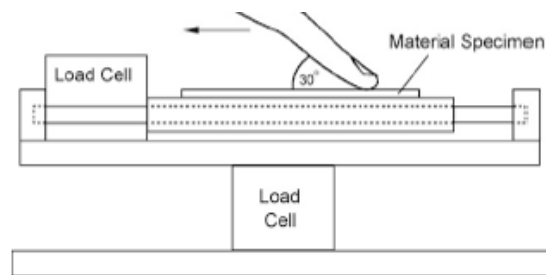


Figure 2.9 – Finger friction measurement rig, reproduced with permission from Lewis [60].

In 2005, Zahouani *et al.* [61] measured friction using the acoustic emissions produced when skin interacts with a surface, illustrated in Figure 2.10. The measurements were confined to 20 Hz – 20 kHz, since the acoustic emissions from the stratum corneum have been found to be in the audio band 20 – 5000Hz, and friction noise is the white noise. The diameter of the probe used was 20 mm. The results gained seem to correlate well with the roughness and stiffness of the skin, but they were unable to quantify the friction coefficient between the skin and the object. This method has been implemented in a more recent study [62] and the results show some correlation between the acoustic emissions and roughness and skin stiffness.

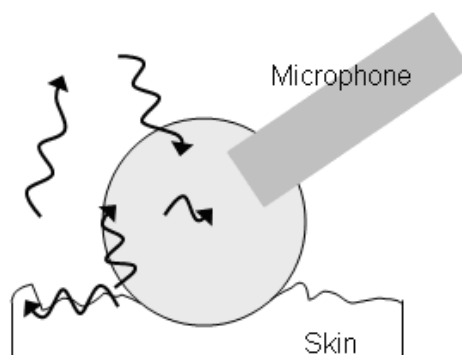


Figure 2.10 – Acoustic emissions method, redrawn from [61]

The majority of these tests have involved examining the dynamic coefficient of friction. Very few consider the static friction, especially when testing fingers. The static coefficient is difficult to measure, due to the velocity dependence seen with viscoelastic materials [29]. However, Lewis *et al.* [60] and Koudine *et al.* [51] measured the static coefficient of friction for fingers and forearm, respectively, and found under their test conditions, it was greater than the dynamic coefficient of friction.

2.5 Parameters Influencing Friction

The coefficient of friction does not depend on the contacting material alone. Other parameters such as the normal force, sliding speed, contact area and person tested can also influence the results. Table 2.2 shows a summary of some of the tests carried out. The coefficient of friction can be seen to vary substantially but this is thought to be mainly due to the different test materials and methods, as well as skin hydration [63].

Table 2.2- Measured coefficients of friction

Ref.	Area	Test Material	Test Method	Normal Load	Speed	Coefficient of Friction
[17]	Forearm	Polymeric	Probe	0-30 g	0.27 mms ⁻¹	0.42
[64]	Finger	Smooth Polycarbonate	Moving belt	1-20 N	45 -55 mms ⁻¹	1.4
		Rough Polycarbonate				0.7-0.8
[65]	Finger	Sandpaper (grade 0)	piezoelectric mini force plate	Applied by hand		1.361
		Perspex				1.475
[56]	Finger	Rubber	Finger moving on plate			2.5
		Polycarbonate				2.5
		Paper				0.5
[54]	Finger	Acrylic	Plate moving stationary finger	0.5-1 N		1.5
				4-6 N		0.4
[58]	Finger	Latex glove				1.2
[53]	Forearm	Stainless steel	UMT Probe	20 g	0.4 mms ⁻¹	0.33-0.55

2.5.1 Normal Force Applied in the Contact

The stress-strain behaviour of the skin is non-linear, as illustrated in Figure 2.11 [45]. The skin contains elastins and collagen fibres in the dermis and these fibres show linear stress-strain behaviour. However, the structure of these strands is non-uniform, resulting in non-linear behaviour of the skin. The first stage (I in Figure 2.11) is due to the elastins causing the skin to stretch in a linear manner. The second stage (II in Figure 2.11) starts to become non-linear as the straightening of the collagen fibres causes an increase in stiffness. Then in the third phase (III in Figure 2.11) the collagen fibres are straight, causing the stress-strain relationship to become linear.

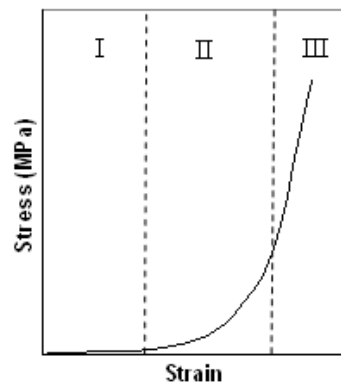


Figure 2.11 – Stress strain curve for skin, modified from [45]

In this non-linear section (II on Figure 2.11), the general trend is a decreasing coefficient of friction with increasing normal force [53, 54, 64]. This is because as the skin becomes stiffer, due to the straightening of the collagen fibres, less deformation occurs, which therefore means a reduction in the hysteresis friction mechanism resulting in a lower coefficient of friction.

Previous work, excluding that of Asserin *et al.* [17] and Ramalho *et al.* [63], found the relationship between the friction force and the normal force to be described by Equation 2.5 [37, 66].

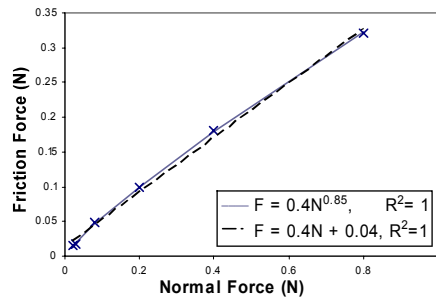
$$F = c \cdot N^m \quad 2.5$$

where F is friction force, N is normal force, c is a constant, and m is a constant less than 1. m is suggested to have a value of approximately 0.67 [51, 53].

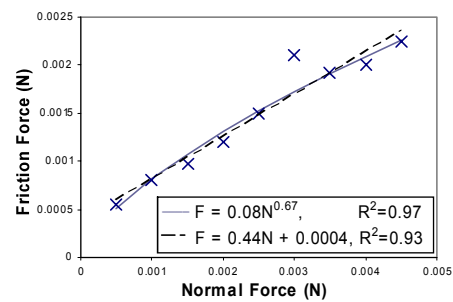
Tests carried out by Asserin *et al.* [17] showed the coefficient of friction to be proportional to the normal force applied, in the range of 0.05 - 0.3 N. Ramalho *et al.* [63] also found a linear relationship between friction force and normal force, however, for the palm he suggested that there is one initial

linear relationship and then at a critical force this relationship changes to a second linear relationship. Asserin *et al.* [17] and Ramalho *et al.* [63] present their data differently to that of the other authors, in that they look at the relationship between friction force and normal force, rather than the coefficient of friction and normal force. To investigate the relationship between friction force and normal force further the results from three different investigations were taken and manipulated to show the friction and normal forces. The three sets of data chosen for analysis were that of Koudine *et al.* [51], Sivamani *et al.* [53] and Han *et al.* [54]. The coefficients of friction were measured using a glass probe on the forearm (dorsal side), a steel probe on top (not palm) of the middle finger and transparent acrylic board moving on the fingertip, respectively. The coefficients of friction stated by Koudine *et al.* [51], Sivamani *et al.* [53] and Han *et al.* [54] were multiplied by the normal force to give the friction force. In all cases, the equipment measured the normal and friction force, so it is assumed that the coefficient of friction stated is the ratio of these. These plots are shown in Figure 2.12.

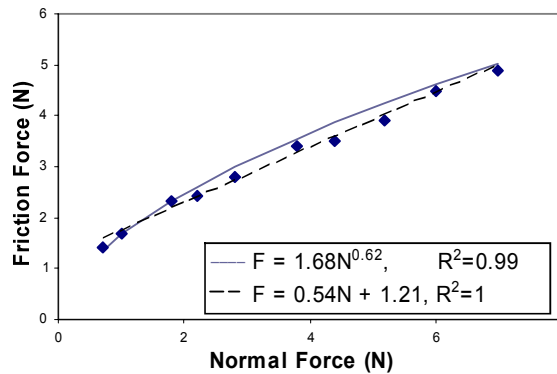
When these results were plotted they seemed to show a linear relationship between normal and friction force, which is in agreement with that stated by Asserin *et al.* [17]. Figure 2.12 shows two lines of best fit; the first is based on a linear relationship and the second is based on the form $F=cN^m$, where c and m are constants. The equations of best fit for the data, in these two forms, and the Pearson squared correlation coefficients are shown on each graph. This shows a linear relationship, or a power relationship could be plotted through the data points. The data from Sivamani *et al.* [53] and Han *et al.* [54] agree with the relationship predicted from Hertz theory, however, the power is slightly higher for the data from Koudine *et al.* [51]



Koudine *et al.* [51]



Sivamani *et al.* [53]



Han *et al.* [54]

◆ Test equipment using a plate ✕ Test equipment using a probe

Figure 2.12 – Comparison of results from various authors

To analyse this relationship further the results were all plotted on a log scale graph, shown in Figure 2.13. The interesting point about this is that although they are all testing different materials, testing different people and using different equipment, they show a general linear trend, however, it could also be argued that they all lie on their own individual line. Due to the different structure of the finger compared to the forearm, it could be that it behaves differently to that predicted by Hertz, so is worth further analysis.

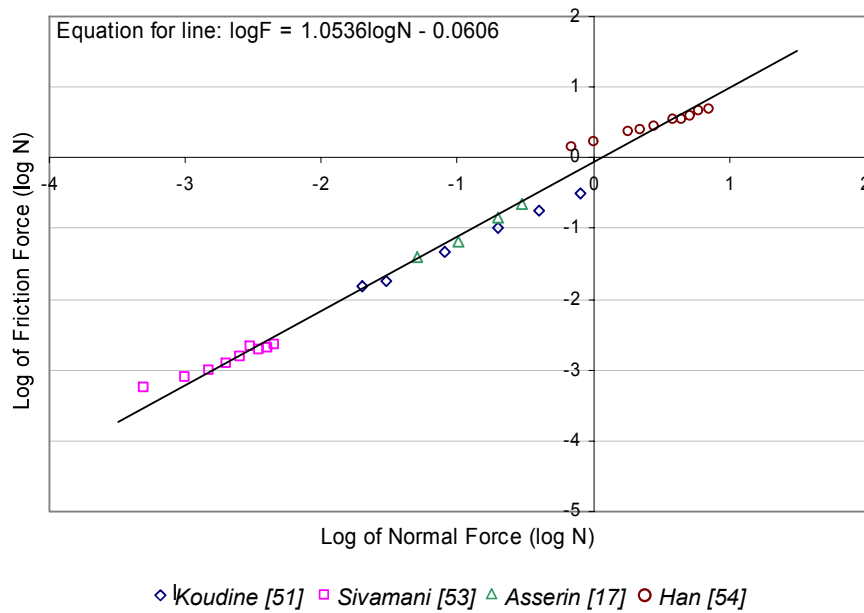


Figure 2.13 – Plot of all results on a log graph

2.5.2 Contact Parameters

The surface area, of the fingertip, alters from person to person (i.e. large or small fingertips), but also by varying the angle of contact between the finger and the surface, or the way in which the finger deforms in the contact. The exact contact area used in gripping is difficult to determine due to the unknown asperity-asperity contact. Pressing the finger against Perspex shows that the ridges do not deform to a point where the apparent area of contact is flat [67]. Levesque and Haywood [68] have developed a digital imaging technique to examine the deformation of the finger on both a flat surface and one with features, such as a bump or a hole. Their equipment needs refinement to provide accurate information on the contact; however, they did report significant deformation of the fingers and ridges, when moving. At decreased angles of contact, and therefore larger contact areas, the coefficient of friction was found to increase [54]. This is explained because an increase in surface area leads to an increase in the adhesive friction mechanism.

2.5.3 *Direction of Motion*

The ridges of the finger are arranged in such a way that parts of the ridges are always perpendicular to the friction force; this should mean that in terms of gripping an object, the direction of motion should have little effect on the gripping capability [69]. However, the direction of the motion will affect the deformation of the finger, which in turn affects the coefficient of friction. Srinivasan *et al.* [55] found this not to be the case, whereas Han *et al.* [54] found the coefficient of friction to be larger for movement, of the finger, towards the body when compared to motion away from the body. This disagreement could be caused by the difference in the test procedures. Srinivasan *et al.* [55] made use of a probe test and Han *et al.* [54] tested the friction by running the finger along a flat plate. The deformation of the finger in these two tests will be different, and the amount of deformation and type will alter the coefficient of friction.

2.5.4 *Sliding Speed*

There seems to be little work carried out on the effects of sliding speed. The work that has been done, with probe on finger, suggests that increasing the speed will increase the coefficient of friction [55]. This would agree with what is already known about viscoelastic materials. For example, with rubber the coefficient of friction increases with speed, because this increases the surface temperature, which in turn increases the contacting area [30], and therefore the amount of adhesive friction. Tang *et al.* [36] did work looking at the effect of speed on the forearm. They found a non-linear relationship between speed and coefficient of friction, with the friction increasing as speed increases. Tang *et al.* [36] attribute this to the hysteretic contribution to friction. When moving at a slower speed there is more time to recover the energy required to deform the skin. However, at a faster speed this 'recovery time' is reduced, so more energy is dissipated, increasing the hysteresis friction. However, considering that deformation has been shown to only contribute by a small percentage to the overall friction [70], this may not be

the case. It could in fact be a modification of the adhesive mechanism. Due to the increase in time for adhesive bonds to form, at lower speeds, however, this needs to be investigated further.

2.5.5 Hydration

The natural hydration of the skin affects the coefficient of friction, but friction can also be affected by moisture from external additions. Moisture can be as a result of something 'unwanted', such as rain, or from a chemical added to the hand voluntarily, for example hand cream. Sweating is another source of additional moisture. The effect of this moisture varies depending on the material and the degree of hydration. It has been found that dry skin (chemically dried [53, 71] and without added hydration [53, 57]) has a lower coefficient of friction than slightly hydrated skin. Increasing the hydration of the skin increases the coefficient of friction, up to a point. There are three possible reasons for this, depending on the type of moisture. When considering surface moisture, the increase in friction is due to liquid bridging between the ridges of the skin and the contacting surface. This bridging effect causes increased friction due to the shear forces set up [57], and/or an increase in contact area from capillary adhesion [72]. Past this point a further increase of hydration has the effect of decreasing the coefficient of friction [53, 57, 59, 71, 73]. If the hydration is increased more on an internal level, e.g. moisturisers that have been absorbed into the skin or soaking of the finger in water, the increase in friction is due to the skin becoming more supple. This increases the possible area of contact between the skin and counter-face, which increases the amount of adhesion possible, thus increasing the friction [74]. Contaminants such as oil have the effect of reducing the coefficient of friction [64], this is true for even a small amount of natural oil [59].

Changing the roughness of the material can alter the effect of moisture. Ding *et al.* [57] explained that increasing the roughness, increases the distance

between the surface and the ridges, allowing fewer bridges to form. Therefore, the coefficient of friction decreases with increased roughness. Bobjer *et al.* [64] found this to be to such a degree that there was no increase in friction with a small amount of moisture, instead an immediate decrease, for the extremities of roughness.

One of the functions of the sweat produced by the hands is to increase the coefficient of friction between the hand and contacting surface. This was studied by Mackenzie and Iberall [69] who found that a single gland produces more sweat when the hand is grasping a dynamometer than when the hand is at rest. It is also thought to be part of the “fight or flight” mechanism. When a person is scared they sweat more, this increases the friction between the ground and the sole of the foot making running an easier task. When an object is held for a long time the build up of sweat can become too high and the coefficient of friction reduce, this does not happen when running (barefoot) because the sweat is continually deposited [75].

2.5.6 *Deformation of the Finger When Contacting a Surface*

The deformation of the finger has been modelled analytically and tested experimentally. One such analytical model was based upon an inflated membrane [76]. This model was experimentally validated and it was found that the force-displacement behaviour resembles that of a hardening spring, with most of the displacement occurring below 1 N. However, this model is based upon a contact where the finger is 45° to the surface, thus forming a circular area of contact. However, the upper part of the finger (distal phalange) is usually flat against the surface when gripping an object, so the contact area will be an ellipse.

Experimentally, the relaxation with shear has been measured [77]. This work highlighted the viscoelastic nature of the fingertip. When the normal load

was constant there was a large decrease in the tangential force of the finger contact, for the first 3 – 4 seconds after the shear force had been applied. This rate then decreased, and is described by Equation 2.6. This experiment highlights the non-linear viscoelastic behaviour of the finger, which should be considered when analysing finger friction.

$$\frac{dF_t}{dt_s} = \alpha_1 \cdot \ln(t_s) + \alpha_2 \quad 2.6$$

where α_1 and α_2 are constants, F_t is tangential force and t_s is time.

2.5.7 Modelling the Contact of a Finger with a Surface

Although the main mechanisms of finger friction are said to be adhesion and hysteresis, the majority of finger friction models assume only adhesive friction. Most of the models are based on Hertzian contact. The assumptions of this contact are:

- the materials in contact are homogeneous and the yield stress is not exceeded
- contact load is caused by the load that is normal to the contact, which effectively means that there are no tangential forces acting between the solids
- the size of the contact is small compared to the size of the curved bodies
- the contacting solids are at rest and in equilibrium
- the effects of surface roughness are negligible, and surfaces are frictionless

Hertz theory was originally constructed for smooth elastic contacts. Contact with the skin is neither smooth nor elastic; therefore, the assumptions are not valid for use with human skin. The skin is not homogeneous, there are

several different layers, and in experiments these are considered as a whole material. Considering a finger on a flat surface, the radius of the curved body needs to be considered as the radius of the curved 'fleshy' part of the fingertip. The contact will also never be 'clean', in that there will always be a layer of sweat or oil between the finger and the contact, modifying the interaction of the bodies further. The finger is also not elastic, but viscoelastic. Creep also needs to be considered with viscoelastic materials. Full details of how this can be implemented for static contact can be found in Johnson [78]. Johnson [78] found that the pressure distribution of the contact is not different to that of Hertz contact, for any stage of the contact, however, the area does change. Figure 2.14 shows how the area changes for a '3 parameter' and 'Maxwell model' of a viscoelastic material. In dynamic skin friction experiments, the finger is not in static contact with the surface, and the change in area is small, so Hertz contact is often assumed.

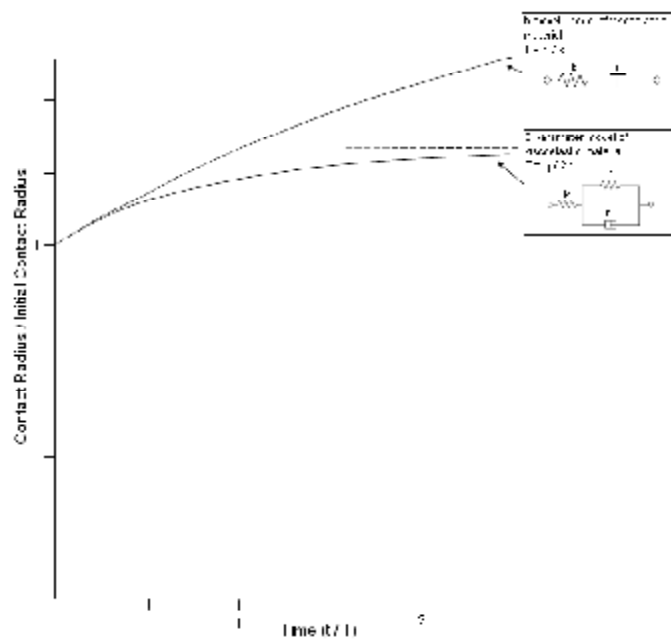


Figure 2.14 – Increase in radius of contact with time for a 3 parameter and Maxwell viscoelastic solid. Modified from [78]. Where η is dynamic viscosity and k is the spring constant

From Hertz's theory, the area of contact can be assumed to follow Equation 2.7 [54].

$$A = c \cdot N^m \quad 2.7$$

where c and m are constants, A is real area of contact and N is normal load.

Moore [23] assesses the contact in reverse (solid sphere on flat elastomer) and finds the value of $m = 2/3$. This is of the same form as Equation 2.5 used to describe the relationship between normal force and friction force, because in adhesion, the friction force is said to be proportional to the area of contact.

Adhesive friction is dependent upon the shear strength and contact area. It can therefore be expressed using Equation 2.8 [54].

$$F = A \cdot \tau \quad 2.8$$

where F is friction force, A is real area of contact and τ is mean shear strength at the contact area.

Assuming that the real area of contact is directly proportional to the nominal area of contact (A_0) the friction force can be expressed using Equation 2.9 [54].

$$F = \psi \cdot A_0 \cdot \tau \quad 2.9$$

where ψ is a proportionality constant, and τ is the shear strength.

One method of describing the shear strength, is to use Equation 2.10, which accounts for pressure effects [54, 74].

$$\tau = \tau_0 + \alpha \cdot p \quad 2.10$$

where τ_0 and α are constants and p is the average contact pressure.

Combining Equations 2.7, 2.8 and 2.10, forms Equation 2.11, describing the coefficient of friction (μ) [54, 74].

$$\mu = \frac{F}{N} = \frac{A \cdot \tau}{N} = \frac{c \cdot N^m (\tau_0 + \alpha \cdot p)}{N} = c \cdot N^{m-1} \cdot \tau_0 + \alpha \quad 2.11$$

However, considering Johnson, Kendal and Roberts (JKR) theory [78, 79], Pailler-Mattéi [80] found Equation 2.12. JKR theory describes how surface energy modifies Hertz contact theory, leading to a larger area of contact. This is not as easy to apply to test data as Equation 2.11, due to the need to quantify the adhesion energy (w_a).

$$F_a = \frac{3}{2} \cdot \pi \cdot R \cdot w_a \quad 2.12$$

where F_a is the adhesive friction and R is the radius of curvature of the finger.

2.6 Discussion

2.6.1 Normal Force

The way an object is gripped and the forces involved in the grip are determined by the frictional properties and shape of the object. Naturally adult humans try to apply the minimum force they can by using the information provided by touch and small slips to obtain surface characteristics, such as shape and texture, which they can then use to optimise the applied normal force.

The results, shown in Figures 2.12 and 2.13, support the argument that the relationship between the friction force and normal force is linear. This is also supported by the physical deformation of the skin when a load is applied. The tests on the forearm and top of the finger are done at low loads, comparatively. There would not be much deformation expected on the top of the finger (compared to other parts of the body) and the low loads on the forearm mean that not much deformation is expected. Also, observing the deformation of the fingertip; there is a large initial deformation with load and then this appears to either stop or reduce to a very small amount. The deformation will contribute to non-linearity. If it is assumed that the data examined in this comparison is above the load for deformation, the linear relationship fits the data and the physical process most appropriately, in the range of forces tested. This seems to contradict the behaviour of other viscoelastic materials.

To fully understand this relationship, extensive tests over a wide range of forces, on the same material should be done to see whether at lower loads, the relationship is non-linear due to the deformation of the finger.

2.6.2 Contact Parameters

Although it is clear that the surface of the fingertip varies from person to person, the extent of this variability in terms of friction is not yet known. There does not seem to be any difference in the skin's frictional properties between males and females [59] and there is also no measured difference between people of different races [16]. However, it has been found that the increase in forearm skin friction with water addition is greater for females than for males [81]. This is thought to be due to the forearm skin of premenstrual women having a greater dermal and epidermal thickness, greater corneocyte (the complex proteins that form the stratum corneum) surface area, higher furrow density and lower surface roughness. The variability between people could be due to a large number of factors including, different

levels of moisture in the skin and also the actual area of contact between the finger and object.

Increasing the surface area of the contact increases the coefficient of friction. This is because, with a larger area, there is a greater possibility of adhesion. Considering the direct link between contact area and friction force, for adhesive friction, a method to measure the real area of contact would be very beneficial.

All tests found in the literature, except Roberts work on surgeons' gloves [58], used standard non-viscoelastic engineering materials (e.g. steel), therefore it is not known as to what extent the relationships shown hold for viscoelastic materials such as rubber. Knowledge of this is important because, for comfort or functional reasons, many items are made from viscoelastic materials, for example, the handles of kitchen utensils or tennis rackets.

2.6.3 Hydration

A certain amount of water involved in the object hand contact will increase the coefficient of friction, due to the modification of the adhesive forces either due to a larger contact area or (in the dynamic case) viscous shear forces. However, in the dynamic case, increasing this hydration further will start to reduce the coefficient of friction as the water (or other moisture) film thickness increases. Studies into the effect of water on different types of materials have not been comprehensive. It would be interesting to compare the trends for a variety of different materials to examine whether the same level of moisture increases friction for all materials, what these levels are, and how these relate to gripping conditions.

2.7 Conclusions

The skin is a viscoelastic material so it does not obey the traditionally accepted laws of friction; Amonton's laws. The frictional properties of the contact are dependent upon normal force, sliding speed, area of contact, motion type and hydration. Larger areas of contact increase the coefficient of friction, as can a certain amount of moisture; however, too much hydration will result in a decrease in coefficient of friction.

There are many gaps in the knowledge of finger friction. However, when considering improved grip, the effect of normal force, texture and hydration can be highlighted as two principal areas for further research. Other areas include sliding speed, person to person variation and material type. To extend the knowledge of the effect of normal force on the friction force, tests performed over a much larger range on the same material would give a better picture of exactly what the relationship is, rather than taking sections of it. It may also be interesting to look at the effect of normal force on viscoelastic materials. Understanding the behaviour of viscoelastic materials is important, as they may not exhibit the same friction characteristics as standard materials, yet they are used in many situations where a good grip is required, for example; some handles on walking frames and some steering wheels.

The amount of hydration may also be able to be utilised to improve grip. This will require a good understanding of the points at which the coefficient of friction increases with water, and then starts to decrease. This level may or may not be the same for all materials.

Bobjer *et al.* [64] (ridges) and Smith *et al.* [82] (raised and recessed squares) investigated texture. However, these studies only examined a few different textures, and were therefore limited in their findings. Textures are used

frequently to improve grip. It is therefore important to understand how to design these effectively. This aspect is therefore also important for further investigations.

Investigating these factors; normal force, hydration, viscoelastic materials, inter-person variation and texture, will contribute greatly to improving the understanding of the friction mechanisms in finger contact.

3 Equipment and Testing Procedure

This chapter outlines the design improvements made to the original finger friction rig (Rig A) at The University of Sheffield and a description of the friction rig (Rig B) used at Philips Applied Technologies. It also outlines the standard test procedure followed for each friction test, and the method of skin moisture and roughness measurement.

3.1 Original Rig (A) Design

The rig is operated by attaching the material to be tested to the upper plate (Figure 3.1) and then running the finger along the surface, in a direction towards or away from the tangential force load cell. The voltage output of the two load cells can then be calibrated to force. The original rig [60], consisted of two load cells, as shown in Figure 3.1, rated at 200 kg (maximum load).

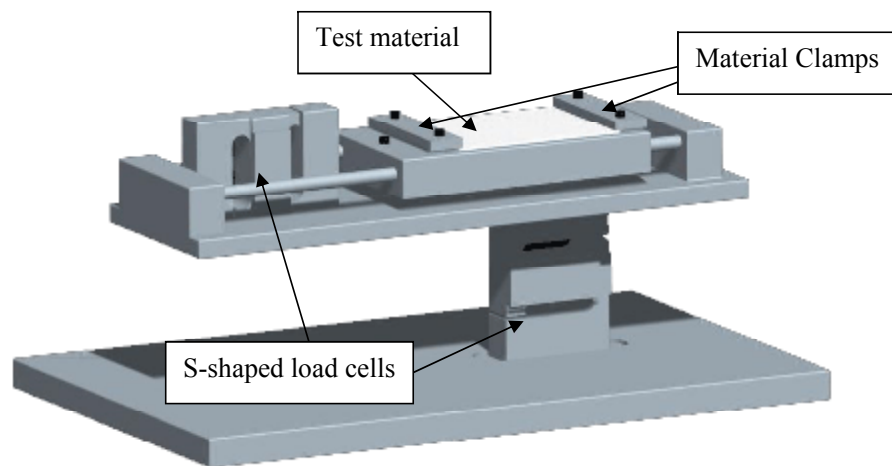


Figure 3.1 – Schematic of Finger Friction Rig (Rig A). The Schematic of the rig is the same for the original and final design, since in terms of the physical appearance of the rig, only the load cells were changed

The data acquisition system consisted of two strain indicator boxes and a Picoscope 3204. The strain indicator box was used to condition and amplify

the signal and the Picoscope 3204 sampled the signal, which could then be displayed on a computer interface. The reliability of the rig was confirmed by using the rig to measure the friction between two engineering materials, the friction of this contact was tested and compared to results from an established friction measurement rig, and a full account of this can be found in [83]. This set-up resulted in low sensitivity due to the high rating of the load cells. The rig also needed to be transportable and the bulkiness of the data acquisition system did not easily allow this. The set up of the Picoscope gave a maximum sampling frequency of 500 Hz. A higher sampling frequency would be better at detecting sudden friction changes, for example that due to a ridge on the surface.

3.2 Modifications to Rig A

There was no data available on the maximum force one finger can apply to a flat surface. To estimate this, the existing load cells on the friction rig were used. Twelve volunteers were asked to apply the maximum force (comfortably) possible using their middle finger, to the load cell. A maximum force of 76 N was measured, which is comparable to the ergonomic data for the maximum pinch grip, of 100 N [84]. Information for the load cell manufacturers (Vishay) indicated that the 200 kg rated load cell could measure in the range of 1 kg to 340 kg, and can detect every 0.1 kg division. This range is far larger than our requirements and is not a high enough sensitivity. There is approximately a 6 kg pre-load on the normal force load cell, to also be taken into account.

The advantage of the original design is the simplicity of direct measurement of the force applied. The s-shaped nature of the load cell (see Figure 3.1) means that it can be used to support the top plate. This means that any force applied to the top plate is measured directly by the load cell. Bearing this in mind, the load cell was changed to a 50 kg rated s-shaped load cell

(the minimum rated s-shaped load cell). This is capable of measuring 0.05 to 50 kg in 0.05 kg increments.

To address the need for a portable rig, the strain indicator boxes were replaced with a simple amplification unit. This uses a differential amplifier and a series of trimmers (variable resistors) and processes the signal, to reduce noise. The different trimmers add the option to increase sensitivity at low loads, but increase the range of measurement (decreasing sensitivity) at higher loads, between output voltages of ± 5 V. There are four levels of gain (amount the circuit can increase the amplitude of the signal) to do this; 5000 dB, 2500 dB, 1000 dB and 500 dB. The rig was calibrated at each gain using dead weights, and this calibration was checked regularly. This amplification unit was designed and built at The University of Sheffield.

3.3 Rig B – Test Equipment used at Philips Applied Technologies

The tests on textured surfaces and at low loads were done at Philips Applied Technologies, Eindhoven, and used alternative equipment that was more sensitive to low loads. A Kistler Multicomponent Dynamometer Type 9256 C (3-directional force transducer) was used. This was clamped to a table top and the materials clamped to the surface using 4 screws, as shown in Figure 3.2. The output was conditioned and amplified using a Kistler multichannel charge amplifier type 5019B and the data captured using a DATAQ DI-720 Series data acquisition box and Windaq software. The results at larger loads were comparable to the friction measurements taken at The University of Sheffield (Rig A) (See Chapter 4 for details).

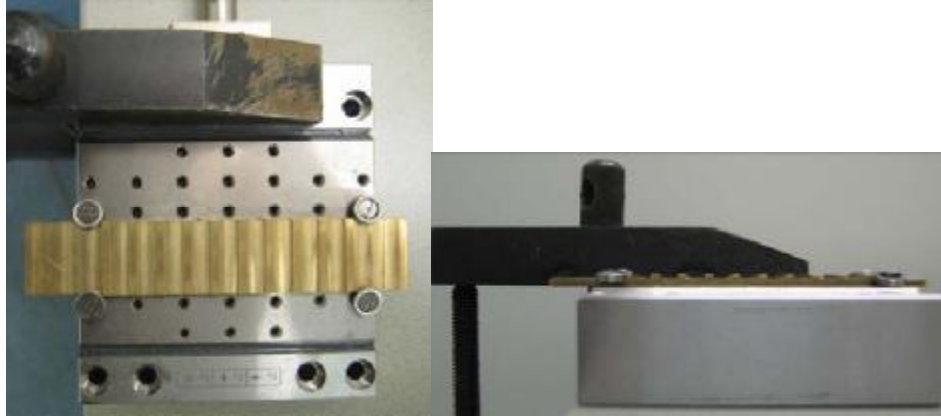


Figure 3.2 – Kistler dynamometer and attached plate for textured friction tests

3.4 Testing Procedure

There were variations to the test procedure depending on the specific test. However, this section provides an outline of the general procedure followed in each finger friction test. Test specific conditions will be explained in the corresponding chapter.

The test procedure had ethical approval from The University of Sheffield, Department of Mechanical Engineering, Ethics Committee. Following the ethical procedure, all participants gave full consent for the tests, filling in the relevant paperwork. In all tests the age, race, and gender were recorded, and an estimate of the maximum nominal area of finger contact used in the tests was printed using a mixture of poster paint and washing up liquid. Before the tests started and at regular intervals, the volunteers hands were washed with soap (Boots Sea Kelp and Water Mint Hand wash), using lukewarm water, and the method prescribed in Appendix 4. They were then towel dried (using a paper towel) and given time to further air dry. The contacting surface material was also cleaned before tests, using a mixture of Janitol Degreaser and water, towel dried and allowed to further air dry. For the tests done at Philips Applied Technologies, the samples were cleaned with ethanol using an ultrasonic cleaner before each test run. The hands

were washed before each test batch (21 tests for textures and 6 tests for low loads), since it took 30 minutes to acclimatise to the room. There was no sink in the climate controlled room, and a balance was required between the removal of contaminants or natural oils from the hands, and not over-drying the skin through the use of too much soap.

The test materials were attached to Rig A using both double-sided adhesive tape and the clamps, shown in Figure 3.1, depending on whether flat contact was possible without tape. For the tests done at Philips Applied Technologies, the materials were attached using four screws, as shown in Figure 3.2.

It was previously found that the middle finger of the writing hand produces the most controlled runs and consistent results [83]. Therefore, this finger was used in all tests. It was also found that movement of the finger towards the body rather than away gave the most consistent results; again this method was employed in all tests. The experiments are concerned with friction in grip, so a large amount of the upper section of the finger (distal phalanx) was in contact with the surface. The angle of the finger after the interphalangeal joint ranged between 22° to 26°. However, this angle was larger for the rectangular ridged surfaces, ranging from 34 to 44° across all tests. Also, for the rectangular ridged surface the angle varied from 1 to 5° along the slide, due to the motion over the ridges. The velocity of the finger moving on the surface was controlled by asking the participants to count slowly to five from the start to the finish of the slide. The range of speeds this produced for each test is shown in Table 3.1.

Table 3.1 – Range of approximate speeds recorded for each set of friction tests

Friction Test	Speed (mms^{-1})
Flat surface; Multiple volunteers (All Tests)	7.2 to 18.4
For a single volunteer (maximum difference between maximum and minimum speed)	3.8
Flat Surface; Single Finger	14 - 20
Moisture Tests	19 - 31
Small, triangular ridges	19 - 30
Large, rectangular ridges	34 - 44

Figure 3.3 shows the data acquired from the measurement system. In tests where the average values of friction and normal force are used, these are taken from the area of constant friction force, illustrated in Figure 3.3. In such tests, Matlab® was used to select the force range, and then calculate the average and standard deviation of this range. The user interface and coding of this program are shown in Appendix 5.

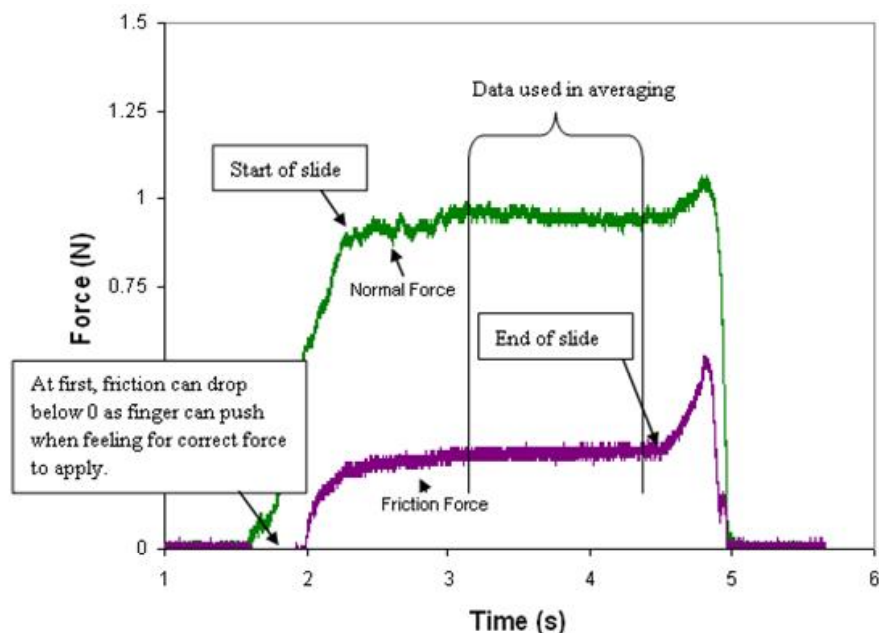


Figure 3.3 – Data acquisition of one slide

3.5 Moisture Measurement

Previous work has shown that moisture can have a large impact on the friction of an interaction. Therefore, the moisture of the fingers was monitored in all tests, where possible, and the effect of moisture was investigated. The device used for this monitoring, at The University of Sheffield, was a commercially available device called the Moistsense (by Moritex). As the water level of the skin changes, the dielectric constant is altered, thus altering the capacitance measured, providing a measure for the amount of moisture in/on the finger. Due to the commercial applications of this device, it provides a scale value from 1 to 99, depending on the capacitance measured; this scale value will be denoted by “au” (arbitrary unit). This number is calibrated against data from 300 people; i.e. a measurement of 50 au corresponds to the average capacitance reading from the sample of 300 people. The relative dielectric constant of skin has been recorded to be 28 – 48 [85] (however this depends on the depth of measurement), comparably, the relative dielectric constant of water is 79 (at 25 °C) [86]. During the tests at Philips Applied Technologies, the Corneometer © CM 825 (Courage + Khazaka electronic GmbH) was used. The operation of this device is based on the same principles at the Moistsense, however the Corneometer has been used widely in the skin research community [87]. The Corneometer has a scale of 0 – 120 AU (Arbitrary Units). Note that the arbitrary units for the Moistsense (au) are different to those for the Corneometer (AU).

The operation of the Moistsense is explained by the manufacturers as working on the principles of a parallel plate capacitor, as illustrated in Figure 3.4. However, with additional confidential information from the manufacturer and disassembling the appliance, it is thought to work in a similar manner to the Corneometer. The arrangement of the device, is the same as shown in Figure 3.4, however the equation is not applicable. The Corneometer utilises the scatter field, often seen at the end of capacitor plates, as illustrated in Figure 3.5 [88]. The wires in the sensor are separated by an insulator, if the operation of the Moistsense was not similar to the Corneometer, the

capacitance of the contacting skin could not be measured. Since, this means that now it is no longer a simple parallel plate problem (obeying the equation in Figure 3.4), the amount of water present (in a measure of grams of water, for instance) cannot be calculated directly from the Moistsense reading. If it were a parallel plate problem, the dielectric of skin and water could be used to calculate an estimate of the percentage water in the contact. However, for the scatterfield arrangement, it can only be calibrated by adding different (known) levels of moisture to the finger, and measuring the capacitance.

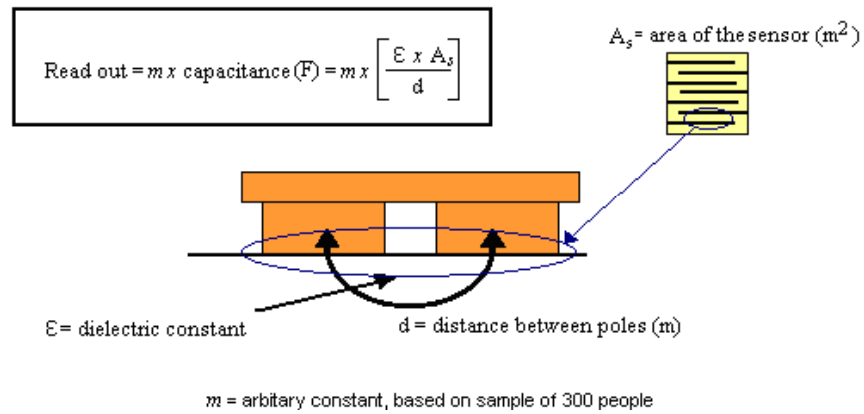


Figure 3.4 – How Moistsense is claimed to work (modified from Moritex promotional material)

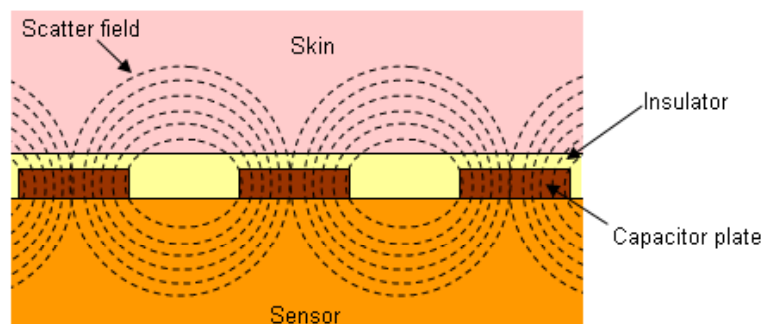


Figure 3.5 – Scatter field utilised by the Moistsense and Corneometer, to measure the change in capacitance of the skin due to water addition

Due to the commercial (cosmetic industry) rather than research application of the Moistsense, calibration checks were done. Three methods were used to calibrate the reading on the Moistsense to a capacitance reading, and/or to ensure that the scale was linear. The first method had the largest inherent error; however, it tested the Moistsense as a whole. The Moistsense sensor was attached to a capacitance meter. Different fruit skins were then placed on the sensor and the capacitance recorded, the same fruit peel was then immediately tested in the same place with the Moistsense device as a whole. Fruit peel was used since it has a similar dielectric constant as the skin, and it is flexible, so makes good contact with the device. Changing the type of fruit gave a wide range of readouts on the Moistsense. The results from this test are shown in Figure 3.6.

The second method was to remove the sensor from the Moistsense and in its place attach different capacitors. This then showed the capacitance required to produce a given readout. The results for this are shown in Figure 3.7.

The third method was to compare the Moistsense readings to that of the Corneometer © CM 825. The Corneometer was used as a calibration comparison to the Moistsense, since it is widely used in skin research. The two devices were compared using moisture measurements from different skin locations. Since the skin varies in moisture content across the body, a range of readings was possible. The results from this test are shown in Figure 3.8.

Considering the increased error in method 1, the two capacitance tests can be seen to agree with the relationship between capacitance and Moistsense reading. This coupled with the linear relationship between the Moistsense reading and Corneometer CM 825 reading indicates that the sensor is linear.

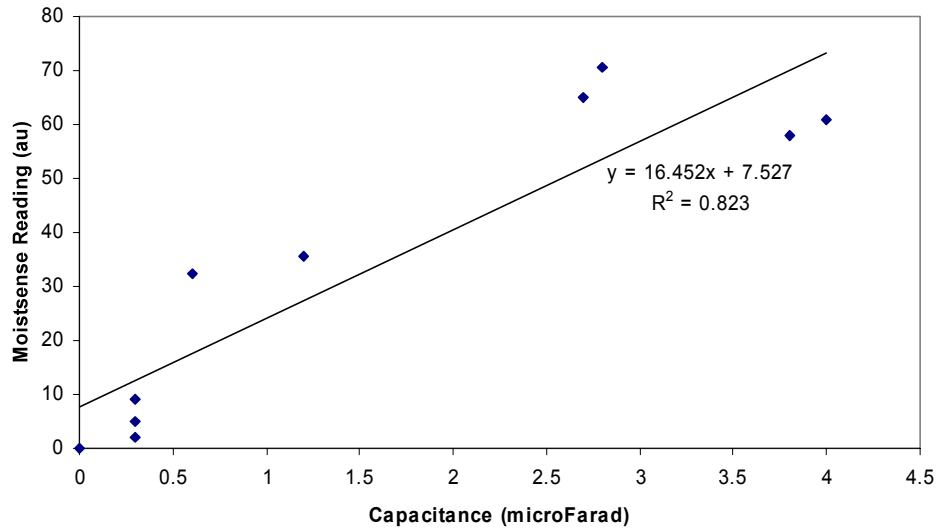


Figure 3.6 – Capacitance plotted for the Moistsense readout, when tested on various fruit peel

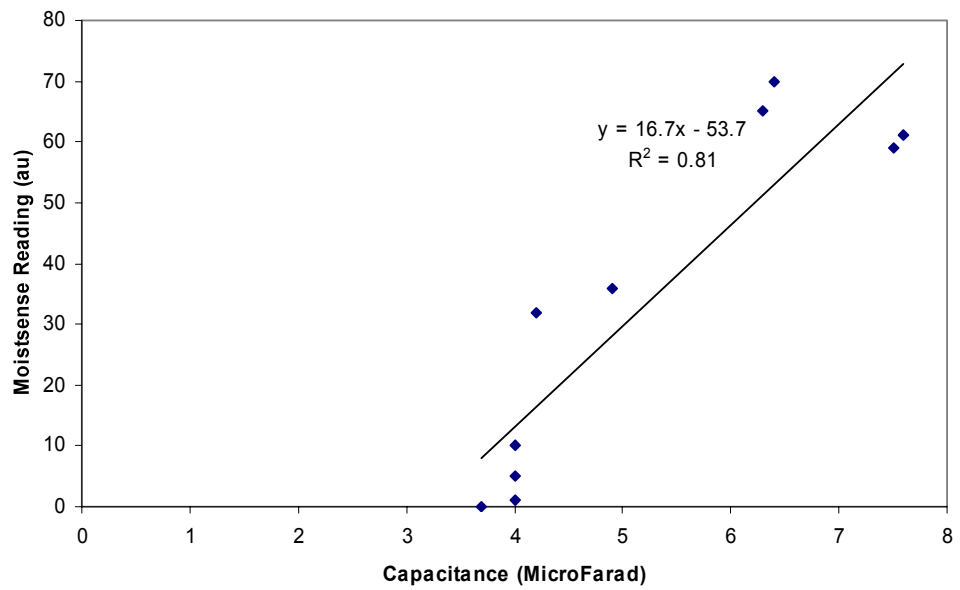


Figure 3.7 – Plot of varying capacitance against reading of the Moistsense, when different capacitors were attached to the Moistsense

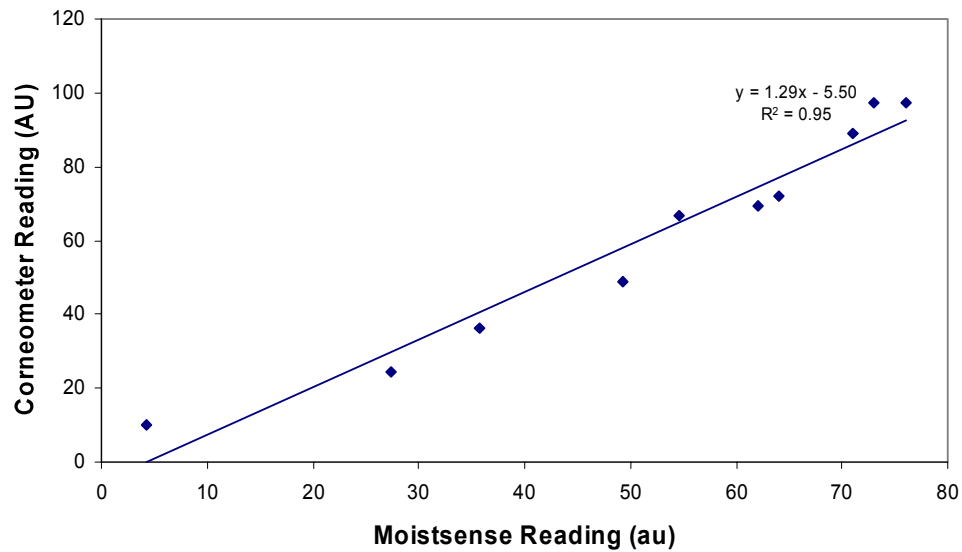


Figure 3.8 – Plot of Moistsense reading against Corneometer reading when tested on the same skin area

3.6 Roughness Measurements

Roughness profiles of the test surfaces were measured using a Mitutoyo SurfTest SV-600 profilometer and the data collected and analysed using Mitutoyo Surfpak-SV Version 1.3. The measurement distance depended upon the test; it was 25 mm for nominally flat surfaces and 6 mm for the small ridged surfaces. The test was repeated in three different positions on the surface, and the profilometer needle was moved in the same direction as the finger in the friction tests. The speed of the probe was; 0.5 mms^{-1} (for 25 mm length) and 0.1 mms^{-1} (6 mm length). The number of data points were 2500 (25 mm length) and 6000 (6 mm length).

Since it is not possible to keep the finger still enough for the profilometer, a cast (negative) of the finger was made using an addition cured silicone (Aquasil Ultra from Densply). The roughness of the cast was measured using the procedure above, over a distance of 2 mm, a speed of 0.1 mms^{-1} , and 10000 data points were recorded.

3.7 Finger Properties

In Chapter 4, a number of different people were tested; however, following this, in the majority of cases, the finger of one person was used. The surface dimensions of this finger are shown in Table 3.2.

Table 3.2 – Surface dimensions of the finger (for the finger used in the majority of tests)

Length (from tip to interphalangeal joint) (mm)	25
Height (from finger pad surface to nail surface) (mm)	12.5
Width (mm)	14
Roughness (R_q) (μm) (area dependent)	7.5 - 17
Ridge Pattern	Double loop

4 Relationship Between Friction Force and Normal Force

In the literature review (Chapter 2), previous work analysing the relationship between the friction force and normal force, for human skin, was assessed. This found contradicting conclusions about the relationship between the friction force and normal force: Ramalho [63] found a two part linear relationship for friction on the palm, as opposed to the power relation suggested by studies on the forearm [51, 53]. This highlights the need for finger specific tests to be done, since like the palm, the finger could behave very differently to the forearm. This chapter investigates the relationship between the friction force and normal force for the finger contacting a nominally flat surface. This research has importance in terms of understanding finger friction for a wide number of applications. The normal forces used in everyday tasks (such as opening a bottle or holding a hand rail) are often unknown. These are measurable, but when trying to gain an understanding of the friction in grip, it is more useful to know how the friction force varies with load.

4.1 Test Method

The tests in this study were split into three categories. Initially thirty two volunteers (6 female and 26 male), aged 20 – 49 years, were tested to gain an idea of the friction behaviour for a large number of people. Volunteers over the age of 50 years were not tested, due to Cole *et al.*'s [14] findings that friction for acetate decreases at the age of 50 years. The sample included university students, lecturers and technicians. The test procedure described in Chapter 3 was used. The materials tested were microscope slide glass ($R_a = 0.076 \mu\text{m}$), steel ($R_a = 0.479 \mu\text{m}$) and smooth rugby ball material ($R_a = 5.926 \mu\text{m}$). The material properties of the rugby ball material are unknown. However, it was observed that the deformation of the finger was distinctly greater than that of the rugby ball material. These were chosen as widely used examples of materials that are gripped; for example glass in packaging, steel in hand rails and rugby ball material in sport. The

sequence in which the materials were tested was rotated, to average any effects of test order. Volunteers were asked to do five tests on each material. Each test was done at a different load, ranging from the minimum to maximum force the volunteer was able and found comfortable to apply.

The second set of tests investigated the relationship between the friction force and normal force in more depth, with a larger number of sample points, but was only conducted on one finger to eliminate the inter-person variation. The test procedure as outlined in Chapter 3 was used, on a single finger. The materials tested were; Aluminium 2024 ($R_a = 1.616 \mu\text{m}$), Stainless Steel 316 ($R_a = 1.439 \mu\text{m}$), Brass ($R_a = 1.71 \mu\text{m}$), Nylon ($R_a = 1.491 \mu\text{m}$), HDPE ($R_a = 4.095 \mu\text{m}$), Acetal ($R_a = 2.615 \mu\text{m}$), Polypropylene ($R_a = 1.234 \mu\text{m}$), PVC ($R_a = 0.734 \mu\text{m}$) and elastomers 408 ($R_a = 0.906 \mu\text{m}$), 803-30 ($R_a = 1.383 \mu\text{m}$), 908SP ($R_a = 1.513 \mu\text{m}$) and 7265 ($R_a = 2.545 \mu\text{m}$). The loads applied varied between 0.4 N and 34 N; however, this maximum value depended on the material, as tests were stopped when the applied force caused pain. Forty tests were done in this range of forces for each material. The temperature and humidity were measured to ensure that these were not affecting the tests. The overall ranges of these throughout all tests were a humidity of 30 – 46 % and temperature of 21.5 – 24.5 °C. No effects on the results in this test were found, at this range of temperature and humidity. The moisture of the finger was also monitored. When analysed it was shown that a moisture level above 65 au, where au denotes the arbitrary units for the Moistsense device, (60 au for brass) increased the measured coefficient of friction, so these results were omitted. The range of moisture was therefore 45 – 65 au (60 au for brass).

Finally, the third stage of testing investigated the relationship between friction force and normal force at low loads. These tests were done at Philips Applied Technologies, The Netherlands. The equipment and test method used is described in Chapter 3. These tests were done on Brass (CZ 121),

PVC, Polypropylene, Nylon 6, Acetal and HDPE, and they were done using the same person and finger as the tests at The University of Sheffield. Forty tests were done at varying loads, but some of these results were discounted from analysis, due to the large amount of stick-slip observed during the test. Thirty of the forty tests aimed to have a normal force below 5 N, with the remaining tests done at larger loads so data was available to compare to the previous tests. The recording equipment was outside of the climate controlled room, and therefore not visible during tests, so control of the force applied was limited. However, with the large number of tests done, a range of data was collected at low loads. The climate controlled room was set to a temperature of 20 °C and a humidity of 45%. The moisture level of the finger was measured before each test using the Corneometer © CM 825, the moisture level varied from 33 to 44 AU, throughout the duration of the tests (where AU defines the arbitrary units of the Corneometer).

4.2 Results

4.2.1 Results from the Experiments Involving Thirty Two Volunteers

A general trend of linearly increasing friction force with normal force was seen for all materials and people tested. An example for one person is shown in Figure 4.1, and the details of all the plotted lines of best fit for each person are shown in Appendix 6. The steel and glass lines of best fit, in Figure 4.1, do not intercept the friction force axis at zero. The line of best fit for the rugby ball material does intercept the friction axis at zero, for the example shown, but this was not the case for all volunteers.

The glass results are unreliable since a constant friction profile (as seen in Figure 3.2, in the previous chapter) was not achieved. The data at the end of the profile was used as this is the region where the friction values were more constant.

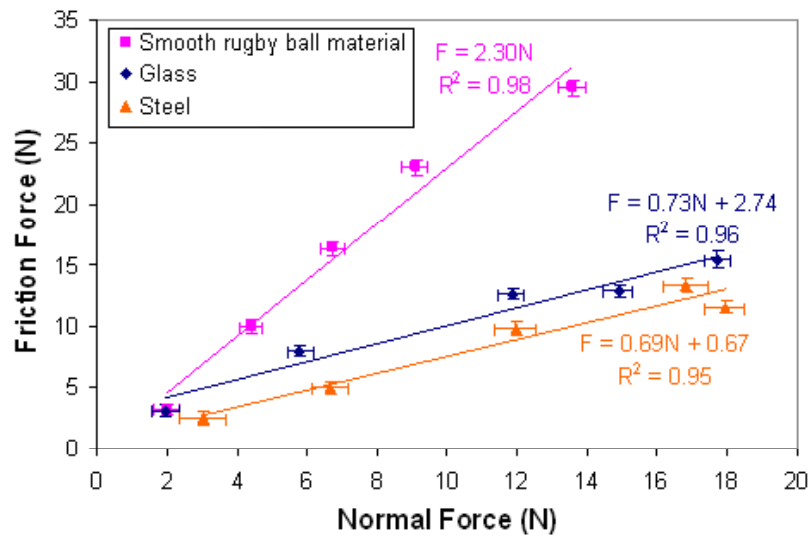


Figure 4.1 – Plot of friction force against normal force for three materials tested with a 24 year old male, error bars indicate one standard deviation

Although there was a trend of linearly increasing friction force with normal force for all volunteers, the gradient of the line of best fit varied dramatically between people. Figure 4.2 highlights this variation, it shows the average gradient of the friction vs. normal force graph for all the volunteers tested, displayed in age groups and gender. The error bars display the 95 % confidence intervals. The value of the friction force axis intercept varied depending on the person and material tested, the average of these can be seen in Figure 4.3. This shows that the friction force axis intercept was averaging a positive value for steel on all occasions (this was true for all volunteers excluding one). The intercept, however, varied between a positive and negative value for glass and the rugby ball material. The error bars in Figure 4.2 show that there is a large variation of the coefficient of friction measured within groups. However, the average value of friction force does not vary between age and gender groups, except for the rubber at an age of 40 – 49 years, but this is skewed due to it only being populated by two people. The average coefficient of friction (gradient of the graph) is similar for steel and glass, but larger for the rugby ball rubber.

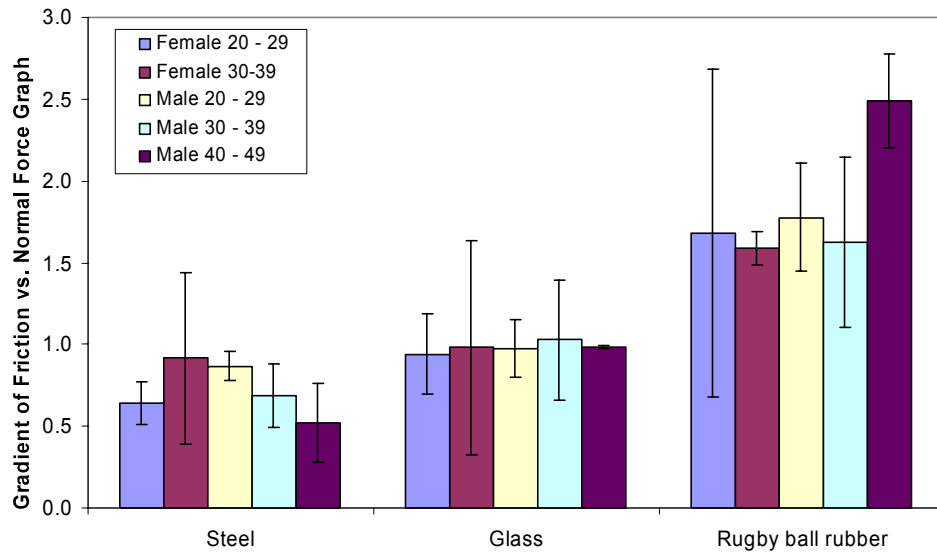


Figure 4.2 – Average gradient of Friction vs. Normal Force Graphs for all volunteers tested

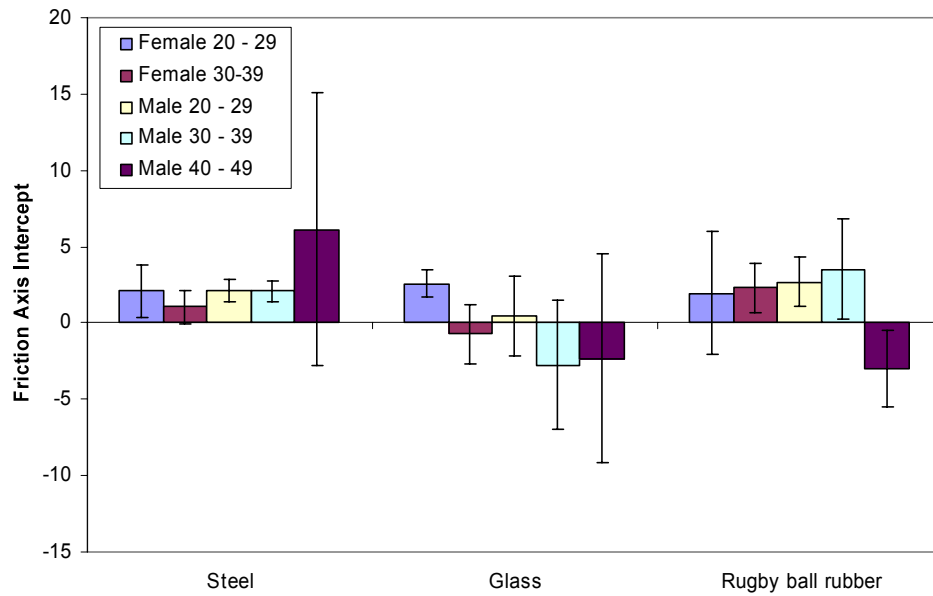


Figure 4.3 - Average friction force axis intercept values, when plotted against normal force, for each age group and material

4.2.2 Results from Tests Involving One Finger at Larger Loads

The results for the plastics are shown in Figures 4.4 and 4.6, the results for the metals are shown in Figure 4.5, and the results for elastomers are shown in Figures 4.7 to 4.9. These figures show that it is reasonable to plot a linear line of best fit through the data, within the force range tested. Figure 4.6 shows the friction results from testing Acetal. This material is highlighted because it deviates the most from the linear line of best fit. A power curve is also plotted through the results, to compare the fit to a linear one. The data best correlates to the linear line of best fit. Later analysis in this section will show that a two part linear relationship is valid for all results, and this would further better represent the results.

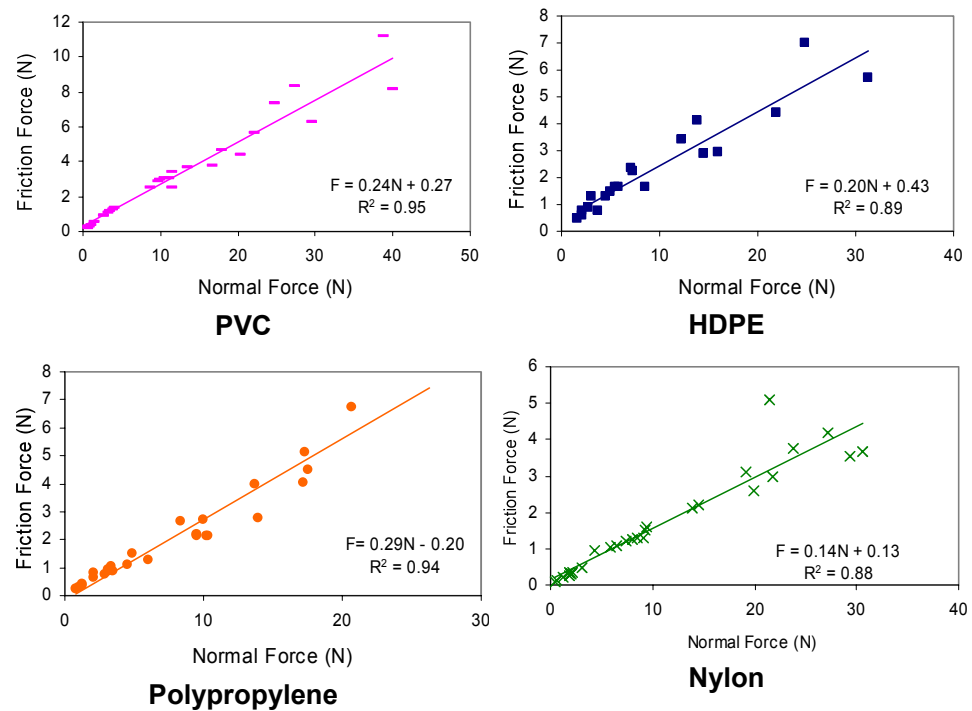


Fig. 4.4 – Plots of normal force against friction force for all plastics, except Acetal (See Figure 6 for Acetal results)

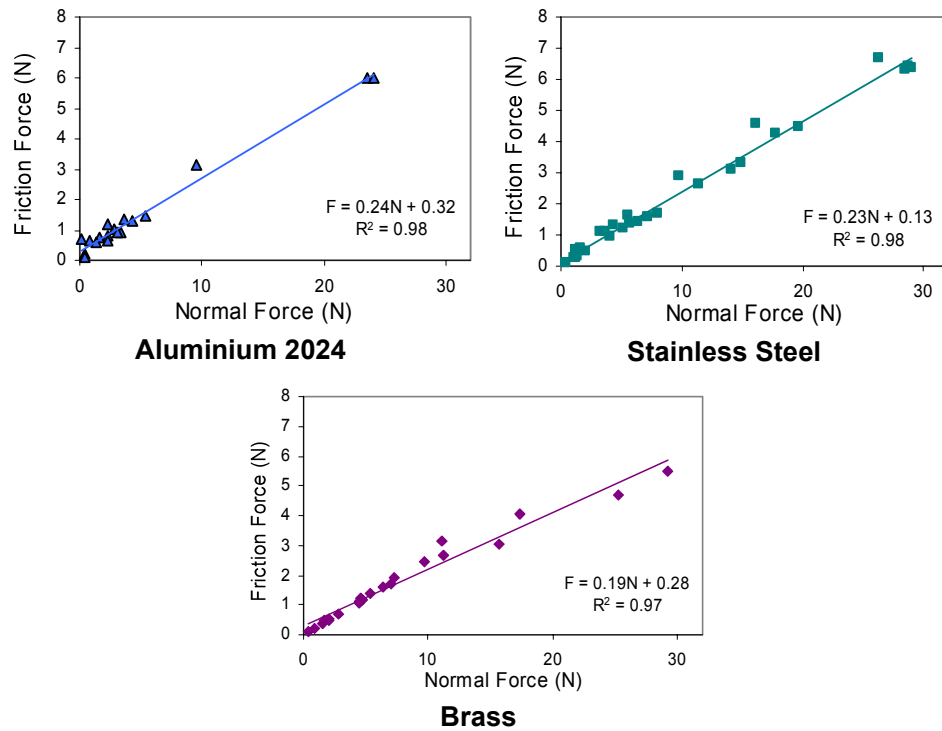


Fig. 4.5 – Plots of normal force against friction force for all metals

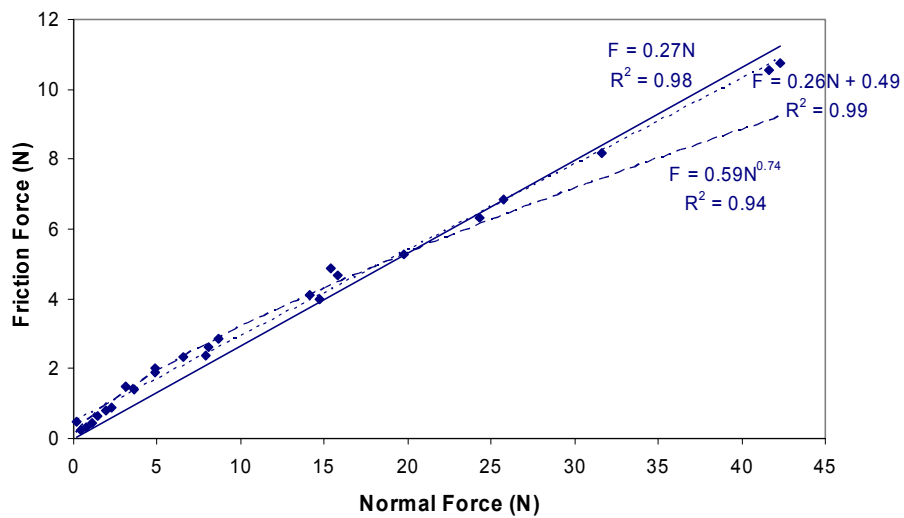


Fig. 4.6 – Plot of friction force against normal force for Acetal

The relationship between the friction and normal force for the elastomers tested is shown in Figures 4.7 to 4.9. Most of the elastomers, excluding

elastomer 803-80, exhibited large scale stick-slip behaviour, past a certain load, as illustrated in Figure 4.10. This load is the maximum load displayed in Figure 4.7, for each elastomer individually. Large scale stick-slip refers to the finger moving along the surface and then noticeably stopping, due to an increase in friction (at the same normal force). The finger then overcomes this friction and starts to slide again. At larger loads, there was also small scale stick-slip observed, illustrated in Figure 4.10. Elastomers are composed of chains of molecules, so the small scale stick-slip could be due to the elongation of rupture of the molecule chains. Once a chain has been stretched to a maximum it ruptures and returns to its original position [89].

Figures 4.8 to 4.9 show three lines of best fit for the elastomers which exhibited the large scale stick-slip. Figure 4.8 displays the results for the ‘slip’ part of the slide and Figure 4.9 shows the results for the ‘stick’ part of the slide. An interesting observation from these results is that there is a linear relationship between the friction and normal force in all the three regions of the slide (Figures 4.7 to 4.9).

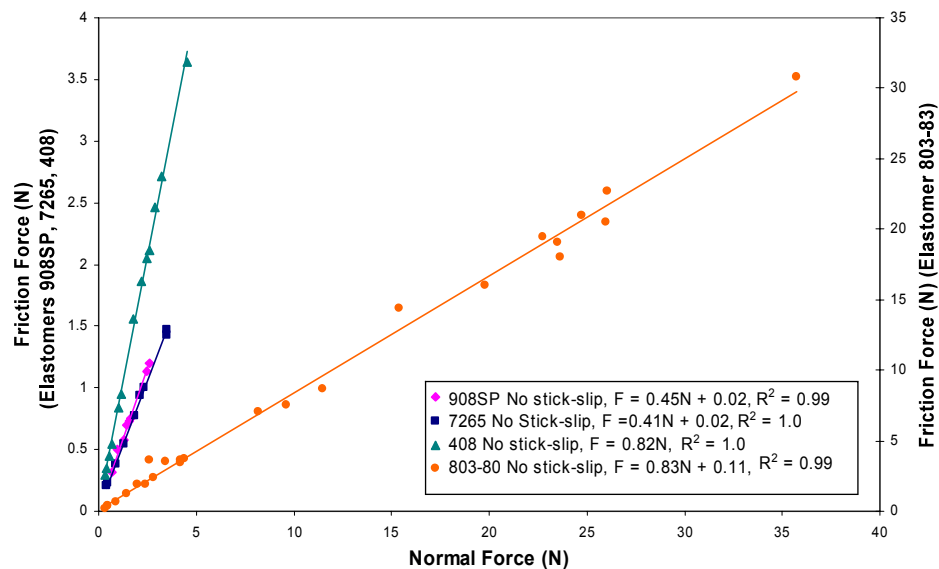


Fig. 4.7 – Plot of friction against normal force for the four rubbers tested, in the area of no stick-slip

Chapter 4 Relationship Between Friction Force and Normal Force

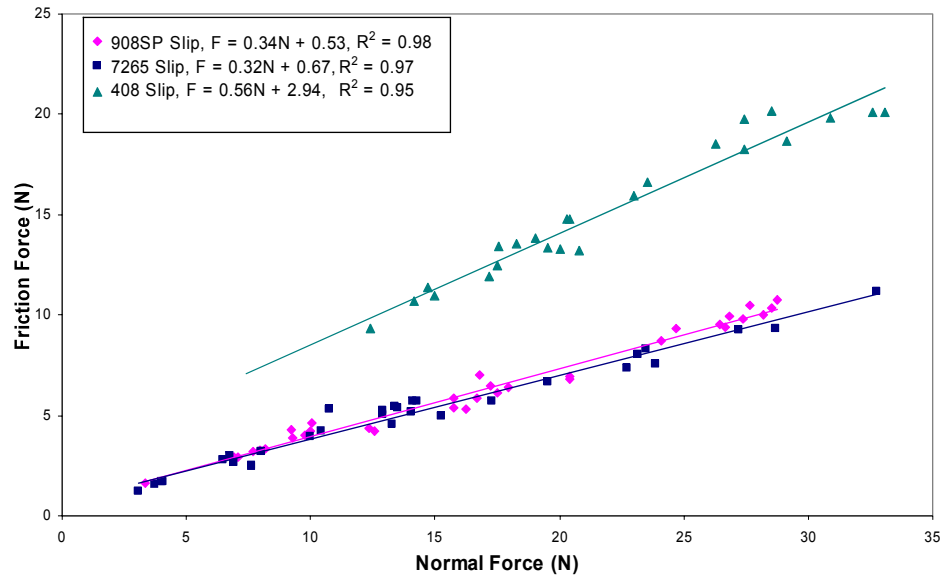


Fig. 4.8 – Plot of friction against normal force for the three rubbers tested (which showed stick-slip behaviour at increased load), in the area of slip

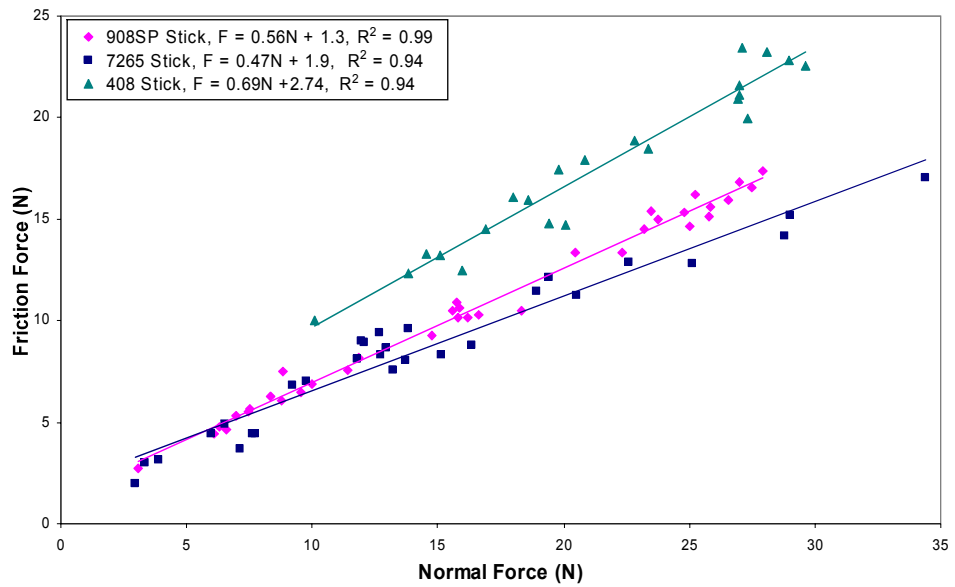


Fig. 4.9 – Plot of friction against normal force for the three rubbers tested (which showed stick-slip behaviour at increased load), in the area of stick

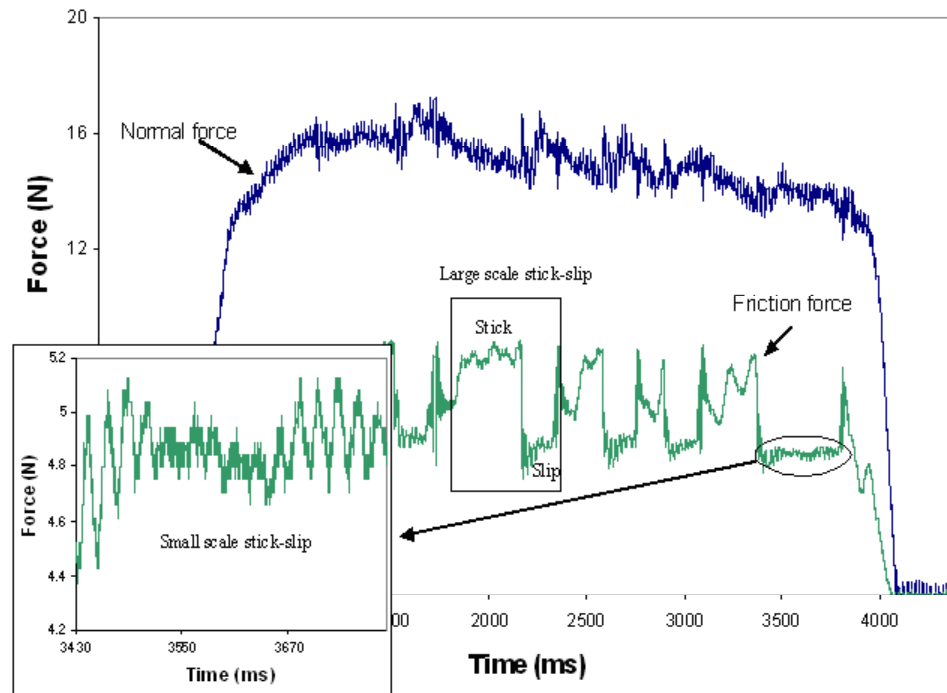


Figure 4.10 – Typical signal from a test with stick-slip. The test shown is for the finger contacting Elastomer 7265

Table 4.1 shows a comparison of all the coefficients of friction measured. These coefficients are the average value of the friction force divided by the normal force for each data point, in the range of 2 N to 20 N. The coefficients of friction displayed for the elastomers are for the no stick-slip data (the data displayed in Figure 4.7). This table shows that in the majority of cases the coefficient of friction is similar for each metal and plastic. However, aluminium and acetal have a slightly higher coefficient of friction than the other materials, and nylon 6 has a slightly lower coefficient of friction. That said; the average coefficient of friction does not give the full picture, due to its load dependence. To illustrate this difference, the coefficient of friction, calculated from linear lines of best fit plotted through the data in Figures 4.4 to 4.6, above loads of 2 N (so slightly different to those shown in Figures 4.4 to 4.6), was plotted against normal force in Figure 4.11. The line was plotted at loads above 2 N, since the relationship changes for loads below this. This

Chapter 4 Relationship Between Friction Force and Normal Force

graph shows that below 7 N, the materials with the largest coefficient of friction will be dependent upon the testing load.

Table 4.1 – Average coefficient of friction for each material, for data in the load range of 2 N to 20 N

Material	Average Coefficient of Friction
Stainless Steel 316	0.25
Aluminium 2024	0.34
Brass CZ 121	0.25
HDPE	0.28
Polypropylene	0.26
PVC	0.30
Acetal	0.34
Nylon 6	0.16
Elastomer 803-80	0.90
Elastomer 908SP	0.46
Elastomer 408	0.83
Elastomer 7265	0.43

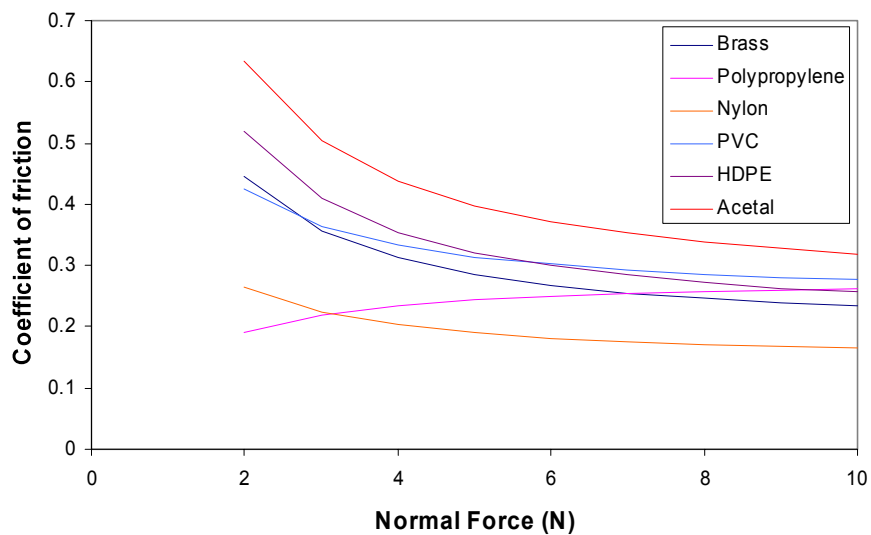


Figure 4.11 – The coefficient of friction against normal force, calculated using a linear line of best fit, through data measured above a normal force of 2 N (in an area where the friction force definitely varies linearly with the normal force).

4.2.3 Results from the Low Load Tests

The results from the low load tests are shown in Figure 4.12. The graphs are plotted individually for each material. Two possible relationships between the friction force and normal force are plotted on these graphs. Firstly in blue, a two part linear relationship is shown. The low load data showed that the line of best fit for the friction force vs. normal force graph does indeed pass through zero. The data from approximately 0 to 2 N indicates a linear relationship between the friction force and normal force. After this there is still a linear relationship, however, this is at a different gradient to the lower load relationship and does not intercept the friction force axis at zero.

The results could also be described using a power relationship, but the normal force is raised to a power greater than 0.67 (expected from the Hertzian based derivation of adhesive friction). The power in fact ranges between 0.81 and 1.06.

Chapter 4 Relationship Between Friction Force and Normal Force

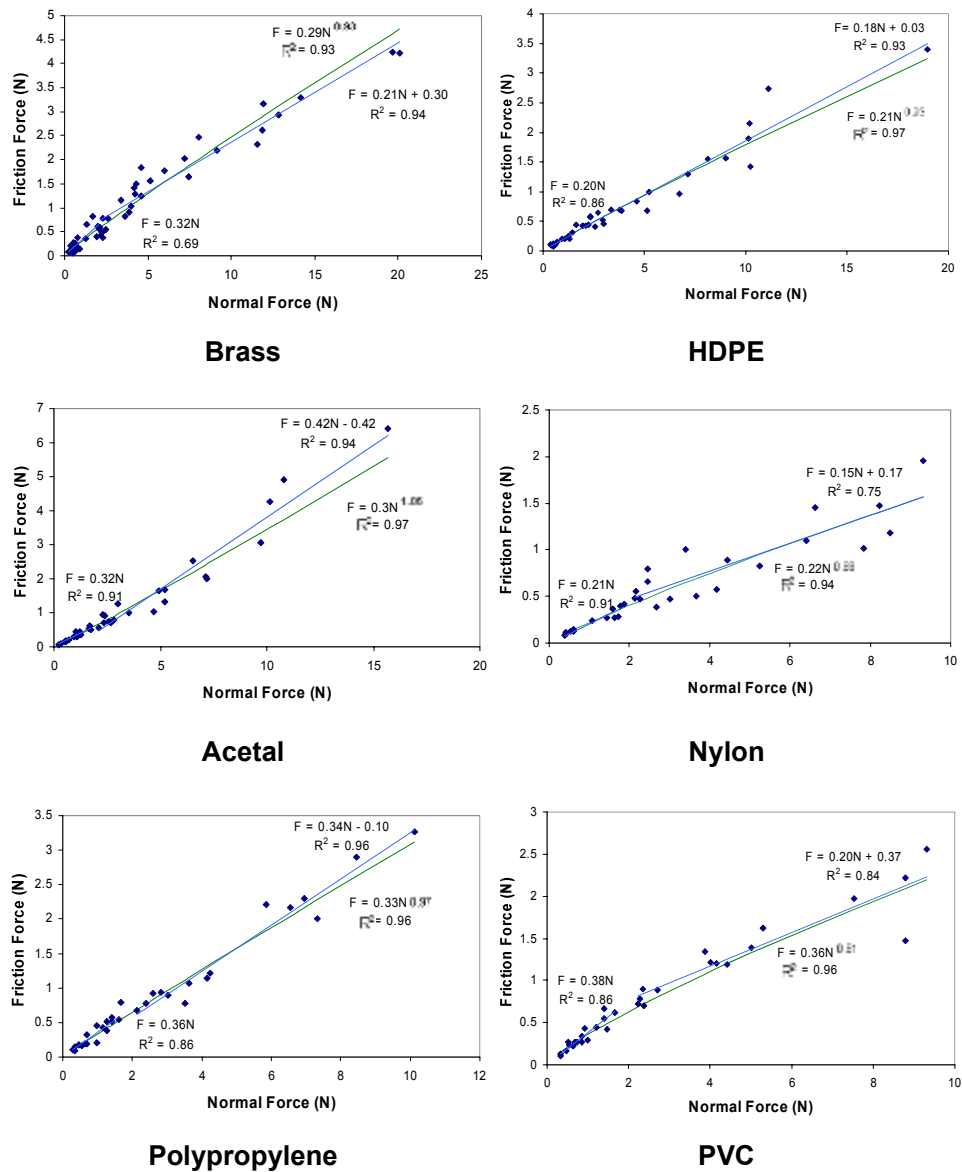


Figure 4.12 – Results from low load friction tests

To ensure no discrepancies between the measuring techniques used at The University of Sheffield to those at Philips Applied Technologies, a comparison of the high load tests was done. Table 4.2 shows the equations of the linear lines of best fit for both tests. Most of the lines of best fit at the larger loads are similar for both tests; the largest difference is seen for acetal and

Chapter 4 Relationship Between Friction Force and Normal Force

polypropylene. Figure 4.13 shows the results for tests done on PVC both at Philips Applied Technologies and at The University of Sheffield. This shows that for the larger loads tested at Philips Applied Technologies, there is good agreement with the results from the tests at The University of Sheffield. It also provides a larger picture of how the friction force varies with normal force from 0 – 25 N.

Table 4.2 – Equations for the lines of best fit for the tests done at The University of Sheffield and Philips Applied Technologies

Material	Philips Results		Sheffield Results	
	At low normal force	At high normal force	All data	Larger loads
PVC	0.38N	0.20N + 0.37	0.24N + 0.27	0.24N + 0.37
HDPE	0.20N	0.18N + 0.03	0.20N + 0.43	0.19N + 0.66
Poly-propylene	0.36N	0.34N - 0.10	0.29N - 0.20	0.28N - 0.18
Nylon	0.21N	0.15N + 0.17	0.14N + 0.13	0.14N + 0.25
Acetal	0.32N	0.42N - 0.42	0.26N + 0.49	0.24N + 0.79
Brass	0.32N	0.21N + 0.30	0.19N + 0.28	0.18N + 0.53

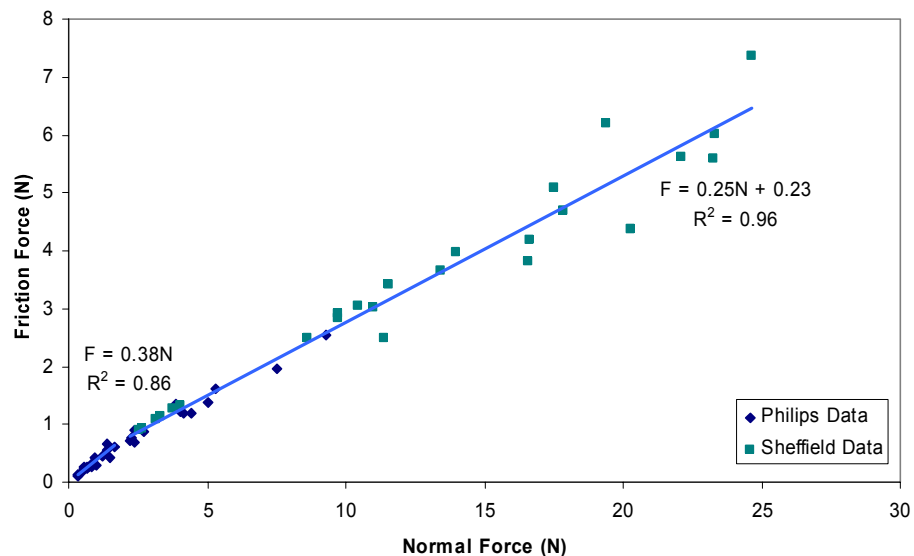


Figure 4.13 – Plot of all the results from both the tests done at Philips Applied Technologies (Philips Data) and The University of Sheffield (Sheffield Data), for the finger contacting PVC. The lines of best fit shown include all data at low and then high loads.

4.3 Discussion

4.3.1 *Variation of Friction Force with Normal Force*

There is a large variation between individuals, in the gradient of the friction force vs. normal force graphs. However, the general trend of linearly increasing friction with normal force, across the loads tested, is seen for all subjects. Since this study is interested in behaviour, rather than a quantification of friction, these results indicate that tests on a single finger will yield information that can be applied generally to the larger population. The single finger tests were in agreement with these tests, in that, in the region tested the relationship between the friction force and normal force is linear, this was seen for all materials, including elastomers. However, the line of best fit does not cross the friction force axis at zero (see Figures 4.4 to 4.7), except for the elastomers (no stick-slip), where in most cases, it does intercept the friction force axis at zero. This is in agreement with the tests done on the thirty two volunteers. The non-zero intercept could initially have had several interpretations. It could have been due to a non-linear relationship at lower loads, or, as discussed later, a linear relationship at low loads different to that at higher loads. It could also have been due to there being a friction force at zero normal force, due to the surface energies of the finger and counter-surface, as predicted by JKR contact theory [79]. However, Figure 4.3 shows that the friction force axis intercept is not always positive, thus negating this explanation.

The tests done at Philips Applied Technologies furthered the understanding of the relationship between friction and normal force, by investigating in more depth the relationship at low loads (Figure 4.11). These tests highlighted two possible relationships between the friction force and normal force: A two part linear relationship or a power relationship. These force tests alone cannot determine which best describes the contact. A two part linear relationship for palmer skin has previously been discussed by Ramalho [63]. However, his work was done at much larger loads, and the results don't show a large

population of data points below a force of 5 N. Ramahlo's results showed a change in linear relationship at approximately 28 N. This is a larger load than the test method used in this study can measure, due to the physical constraints on how hard a human can consistently press with their finger. It is also a load much larger than would be applied by a single finger when gripping. Although it is not possible to use this technique to measure at high loads, these results imply the relationship between friction force and normal force could be a three part linear relationship: Two parts in the region tested, and a further part at a larger load (around 28 N, but this is expected to vary between people).

The friction mechanisms of the finger are complex, due to a number of different aspects influencing the properties of the surface. There will be contacts of asperities, therefore adhesive friction. The fingers have a self lubrication system of natural grease and sweat, in fact the finger sweats more when in contact with a surface. This introduces another friction mechanism from the capillary effects or viscous shear effects, which will be further examined in Chapter 6. There will be a contribution to friction due to the delayed movement and deformation of the ridges, the work of Levesque and Haywood [68] is looking to improve the knowledge of this friction mechanism. Observing the finger movement, there is also a contribution of friction due to the deformation of the finger. Taking all these factors into account, the friction, for a finger contacting a flat surface, can be described using Equation 4.1.

$$F_T = F_a + F_d + F_v + F_r \quad 4.1$$

where F_T is the total friction, F_a is the adhesive friction, F_d is the deformation friction, F_v is the friction due to capillary adhesion or viscous shearing, and F_r is the friction due to deformation of finger ridges

For a flat surface, the deformation component of friction replaces the hysteresis component usually concerned with skin friction. This is due to the difference between the two friction systems. Hysteresis friction is referred to when a probe (usually spherical) is moved along the skin, for example along the forearm. The skin in front of the probe deforms, this requires work to be done on the skin, but, the skin behind the probe deforms back to its original position; an energy return. However, the work done is greater than the energy return, due to the viscoelastic nature of the skin. The hysteresis component of friction refers to the additional force required, due to this dissipation of energy. The finger is not deforming and un-deforming, so the mechanism is different. Since, the test is dynamic there is no dwell time, so the creep previously observed with finger contacts [77] will not be of consequence. Considering the static case of friction, work is done on the finger to deform it, in placing it on a surface the work done is described by Equation 4.2 [90]

$$U = \frac{3}{10} \cdot \frac{N^2}{a^2} \cdot \frac{1}{E^*} \quad 4.2$$

where U is the work done, N is the applied Load, a is the radius of contact area, and E^* is the reduced Young's modulus

The finger can be observed to compress, and then when a lateral force is applied, there is a movement of the bulk of the finger (in the apposing direction), however the contacting surface of the finger does not move. The bulk of the finger, then remains in this relative position (to the contacting surface) during the slide; this requires an energy input. Tabor [91] modelled the work done for a sphere (rigid) moving along a flat (less rigid) surface. This calculation is based upon the area of contact and deflection, from Hertz theory. Since the area and deflection for a sphere are the same whether it is the sphere or the flat is the softer material, this model can be applied to the finger; assuming of course that the finger can be modelled as a sphere.

Tabor [91] found the work done per unit length in rolling a sphere along a flat is described by Equation 4.3.

$$\Phi = \frac{9}{64} \cdot \frac{N^2}{a^2} \cdot \frac{1}{E^*} \quad 4.3$$

where Φ is the work done per unit length

Since work done is the integral of force with respect to distance, the force required to apply this deformation is described by Equation 4.4 and is the friction force due to deformation. However, once the finger starts to move (the kinetic case) there is no more work done on the finger, because the deformation remains the same. However, there will still be some force required to maintain the finger in its deformed state. An analysis of the energy required to deform the finger, compared to that required for sliding can provide information about the contribution of this deformation component to the overall friction. However, to do this, information about the deformation of the finger with applied load is required. This will be assessed in Chapter 5.

$$F_d = \frac{9}{64} \cdot \frac{N^2}{a^2} \cdot \frac{1}{E^*} \quad 4.4$$

This chapter has investigated how the total friction force varies with normal force. In many other skin tests, adhesion is the principle mechanism of friction, and it would not be surprising if this is also the case for the finger. However, since the adhesive contribution of friction is dependent upon the area of contact, and is described by Equation 4.5, the area of contact needs to be further investigated. This will be examined in Chapter 5.

$$F_a = \tau \cdot A \quad 4.5$$

where τ is the shear strength at the asperity junctions and A is the real area of contact

The equipment available is not capable of measuring the contribution of friction due to deformation of the ridges. As mentioned previously, the exact motion is being investigated by Levesque and Haywood [68]. It is, however possible to calculate an over estimation of the contribution to friction due to ridge deformation. There are two possible mechanisms of friction from the ridge deformation on a nominally flat surface. The first is the deformation of the finger ridges, similar to the bulk of the finger. This requires an initial force to cause the deformation, then a small applied force to keep the ridge in its deformed state. The force to maintain the deformed state is not known, but the initial larger force can be estimated. The second possibility is related to the movement of the ridges and hysteresis losses associated with this. This can be over estimated, again using the work done to deform the ridge, this is then multiplied by a loss fraction (so will be less than the calculated force). This analysis also needs information on the area of contact, so will be fully assessed in Chapter 5.

4.3.2 The Variation in Coefficient of Friction Between the Materials Tested

Table 4.2 shows little variation between the measured coefficients of friction for each material. It does, however, show that Nylon 6 has a lower coefficient of friction than the other materials, and acetal and aluminium have a slightly higher coefficient of friction. Table 4.3 shows the properties of the different materials and Table 4.4 shows the Pearson correlation coefficients (R_p) for a linear relationship between each material property and the measured coefficient of friction. These correlation coefficients show no linear correlation between the coefficient of friction and any of the material properties. Except when considering metals alone, in which they may be a correlation between density and measured coefficient of friction, but, since only three metals were tested, more experiments need to be done.

Chapter 4 Relationship Between Friction Force and Normal Force

Table 4.3 – Material properties of metals and plastics. E is Young's Modulus, K is thermal conductivity and μ is the coefficient of friction against hardened ground steel (pressure = 0.05 Nmm^{-2} , velocity = 0.6 ms^{-1}).

Material	Density (g/cm^3)	E (MPa)	K (at 20°C) ($\text{Wm}^{-1}\text{K}^{-1}$)	Roughness ($R_q, \mu\text{m}$)	Shore Hardness Scale D	μ	Surface Energy (mNm^{-1}) [92, 93]
HDPE	0.95	900	0.43	4.749	62	0.3	35.3
Polypropylene	0.91	1450	0.22	1.459	70	0.3	30.1
PVC	1.36	3000	0.14	0.936	82	0.6	41.5
Acetal	1.39	2600	0.31	3.084	85	0.35	42
Nylon 6	1.13	1700	0.28	1.778	77	0.42	42
Brass	8.75	115000	159	2.011			
Stainless steel 316	7.99	193000	16.2	1.684			
Aluminium 2024	2.78	73100	193	1.966			
Elastomers							
Elastomer	50% Elastic Modulus (MPa)	100% Elastic Modulus (MPa)	Tensile Strength (MPa)	Elongation at break (%)			
803-80	6.1	15	27.4	224			
908SP	5	9.25	15.8	177			
408	3.5	7	17.2	272			
7265		14.2	16.6	137			

Chapter 4 Relationship Between Friction Force and Normal Force

Table 4.4 – Correlation table for each material property against the coefficient of friction of the material against the finger

Property	Materials	Number of samples	R _p	p value (two tailed)
Young's modulus (MPa)	All	12	-0.341	>0.1
	Metals	3	-0.376	>0.1
	Plastics	5	0.258	>0.1
	Elastomers	4	-0.135	>0.1
Density (gcm ⁻³)	All	8	-0.226	>0.1
	Metals	3	-0.931	<0.01
	Plastics	5	0.127	>0.1
Thermal Conductivity (Wm ⁻¹ K ⁻¹)	All	8	0.033	>0.1
	Metals	3	0.214	>0.1
	Plastics	5	-0.507	>0.1
Roughness (R _q) (µm)	All	12	-0.259	>0.1
	Metals	3	-0.094	>0.1
	Plastics	5	-0.307	>0.1
	Elastomers	4	-0.779	>0.1
Coefficient of friction to DIN 53375 (Plastics only)	Plastics	5	0.108	>0.1
Shore Hardness D Scale (Plastics only)	Plastics	5	0.159	>0.1
Surface Energy (mNm ⁻¹)	Plastics	4	-0.514	>0.1

The predominant mechanism of adhesion is adsorption [94]. This is where intermolecular bonds, such as van der Waals and/or hydrogen bonds, form between the two surfaces. Considering this mechanism, the work done in adhesion is dependent upon surface energies as described by Equation 4.6 [78].

$$\Phi = \gamma_a + \gamma_b - \gamma_{ab} \tag{4.6}$$

where Φ is the work done to separate the surfaces, γ_a and γ_b are the surface energies of each surface and γ_{ab} is the energy of the interface.

However, there is no correlation between the surface energy of the plastics and the measured coefficient of friction, since nylon has a much lower coefficient of friction than acetal, yet they have the same nominal surface energy. The interfacial energy is a more difficult quantity to measure and this could provide some more information to explain this difference. The manufacturers tested the water absorption, at equilibrium, at 23°C and 50 % (in line with DIN EN ISO/ASTM 63). These tests showed that nylon had a level of 3 % absorption, whereas the other plastics ranged between 0.01 and 0.2 %. This could account for the difference seen, but the physical reason is unknown. For acetal, the water absorption was in the same range as the other materials (0.2 %).

There are four mechanisms of adhesion (which will not be discussed in detail). Adsorption is the principal mechanism, and the other mechanisms are [94]:

Mechanical Interlocking – this occurs when the width of the asperities of one mating surface are much smaller than the other. The smaller width asperities then climb up and down the broader ones, energy is lost in the descent by impact deformation or generation of phonons (particle vibrations) [95].

Diffusion – diffusion of molecules from one material to the other, across the contact surface (applicable for polymers).

Electrostatic – there is a transfer of electrons between the two materials (applicable for when one surface is metallic). This creates opposite charges at each surface, and therefore an electrostatic attraction.

This study does not investigate these mechanisms, and therefore can not determine the percentage contribution of the mechanisms. However, further analysis of these mechanisms could help to further explain the results. For example, diffusion may be occurring in the finger on polymer (plastics and elastomers) contacts, and electrostatic adhesion may be present for finger on

metal contacts. The amount of adhesion is dependent upon the contacting materials having a similar solubility parameter (Equation 4.7). If this could be found for the skin of the palm; comparison to the parameters for the polymers (also needing to be measured and calculated) could provide an explanation to the different coefficients of friction measured.

$$\delta_s = \left(\frac{\Delta H_v - R_g \cdot T}{V} \right)^{1/2} \quad 4.7$$

where δ_s is the Solubility parameter, ΔH_v is the molar heat of vaporisation, R_g is the gas constant, T is the temperature and V is the molar volume

These tests show, that in terms of friction, either metal or plastics can be used as surfaces (flat) for grip, with very little discernable difference between them. The elastomers have a higher coefficient of friction than the other materials. This was initially thought to be due to their viscoelastic nature, which adds a hysteresis contribution to the friction mechanism, when the material deforms. However, approximate calculations do not estimate that the deformation contribution to friction would contribute to the whole increase in friction seen for the elastomers. A sample calculation is shown below for Elastomer 7265. There have been many assumptions made in these calculations, so it is only good for a very rough first approximation. This calculation suggests the hysteresis contribution to friction is only 0.5% of the total friction, so it is considered that another reason is possible for the increase in friction, such as the chemical construction of elastomers compared to polymers.

Deformation calculation for Elastomer 7265:

The friction due to hysteresis (F_h), for a rigid sphere contacting a flat elastomer, can be described using Equation 4.2 [91].

$$F_{hys} = \beta \cdot \left(\frac{9}{128 \cdot R} \right)^{2/3} \cdot \left(\frac{1 - \nu^2}{E} \right)^{1/3} \cdot N^{4/3} \quad 4.8$$

where β is the loss fraction, R is the radius of the sphere, ν is the Poisson's ratio, N is the normal force and E is the Young's modulus

The deformation of the finger contacting the different materials, whilst mounted on the friction rig, was filmed using high speed video. From this the deformation of the finger with normal force is known (full details of the experiment and results will be explained in Chapter 5). At 5.7 N the finger was fully deformed, therefore it is assumed that at this force, the finger can be approximated to a 'rigid' body. Calculating the difference between the maximum deformation of the finger on steel (1.58 mm) and then on elastomer 7265 (1.78 mm), the compression (δ) of elastomer 7265 is shown to be approximately a 0.2 mm. The deformation cannot be easily measured directly from the equipment setup due to its opaque nature. Making the crude assumption that at this point of deformation the finger is behaving as a rigid body, the Young's modulus (E) can be estimated from Hertz Theory of Contact [70]. The equations used for this are Equations 4.9 and 4.10. If the finger is considered to be rigid, such as a steel ball, the modified Young's modulus is equal to the Young's modulus of the elastomer. So, the Young's modulus at 5.7 N, of elastomer 7265, is 14 MPa.

$$N = \frac{4}{3} \cdot R^{1/2} \cdot E^* \cdot \delta^{3/2} \quad 4.9$$

$$E^* = \left(\frac{1 - \nu_1^2}{E_1} \right) + \left(\frac{1 - \nu_2^2}{E_2} \right) \quad 4.10$$

The assumption is made that the loss fraction of the rubber is approximately 0.18. The actual loss fraction is unknown. The loss fraction for a hemisphere moving over the forearm is approximately 0.24 [70], the rubber is

seen to deform to less extent than the forearm, so it is assumed that the loss fraction will be less. The Poisson's ratio is assumed to be 0.5 [40, 41]. Equation 4.8 is used for a rigid sphere contacting an elastomer surface. The finger therefore needs an assumed radius and this is based on extending the profile of the finger, as illustrated in Figure 4.14, and using the average of the two radii in the calculations. Substituting these assumed, calculated and measured values into Equation 4.8, yields a contribution to deformation friction of 0.023 N from the elastomer itself, which is only a contribution to the total friction of 0.5%. At this load, the friction force for elastomer 7265 is 1.75 times greater than that for stainless steel 316. Thus, implying that, the deformation of the rubber has little impact on the overall friction of the contact. Therefore, to understand why the friction is larger for elastomers, the mechanisms of adhesion need to be analysed and tested. It should also be noted, if the assumed loss fraction had been as high as 1, it hysteresis friction (0.13 N) would still not account for the increase in friction.



Side view of fingertip End view of fingertip

Figure 4.14 – Circles used to calculate the radii of the finger (average $R = 12 \text{ mm}$)

4.3.3 Variation in Friction Between People

The tests on thirty two volunteers showed a large variation in the average gradient on the friction force vs. normal force graph. Knowledge of finger friction suggests that the main reasons for the variation between people are the different hydration levels of skin, and the size of the area of contact, although the quick area measurements taken alongside these experiments did not show any correlation between the average coefficient of friction and the area of contact. However, these areas were measured crudely (using poster paint finger prints). There are also other factors that could affect

friction but are less understood, such as the variation of ridge patterns from person to person (and between fingers).

Referring to Figure 4.2, the average coefficient of friction does not vary greatly between age groups, except for males aged 40 – 49, when contacting the rugby ball material. However, there were only two people in this sample. If this were shown to be the case for a larger sample, it would be interesting to compare the results to the work of Cole *et al.* [14]. However, since age is not a concern for this specific research it will not be assessed in further detail.

4.3.4 Errors in the Results

There is some scatter seen in the results which could be due to several uncontrolled parameters; for example, speed and moisture change during a slide, since these have been shown to directly affect finger friction. Although the aim of the tests was to achieve a consistent speed for all tests, the nature of the test procedure dictates that this will change due to the human subject, not the test rig, controlling the applied speed (speed range = 0.014 ms^{-1} – 0.028 ms^{-1}). For the plastics, the scatter also seems to increase with larger forces, see Figure 4.4. Fingers sweat when gripping [15], i.e. when applying a force to an object. This sweat will alter the friction and the effect of this will be more apparent at higher loads, which could be an explanation for the scatter. To confirm this, an integrated measurement system such as that used by André *et al.* [87] could be used. However, this was not done as part of this study.

The results from the friction tests at Philips Applied Technologies (high loads) compare well to those done at The University of Sheffield. This validates the use of both tests. There is a small amount of variation between the tests, but this is thought to be due to the natural variation of the skin from day to day.

4.4 Conclusions

These tests showed there to either be a piece-wise or a power relation between the friction force and the normal force. If it follows a power law, the power (0.81 – 1.08) is greater than the 0.67, previously suggested. This difference in power is possibly due to the additional contributions to friction, resulting from the deformation of the finger, liquids naturally on the finger, and ridge deformation. More work needs to be done, to look at the area of contact, and the deformation of the finger. This will provide more information on the contribution, to the total friction, of the different friction mechanisms. The information can also be used to validate the use of the existing models, and the application to the finger, by simplifying it to a spherical elastomer.

Excluding the elastomers, there is very little difference in the friction of the contact between the finger and the materials, and surface conditions tested. This indicates that the finger may be dominating the friction mechanism.

The elastomers have a much larger coefficient of friction than the other materials. A quick analytical analysis implies that for the elastomers tested (relatively stiff), the increase is not due to hysteresis friction. Therefore, it is assumed that the increase in friction is due to the chemical composition of the elastomer, compared to that of a plastic or metal.

5 Area of Contact in Finger Friction Tests

The work outlined in Chapter 4, examining the relationship between the friction force and the normal force showed that it is either a power relation (raised to the power of approximately 0.8 – 1.1) or a two part linear relationship. Examining the deformation of the finger and area of contact, could provide a better understanding of the friction mechanism, and therefore how friction varies with load.

This chapter describes three methods that were used to examine the deformation and area of contact of the finger with the counter-face. These methods are compared for effectiveness, and then the results are used to analyse the relationship between the friction force and normal force.

5.1 Methods for Measuring the Area of Contact and Deformation of the Finger

5.1.1 High Speed Video Camera Analysis

High speed video analysis was conducted in two stages. Initially, the deformation of five volunteers' middle fingers was analysed, when contacting glass. The cameras were set-up such that one viewed the area of contact from below the glass, and one viewed it from the side of the finger, as illustrated in Figure 5.1. The settings for the cameras were: Resolution 512 x 512, Sample rate 160pps and Exposure 300 μ s. The glass was supported by two load cells (used to measure the normal force) and these were attached to two aluminium beams (stilts), which allowed the glass to be positioned above the high speed video camera. Each volunteer then pressed his or her finger onto the glass surface and removed it; this was repeated twice for each volunteer. The area of contact and deformation of the finger was then analysed in Matlab® using a program written by Choppin [96]. The video is converted to bitmaps; the Matlab® program then enables the user to pick

points on the picture. The coordinates of the pixels are then written to a spreadsheet. To determine the pixel length (for distance calculations), graph paper was attached to the glass, for the view from beneath, and for the side view the finger was marked in 3 positions, 1 cm apart (Figure 5.2). Mark 3, shown in Figure 5.2, was used to track the compression of the finger.

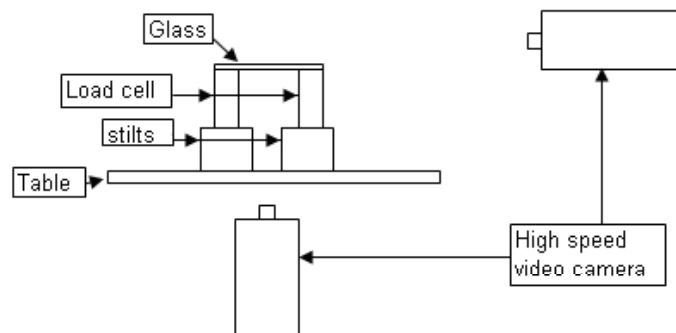


Figure 5.1 – Schematic of high speed video camera set-up for tests on glass

This method was then advanced, using the friction rig to measure the deformation of the finger, against all the materials tested in the normal force tests (see Chapter 4). These tests were done using the same person's middle finger as used in the normal force tests. Since the materials are not transparent, the side camera alone was used to measure the length of contact and the compression of the finger. The finger friction rig was used to measure the normal load. Tests were then done examining the area of contact and the deformation of the finger, when it is pressed onto a surface, and when the finger is sliding along the surface.

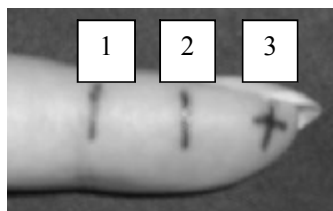


Figure 5.2 – Markings on the finger. Marks 1, 2 and 3 are 10 mm apart and used for calibration. Mark 3 was also used to track the compression of the finger

5.1.2 *Finger Print Ink*

The fingers are not smooth; there are ridges on them. Cutkosky *et al.* [67] found that the ridges do not compress to form a fully flat surface, even at high pressures. Therefore, the contact area is much less than the oval outline measured, in the high speed video tests, even before considering the contact area at an asperity level. The nominal area of contact is the contact that can be measured from a given technique. For example, the nominal area from the high-speed video footage is an oval of the measured diameters, whereas for the ink prints, it includes the ridges. The real area of contact, refers to the contact of the asperities, this will therefore be less than the nominal area of contact. The ridges on the fingers mean that the high speed video results are giving a large over estimation of the nominal area of contact. If the area of contact occupied by the ridges is known, the high speed video results can be modified to take the ridges into account, thus providing a better estimate of the nominal area of contact; however, this will still not be an estimate of the real area of contact.

These tests were carried out on the same finger as the normal force tests. This is to match the results up to the high speed video results, and then relate the area results to the friction measurements. The finger was inked using fingerprint ink and then pressed onto the surface of a white sheet of paper at varying loads, with the same orientation as in the friction tests. The area of the finger was then correlated to the length of contact measured in the high-speed video tests. This allowed analysis of the ridge contact for each of the areas measured, so that the area from the high speed video tests could be modified to a better area prediction. Matlab® was used to determine the area of ink and no ink; this was done by converting the print to a binary image. The number of zeros (black) can then be counted, giving an area of the ridges, this can then be compared to if the whole print was black (giving a ratio of ridge area). There will be some error in these calculations due to ink spreading, which may take place in the process of making the prints.

5.1.3 Electrical Resistance

A method of measuring the area of contact from electrical resistance was developed. This was based on the method currently used in Tribology for measuring the contact area between two inanimate, electrically conductive objects loaded together (such as two steel cylinders). In this case, the resistance of the contact is inversely proportional to the number of contact junctions, therefore providing a measure of real contact area (on an asperity level) [97]. However, in the case of the finger, due to the moisture and oil on the fingers, and the low conductivity of the stratum corneum [98], the real area of contact is not measured. These factors also mean that no difference was seen in the area of contact when the finger was sliding, to when it was momentarily stationary. Therefore, sliding was not used in these tests.

This method was done initially on the stainless steel surface, used in the normal force tests ($R_a = 1.439 \mu\text{m}$). The steel was attached to the friction rig to measure the load. The current used was of the order 10^{-7}A , as is used in previous skin resistance measurements [99]. The resistor in the circuit was altered between $1 \text{ M}\Omega$ and $3 \text{ M}\Omega$; $1 \text{ M}\Omega$ was found to give an appropriate level of sensitivity. This is based upon a finger moving over a ridged surface, the circuit with a resistance of $1 \text{ M}\Omega$ was able to detect the change in area as the finger moved over the ridges, whereas the $3 \text{ M}\Omega$ resistor circuit was not. Gels are often used to improve the contact of electrodes with the skin [100], thus a pad from a TENS (transcutaneous electrical nerve stimulator) machine was used in these experiments. This is a commercially available pad for establishing good electrical contact with the skin. The pad was also chosen due to its size (dome-shaped 46 mm at each extremity of width and length). Creating a good electrical contact with the pad minimises the resistance between the circuit and skin, improving the measurement of the resistance of the finger contact. Figure 5.3 shows the circuit used for these tests: the buffer amplifier provides a low impedance output voltage to drive the NI USB DAQ.

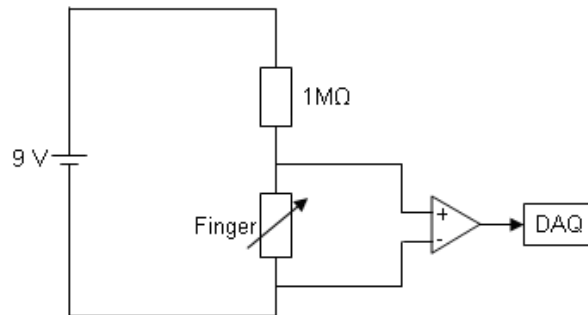


Figure 5.3 – Circuit used to measure the change in resistance of the finger contact

To improve the contact, the back of the hand and the finger tip were exfoliated before use. The TENS machine pad was connected to the circuit and then attached to the back of the hand. The test finger was pressed onto the stainless steel and the change in contact voltage and normal force were recorded. This was repeated 10 times. The positioning of the TENS pad was verified by positioning it on each finger as well as the back of the hand. The results were comparable so the back of the hand was chosen due to the increased area of contact. These tests were then repeated at Philips Applied Technologies to gain data at lower loads on brass, and three repeats were done.

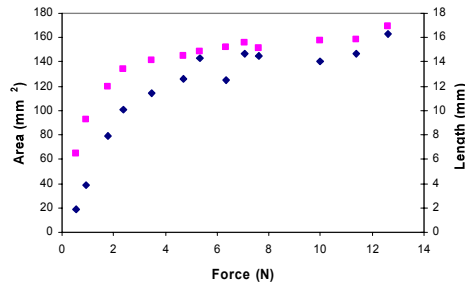
5.2 Results from Area Tests

5.2.1 High Speed Video Camera Results

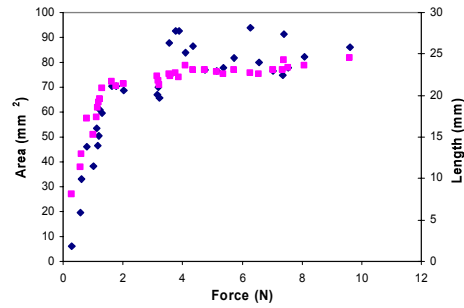
Figure 5.4 shows the results from the high speed video tests for a finger contacting glass; displaying results for each volunteer and the data from the lower camera (area) and the side camera (length). The plots show that the trend of increasing length of contact follows the same trend as the area of contact. The squared Pearson correlation coefficient (R^2) was calculated for a linear relationship between length of contact and area of contact. These values are shown in Figure 5.4. They show that in most instances there is a good correlation between the area of contact and the length of contact.

There seemed to be more error in the area calculations than the length calculations, due to an increased difficulty in selecting points of contact and no contact for the area measurements. This was due to there being no clear distinction between contact and no contact in the zoomed-in view, increasing the difficulty of pixel selection (when using the Matlab® program). This could be the cause of any discrepancies in the correlation. However, later examination found that the width and length of the contact do not increase at exactly the same rate – this will be discussed later in this chapter.

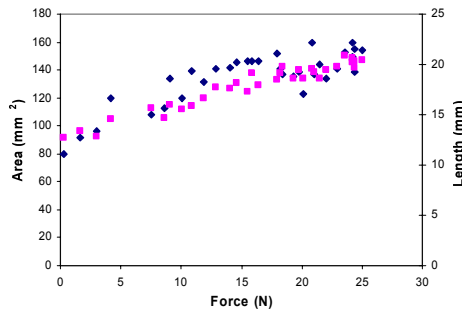
Figure 5.4 also shows that there are different trends of increasing contact with load for each volunteer. The forces at which the amount of contact plateaus are shown in Figure 5.4, highlighting the differences between people.



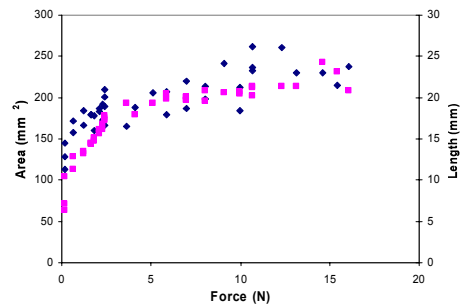
Volunteer 1, Plateau = 4.7 N
Area vs. Length (linear) $R^2 = 0.96$



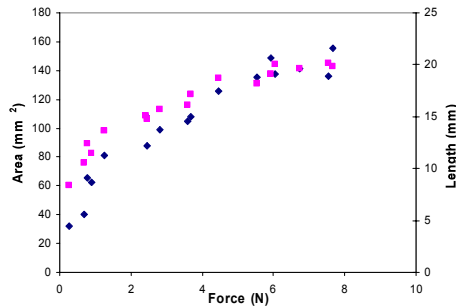
Volunteer 2, Plateau = 2.0 N
Area vs. Length (linear) $R^2 = 0.90$



Volunteer 3, Plateau = 4 – 7 N
Area vs. Length (linear) $R^2 = 0.74$



Volunteer 4, Plateau = 2.4 – 3.6 N
Area vs. Length (linear) $R^2 = 0.66$



Volunteer 5, Plateau = 5.5 N
Area vs. Length (linear) $R^2 = 0.96$

◆ Area ■ Length

Figure 5.4 – Applied load against measured area of contact and the length of contact, for the middle finger of five volunteers contacting glass

The correlation between contact area and length, in terms of trends of finger compression, indicates that for the non-transparent materials it is acceptable to use the side camera view as a measure of the amount of contact between

the finger and counter-surface. The results of the finger compression for the materials and finger used in the normal force tests (Chapter 4) are shown in Figures 5.5 to 5.8. Figures 5.5 and 5.6 show the change in the length of the contact, with normal force (as viewed from the side camera). They show that the finger reaches a maximum area of contact at approximately the same load for each material. Figures 5.7 and 5.8 show how the compression of the finger changes with load. These plots indicate that the point of maximum compression is the same as the point of maximum area of contact, as would be expected. Each figure displays the moving average data, averaged over three data points.

The final area of contact varies between the materials. Serina *et al.* [101] conducted experiments looking at the finger deformation when volunteers tapped at different frequencies; they observed that the deflection was frequency dependent. This is a different situation, however, comparing the loading rates, it follows that the materials with a larger final contact length, and deformation, were loaded more rapidly. For example, the initial loading rate for Nylon was 9.87 N s^{-1} , whereas it was only 5.98 N s^{-1} for Polypropylene; only the initial loading rates are quoted, since the loading was non-linear.

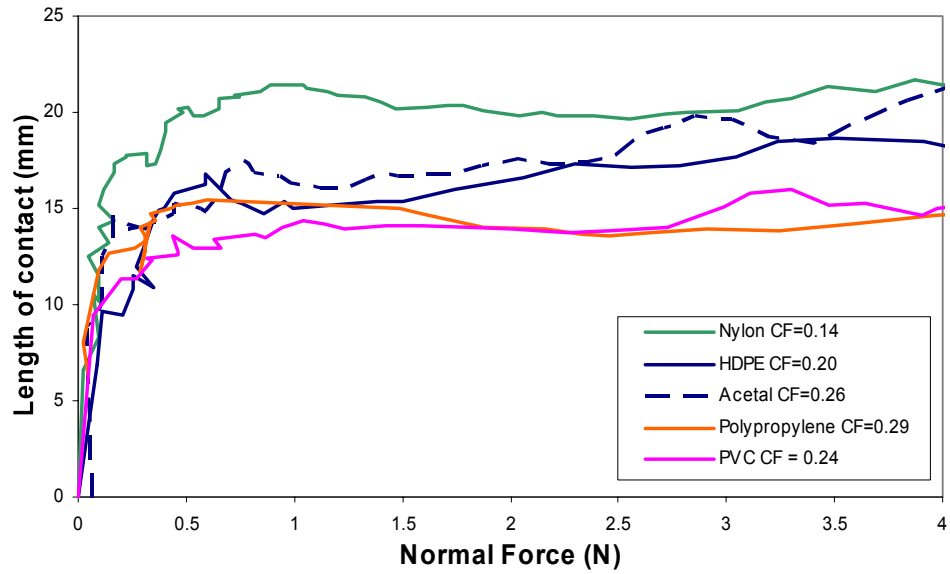


Figure 5.5 – Length of contact of the test finger and counter-surface, at varying loads, for the plastics tested

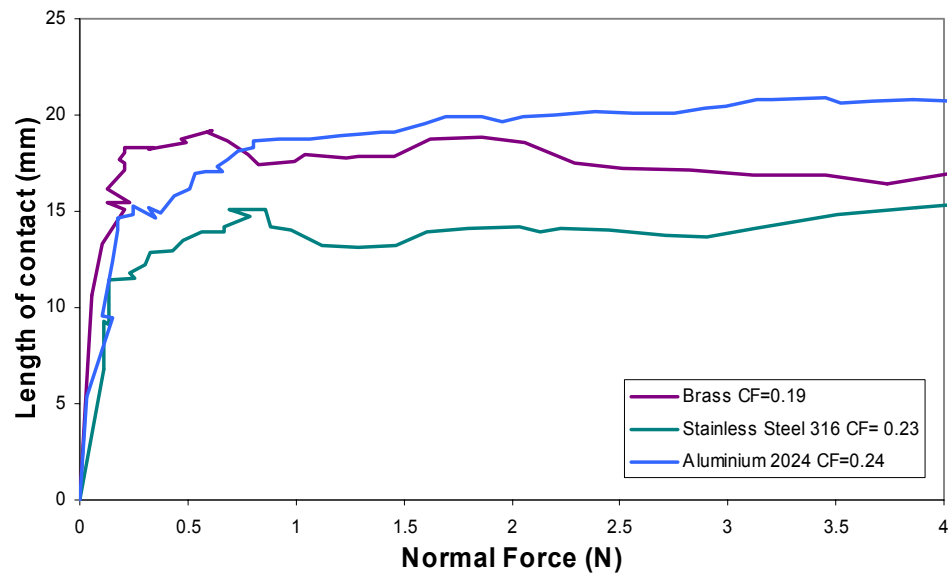


Figure 5.6 – Length of contact of the test finger and counter-surface, at varying loads, for the metals tested

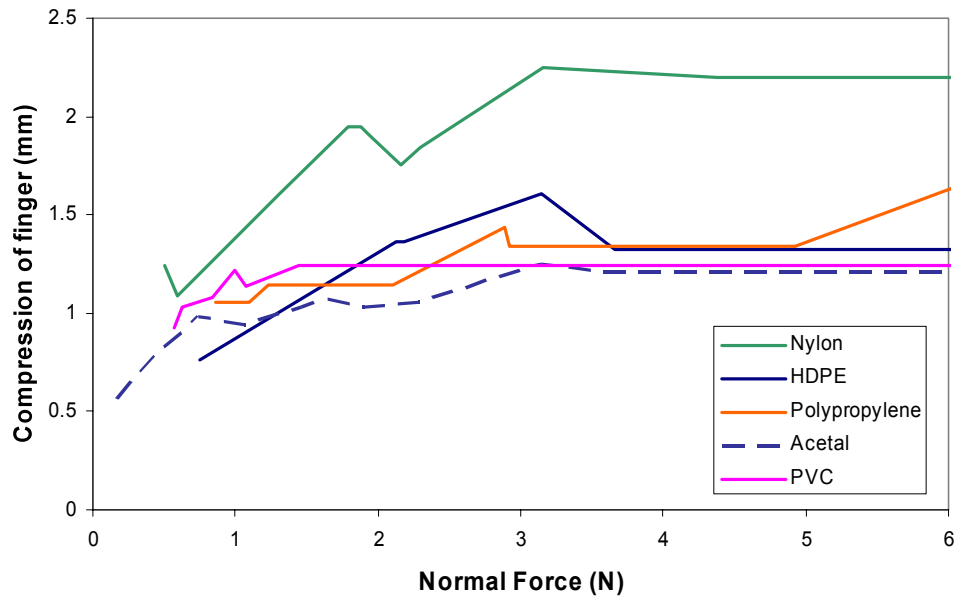


Figure 5.7 – Compression of finger, measured by tracking the vertical movement of point 3 (Figure 5.2), for the plastics tested

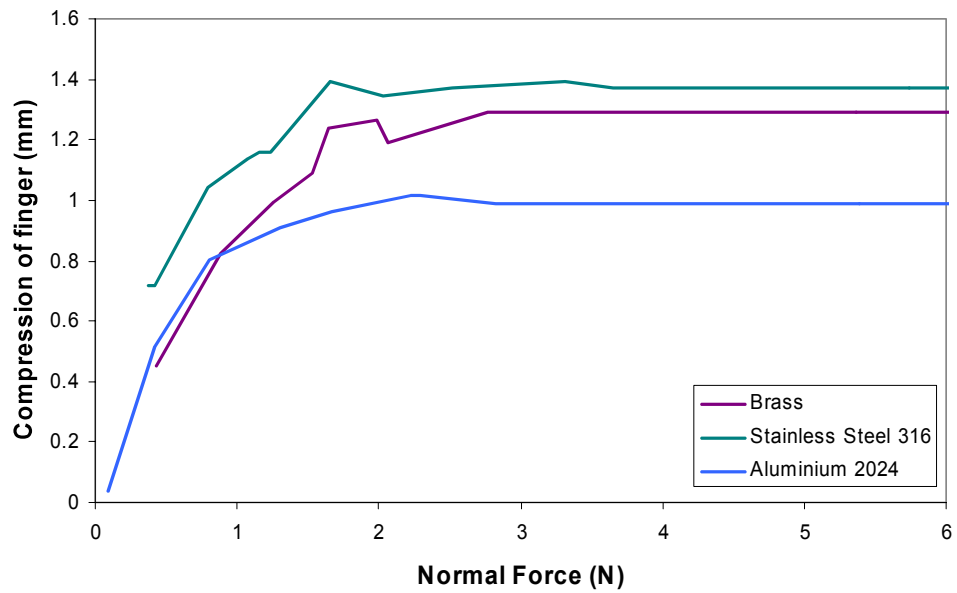


Figure 5.8 – Compression of finger, measured by tracking the vertical movement of point 3 (Figure 5.2), for the metals tested

5.2.2 *Electrical Resistance Results*

The electrical resistance experiments were carried out on both the finger friction rig, at The University of Sheffield, and the Kistler Dynamometer, at Philips Applied Technologies. Figures 5.9 and 5.10 show the results from the tests done at Philips Applied Technologies. These results are from two separate tests. The first (Figure 5.9) clearly shows that the relationship between the area of contact and the normal force, is a two part linear relationship. Figure 5.10 suggests that there may be a small area of non-linearity in the transition between the two linear regions, which is in agreement with the other contact measurements presented previously in this chapter. The transition point on Figure 5.9 and 5.10 is different, although the material and conditions were the same. However, this could be associated with matching the data from the area circuit and the dynamometer, since they used different data acquisition hardware and software. Also, similar to the high speed video tests, the loading rate of the finger will affect the area of contact. The sampling rate for both tests was the same; however, Figure 5.10 shows a larger population of data in the transition zone, suggesting a slower movement, than the case of Figure 5.9. This implies that not only does the loading rate have an effect on the final contact area, but also the area (inverse resistance in this case) vs. load profile.

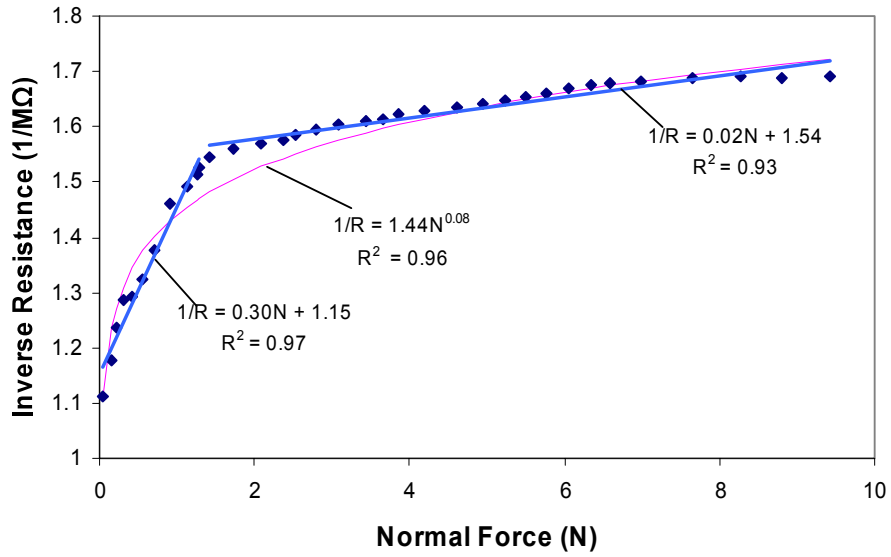


Figure 5.9 – Relationship between inverse contact resistance and normal force, for tests done on the Kistler Dynamometer, on Brass CZ 121

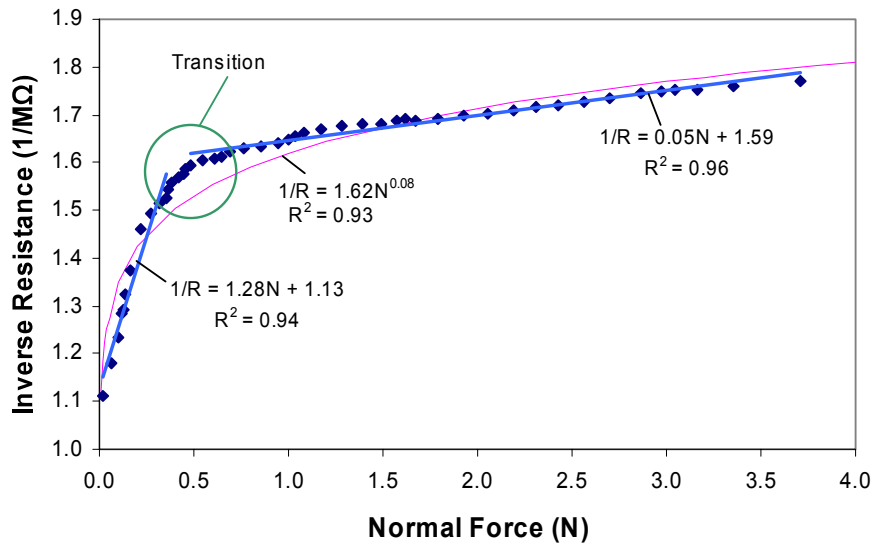


Figure 5.10 – Relationship between inverse contact resistance and normal force, for tests done on the Kistler Dynamometer, on Brass CZ 121

5.2.3 Finger Print Results

Table 5.1 shows the overall area of contact, the area percentage of ridges calculated using Matlab® and the calculated area of ridges in contact. This shows that the ridges account for approximately 50 % of the total area. Therefore, it can be assumed that the actual ridge area of contact is half that of the measured area of contact, for all contact areas measured using the high speed video. Examples of the fingerprints at three different loads are shown in Figure 5.11.

Table 5.1 – Area of contact of ridges

Length of contact (mm)	Area of contact (mm²)	Percentage of ridges (%)	Ridge area (mm²)
6	23	51	12
11	72	52	37
14	108	38	41
17	136	43	58
18	152	48	72
19	163	55	89
20	171	56	96
21	194	59	114





Area = 23 mm ² 51 % ridges	Area = 72 mm ² 52 % ridges	Area = 152 mm ² 48 % ridges	Area = 182 mm ² 53 % ridges
			

Figure 5.11 – Examples of fingerprints

5.3 Comparison of the Effectiveness of Each Method

Table 5.2 displays the advantages and disadvantages of each method of area measurement. The ink method could potentially be expanded to look at the area of contact on the surface of different materials with normal force (however, using the current ink, it could not be used on dark coloured materials). This expanded version of the method is considered in Table 5.2.

Table 5.2 – Advantages and disadvantages of each method of area measurement

Method	Advantages	Disadvantages
High-Speed Video	<ul style="list-style-type: none"> ▪ Can be used on all materials ▪ Direct length measurement, two length measurements would enable better area prediction ▪ Could be improved if the contact could be measured computationally, rather than from manual point selection 	<ul style="list-style-type: none"> ▪ In current method; large error due to human input in point selection ▪ Not a measure of total area of contact ▪ In current method; data analysis is time consuming
Electrical Resistance	<ul style="list-style-type: none"> ▪ Fast and simple method ▪ Greater accuracy ▪ Higher sampling frequency 	<ul style="list-style-type: none"> ▪ Cannot be used on insulating materials ▪ Not a direct area measurement
Ink print	<ul style="list-style-type: none"> ▪ Direct area measurement ▪ Could be used on various materials using other methods, such as finger print dusting 	<ul style="list-style-type: none"> ▪ Cannot be used on dark materials (with current ink) ▪ Errors due to ink spreading ▪ Ink is contaminating contact ▪ Cannot be used during a sliding contact

Comparison of the results from, the resistance tests and the change of the finger print width with length for the ink tests highlights a flaw in the high speed camera method, which was not initially highlighted in the glass area tests. Table 5.3 shows the ratio of width to length of the finger prints at varying areas of contact. The lengths and widths were measured using a ruler. This table highlights that the width and length of the contact do not increase at the same rate. Therefore, a single length of contact does not effectively describe the contact area, since this method assumes the minimum and maximum radii, of contact, increase at the same rate.

Table 5.3 – Finger print dimensions

Length (mm)	Width (mm)	Length/Width
6	4	1.5
7	7	1.0
8	5.5	1.5
9	5	1.8
11	7	1.6
14	7.5	1.9
15	8	1.9
17	8	2.1
18	9	2.0
19	9	2.1
20	9.5	2.1
21	10.5	2.0
22	11	2.0
23	11	2.1

Overall, it is considered that the electrical resistance method is preferable when using conducting materials. This is due to its ease of use and also the lack of human input required in the results analysis. There are, however, errors that should be considered in using this method, such as the dependence upon the amount of moisture and grease on the skin. Care should be taken to always exfoliate the skin well before tests to reduce this error, and also create a better contact.

When using an insulating material the high-speed video analysis should be used. This could be improved if it were possible to use an automated tracking system and a camera viewing the end of the finger as well as the side. The advantage of this method over the ink prints is the lack of external contamination. When using ink to measure the area of contact the ink is changing the conditions of the interface, so the results may not be fully

representative of the contact. There is also spreading associated with the ink. This method has, however, been useful to establish that the nominal area of contact measured in the high-speed video tests is approximately half of that in reality, due to the ridges on the finger.

5.4 Area of Contact

Assuming that the real area of contact is (at lower loads) a constant fraction of the nominal area, all measurements, within their capabilities, showed an initial linear increase in area with normal force. This was followed by a secondary linear relationship in the resistance measurements, and a plateau in the other tests. There could be a very small area of non-linearity in the transition between the linear zones. This is different to what would initially be expected when applying Hertz contact analysis, or JKR theory. Initial thoughts when thinking about the contact in terms of Hertzian contact, is that the area should vary with normal force by a power of approximately 0.67. JKR theory suggests that due to the surface energies of the contacting surfaces, there is an attractive force, and therefore an area of contact, even when no load is applied [79]. This would infer that at no load there should be a small area of contact. This section will discuss the results with regards to these two theories, to try to better understand the results.

5.4.1 Hertzian Contact

Hertz's theory of contact states that the radius of a circular area of contact can be described using Equation 5.1. Therefore, the area of contact varies with normal force, raised to the power of 0.67. However, this is assuming that the Young's modulus of the finger does not change during the contact, which for the finger is not true. As the finger compresses against the surface, it is becoming stiffer, i.e. the Young's modulus is increasing. The change of this can be estimated using the data from the high speed video tests and Equation 5.2. The high speed video data provides the deflection

(compression) of the finger associated with an applied normal load. Assuming a Poisson's ratio of 0.5 [40, 41], the Young's modulus can then be calculated with load, using Equation 5.2. Allowing for this change in Young's modulus shows interesting results, which are shown, in Figure 5.12, for the finger contacting Brass CZ 121. This figure shows that when allowing for the change in Young's modulus, the contact actually obeys that predicted by Hertz, in terms of behaviour, but not in terms of magnitude. The behaviour can be explained mathematically by combining Equations 5.1 and 5.2, this results in Equation 5.3. This equation shows that the area of contact is proportional to the deflection, which intuitively makes sense. Since the finger is observed to reach a maximum bulk compression, it is logical that the rate of change of area with load should also change at this point. Figure 5.12 shows the area to plateau, this is not what is observed in the resistance measurements, and is due to the calculations being based on compression. At these larger loads there is no compression recorded, however, this is more likely to be due to it being too small to be observed by the pixel size used and the naked eye. Yang and Persson [102] observed that for rough elastomers, using increased magnifications, there is a small compression with increased loads, it is assumed that this will also be the case for the finger.

$$a = \left(\frac{3 \cdot N \cdot R}{4 \cdot E^*} \right)^{\frac{1}{3}} \quad 5.1$$

where a is the radius of the contact area, N is the Normal Force, R is the estimated radius of finger, E^* is the reduced Young's modulus $= \frac{1-\nu^2}{E}$. E is the Young's modulus of finger and ν is the Poisson's ratio of skin (approximately 0.5). The reduced modulus is restricted to the properties of the skin due to it being much softer than the contacting surface.

$$N = \frac{4}{3} \cdot R^{\frac{1}{2}} \cdot E^* \cdot \delta^{\frac{3}{2}} \quad 5.2$$

$$A = \pi \cdot R^{2/3} \cdot \delta$$

5.3

where A = area of contact and δ = compression of the finger

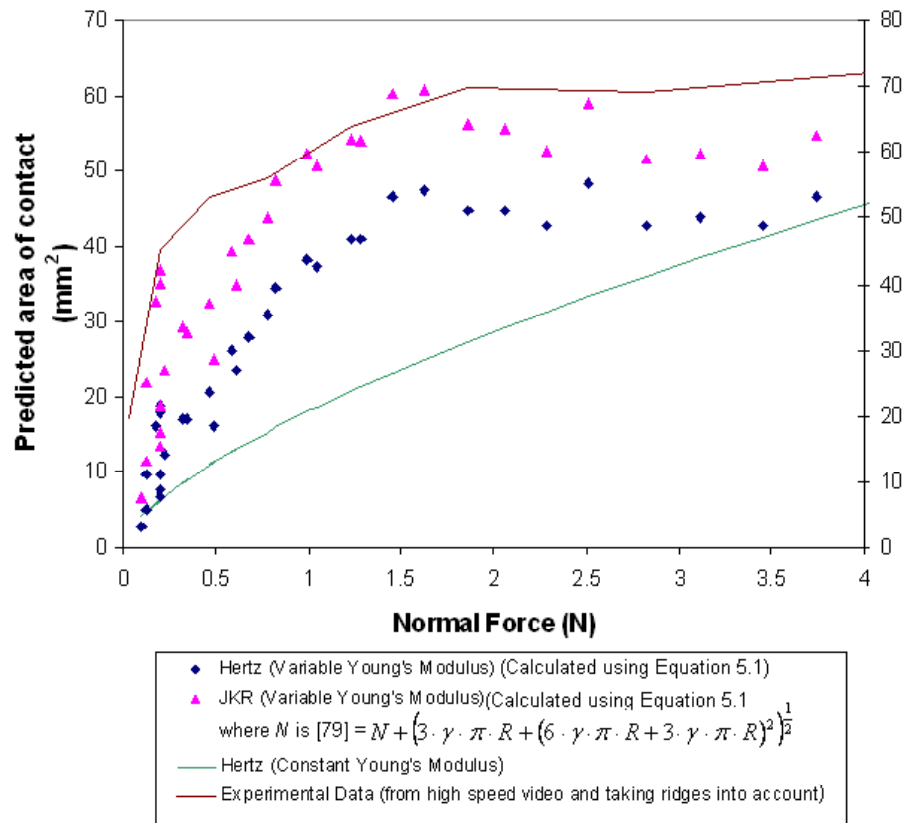


Figure 5.12 - Predicted area of contact using Hertz theory when the Young's modulus is allowed to vary and when it is kept constant ($E = 0.49$ MPa), and area of contact calculated using varying Young's Modulus and JKR theory. The experimental data, is a moving average of 50 % of the total area (to account for ridges). The Young's modulus is calculated using Equation 5.2 and deflection data from the experiment. N = normal force, γ = total surface energy and R = radius of the finger.

In many low load applications, the area of contact has been observed to be larger than predicted by Hertz contact theory. This observation resulted in Johnson *et al.* [79] investigating the contact further and forming the JKR theory of contact.

5.4.2 JKR Theory

The original tests using the high speed video camera, which analysed the contact on a number of volunteers, suggested that JKR theory could be applicable, in that the graphs suggest that the area of contact is not zero at zero load. This is more difficult to judge and see from the other graphs. Figure 5.13 shows a zoomed view at the start of the data from the resistance tests. The measurements were taken continuously and using the same equipment, so there is no issue of matching up the time (this, however, is from The University of Sheffield's Friction Rig). Figure 5.13 shows that contact is detected at point a, however, there is not a load increase until point b. This would indicate that there is an area of contact when there is no applied load, however, the discrepancy is for such a short time, it is difficult to say whether this is a physical observation or due to the sensitivity of the load cells on the friction rig.

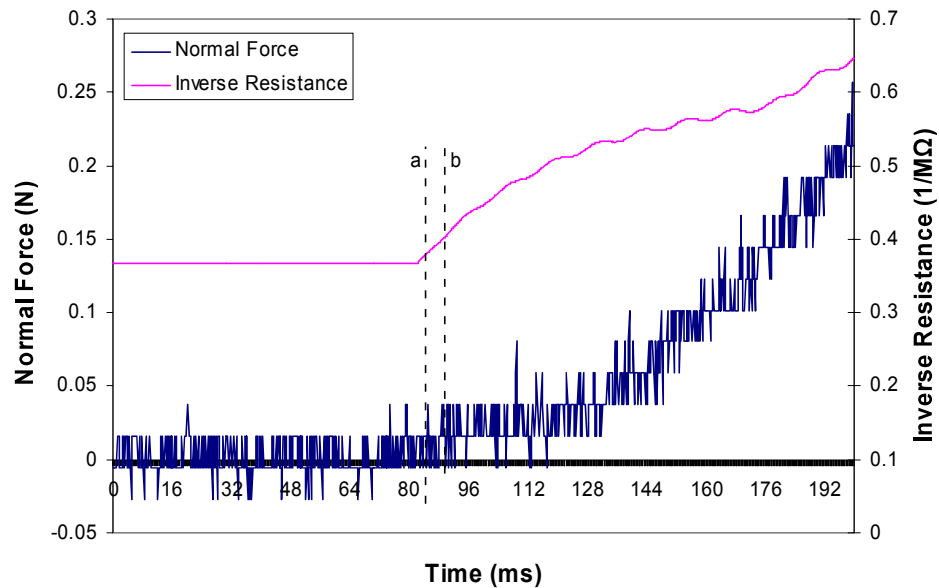


Figure 5.13 – Zoomed view of the start of an area test, using the finger friction rig at the University of Sheffield

Assuming that the Young's modulus changes with applied load, and that Equation 5.2 is applicable, the general trend, in the change of area with normal force is the same for both theories; however, JKR theory predicts a larger contact area. The total surface energy is not known, so the total surface energy was varied from 0.5 to 1.5 Jm⁻². The change did not make a large difference to the results. The results shown in Figure 5.13 are for a total surface energy of 1 Jm⁻².

5.4.3 Contact for Rough Spheres

Greenwood and Tripp [103] found that for a rough elastic sphere, the area of contact was in fact greater than that predicted for smooth spheres, at low loads. This is due to the ridges, protruding from the mean profile of the surface, contacting the counter-surface, before contact would be predicted with Hertz theory. At higher loads, approximately loads above 10 N, for the sphere modelled (radius = 10 mm, asperity density = 500 mm⁻², asperity radius = 0.2 mm, standard deviation of asperity height = 5 x 10⁻⁴ mm, and elastic constant = 10⁴ kgmm⁻²), the effect of roughness was less apparent and the contact tended towards that predicted using Hertz theory. This is not expected for the finger, since the ink tests show that the area of contact is still 50 % of the total area, even at large loads. This difference is due to the material of the ridges being different to the bulk material (the subcutaneous tissue is responsible for the bulk deformation, whereas the ridges are part of the stratum corneum layer). Greenwood and Tripp's work resulted in Equation 5.1, being modified to take the effect of roughness into account, such that the radius of curvature was raised to the power of 0.37 as opposed to 0.3. The problem of modelling roughness on a sphere is complex, the solution produced by Greenwood and Tripp [103] was only a crude approximation. This has since been improved upon; Bhushan [104] reviews many of these methods and Polonsky and Keer [105] also suggested a new computational method which reduces the computer processing time. However, none of these solutions are trivial and require expert mathematical and computer programming knowledge to perform accurately and well. This

is an area where this work could be expanded by someone with the appropriate knowledge, skills base and computing power.

The analysis in this chapter did not allow the measurement of the real area of contact. The nominal area of contact reaches a maximum of approximately 86 mm², from the high speed video tests, and accounting for ridges. The JKR theory calculations predict a maximum area of approximately 60 mm². There are several factors that would suggest the real area of contact should be greater than this, including roughness (as discussed), the shape of the contact and also creep of the finger (if it is held there for any length of time). With initial contact, the area is circular, but with increasing load, it progresses to an oval shape; Hertz and JKR theory both assume a circular contact. To account for this, the larger radius of the finger was also used in calculations; this served to bring the Hertz results more or less in line with the JKR results. Figure 5.12 shows that JKR or Hertz Theory (using the maximum radius of contact) predicts the limiting area of friction fairly well. The model mainly fails at larger loads, when the compression is not visibly changing, but the area is increasing (relating to experimental limitations). The area of contact increases more rapidly at lower loads, than at larger loads.

The finger is a layered structure, consisting of the stratum corneum, epidermis, dermis, subcutaneous tissue and bone. Each of these layers has their own individual properties, such as Young's modulus. In treating the finger as a single material the influence of these layers, probably in particular the stiff bone, are being neglected. Both of these contact theories were developed for a homogeneous material, which the finger is not, so could result in the different behaviour seen. The development of this model is an area for further work. This could include some modification of the JKR theory, similar to that done for elliptical contacts [106] (for the case of two cylinders presented at angles to each other). In future calculations, in this thesis, the area of contact will be approximated using Hertz theory, but using the maximum radius of the finger (16 mm).

5.5 Relationship Between Friction Force and Normal Force

As discussed previously in Chapter 4, the total friction can be described by Equation 5.4. Chapter 4 introduced how these friction contributions can be analysed, but numerical analysis required the results from the area study. This section will discuss the contributions of each mechanism, excluding that due to moisture/grease that will be assessed in more depth in Chapter 6.

$$F_T = F_a + F_d + F_v + F_r \quad 5.4$$

where F_T is the total friction, F_a is the adhesive friction, F_d is the deformation friction, F_v is the friction due to capillary adhesion or viscous shearing, F_r is the friction due to deformation of finger ridges

5.5.1 Friction due to Bulk Deformation of the Finger

Chapter 4 discussed how the calculations used for other areas of the skin are not applicable for the fingers. It also discussed how the contribution of friction due to deformation (F_d) is from the force required to keep the finger in its deformed state. This force cannot be directly measured, due to the sensitivity of the equipment, but the energy required for the initial deformation can be approximated, using Hooke's Law. The results in this chapter provide information about the deflection of the finger with load; the initial linear part of loading is shown in Figure 5.14, after this the deformation plateaus with force. The energy required to deform the finger, according to Hooke's law is described by Equation 5.5.

$$U = \frac{1}{2} \cdot k \cdot \delta^2 \quad 5.5$$

where U = strain energy, k = spring constant and δ = deflection of finger

At the maximum deflection, $\delta = 1.23$ mm. The gradient of the graph shown in Figure 5.14 is equal to $1/k$, therefore $k = 1.03$ kNm⁻¹. Substituting these

values into Equation 5.5, shows that the energy required to deform the finger is 77.8 mNm. This is of course an approximation, as it describes the vertical deformation. However, there is only a very small amount of deformation in the lateral direction, so this is taken as a good first approximation.

The work done to slide the finger along the surface is the multiple of the friction force and distance travelled. Equating this value to the energy required to deform the finger, it can be shown that the same amount of energy to deform the finger, would slide the finger 2 mm. As a percentage over a 5 cm slide, the deformation only accounts for 3.9 % of the total required energy.

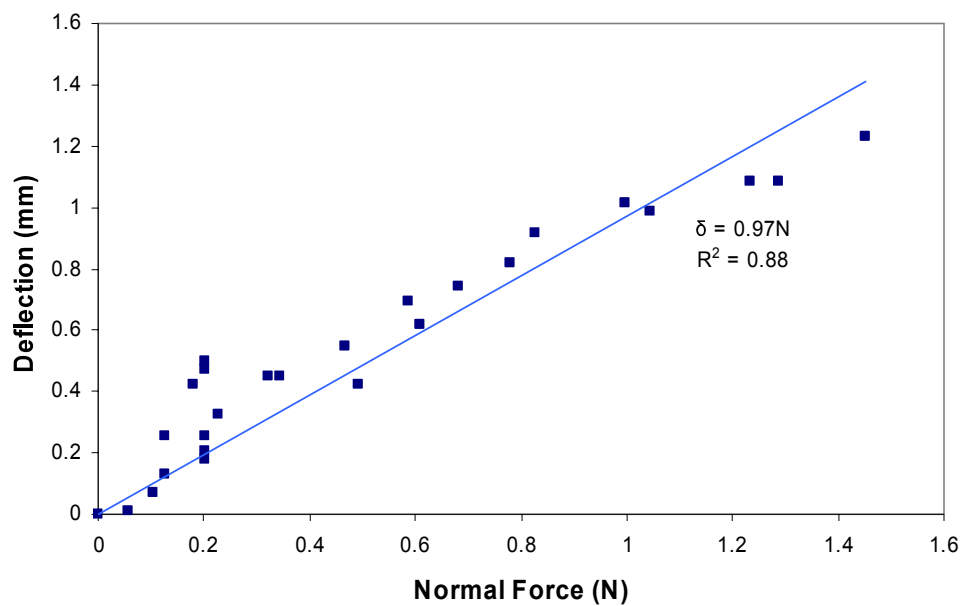


Figure 5.14 – Initial (linear) part of the deflection (δ) vs. normal force (N) curve, for a finger contacting brass

5.5.2 Friction due to Deformation of the Ridges

Chapter 4 discussed how it is possible to over estimate the contribution of the ridge deformation to the total friction, by calculating the deformation of the ridges. The data from these tests can be used to numerically calculate this overestimated contribution. The ridge of the finger is considered to be a cylinder, therefore the work done, to compress it, is described using Equation 5.6 [107].

$$Workdone = \frac{2}{3} \cdot \frac{N \cdot b}{R_r} \quad 5.6$$

where b is the width of the contact (of length L), and described by Equation 5.7, and R_r is the radius of the ridge, estimated from the roughness profile to be 0.29 mm.

$$b = \left(\frac{4 \cdot \left(\frac{N}{L} \right) \cdot R_r}{\pi \cdot E^*} \right)^{\frac{1}{2}} \quad 5.7$$

The length (L) of the cylinder (ridge) is not known, so it is estimated. Assuming that the ridges occupy half the area (as seen in the fingerprint tests), the length can be described using Equation 5.8.

$$L = \frac{A}{2 \cdot R_r} \quad 5.8$$

A = Area of contact and is calculated using Hertz Theory (with the maximum radius of the finger (16 mm))

Calculations for the finger contacting brass showed the percentage contribution of the ridge deformation to the friction (using this over estimate) is related to the normal force by Equation 5.9. This means that at 18 N, only

0.15 % of the friction is due to the deformation of ridges. It also needs to be remembered that this calculation is a large over estimation of the actual friction force, so the actual contribution is thought to be much less than this. This is for a flat surface, if there is texture on the surface, the ridges on the finger may start to interlock with the surface asperities/texture, which will increase this contribution to friction.

$$\%e \text{ of total friction due to ridge deformation} = 0.0076.N + 0.0198 \quad 5.9$$

5.5.3 Friction due to Adhesion

All methods of measuring the area presented, in this chapter, determined the nominal area of contact, rather than the real area of contact (on an asperity level). The real area of contact is of interest when considering adhesion friction. The assumption in the following discussion of friction is that the real area of contact varies in proportion to the measured area of contact.

Since the other mechanisms of friction have been shown to be negligible for the finger sliding on a nominally flat surface, the main mechanism of friction, in this case, is adhesion. The viscous forces have not been accounted for here, but since the hands were cleaned and dried before the tests, and also, in actual fact, the thin layer of grease on the skin will be accounted for in the following adhesion calculation. The results from both the area of contact tests and the normal force tests, suggest that the friction (adhesion) varies with normal force according to Equation 5.10.

$$F_a = \begin{cases} \mu_1 \cdot N & N < N_L \\ \mu_2 \cdot N & N > N_L \end{cases} \quad 5.10$$

where μ_1 and μ_2 are the coefficients of friction in the respective zones.

The Young's modulus of the finger, up to a load of 14 N, varies in 2 linear parts. The initial part (below 1.6 N) has a lower Young's modulus than the second part (above 1.6 N). The two equations relating load and Young's modulus can be seen in Equation 5.11.

$$E = \begin{cases} 16893 \cdot N + 130663 & N < N_L \\ 102496 \cdot N - 22736 & N > N_L \end{cases} \quad 5.11$$

where E is the Young's modulus of the finger tested

The adhesive friction for a surface covered with an organic layer has previously been described using Equation 5.12 [74, 108]. This was applied to the data (See Appendix 7), and is shown in Figure 5.15. When the data was considered as a whole, the theory predicted the behaviour, but with a degree of error. However, if the data were split and considered in two parts, the predictions fit the measured values exactly. That is, there is a two part linear relationship between the interfacial shear stress and the contact pressure, used to derive equations 5.12 and 5.13 (See appendix 7). This further provides evidence for a two part linear relationship, rather than a single power relationship. In fitting two individual lines, Equation 5.12 is modified to obtain Equation 5.13. The term τ_0 in the equation refers to the intrinsic material shear strength, and the term αN refers to the pressure dependence of shear stress, this has been described as the energy required to plastically deform the asperities. Applying these definitions to the model of friction obtained for the finger, they would imply that at low loads, the intrinsic shear strength has very little effect on the friction, due to the large amount of bulk deformation. The energy required for the compression of the bulk of the finger, is the factor dominating the friction. However, once the transition load (N_T) is met (1.6 N for the finger tested), the intrinsic material shear stress is more important to characterising the overall friction. The deformation aspect is then dependent upon the deformation of ridges and asperities. Future work could be done to confirm this theory, if it were possible in some way to separate the mechanisms and investigate them separately.

$$F_a = \tau_0 \cdot A + \alpha \cdot N \quad 5.12$$

$$F_a = \begin{cases} \alpha_1 \cdot N & N < N_T \\ \tau_0 \cdot A + \alpha_2 \cdot N & N \geq N_T \end{cases} \quad 5.13$$

where τ_0 , α , α_1 and α_2 = constants specific to the contact system

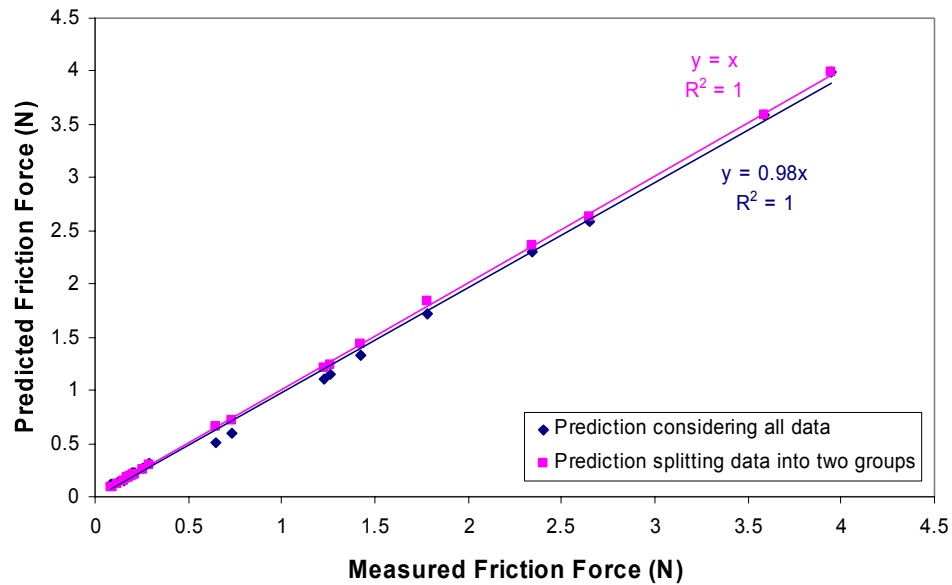


Figure 5.15 – Comparison of the predicted and measured adhesive friction measurements

5.6 Conclusions

The area of contact is a two part linear relationship. The initial linear part is determined by the bulk properties of the finger and the secondary part is determined by the deformation of the finger ridges and asperities. The main mechanism of friction for a finger sliding on a flat surface is adhesion. Since, the friction due to the deformation of the finger (F_d) and the ridge deformation (F_r) has been shown to be negligible; it will be discounted in future discussions of mechanisms (within this thesis).

6 Effect of Moisture on the Measured Friction

Finger friction has been found to increase when a certain level of moisture is added to the contact [57]. There have been several explanations for the increase, these are that: the finger absorbs the water and becomes more supple, which increases the contact area and therefore increases the coefficient of friction [74]; liquid bridges form between the ridges on the finger and the increase in friction is due to viscous shearing [57]; and that capillary adhesion increases the friction [72, 109]. Increasing moisture above a certain level causes the friction to decrease. The dependence of the magnitude of friction, upon the amount of moisture in the finger contact, means it is an important factor, when considering the grip of objects. In fact, even more so, since Mackenzie and Iberall [69] have shown that gripping an object causes the hands to sweat. In this chapter, the initial section shows some work looking at the variation in moisture between people and during various activities. Further sections examine friction tests, done to assess the effect of adding moisture to the finger.

6.1 Survey of Moisture Variation Between People and During Different Activities

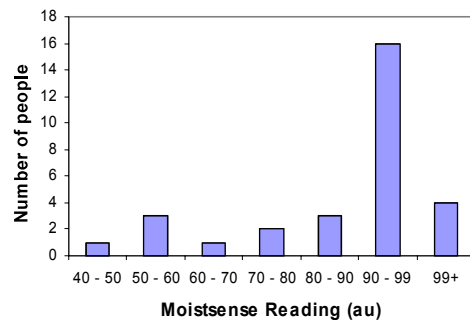
Some of the surveys of moisture levels were done by a summer placement student (Caroline Texier), under my supervision, I then analysed all the results. The initial surveys of moisture looked at variation from person to person. These were done by taking measurements of a group of people participating in the same activity. These activities included using a computer (30 people), sitting in a lecture theatre (15 people) and also before and then after an aerobics class (9 people). The readings were taken from the middle finger of the writing hand (same as used for friction tests) and all tests were done three times before an average was taken. The Moistsense was used as a measure of skin hydration (this device is explained in Chapter 3).

The second series of tests looked at the variation for a single person. Studies of how people's moisture changed during the day were done using individual surveys (5 people (3 male, aged 24 – 36, and 2 female, aged 25 - 27). There were also more focussed studies done on one person's finger, to examine in more detail how the moisture on the finger changes when gripping an object. These tests consisted of a comparison between the left and right hand to confirm the moisture readings were similar. Following this, tests were done where one hand was used to write with a plastic biro and the other was at rest. The change in moisture was monitored every minute.

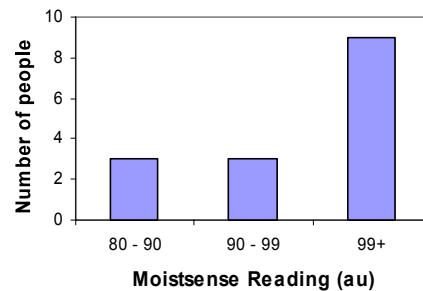
The results from these tests are shown in Figures 6.1 to 6.4. The moisture is shown to vary from person to person, whilst in the same environment or doing the same activity. Figure 6.1a shows that there is variation from 40 to 99 + au, for people in the same computer room. The maximum reading of the Moistsense is 99 au, after which it gives an error reading, so the distribution of moisture levels above this cannot be quantified. The activity people were doing, in the computer room, will have varied slightly; some people doing more typing, others using the mouse more and others doing more written work. There was a variation in hydration levels seen in the Lecture Theatre, Figure 6.1b), however, this was not as great as that seen in the computer room. This is thought to be because the participants were mainly at rest. The values are very high, but the room was very hot, however the temperature and humidity were not recorded to quantify this. Figure 6.2 groups all the data of the individual surveys together, but when analysed in more detail, they show a large variation between people doing nominally the same activity, but also for a single person. For one person's survey (male aged 36) he recorded 65 au for typing at one point in the day, and then 93 au for typing later on in the day. Again, Figure 6.3 (the results from the aerobics class survey) shows a range of readings from 64 to 95 au.

The hydration of the fingers varies depending on a given activity. In the survey of people in the computer room (Figure 6.1a) it was found that the majority of people had a high hydration level, since they were all operating a computer or writing. Also, Figure 6.2, the survey of hydration throughout the day, shows that there is a significant increase in the Moistsense reading from at rest to when the person is taking part in an activity. Figure 6.4 examines this in more depth looking at how the moisture on the finger increases when gripping a pen. This shows that the longer length of time the pen is used for, the greater the level of finger hydration.

The results from the aerobics class, Figure 6.3, were not as expected, in that, in a lot of the cases the moisture level was lower after the class than before. However, the first reading was taken as people entered the class, so may have been running or rushing to get to the class. The second reading was taken when they were leaving, so after they had cooled down (during the class) and then perhaps had a chat to their friends before leaving.



a) Moistsense readings from the Computer Room



b) Moistsense readings from the Lecture Theatre

Figure 6.1 – Results from survey of people in the computer room and lecture theatre

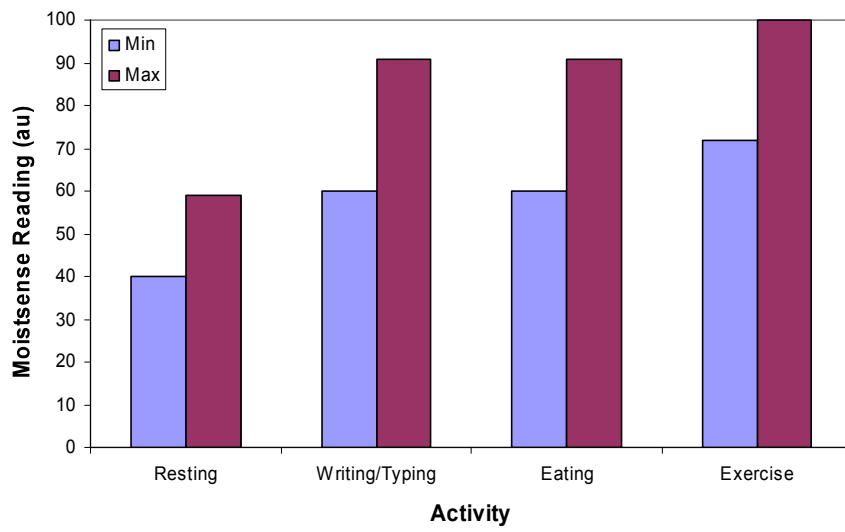


Figure 6.2 – Variation of moisture throughout the course of a day. Error readings (because of too much moisture) are displayed on this graph as 100 au.

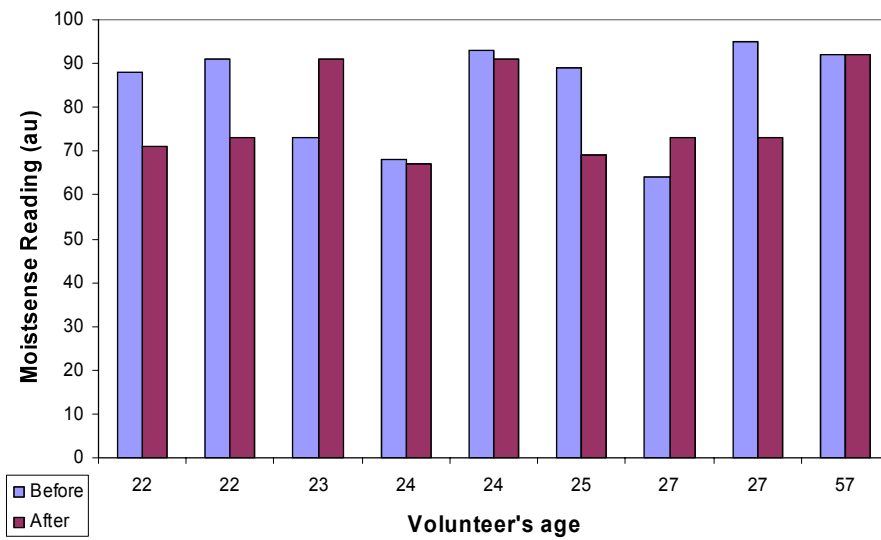


Figure 6.3 – Variation of moisture before and after an aerobics class

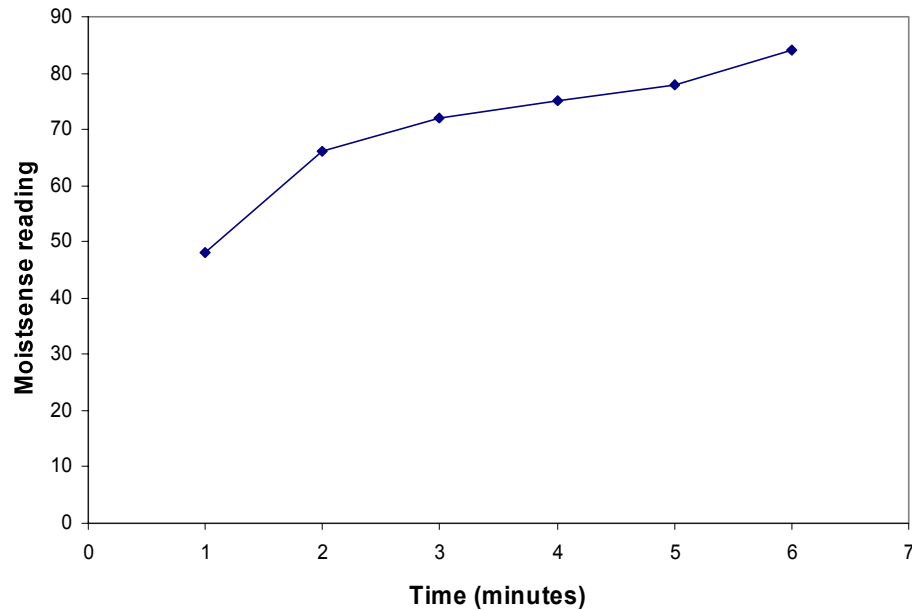


Figure 6.4 – Change in skin hydration, with time, whilst writing

6.2 Friction Tests at Varying Levels of Finger Moisture

The general procedure, for the friction tests, followed that described in Chapter 3. The hydration/moisture on the skin was measured using the Moistsense. Although the Moistsense is designed to measure the moisture in the stratum corneum, its mechanism of measuring a change in capacitance is such that it will also measure the amount of surface water, up to a limiting level. Initially tests were done on; Acetal ($R_a = 0.171 \mu\text{m}$), Polypropylene ($R_a = 0.221 \mu\text{m}$), HDPE ($R_a = 0.307 \mu\text{m}$), PVC ($R_a = 0.201 \mu\text{m}$), Steel ($R_a = 0.25 \mu\text{m}$), Aluminium ($R_a = 0.465 \mu\text{m}$) and Brass ($R_a = 1.71 \mu\text{m}$). These tests were done by a summer placement student (Caroline Texier), under my supervision, and then the results analysed by me. The water was applied using a combination of drying and wetting the finger with paper towels and a water spray. The normal force was not controlled to a sufficient level in these tests. The range of loads applied can be seen in Table 6.1 and at times the load was not at a high enough level. This is a level above approximately 1.6 N, for the finger tested in Chapter 4, which is the point at which there is a transition from one linear relationship to another.

The Moistsense reading was taken from the same finger as the friction test. The Moistsense is a contact measurement device, so it could be removing some of the moisture during the measurement.

The tests were repeated (by me) on PVC, with increased control of the variables. The normal load applied was 11.7 ± 1.8 N. The time between water application and test was also recorded and was 12 ± 3 s. This was kept as short as possible to try and avoid too much absorption of water into the stratum corneum or evaporation. Following a test run the finger was dried and rested until the Moistsense reading of both the middle and the ring finger returned to 40 ± 2 au, this was the Moistsense reading recorded when the finger was in its 'dry' state. These tests were done at a temperature of 19.8 °C and relative humidity of 45 %. Over several readings, the largest variation in moisture between the ring finger and middle finger was 2 au (see Chapter 3 for unit description). Since the action of taking a Moistsense reading from the finger, can alter the level of water on the finger, the ring finger and middle finger were both wet in the same way at the same time. The Moistsense reading was then taken from the ring finger, and the friction test was done on the middle finger. Water was applied to the finger using a wet paper towel and a dry paper towel, the methods of application and corresponding Moistsense readings are shown in Table 6.2. There are a varying number of readings for each method, since some methods were more consistent than others, so required less repeats.

Table 6.1 – Force range applied across all tests on each material

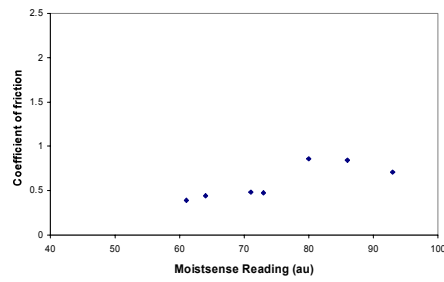
Material	Normal Force Range (N)
PVC	10.9 – 17
Polypropylene	0.86 – 3.2
Nylon	0.3 – 6.4
HDPE	7.3 – 20
Acetal	20.4 - 25.3
Brass	0.21 – 1.29
Aluminium 2024	1.68 – 4.15
Stainless Steel 316	1.26 – 3.68

Table 6.2 – Method of water application and corresponding Moistsense reading

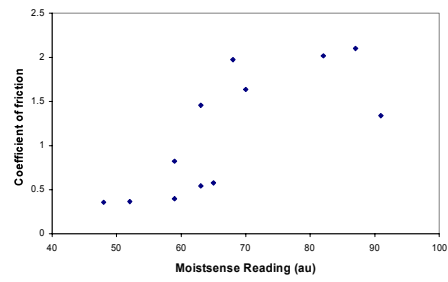
Water Application Method	Moistsense Reading (au)
Dry	41/40
3 sprays of water on paper towel, dab finger in wet patch, then one dab on dry towel	50/52
1 spray of water on paper towel, wait 5 s and then dab finger in wet patch	58/63/65
3 sprays of water on paper towel, wait 5 s and then dab finger	75/85
Fully wet paper towel and finger dabbed for 3 s	95/95/95

6.2.1 Results from Friction Tests

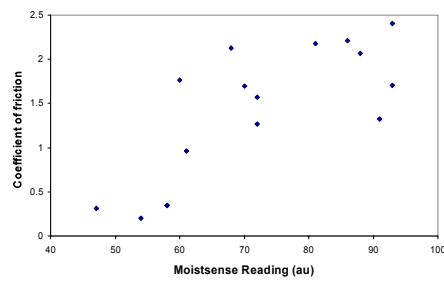
Figure 6.5 shows that the friction is increasing with a small amount of moisture, and then a subsequent decrease in the measured friction is seen at a certain level of water. The peak in friction is similar for most materials; the friction peaks at a Moistsense reading of approximately 70 – 83 for polypropylene, HDPE, acetal, brass, stainless steel 316; and it is between approximately 80 – 88 for PVC, nylon and aluminium 2024.



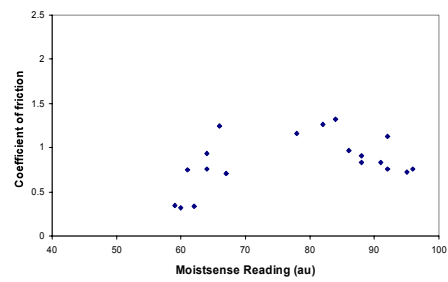
a) Acetal



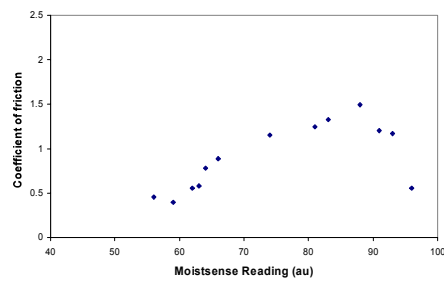
b) Polypropylene



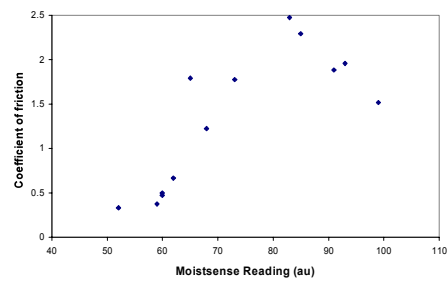
c) Nylon



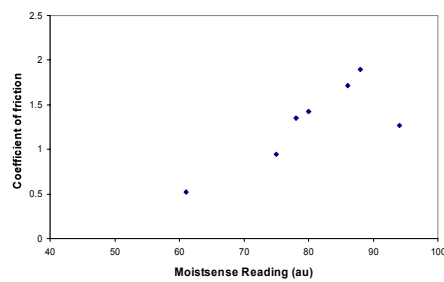
d) HDPE



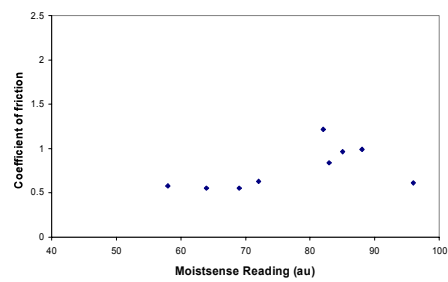
e) PVC



f) Brass



g) Aluminium



h) Steel

Figure 6.5 – Variation of coefficient of friction with moisture for all materials initially tested

The results from the second set of friction tests done on PVC are shown in Figure 6.6. The general trend of friction follows that of the previous PVC tests, with the maxima being located at the same Moistsense reading. The measured coefficient of friction is different to the previous tests due to a different person's fingers being used in these tests. The increase in friction force is equivalent to an increase of 10 N, due to moisture addition alone, for a nominal force of 11.7 N.

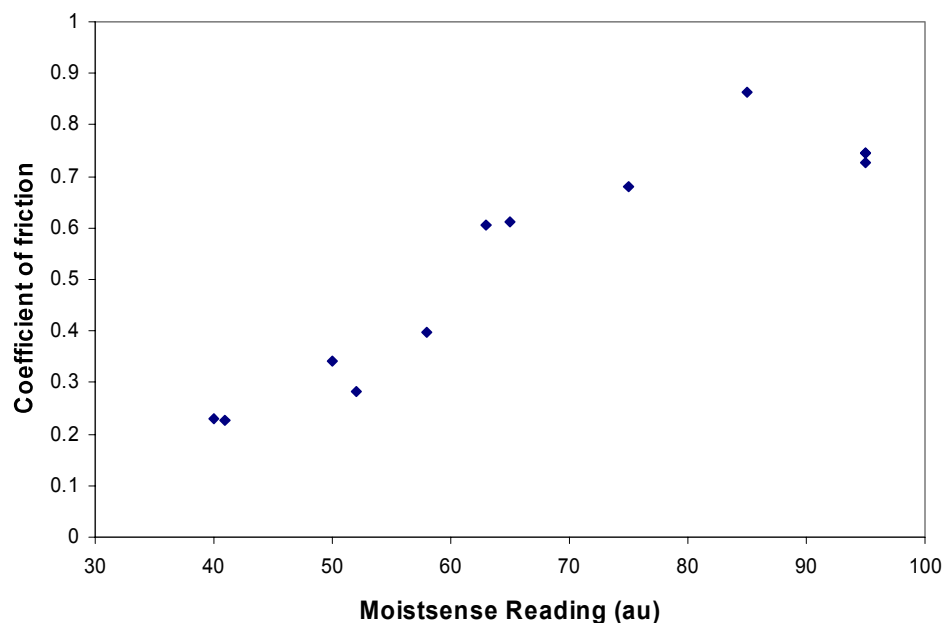


Figure 6.6 – Change in coefficient of friction with added water, for a finger-PVC contact

6.3 Discussion of Moisture Test Results

All the friction tests showed an increase in friction with a small amount of water addition. This discussion will concentrate mostly on the results in Figure 6.6, where the normal force was controlled, however the other results will be considered, since the increase in friction is not the same for all the surfaces. The results will be discussed in terms of the proposed

mechanisms causing the friction increase; water absorption, viscous shearing and capillary adhesion.

6.3.1 Absorption of Moisture Causing a Change in the Young's Modulus of the Skin

Adams *et al.* [74], examined the friction of a hemi-spherical glass probe contacting the forearm. They found that when water is added to the forearm, the skin swells to the extent that the surface can be considered as smooth. The Young's modulus also reduces with water addition, even before the 'smooth' state is reached. The finger, however, is different to the forearm, in that it has ridges on the surface. These ridges do not fully deform in contact [67], so it cannot be assumed that water addition will have the same effect on the finger as on the forearm. In one of the experiments by Adams *et al.* [74] the skin was left for 30 minutes after water application, to allow it to absorb into the skin. However, in another of their tests water was added to the forearm during the friction test. The results from this test suggest that it takes very little time for the skin to absorb moisture; they noted a triple increase in the friction coefficient only three seconds after application, and a constant 'wet' state friction was reached after three minutes. This indicates that although, in this current study, water was applied and then the friction test was done (with no dwell time), there could still be some water absorption.

To try and test the theory of whether moisture was absorbed in such a short time, an approximation of the Young's modulus was made using Hertz's Theory. This is a crude method, since there are assumptions made in Hertz Theory, which are not applicable to skin contact (as discussed in Chapter 2), and this theory does not account for the presence of ridges. A 10 mm diameter steel ball bearing was placed on to the fingertip under various loads (0.66 N, 1.16 N, 1.64 N, 2.14 N and 2.67 N). The positioning of the finger was regulated, using a finger guide and an end plate. The middle finger and ring finger were wetted to the appropriate amount, and the moisture reading

was then taken from the ring finger, simultaneously as the middle finger of the writing hand was placed on the test rig, the load applied and a photo taken. Calibration of the pixel length, allowed the compression of the finger to be measured from the photo. The test was then repeated at either a different load or moisture level. A photograph of the set-up is shown in Figure 6.7.

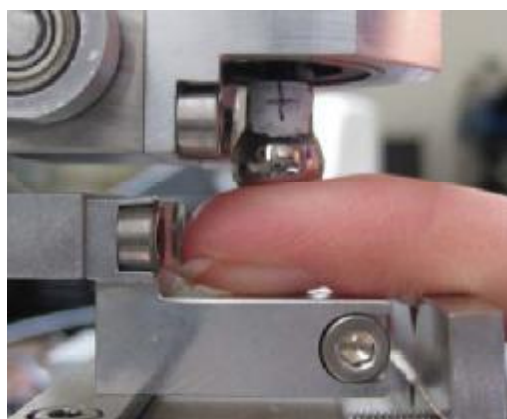


Figure 6.7 – Rig for loading the finger with a ball bearing, and then measuring the compression

The change in Young's modulus, resulting from the softening of the stratum corneum, could then be estimated using Equation 6.1 [74]. These calculated values of Young's modulus, were plotted against the Moistsense readings, as shown in Figure 6.8. This shows that there was a decrease in the Young's modulus from 30 au to 50 au. However, at a moisture level above 50 au there is no obvious change in the Young's modulus. These results show that there is a definite change in the Young's modulus from the dry to the wet state; however, it cannot quantify the change between different Moistsense readings, in the wet state. This is because there will only be a small change in the Young's modulus, since the majority of the deformation is in the subcutaneous layer, which does not absorb water. The test may not be sensitive enough to detect such small changes due to its reliance on pixel size and human point selection. Also, there are errors due to the use of

Hertz's contact theory. In this test, it took approximately 30 minutes for the finger to return to its original moisture state after tests of a Moistsense reading greater than 70 au (this was also true for the friction tests), thus further implying that there is definitely some absorption of water into the stratum corneum when water is added to the finger. Therefore concluding, that there is some contribution to the overall friction due to water absorption in the stratum corneum, but this cannot be quantified from these tests alone.

$$E = \frac{3}{4} \cdot N \cdot R^{-\frac{1}{2}} \cdot \delta^{-\frac{3}{2}} \cdot (1 - \nu^2) \quad 6.1$$

where N is normal force, R is the radius of the finger (maximum radius used (16 mm)), δ is the compression deflection of the finger, and ν is the Poisson's ratio of skin (0.5 [39]).

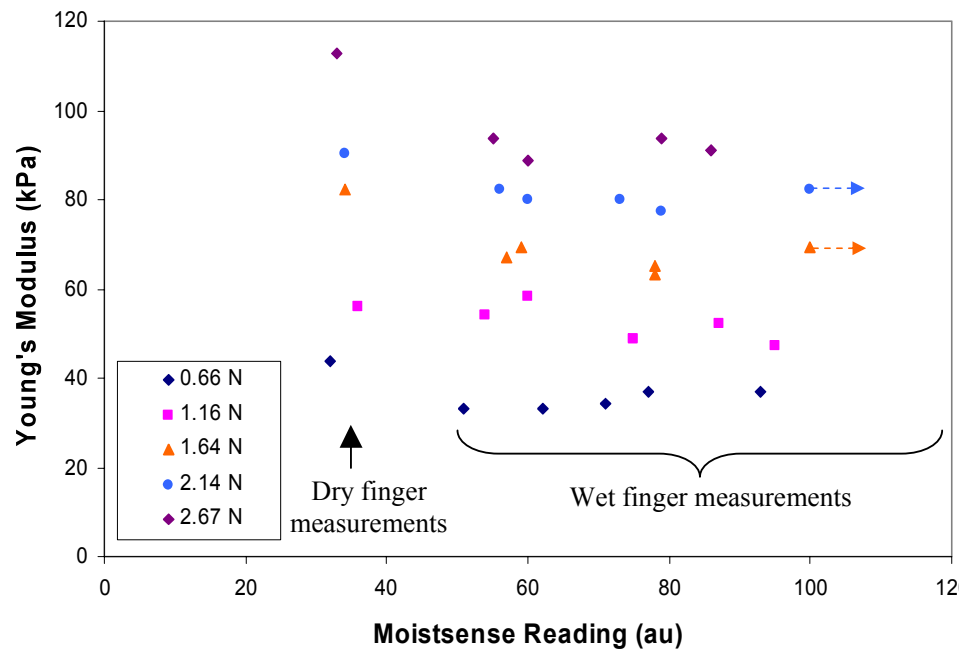


Figure 6.8 – Graph of estimated Young's Modulus of the finger, calculated using compression by a steel ball bearing, for different Moistsense readings (levels of hydration)

6.3.2 Viscous shear in liquid bridges

Dinç *et al.* [57] suggested that friction increases in the presence of moisture due to liquid bridges forming on the ridges of the fingers and asperities. Viscous shear forces owing to the formation of these bridges then increase the friction force. They did not, however, prove this and only stated this as a possible theory.

There have been several studies examining the lubrication of a steel ball sliding and rolling on a soft elastomer surface [110-112], however, while in some cases the Young's modulus of the elastomer is comparable to the skin of the finger, in many cases the diameter of the ball is too small. If it is assumed that the finger can be modelled as an elastomer sphere, the reverse of these test conditions is established, and since the area of contact is similar, the area dependent friction properties are comparable. Adams *et al.* [74] addressed the problem for the forearm skin using a 16 mm diameter glass probe, at a load of 0.2 N; this is the smallest diameter of the finger (measured in Chapter 4, for the finger used in tests), but the load is too low. A current literature search did not find a Stribeck curve applicable to the finger. However, these studies indicate that when considering the lubrication of the finger, there are three regimes of lubrication; boundary lubrication, mixed regime lubrication and isoviscous elastohydrodynamic lubrication (IEHL). IEHL is applicable to both 'hard' and 'soft' contact surfaces where there is significant elastic deformation, but this does not increase the lubricant viscosity [110]. In this case due to the low Young's modulus of the finger, the finger deforms substantially (elastohydrodynamic), but the viscosity of the water in the contact is not affected by the applied load (isoviscous). The coefficient of friction due to IEHL (μ_{IEHL}) alone can be calculated using Equation 6.2 [74].

$$\mu_{IEHL} = 1.51 \cdot (\eta \cdot u)^{0.36} \cdot R^{-0.134} \cdot E^{-0.247} \cdot N^{-0.113} \quad 6.2$$

R is the radius of the finger, E is the Young's modulus of the finger (an average value of 0.49 MPa was used) (Poisson's ratio is assumed to be 0.49 in formulation of Equation 6.2), N is the normal load, η is the dynamic viscosity and u is the sliding velocity.

Using this calculation the friction coefficient is 0.001, for the finger contacting the PVC. This corresponds to an increase in friction force of only 0.013 N, for an applied load of 11.7 N. However, this is possibly an underestimate, since Equation 6.4 is assuming a smooth surface contact, of which the finger is not. However, Bongaerts *et al.* [111] found roughness to have no effect in the IEHL regime, but these were at much lower root mean square roughness's (6.6 nm to 3.6 μm) than that of the finger (7.5 to 17 μm).

Adams *et al.*'s tests suggest a glass probe (8 mm radius) moving at the finger friction test speed will be in the boundary lubrication regime (at 0.2 N load) and Myant *et al.*'s [113] studies of different compliant contacts, show that for PDMS (Young's modulus of 5 MPa) contacting a stainless steel ball (9.5 mm radius), with the viscosity of water and speed used in this test, the contact is in the boundary lubrication regime. The Young's modulus of the skin varies depending on the person, environment and the location on the body. Tests in the study of Myant *et al.*, analysing the effect of Young's modulus, suggest that the transition to the mixed lubrication regime is at lower speeds (for the same viscosity of fluid), when the Young's modulus is reduced. Therefore, if the Young's modulus is lower than the forearm tested by Adams *et al.* the finger may not be quite in the boundary regime. However, for completeness, boundary lubrication will be considered. Since the literature review did not find a Stribeck curve directly related to the finger, the corresponding coefficient of friction is not known. At the correct corresponding viscosity and speed, Adams *et al.* suggested a friction coefficient of approximately 0.3. Bongaerts *et al.* [111] looked at the effect load (for elastohydrodynamic lubrication (EHL)) had on the Stribeck curve and found that in the boundary

and EHL regime the friction coefficient decreases as a function of load. However, in the boundary regime these results are not scalable. All the previous tests have been done on smooth discs, but their research also found that for increased roughness, the Stribeck curve shifts along the x-axis (to larger values of velocity multiplied by dynamic viscosity), and the minimum coefficient of friction is increased.

A simple estimation of the friction due to shear stress in the boundary regime can be predicted using Equation 6.3. This is also assuming that the liquid bridges are forming between the contacting surface and the finger, rather than solely along the finger surface.

$$\tau = \eta \cdot \frac{du}{dy} = \eta \cdot \frac{u}{y} \quad 6.3$$

where η is the dynamic viscosity. In the calculations the dynamic viscosity of water ($1.002 \times 10^{-3} \text{ Nsm}^{-2}$) was used, however, there will more than likely be salts in the water from the finger contact, which may modify the viscosity slightly. u is the velocity (in this case the velocity of the finger slide is used) and y is the distance between the finger and the contacting surface.

The shear stress needed to increase the friction by the amount seen in the tests (10 N) can be calculated using Equation 6.4. The area used is half the total area measured in the area ink tests (Chapter 5), since it is assumed that the water is occupying the area between the ridges.

$$\tau = \frac{F}{A} = \frac{10}{97 \times 10^{-6}} = 0.10 \times 10^6 \text{ Pa} \quad 6.4$$

Substituting this shear stress into Equation 6.3 allows the calculation of the film thickness required to produce the increase in friction seen, as shown in Equation 6.5.

$$y = \frac{\eta}{\tau} \cdot u = \frac{1.002 \times 10^{-3}}{0.10 \times 10^6} \cdot 0.021 = 0.20 \text{ nm} \quad 6.5$$

As theory predicts, there is a larger increase in friction force for a thinner film, as illustrated in Figure 6.9, where the variation of increased friction force with film thickness has been calculated using Equation 6.3 and 6.4.

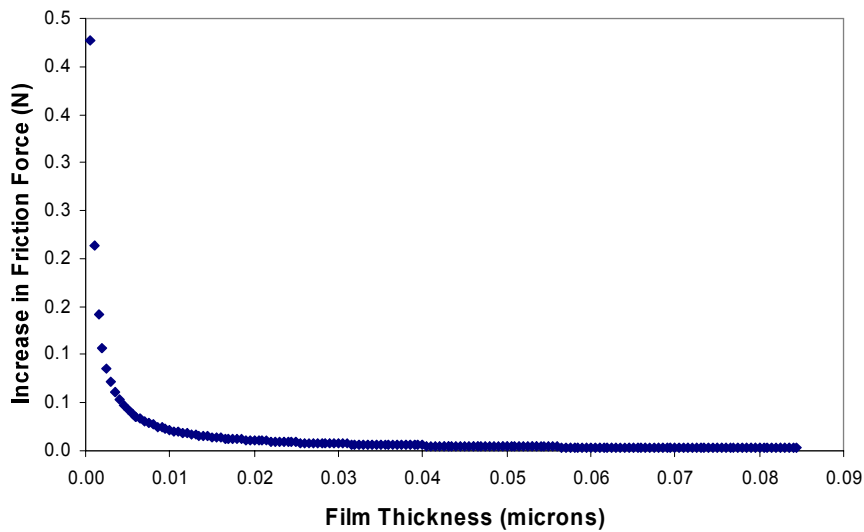


Figure 6.9 – Increase in friction force with water film thickness

If IEHL is applicable to the finger, then the increase in friction force is negligible, compared to the overall measured friction. Viscous shearing would only increase friction significantly for water films less than 10 nm, with a 0.20 nm film accounting for the increase in friction seen in the tests. If water completely filled the furrows between the finger ridges (which range from approximately 20 to 100 μm in height, for the finger tested), viscous shearing is negligible (See Figure 6.9).

6.3.3 Capillary Adhesion

When two contacting materials are rough, but hard, an increase in the water between the two surfaces increases the area of contact. This is due to a force in the capillary, which pulls the surfaces together [72, 114]. However, this is not the case when one of the materials is soft. Persson [72] analysed this situation for a hard, rough surface ($R_q = 6 \mu\text{m}$) contacting a smooth, elastically soft solid at a nominal applied pressure of 0.1 MPa, where the Poisson's ratio of the soft solid was 0.5 and the Young's modulus varied from 3 to 300 MPa. Persson [72] found that for elastically soft solids, when the water level on the surface decreases, there is a large increase in the area of contact. This is thought to be due to the capillary adhesive forces pulling the walls of the ridges into closer contact.

The effect of capillary adhesion is highly dependent upon the Young's modulus of the contacting, elastically soft material [72]. Values of the Young's modulus of the stratum corneum vary greatly, depending on the water content of the stratum corneum [38]. Park *et al.* [115, 116] found in vitro the Young's modulus of skin (pig's ear, which is thought to be comparable to the human stratum corneum) to be approximately 1 GPa at 50% humidity [115] and 3 MPa when submerged in water [116], however, Agache *et al.* [38] found it to be 2.1 MPa for the skin from a human back, at 22 °C and 82 % relative humidity. Agache *et al.* also did experiments in vivo, measuring the properties of the skin, at different locations, and found these to vary greatly across the body. However, it is not possible to separate the results for just the stratum corneum. It is the Young's modulus of the stratum corneum that will be most important in determining whether capillary adhesion will increase friction, since this is the material of the finger ridges. If the stratum corneum does not absorb the water between application and test, and the Young's modulus measured by Park *et al.* (and used in calculations by Adams *et al.*) is assumed, then capillary adhesion will not increase friction significantly. However, if the Young's modulus measured by Agache *et al.* is used, then capillary adhesion would be significant. As

discussed previously, the stratum corneum can absorb water. The stratum corneum is a layer of flat, dead or keratinised cells [117], 85 % of the proteins in the stratum corneum are keratin [118]. The high bipolar nature of keratin allows water to form bonds with the side-chain endings [119], easing absorption of water into the stratum corneum. If water absorption occurs between application and friction test, the Young's modulus of the stratum corneum will reduce and then capillary adhesion will be more applicable.

There is a strengthening argument for capillary adhesion in the experiments by Adams *et al.* [74]. In these experiments the forearm was wet, and the friction increased with this hydration, reaching a maximum after approximately three minutes. This increase in friction is explained due to the absorption of water into the stratum corneum. The majority of the excess water was removed. After this removal of water, there is a peak at a greater coefficient of friction than the 'wet' state friction. The forearm skin is not as rough as the finger, however, if it does not absorb a suitable amount of water to form a smooth surface, it will still be rough. Therefore, this peak in friction could indicate capillary adhesion.

Figure 6.10 shows the results of an initial calculation (unpublished) done by B. Persson, Jülich Forschungszentrum [120], for the stratum corneum with a Young's modulus of 2.1 MPa. In this figure "contact" refers to skin-surface contact area, "wet" refers to the area between the finger and substrate filled with water, and "dry – no contact" indicates the non-contact area not filled with water. Figure 6.11 shows an illustrative schematic of these different areas. The ratio of the real area of contact (area) against the nominal area of contact (A_0) is plotted against the average film thickness. Figure 6.10 shows that the real area of contact will not be enhanced for film thicknesses greater than a few microns. Assuming that the increase in friction is directly proportional to the increase in area of contact, the expected increase in friction force, due to capillary adhesion, can be calculated.

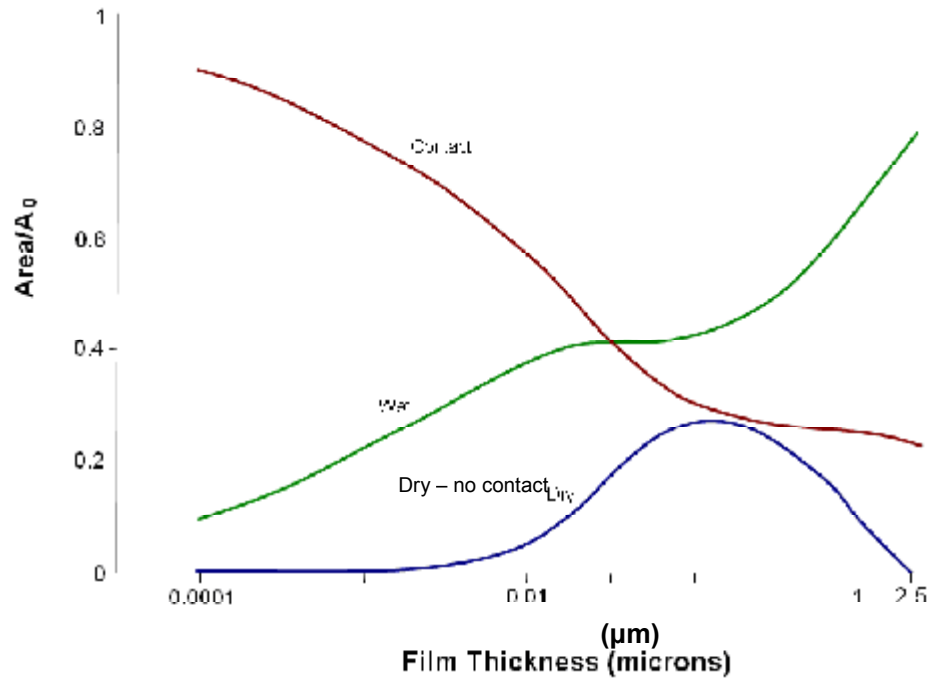


Figure 6.10 – Capillary adhesion calculation results for the stratum corneum with a Young’s modulus of 2.1 MPa and the profile of the skin taken using dental paste negatives and a profilometer. Reproduced with permission from [120].

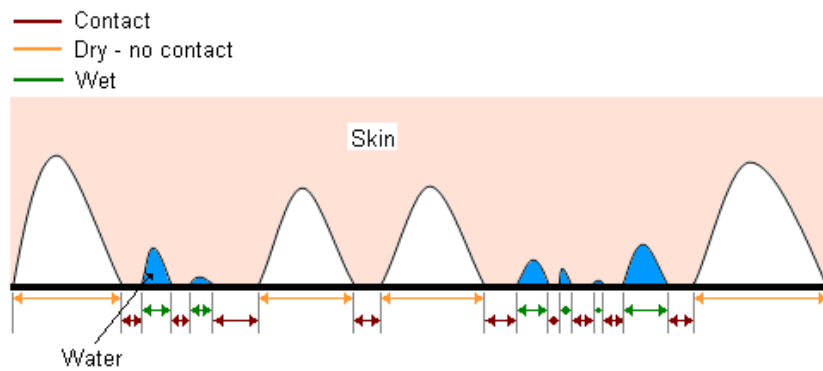


Figure 6.11 – A schematic showing an illustrative version of areas of contact displayed in Figure 6.10

It is assumed that, the increase in friction is directly proportional to the increase in area. This means that the ratio of the wet and dry areas of contact will be equal to the ratio of the wet and dry friction forces; as shown in Equation 6.6. The ratio of real to nominal area of contact, for dry conditions, is approximately that shown for the largest water film (2.5 μm) in Figure 6.10 [120].

$$\frac{F_{wet}}{F_{dry}} = \frac{A_{wet}}{A_{dry}} \quad 6.6$$

where F_{wet} is the friction force in the wet state, F_{dry} is the friction force in the dry state, A_{wet} is the area of contact in the wet state and A_{dry} is the area of contact in the dry state

The ratio of the two areas is the same as the ratio of real area of contact to nominal area of contact, for the wet and dry conditions. Therefore, the enhanced friction force can be calculated, as shown in Equation 6.7. The value shown in Equation 6.7 is for the smallest film thickness (0.1 nm). Figure 6.12 shows the possible friction force increases; Equation 6.7 was used to calculate the wet friction force, then the dry friction force was subtracted from this to calculate the increase in friction. This shows that, in order to achieve a friction increase of 5 N, the film thickness will be approximately 3 nm.

$$F_{wet} = \frac{A_{wet}}{A_{dry}} \cdot F_{dry} = \frac{\left(\frac{Area}{A_0}\right)_{wet}}{\left(\frac{Area}{A_0}\right)_{dry}} \cdot F_{dry} = \frac{0.9}{0.22} \cdot 2.4 = \underline{9.8N} \quad 6.7$$

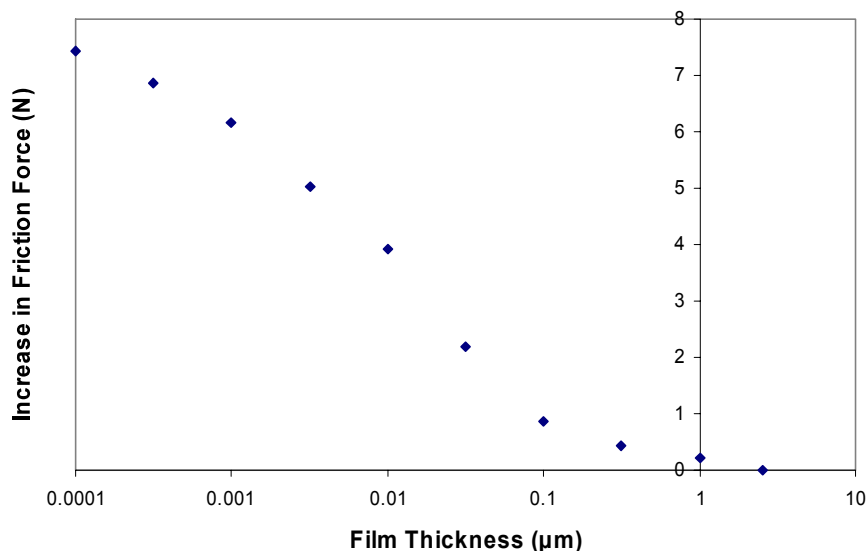


Figure 6.12 - Increase in friction force due to film thickness

In formulating the above calculation, it has been assumed that the film is pure water. This is not likely to be true, since there are salts and oils on the finger (even after cleaning). The salts will dissolve in the water, changing the properties of the solution and the oils may well be providing an additional liquid film; both of which will modify the capillary effects.

The method of water assessment used, does not distinguish between the water on the surface of the finger, and the water absorbed in the stratum corneum. To test the theory of whether capillary adhesion is having an influence on the friction, further tests were done. Water was applied directly to the PVC surface, using a vacuum tube, attached to a Bonaire Ultrasonic Humidifier BU1300W, which emits very fine particles of water at a rate of approximately $46.3 \text{ mm}^3\text{s}^{-1}$ (confirmed via e-mail correspondence with Jarden (parent company of Bonaire)). The tube was held on the surface for varying amounts of time. Friction tests were then done immediately after water application, with a finger that had a Moistsense reading of 38 au before each slide, and in an environment of $19.8 \text{ }^\circ\text{C}$ and 56 % humidity. The

procedure was followed as described in Chapter 3, and the normal force applied was 15 ± 1.7 N. The results from this test are shown in Figure 6.13. This figure clearly shows an increase in friction from the dry state to a partially wet state, and then a decrease when too much water is added. The initial film thickness can be estimated, however, this is likely to be an overestimate due to evaporation. The water output rate is known to be $46.3 \text{ mm}^3\text{s}^{-1}$, the delivery pipe has an area of 855 mm^2 , and the application time is known. Dividing the output rate by the pipe area, and multiplying this by the application time, allows the film thickness to be approximated. It was found that the film thickness was 0.27 mm, before the positioning of the finger, for a 5 s application of water. However, some of the water will be displaced once the finger is applied to the surface, so the average film thickness in contact is still unknown. Again, this method does not fully isolate the mechanism of capillary adhesion, but it reduces the amount of time for absorption.

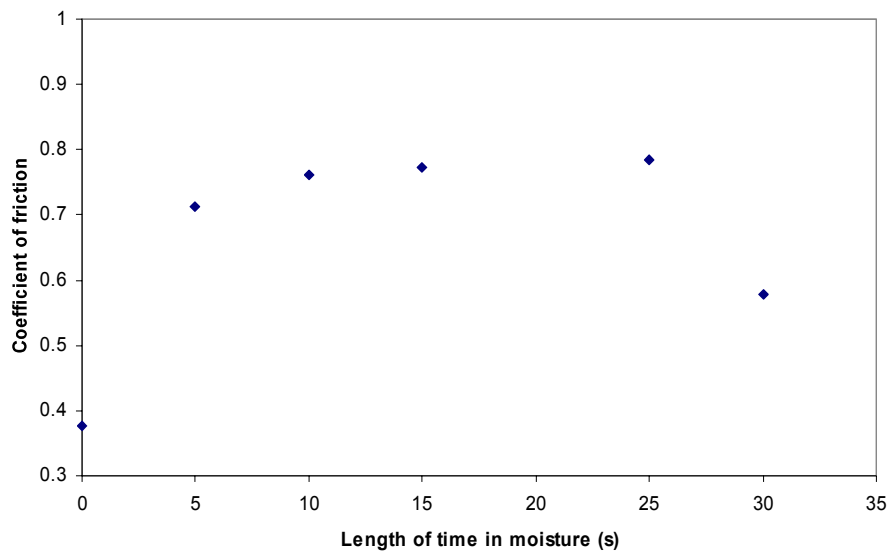


Figure 6.13 - Results from tests where water was applied directly to the surface of PVC

6.3.4 Capillary Adhesion, Viscous Shearing and Water Absorption

The previous three sections have provided a discussion about water absorption, viscous shearing and capillary adhesion. However, the mechanisms have not been separated. To gain a better understanding of the contributions of each mechanism, a small study was done to try and analyse, as much as possible the mechanisms in isolation. These tests were done by another summer placement student (Xiaoxiao Liu), under my supervision, and then the results analysed by me. These tests followed the procedure in Chapter 3, and the normal force was 5.3 ± 1.9 N. In the first tests the finger was soaked in water for varying amounts of time, the finger was then dried with a paper towel, and the friction of the finger contacting PVC was measured. As expected from previous work [74], there was a plateau in the friction after a certain amount of time; Figure 6.14 shows the results from this test. This shows that water absorption does increase friction, but, there could still be some capillary adhesion or viscous shearing, due to it not being possible to completely dry the surface of the finger.

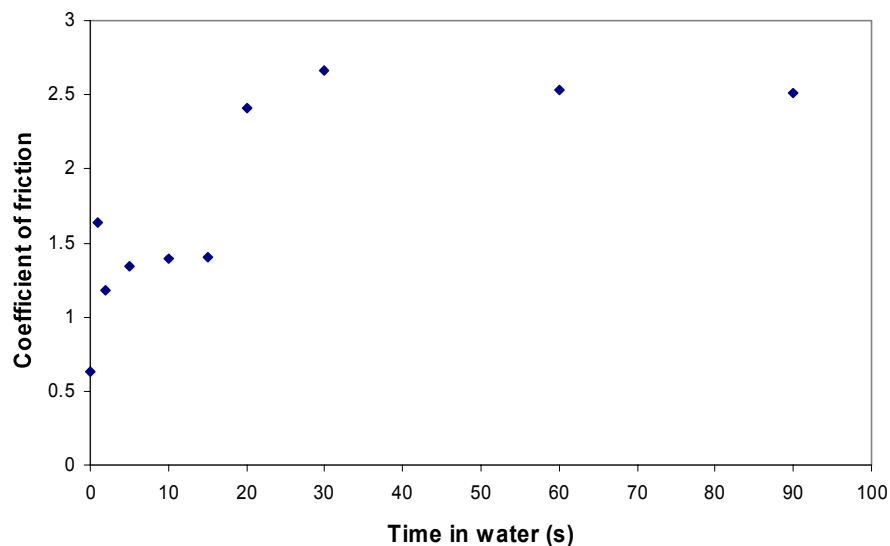


Figure 6.14 – Increase in friction when the finger is soaked in water before the friction test

A further test was done to look at the effect of surface water. The finger was soaked in water for 3 minutes prior to the test. This soaking was to ensure the plateau in water absorption had been reached, so that the surface water was not absorbed into the stratum corneum. The finger was then dried with a paper towel. Water was added to the surface of the PVC using a Bonaire humidifier, with an attached tube for water application, and holding the humidifier on the surface for varying amounts of time. The friction tests were then done as described in Chapter 3, at a normal load of 5.23 ± 1.2 N. The results from this test are shown in Figure 6.15. This shows that an increase in moisture on the surface is decreasing the coefficient of friction. However, these results do not show that capillary adhesion is not present, only that the water film on the PVC is too large for capillary adhesion to be increasing friction. The initial calculations for capillary adhesion indicate that a film thickness greater than $2.5 \mu\text{m}$ will not increase friction. The estimation of the pre-contact film thickness for a 5 second application is 0.27 mm . This means that in the previous tests where water was applied to the surface of PVC, shown in Figure 6.13, there will have been some water absorption.

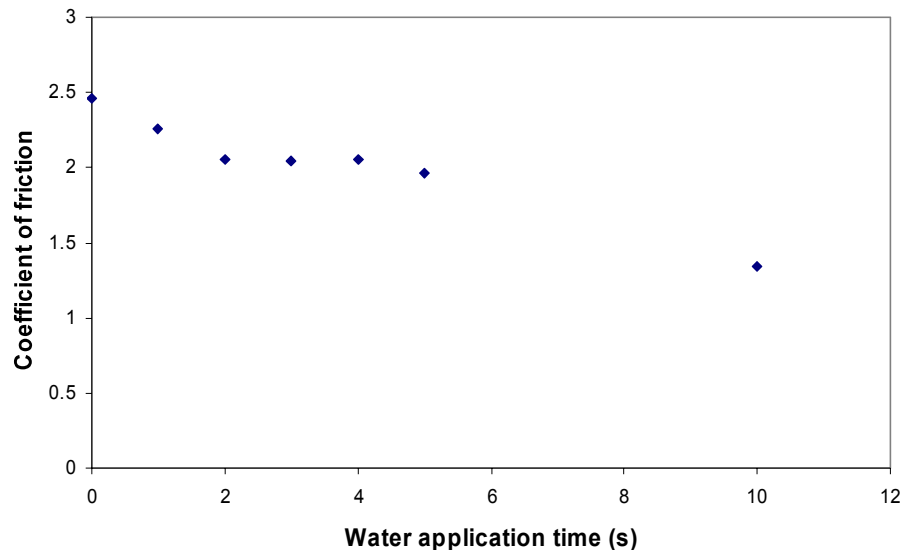


Figure 6.15 – The change in friction when water is applied to the surface of the PVC, after the finger has been soaked in water for 3 minutes

Although these tests have not completely separated the mechanisms of capillary adhesion, they can provide a rough estimate as to the increase in friction, caused by each mechanism. However, this is a crude estimate, due to a different normal force, a different finger and also a different method of water application. The water absorption tests (Figure 6.14) show that after 12 s of water soaking the friction force is 2.2 times greater than the 'dry' case. In the initial friction tests on PVC, Figure 6.6, the maximum friction force is 3.9 times greater than the 'dry' case. Assuming that water absorption is accounting for the total increase in the water absorption tests, this means that water absorption can be said to account for 56 % of the friction increase.

6.3.5 Overall Mechanism of Increased Friction

The work in this chapter has presented three arguments for why finger friction increases in the presence of some moisture. The crude estimates of the contribution of each mechanism, to the maximum increase in friction (10 N) (Figure 6.6) are shown in Table 6.3. This table highlights that water absorption has the highest contribution to the increase in friction. The contribution of the water absorption is two fold; firstly it softens the stratum corneum, enabling a larger area of contact, but secondly, this softening also enhances the amount of capillary adhesion, as this is dependent upon the Young's modulus of the stratum corneum. Capillary adhesion is shown to have the next largest contribution, however, it should be noted that this value is for an average film thickness of 10 nm, which is very small. Increasing this film thickness would decrease the contribution of capillary adhesion, up to a thickness of approximately 2.5 μm , after which capillary adhesion would not increase the friction. In fact, a decrease in friction, from the fully dry case, will be seen (as observed in Figure 6.15). Viscous shearing contributes only slightly to the overall friction, and it would take an extremely small film thickness (in the region of 0.2 nm) to cause a substantial increase in friction. Therefore, it is thought that the two main mechanisms of finger friction are capillary adhesion and water absorption, with water absorption being the most influential. Figure 6.5 shows that there is a difference in the amount the

friction increases for each of the materials tested. There is no discernable difference between them in the dry case. This further implies that a mechanism such as capillary adhesion, and not just water absorption, is increasing friction. Material properties such as surface tension have a large effect on capillary adhesion, but will have little effect on the increase in adhesion, from the dry state, due to water absorption.

Table 6.3 – Estimated contributions of mechanisms to overall friction

Mechanism of friction	Estimate of increase in friction (N)
Water absorption, resulting in a reduction in Young's modulus of the stratum corneum	5.6
Viscous Shearing <i>IEHL</i>	0.013
<i>Boundary layer (≈10 nm)</i>	0.02
Capillary Adhesion (≈10 nm)	4.4

Studies on tyres have shown that the tyres expel water from the contacting surface into the ridges, allowing tyre-road contact rather than tyre-water contact [121]. The same could be occurring for the finger. The increase in friction due to capillary adhesion is also in line with the previous work which suggested that the palms and hands sweat to increase friction and aid the 'flight' part of the 'fight or flight' mechanism. In today's world this transpires as a method to aid grip.

It would be useful to better separate the effects of water absorption and capillary adhesion, this would provide useful information such as, at what point does sweating reduce grip. There are several methods to do this. One could be to use ultrasonic film measurement and the other would be ellipsometry. There are several issues with doing both of these tests on the finger. For example; the salts on the finger may dissolve in the water,

changing the impedance or refractive index. Equally, as the stratum corneum absorbs water, the refractive index or impedance of this may also alter. The ridges will also complicate the quantification of film thickness, however, only an average film thickness is required for the estimation of capillary adhesion. Experiments to modify and verify these techniques for the finger, could be very fruitful in providing a way to separate the two principle mechanisms of friction enhancement. The computer modelling of the finger contact also needs to be furthered, with additional data such as a more accurate measurement of the Young's modulus at different hydration levels.

6.4 Conclusions from Moisture Tests

There is an increase in friction when a small amount of water is added to the finger, and when a small amount is added to a nominally flat surface. The increase in friction is due to a combination of water absorption and capillary adhesion. Past a critical amount of water the coefficient of friction reduces as it enters the mixed lubrication regime (regime between boundary lubrication and IEHL).

7 Influence of Surface Roughness and Fine Ridges on Friction

The effect of surface roughness and texture on friction is important since many objects such as rugby balls and disabled aids use texture to enhance grip. Previously, there has been some work done in this area, but this is not extensive, so it is assumed that manufacturers currently use a trial and error method for texture selection, rather than one based on scientific findings. Understanding how friction varies with texture can provide vital information for the design of product grips. This chapter will discuss the textures currently used to aid grip, and then look at the effects of surface roughness, and triangular cross-section ridges. The following chapter (Chapter 8) will investigate how larger, rectangular ridges affect friction.

7.1 Current Textures used to Enhance Grip

A survey of the current textures used on gripped objects was carried out to establish the current situation. Although these textures were probably not designed from scientific knowledge, they are currently in use, so many have been trialled and found to be effective solutions. A database of the textures was formed with information about the dimensions and descriptions recorded; this can be found in Appendix 8. A wide range of textures were analysed, these were all textures found on dental equipment, sports equipment, aids for the disabled, packaging and household utensils. It was possible to categorise the textures into four categories; criss-cross, dimples, pimples and ridges. A criss-cross pattern is defined as diagonal grooves cut into the surface that creates protruding diamond shapes. A dimpled texture is defined as one where shapes are cut out of the surface. A pimples texture is where shapes protrude the underlying surface. Finally, a ridge pattern is where the texture is protruding from the underlying surface, with a rectangular base, which extends across all or the majority of the surface. The texture, which occurred most frequently, in this survey, was ridges, as Table 7.1 illustrates. This table lists each category of pattern and the number of

Chapter 7 Influence of Surface Roughness and Fine Ridges on Friction

times the pattern was observed, and the texture dimension range, for the population of surfaces analysed.

Table 7.1 – Occurrences of each category of pattern

Category of Pattern	Criss-crossed	Dimples	Pimples	Ridges
Occurrences	13	10	13	33
Min. Height (mm)	0.1	0.1	0.1	0.1
Max. Height (mm)	0.5	1.5	1.5	5.0
Min. Width (mm)	0.1	0.8	0.5	0.2
Max. Width (mm)	1.5	4.5	2.5	9.5
Min. Spacing (mm)	0.2	0.8	0.1	0.2
Max. Spacing (mm)	3.41	12	6.8	5.5

Since, from the surfaces examined in this survey, the ridges were the most popular texture, they were chosen for this study. Table 7.1 shows that the dimensions of the ridges range greatly. Two types of ridges were identified; these were triangular and rectangular in cross section. This chapter examines the smaller ridges; width of 0.1 to 0.5 mm. These ridges will have a triangular cross section. The proceeding chapter will look at larger ridges (width of 1 to 8 mm) with a rectangular cross section. Other surfaces, examined in the survey, used roughness to increase the friction. If surface roughness has a large effect on friction, this could alter the results seen in the ridge tests, because the roughness on the ridge surface may be increasing friction to a greater extent than the ridge itself. Therefore, this chapter will also examine the effect of surface roughness on friction.

To summarise, there were three different types of surface textures examined in this chapter and Chapter 8; firstly the effect of surface roughness was investigated, these surfaces had a root mean square roughness of less than 5.6 μm and the roughness was applied using emery cloths or milling with a boring head. The next type of texture was a fine ridge texture, these were machined using a 60° point tool, which produced ridges with a triangular

cross section, and the root mean square roughness of these surfaces varied from 1.19 to 98.42 μm . The final textures were macro ridged textures; these surfaces were composed of rectangular shaped ridges, varying in height from 0.5 mm to 2.5 mm. The macro ridged textures are to be discussed in the next chapter.

7.2 Procedure for Friction Tests on Different Surface Roughness and Fine Ridges

Tests were carried out on aluminium (HE 30), brass (CZ 121) and steel (S 275). The roughness was varied on the materials using several different techniques. In the first instance the materials were ground using different grades of emery cloth and sand paper (P600, P400, P320, P240 and Grade 60), however, this method proved not to give a wide enough range of roughness to see any relationships between roughness and the coefficient of friction. The next method of applying roughness to the metal was to mill the specimens using a boring head and single point tool at different speeds; 0.5 mm deep cut, 800 rpm and speeds varying from 35 mm/min to 115 mm/min in 10 mm/min increments, this method produced a larger range of roughness.

To produce surfaces with fine ridges, a shaping machine was used to put thin horizontal grooves in the metal. The tool used was a 60° point tool and the grooves were machined at 0.5 mm feed, 0.3 mm deep cut; 0.4 mm feed, 0.2 mm deep cut; 0.3 mm feed, 0.15 mm deep cut; 0.2 mm feed, 0.1 mm deep cut; and 0.1 mm feed, 0.05 mm deep cut. This surface finish represents the fine ridge patterns often seen on gripped objects, which are the lower end of the range of dimensions shown in Table 7.1 (see Appendix 8 for examples of these surfaces). Examples of the finishes achieved for each of these methods are shown in Figure 7.1. The tests were done on the same finger as the normal force, area and moisture tests (Chapters 4, 5 and 6). Five runs were done on each material at varying forces (between 1.6 and 26 N), with the finger moving in a direction perpendicular to the ridges. The procedure

outlined in Chapter 3, for the tests on The University of Sheffield Rig, was followed.

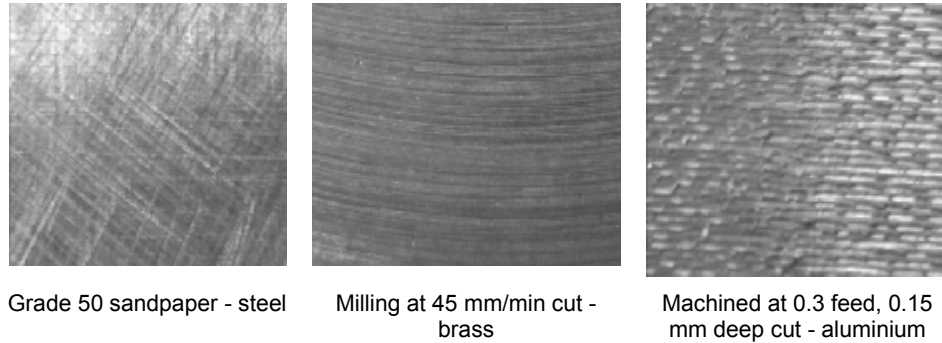


Figure 7.1 – Photos of the three different surface finishes

7.3 Results from Roughness and Fine Ridge Friction Tests

7.3.1 Results from Surface Roughness Friction Tests

Figure 7.2 shows that there is an increase in friction with roughness for steel. However, this is arguably not true for brass and there is no evidence to suggest it to be true for aluminium.

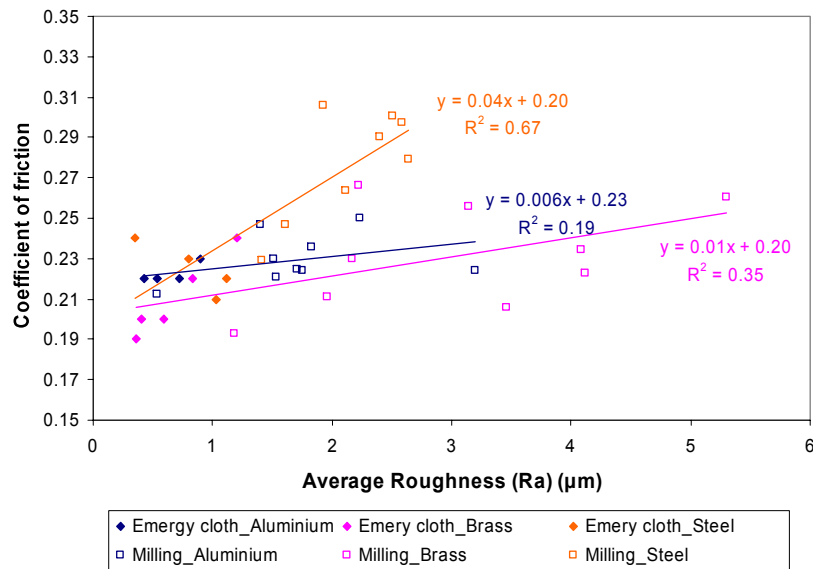


Figure 7.2 –Coefficient of friction (at 10 N) plotted against average roughness. Coefficient of friction calculated by using the linear regression line between the friction force and normal force, from each test, to calculate the coefficient of friction at 10 N

7.3.2 Results from the Fine Ridge Tests

Figure 7.3 shows that all the materials follow the same trend of increasing coefficient of friction with roughness, up to a point (of approximately $R_q = 26 \mu\text{m}$), and then the coefficient of friction plateaus. For the brass and the steel there is a lot of scatter after passing this plateau point. This figure shows all coefficients of friction calculated for each normal load (ranging from 1N to 26 N), which accounts for there being several data points for each roughness measurement.

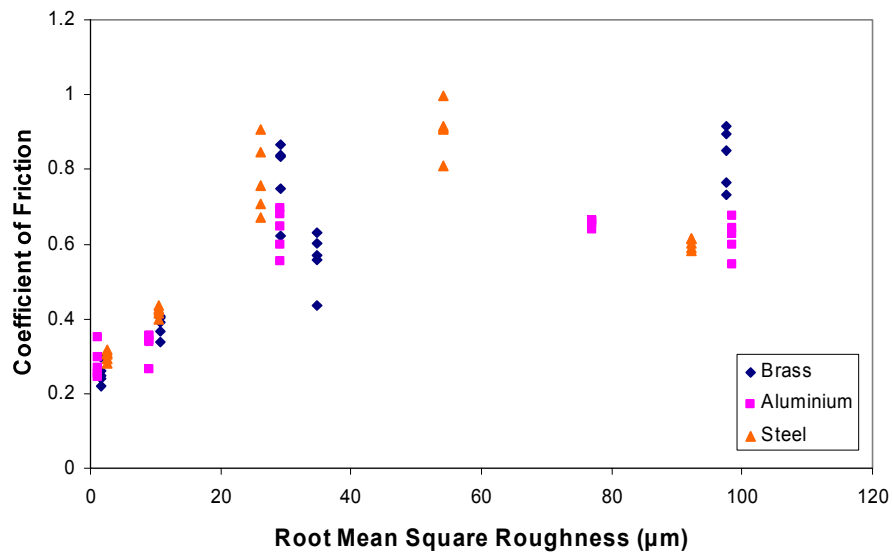


Figure 7.3 – Plot of root mean square roughness (R_q) against the measured coefficient of friction for Aluminium, Brass and Steel. The coefficient of friction at each measured load is shown (load varied from 1.6 to 26 N)

7.4 Discussion of Results from Roughness and Fine Ridge Friction Tests

7.4.1 Discussion of Roughness Friction Tests

In the tests on a flat surface, there was no discernable difference between the three metals, and they are also shown to follow a similar trend in the fine ridge tests. This means it is difficult to explain why steel seems to have increasing friction at low roughness values, however, brass and aluminium

do not show a visible change. This cannot be explained by these tests alone, and further work needs to be done to examine the adhesion mechanisms, which could be responsible for this difference.

Cole *et al.*'s [14] work predicted that the properties of the finger dominate the interaction up to a certain roughness; past this point the overall friction is influenced more by the properties of the counter-surface. The results for brass and aluminium are in agreement with this theory, however, not those for steel. The increase in friction with roughness, at such low roughness levels, could be attributed to an increase in the area of contact, and therefore increased adhesion. Since this level of roughness has little effect on the friction of brass, and other factors such as ease of machining; brass was used in the macro ridge tests (described in Chapter 8).

7.4.2 Discussion of the Fine Ridge Friction Tests

Considering the surfaces machined linearly with a single point tool, the general shape of the surface profile was similar for all materials. Therefore, the width and the height of the ridges were the parameters chosen to describe the surface. The grooves are machined in, so it would be assumed that these measurements were not necessary, and the feed and cut can be used to describe the height and width of the ridges; however, this varies due to the ease of machining one material over another, and there are also errors in the machining process. Due to the manufacturing process the width of the ridges increases with height. To further examine how the height and width of the ridges affected the coefficient of friction, multiple linear regression was carried out. The average height is described using the R_q value. The average width is described by the manually counted main peaks of the profile divided by the sample length. The formula resulting from the multiple linear regression is shown in Equation 7.1, where w is width. The R^2 value for the measured coefficient of friction against the predicted coefficient of friction (using Equation 7.1) is 0.74, as shown in Figure 7.4. This R^2 value shows that although the equation describes the relationship well, it requires

refinement. It does, however, show that width is more dominating than height in the determination of the friction.

$$\text{Coefficient of friction} = 0.15 - 0.06 \cdot \left[\frac{R_q}{R_q} \right] + 0.45 \cdot \left[\frac{w}{w} \right] \quad 7.1$$

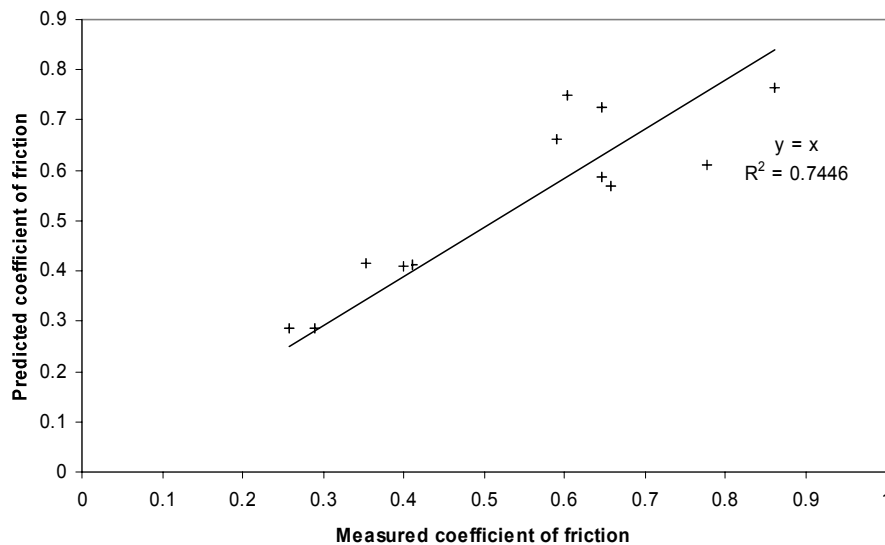


Figure 7.4 – Measured coefficient of friction against the predicted (using Equation 7.1) coefficient of friction

There is a large amount of scatter in Figure 7.3 and this is due to the ease of machining of the metals. That is, the easier it was to machine the grooves into the surface, the more uniform the pattern was. This scatter is greater at a larger roughness, because the ease of machining became more of an issue with increased feed and cut. The scatter can be explained by looking at the profiles of the materials shown in Figure 7.5. The feed and cut can be cross referenced to Figure 7.3, because a higher feed and cut gives a greater value of root mean square roughness. In Figure 7.5 it can be seen that the roughness profile for the aluminium is regular with even peaks for both the 0.4 mm feed and the 0.5 mm feed. This regularity is thought to be the reason that there is hardly any scatter in the results for the aluminium.

Chapter 7 Influence of Surface Roughness and Fine Ridges on Friction

Referring back to Figure 7.3, the brass had a lower than expected coefficient of friction for the stated R_q value, for the 0.4 mm feed. The height of the ridges can be seen to be lower than the other two metals at this feed, however, this is reflected in the R_q value (it is lower than the other two metals). Figure 7.5 also shows that for the 0.4 mm feed, the ridges (brass) have a double peak at the top of the ridge. At a feed of 0.5 mm the profile was again regular, so the value of coefficient of friction was as would be expected. For steel at 0.5 mm feed, the profile is very regular and is as would be expected, however, this is not the case for the 0.3 mm or the 0.4 mm feed (0.4 mm feed profile shown in Figure 7.5). The coefficient of friction for these profiles is higher than would be expected. This is most probably due to the irregularity of the surfaces.

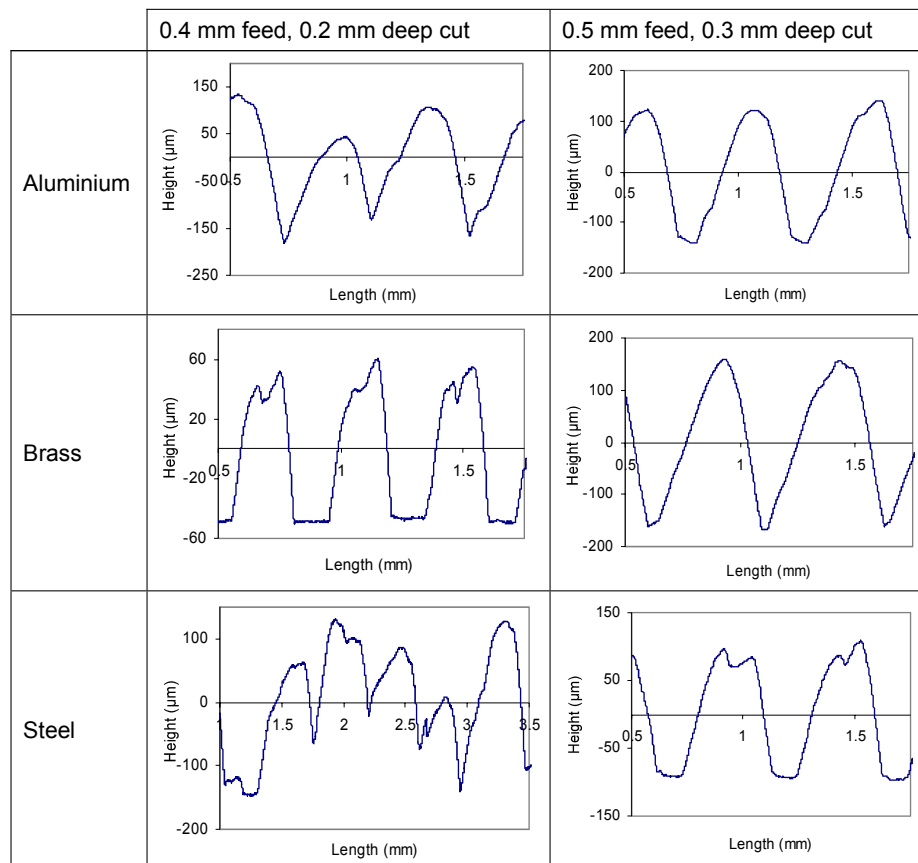


Figure 7.5 – Profiles from profilometer of aluminium, brass and steel at 0.4 mm feed, 0.2 mm cut and 0.5 mm feed, 0.3 mm cut

7.4.3 Friction Mechanisms for a Finger Moving Over Fine Ridges

The main friction mechanisms will be similar to those discussed in Chapter 4 and 5; however, the ridges introduce a hysteresis component to friction. Therefore, Equation 7.2 describes the overall friction. As discussed in Chapter 4, the principle adhesion mechanism is adsorption, however, the presence of ridges on the surface, could also mean that mechanical interlocking is contributing to the adhesive mechanisms. The term for adhesive friction includes all possible adhesion. Interlocking friction usually refers to particles or asperities moving over other particles or asperities. However, in this case the finger ridges are moving over ('climbing') the metallic ridges. The width of the ridges/asperities usually determines whether interlocking will occur [95]; Equation 7.1 highlights width as having a large influence on the overall friction, thus implying that interlocking may be present.

$$F_T = F_a + F_h \quad 7.2$$

where F_T is the total friction, F_a is the adhesive friction, and F_h is the hysteresis friction.

It should be noted that Equation 7.2 has been modified from Chapter 5, since the contributions to friction from lateral deformation of the finger, and the deformation of the ridges, were found to be negligible. Chapter 6 examined the effect of moisture addition. It was found that moisture has the effect of modifying the adhesive mechanism, so is included in the term F_a . The effects of naturally occurring oils on the skin are accounted for (when not in excess) in the shear calculations explained in Chapters 4 and 5, which is used to calculate the adhesive friction.

7.4.4 Hysteresis Friction

The metallic surface ridges will deform the finger (bulk); this means there will be a hysteresis component of friction. To estimate this, a single ridge was considered; Figure 7.6 shows an illustration of the ridge-skin contact. The estimation of the hysteresis friction follows the same procedure as Greenwood and Tabor [91] used for a conical slider. The force required to deform the skin is that on the leading edge, F_D , shown in Figure 7.6.

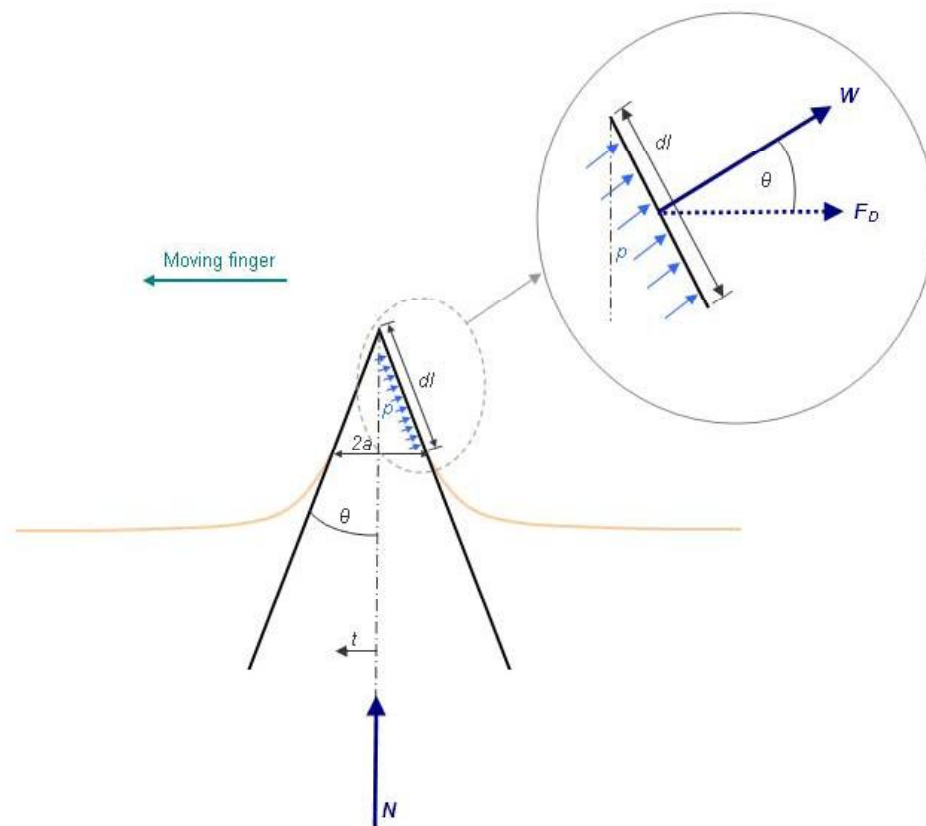


Figure 7.6 – Schematic of a single ridge contacting the skin. N is the normal force, t is the distance from the centre line of the ridge, θ is the angle of ridge, a is the largest distance from centre line to contact of the ridge with the skin, p is the pressure along the contact area of the ridge and skin, dl is the length of the contact area, W is the resultant force due to applied pressure and F_D is the deformation force

Chapter 7 Influence of Surface Roughness and Fine Ridges on Friction

There will be a pressure along the leading edge, which varies along the length dl . The force (W) due to the pressure of the ridge pressing against the skin is:

$$W = \int p \cdot L \cdot dl \quad 7.3$$

where L = length of the ridge contact into the plane of the paper

Equation 7.3 can be re-written as Equation 7.4, since the distance from the central axis (t) varies such that $dt = dl \cdot \sin\theta$. Integrating this between the limits of 0 and a , accounts for the contact area (since a is the distance t where the skin leaves contact with the ridge).

$$W = \int_0^a \frac{p \cdot L}{\sin\theta} dt \quad 7.4$$

The deformation force (F_D) is the horizontal component of the force due to the applied pressure (W). Equation 7.5 describes this force.

$$F_D = W \cdot \cos\theta = \int_0^a p \cdot L \cdot dt \cdot \frac{\cos\theta}{\sin\theta} \quad 7.5$$

The normal force is applied to both sides of the ridge/indenter, and is described by Equation 7.6.

$$N = 2 \cdot \int_0^a p \cdot L \cdot dt \quad 7.6$$

Therefore, the friction force is described using Equation 7.7.

$$F_D = \frac{N}{2} \cdot \cot \theta \quad 7.7$$

There will, however, be a limit to this friction, since there is only so much the finger can deform. An approximation for the maximum deformation of the finger, when a ridge contacts it, was made using a 0.85 mm wide indenter to compress the finger. This showed that the maximum compression of the finger was 4.8 mm, for the ridge size used. The model above, also assumes that the ridge is infinite in height, however, this is not the case, so there is the other limit of the ridge height. None of the ridges tested were taller than 4.8 mm, so the height of the ridges will be the limiting factor.

The model of a single ridge does not fully describe the deformation force, since the adjacent ridges restrict the finger from fully deforming. To take this into account, an equivalent ridge angle or applied load can be calculated. The calculation will be done using an equivalent load (N').

To calculate the equivalent load, it was assumed that the finger deformation, is symmetrical, and can therefore be estimated, in 2D format, using circles (post ridge contact). This physically means that the finger contacts a ridge, and at the point of leaving the ridge it forms an arc. This arc can be modelled by a circle at a tangent to the ridge (the tangent being the point at which the skin leaves contact with the ridge). This is illustrated in Figure 7.7. This model assumes that the deformation profile is constant along the width of the finger (length L). In this figure the larger, blue circle represents the finger that is deforming on a single ridge, and the smaller, green circle represents the deformation of the finger when there is an adjacent ridge.

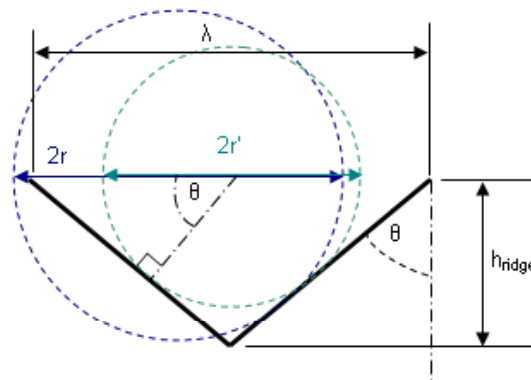


Figure 7.7 – Schematic of the circular representation of a finger deforming on a ridge. r = radius of the circle without an adjacent ridge and r' = radius of circle with adjacent ridge

When Figure 7.7 is drawn to scale, it can be seen that the ratio of the circle radii is equal to the ratio of deformation depths. The deformation depths are considered to be from the tip of the ridge point, to the tangent of the circle with the ridge. For a single ridge contact, the depth of deformation (h_{max}) can be estimated using Hooke's Law, as shown in Equation 7.8. This assumes that the spring constant (k) is linear. This is not the case for a single ridge pressed into an uncompressed finger (see Appendix 9 for details), however, since the finger is already pre-compressed it is thought that a linear spring constant is a reasonable assumption; in Chapter 5, the finger pad as a whole was found to behave as a linear spring.

$$h_{max} = \frac{N}{k} \quad 7.8$$

The ratio of the radii to the finger deformation can then be rearranged to give an equation for the depth of deformation (h), when there is an adjacent ridge.

$$h = \frac{r'}{r} \cdot h_{max} = \frac{\left(\frac{\lambda}{2} \cdot \cos \theta\right)}{h_{ridge}} \cdot h_{max} = \frac{\lambda \cdot \cos \theta}{2 \cdot h_{ridge}} \cdot h_{max} \quad 7.9$$

Chapter 7 Influence of Surface Roughness and Fine Ridges on Friction

Again applying Hooke's law, an equivalent load can be calculated for the new modified deformation, described by Equation 7.10.

$$N^1 = k \cdot \frac{\lambda \cdot \cos \theta}{2 \cdot h_{ridge}} \cdot h_{max} \quad 7.10$$

Since h_{max} can be estimated using Hooke's law (Equation 7.9), the overall equivalent load can be described using Equation 7.11.

$$N^1 = \frac{N}{n} \cdot \frac{\lambda \cdot \cos \theta}{2 \cdot h_{ridge}} \quad 7.11$$

The total normal force is divided by the number of ridges (n), since this then considers the deformation force for a single ridge. This equivalent load is then used as the input to compare whether maximum deformation has occurred yet. If it has, the limiting load (the load at which the deformation reaches a maximum) is used, rather than the equivalent load. This deformation force (for a single ridge) is then multiplied by the number of ridges in the contact, to equate the total deformation.

The number of ridges is calculated using Equation 7.12 where $L = 2a$, a is the radius of contact predicted by Hertz (Equation 7.13).

$$N = \frac{L}{\lambda} \quad 7.12$$

$$a = \left(\frac{3 \cdot N \cdot R}{4 \cdot E^*} \right)^{1/3} \quad 7.13$$

The deformation force is an overestimate of the hysteresis friction (F_h), since the skin is able to return to its original shape, which is a mechanism of

energy return. However, the viscoelastic nature of the skin means that not all of the energy used to deform the skin is recovered. This difference can be represented by the viscoelastic hysteresis loss fraction, β . Therefore, combining Equations 7.8 and 7.11 with the loss fraction, the overall hysteresis friction can be calculated as shown in Equation 7.14. The loss fraction is dependent upon loading and unloading rate, so will vary between ridge patterns. For a finger pressing on a flat surface it is equal to approximately 0.45, with loading compression rate of approximately 0.635 mms⁻¹ and unloading rate of approximately 0.318 mms⁻¹ [77].

$$F_h = \begin{cases} \beta \cdot n \cdot \frac{N}{2 \cdot n} \cdot \frac{\lambda \cdot \cos \theta}{2 \cdot h_{ridge}} \cdot \cot \theta & \frac{N}{n} < N_{max} \\ \beta \cdot n \cdot \frac{N_{max}}{2} \cdot \cot \theta & \frac{N}{n} \geq N_{max} \end{cases} \quad 7.14$$

7.4.5 Adhesive Friction

As previously described, the adhesive (adsorption and electrostatic) friction can be described by Equation 7.15. In the case of the ridged surfaces, it is assumed that the constants τ_0 and α are the same as for a finger sliding on a nominally flat surface. This is probably not entirely true since the ridges on the surface will create pressure peaks; the change in pressure distribution could alter the amount of adhesion. Nether-the-less, the adhesive friction will be greater than a flat surface due to the area of contact increasing with the presence of the ridges. Interlocking friction will also be considered, but this will be discussed later (Section 7.4.6).

$$F_a = \begin{cases} \alpha_1 \cdot N & N < N_L \\ \tau_0 \cdot A + \alpha_2 \cdot N & N \geq N_L \end{cases} \quad 7.15$$

If the contact of the finger is considered to be circular (and approximated using Hertz's theory of contact), there is only one radius that is increased due to the ridges, a' , the other radius a will remain the same length as that predicted for a flat surface; the different radii are illustrated in Figure 7.8. The increased radius a' can be approximated by considering the side of one ridge to be a right angled triangle. The length of contact is the hypotenuse of the triangle. This can therefore be estimated using Pythagoras' Theorem, where the height will be the deformation depth. The amount of deformation has been previously estimated in Equation 7.9. The radius of contact a' is then the hypotenuse multiplied by two (to account for both sides of the ridge), and then multiplied by the number of ridges in the original contact radius a ($n/2$), as described in Equation 7.16. The area of contact can then be estimated using Equation 7.17. This calculated area of contact can then be substituted into Equation 7.15 to calculate the adhesive component of friction. This method makes the assumption that the total pressure can be averaged over the area of contact, however, in reality, it is more likely that there is increased adhesion at the top of the ridge, due to a larger contact pressure, compared to that of the ridge base.

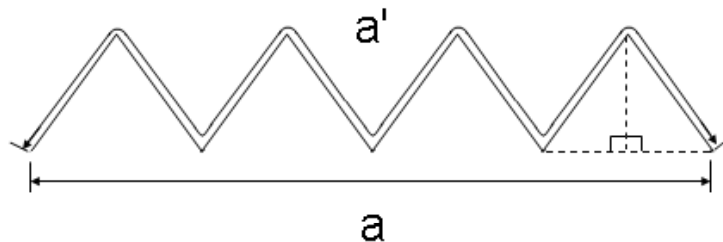


Figure 7.8 – Illustration of the area of contact of a finger when on a ridged surface.

$$a' = \begin{cases} \frac{n \cdot h_r}{\cos \theta} & N \geq N_{\max} \\ \frac{\lambda \cdot \cos \theta}{2 \cdot h_r} \cdot \frac{N}{k} & N < N_{\max} \end{cases} \quad 7.16$$

$$A = \pi \cdot a \cdot a' \quad 7.17$$

Attempts were made to better predict the adhesive friction, by considering an approximation of the pressure distribution. However, these were not successful in providing a better estimate of adhesion. It was assumed that the pressure decreased linearly from a maximum at the tip of the ridge and a minimum at the base. This resulted in the maximum pressure being twice that of the average pressure. This was then used to calculate shear stress along the ridge edge. If the shear stress distribution is taken and multiplied by the area of contact, the overall adhesive friction equates to the same as the method of assuming average pressure. The other method attempted was to calculate the horizontal component of the maximum adhesive friction (horizontal, since it is along the ridge, so acting at an angle θ to the vertical). However, to calculate the adhesive friction from the shear stress, an application area is required. There are two problems with this; firstly, in the approximation of the area, the final result is dependent upon the area chosen for use in the calculation, secondly, in reality the area of contact at the tip of the ridge will vary due to the irregular surface profile.

7.4.6 Interlocking Friction

Assuming that the adhesive friction due to molecular bonding has been fairly well estimated, there is still a large proportion of friction unaccounted for. Considering the friction between a steel indenter and a nitrile rubber [122], past a certain level of roughness ($R_a = 1.6 \mu\text{m}$ for the rubber and $R_a = 1.88 \mu\text{m}$ for the steel) interlocking of the asperities causes an increase in friction. The ridged surfaces are a higher roughness than this ($R_q = 1.19 - 98.42 \mu\text{m}$) and the roughness of the finger is $R_q = 7 - 17 \mu\text{m}$, depending on the test location. This means an additional mechanism of friction could be the finger ridges 'climbing' over the metallic surface ridges; interlocking friction. Adams [123] estimated the coefficient of friction due to interlocking, of one spherical particle climbing over another spherical particle, as described by Equation 7.18. This can be applied to ridges 'climbing' over ridges, with the same result.

$$F_i = N \cdot \tan(90 - \theta) \quad 7.18$$

This may be an overestimate, since in the case of the skin, it can deform, which could provide an additional source of energy to move the finger ridge over the metallic ridge, thus requiring a lower force to move the finger. In the approximations of interlocking friction, Equation 7.18 will be used, since it represents the results well. However, if a better approximation of adhesion from molecular bonding is calculated, the mechanism of interlocking should be reconsidered, which could result in a modification to Equation 7.18.

7.4.7 Comparison of Predicted Friction to Measured Friction

Using Equation 7.2, where the adhesive friction includes interlocking friction, and assuming a viscoelastic hysteresis loss fraction of 0.45 [77], the friction force can be estimated. Figure 7.9 shows the predicted and actual coefficients of friction for the materials tested. There is a fairly good correlation between the predicted and measured values for brass, and there is quite a bit of scatter for the other two materials. The prediction is generally over predicting the friction. The error is thought to come from the assumption that the ridge pattern is regular, uniform and perfectly formed, which Figure 7.5 shows is not the case in reality. There is also error in some of the assumptions made, such as the single assumed loss fraction, and assuming the adhesion (excluding interlocking) equation for a flat surface can be applied to ridges. The equation for hysteresis friction for a sphere contacting an elastomer [91], could be tested by lubricating the rubber. However, this is not possible for a pointed indenter, since it penetrates through the layer of lubricant. Therefore, there is no measure, other than basing it on previous predictions, of how accurate the model for hysteresis friction is.

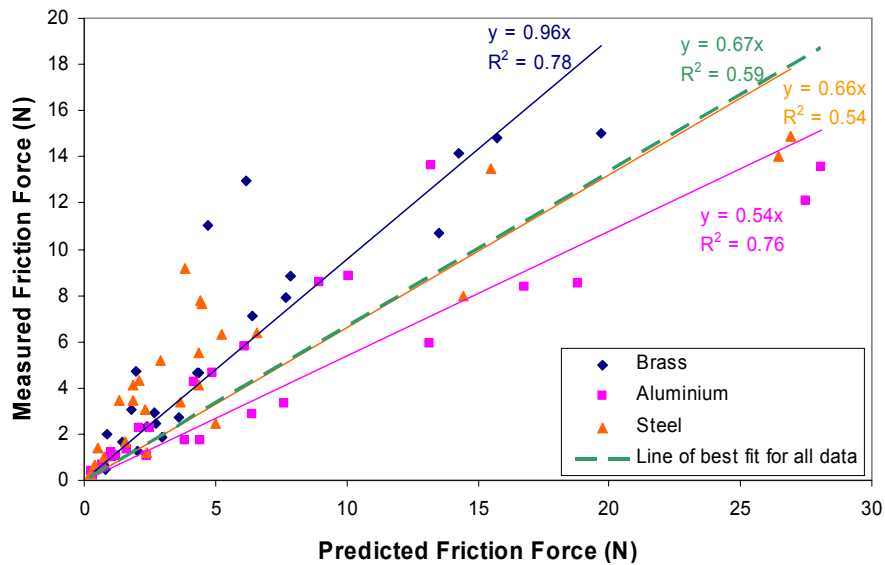


Figure 7.9 – Comparison of predicted coefficient of friction and the measured coefficient of friction, for the ridge patterns tested

Figure 7.3 shows that the coefficient of friction plateaus with roughness, however, from analysis of friction mechanisms, it can be shown that in the range of roughness tested and also the profile type tested, this is not the case. In fact, where a plateau in friction was seen, this was actually related to a change in profile shape (since the machining method did not ensure a constant profile). The measure of roughness used was the root mean squared roughness, which does not account for the different shapes of the ridges.

Figure 7.10 shows the contributions (predicted) of each friction mechanism to the overall friction. This shows that as the size of the ridges increases the percentage contribution of adhesion (to the overall friction), in terms of molecular bonding (e.g.: adsorption and/or electrostatic), decreases and the amount of interlocking (also adhesive friction) increases. The hysteresis friction, does not contribute greatly to the overall friction, except for a ridge height of 250 μm ; the contribution varies from 4 to 12 %, (percentage wise)

decreasing with increased load. Surfaces with larger spaced, and higher ridges, may see a larger contribution of hysteresis to the overall friction.

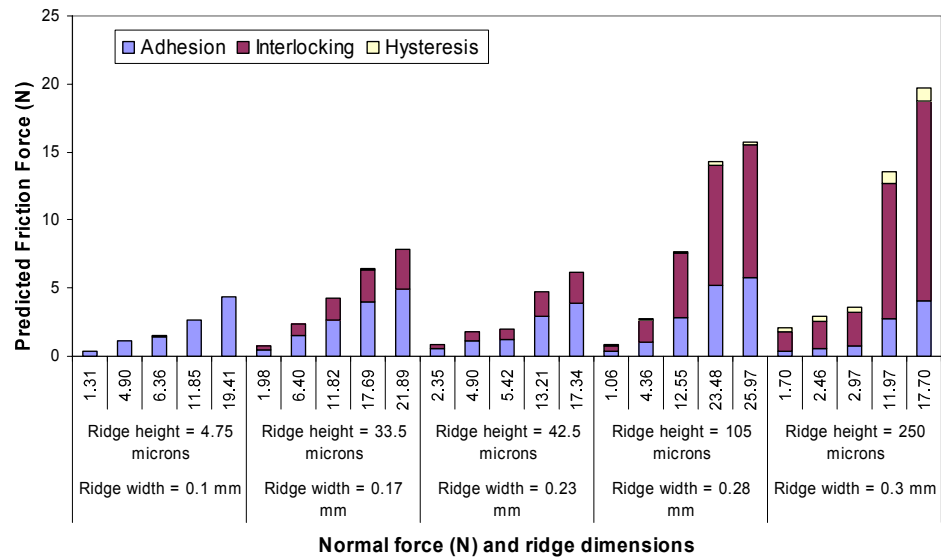


Figure 7.10 – Contribution of each mechanism to the overall predicted friction

7.5 Conclusions

Roughness ($R_q < 5.6 \mu\text{m}$) was shown to have little effect on the measured friction for brass and aluminium, however, for steel it was found to increase friction with roughness. This is thought to be due to an increase in the amount of adhesion possible, with increased roughness. However, this does not explain why the increase was not seen for brass or aluminium. This is an issue to be investigated in a future study.

In these tests, adhesion was the predominant friction mechanism for ridges of a height lower than $42.5 \mu\text{m}$. This is because the metallic ridges are so shallow, they cause an increase in contact area, and therefore adhesion. However, the finger does not deform to a great enough extent for hysteresis friction to have an effect. Interlocking friction contributes more at heights

Chapter 7 Influence of Surface Roughness and Fine Ridges on Friction

greater than 42.5 μm , since the size difference between the two ridges requires the finger ridges to 'climb' the metallic ridges. The amount of interlocking increases as the metallic ridges become sharper, that is, the angle, of the ridge edge to the vertical, decreases. Finally, at a height of 250 μm , hysteresis starts to play a greater part in friction; however, this is still not a dominant mechanism. It is playing a larger part in friction at this height because the metallic ridges are deforming the skin more, due to increased metallic ridge width and height.

8 Finger Friction when Contacting Large Rectangular Ridges

The effects of small, triangular cross section ridges, on the friction between finger and counter-surface, have been investigated in the previous chapter. This chapter will further this study by investigating how larger, rectangular cross section ridges affect friction. Bobjer *et al.* [64] have already analysed these ridges in a small scale study. They tested four ridged surfaces that had 0.5 mm high ridges, and spacing and width ranging from 0.5 to 1.5 mm. This work found that in 'dry' finger conditions, adding ridges to a surface decreased the friction force. This effect was explained by the ridges causing a reduction in contact area, and therefore a decrease in adhesion. However, the previous tests in Chapter 7 have shown that hysteresis friction starts to have a noticeable increase on the total friction for the larger ridges. This study will look at a texture similar to those used by Bobjer *et al.*, but also larger scale ridges, to allow the identification of friction mechanisms, and at what point they occur. The textures were chosen to represent the extremes of height, width and spacing, and a variation of these; the extremes refer to the dimensions where at high load, the finger is only contacting the ridge, and not the underlying surface. Dimension tests were done using FIMO®, which is modelling clay that hardens when cooked. This allowed different ridge dimensions to be analysed, quickly and cheaply. The FIMO® models were used to define the dimension extremities, but they were not used in friction tests. The ridge dimensions were varied until there was no contact with the underlying surface, the maximum dimensions were considered to be; height = 2.5 mm, width = 8 mm and spacing = 12 mm. After the experiments were completed it was found that these were not true estimates of the maximum dimensions, however, this method did provide a large spectrum of texture dimensions.

8.1 Method

To try and separate the individual effects of height, spacing and width, a single dimension was varied across five different surfaces. The textures were such that the spacing was varied from 2 to 12 mm, with a height and width of 1 mm and 4 mm, respectively (general ID prefix 'S' in Table 8.1). The width was varied from 1 mm to 8 mm, with a spacing and height of 5 mm and 1 mm, respectively (general ID prefix 'W' in Table 8.1), and the height was varied from 0.5 mm to 2.5 mm, with a spacing and width of 5 mm and 4 mm, respectively (general ID prefix 'H' in Table 8.1). Then four textures were chosen with a random mixture of width, height and spacing (general ID prefix 'R' in Table 8.1). Table 8.1 shows the dimensions of the surface textures. Figure 8.1 illustrates physically what each dimension corresponds to. All surface ridge patterns were machined from 5 mm thick flat brass (CZ 121) bar.

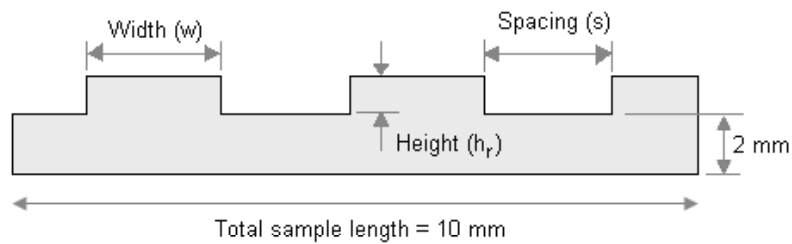


Figure 8.1 – Definition of dimensions

Table 8.1 – Ridge Pattern Dimensions

ID	Ridge height (mm)	Ridge Width (mm)	Ridge spacing (mm)
S1	1	4	2
S2W3H2	1	4	5
S3	1	4	7
S4	1	4	10
S5	1	4	12
W1	1	1	5
W2	1	2	5
S2W3H2	1	4	5
W4	1	6	5
W5	1	8	5
H1	0.5	4	5
S2W3H2	1	4	5
H3	1.5	4	5
H4	2	4	5
H5	2.5	4	5
R1	0.5	1	2
R2	1.5	4	7
R3	2.5	8	12
R4	2	6	10
F1	0	0	0

The friction tests were done at Philips Applied Technologies, using the Kistler Dynamometer (see Chapter 3 for details). They were done in a climate controlled room at 20 °C and 45 % humidity. The procedure followed that described in Chapter 3. Each test was filmed using a digital camera (30 frames per second), to record information on the finger position. A black dot was drawn on the interphalangeal joint to help with position tracking. The position of the finger was tracked using a program written by an R.A, in the Department of Mechanical Engineering, James Hensman, using Python. This uses some typical point tracking code, based upon statistical thresholds,

in terms of the size of the black dot, and where the dot is in relation to the previous frame. Appendix 10 shows a snap-shot from one of the videos, to highlight how the black dot was selected. Twenty six tests were done, on each texture, at varying loads, between the lightest and hardest force the volunteer could apply. This procedure was then repeated at a humidity of 90 % and a temperature of 30 °C, to view the effects of humidity, both in terms of surface water and water absorption. In this case twelve tests at varying loads were done on each textured surface. Less runs were done since, the previous tests were examining the mechanisms, and these tests are analysing modifications to these mechanisms. Therefore, less data was required to draw conclusions.

8.2 Results

Figure 8.2 shows one of the outputs from a friction test. This shows the characteristics that were present in most of the friction tests. The main characteristic being that there is not a constant force applied. The load was applied by the volunteer; they were told to apply a constant normal force, and are able to achieve this with reasonable accuracy on smooth surfaces. However, on a textured surface the ridges and grooves alter the ease of constant load application, so a constant load was not possible in these tests. The friction force was observed to vary much more than the normal force, indicating a change in friction mechanisms. To enable comparison of the friction across the duration of the slide, and between different textures, with varying normal force, the friction force will be normalised by the normal force (the coefficient of friction), in much of the results analysis.

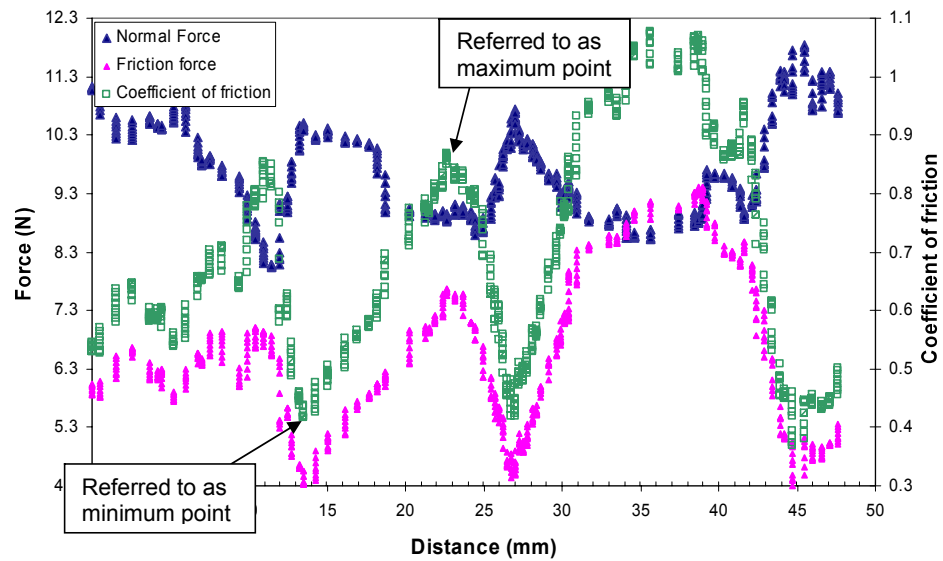


Figure 8.2 – Force and coefficient of friction plot for a test on Texture R4

Figure 8.2 shows that the coefficient of friction is changing constantly, so to compare the influence of the normal force, the points of maximum and minimum coefficients of friction, also shown in Figure 8.2, were compared for each texture. Figure 8.3 shows the results for Texture R4, and the lines of best fit for the remaining textures are shown in Figures 8.4 and 8.5 (Appendix 11 shows the associated equations for the lines of best fit). A linear line fits all the data well, indicating that the friction force varies linearly with normal force at the extremities of the friction measurements. The texture displaying the maximum friction for a given normal force was Texture R2 above a load of 3.5 N and Texture R4 below this load, as shown in Figure 8.4. Both these textures have high, narrow, widely spaced ridges. This figure also shows that the lowest maximum friction force was for Texture S1 (above 2 N), which is a texture with closely spaced ridges. Figure 8.5 shows that the largest minimum level of friction was for Texture W1, which has narrow ridges, but is at the lower end of ridge height and spacing, (above 2 N), and the lowest minimum level was for Texture R3 (above 2 N), this has high, narrow, widely spaced ridges.

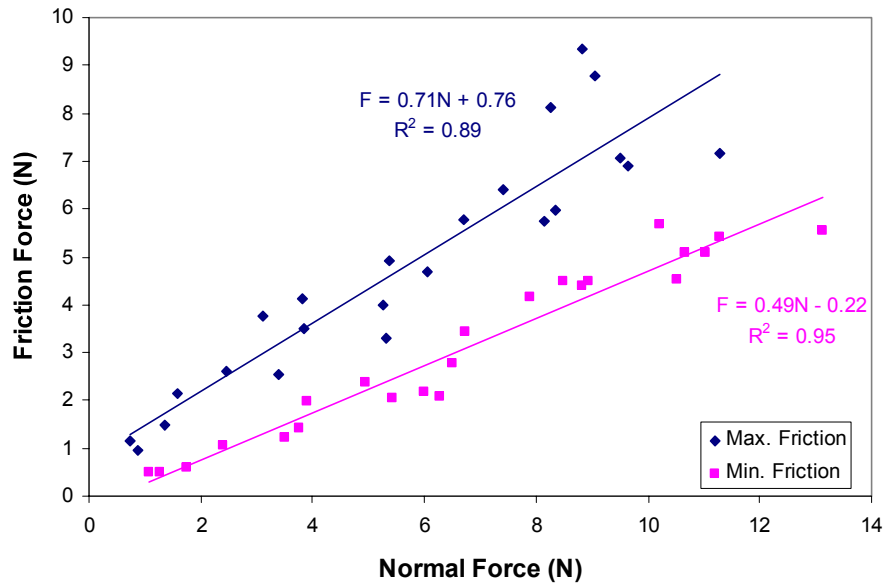


Figure 8.3 – The relationship between friction force and normal force at the points of maximum and minimum friction along the slide

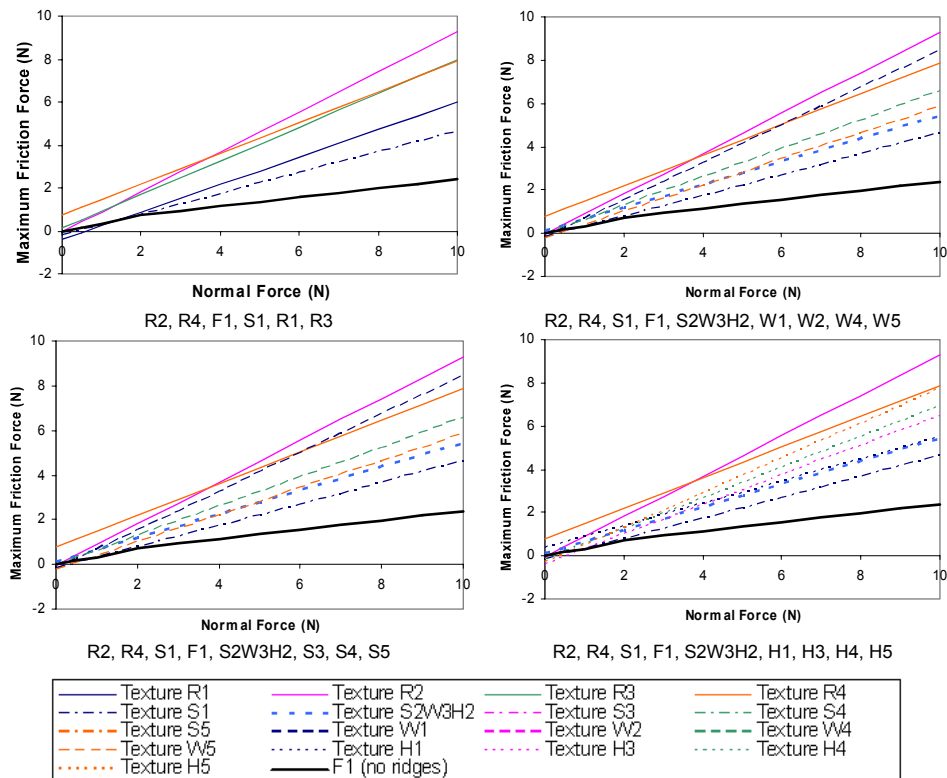


Figure 8.4 – The relationship between the maximum measured friction force (along a slide), and the corresponding normal force, for all textures tested

Chapter 8 Finger Friction when Contacting Large Rectangular Ridges

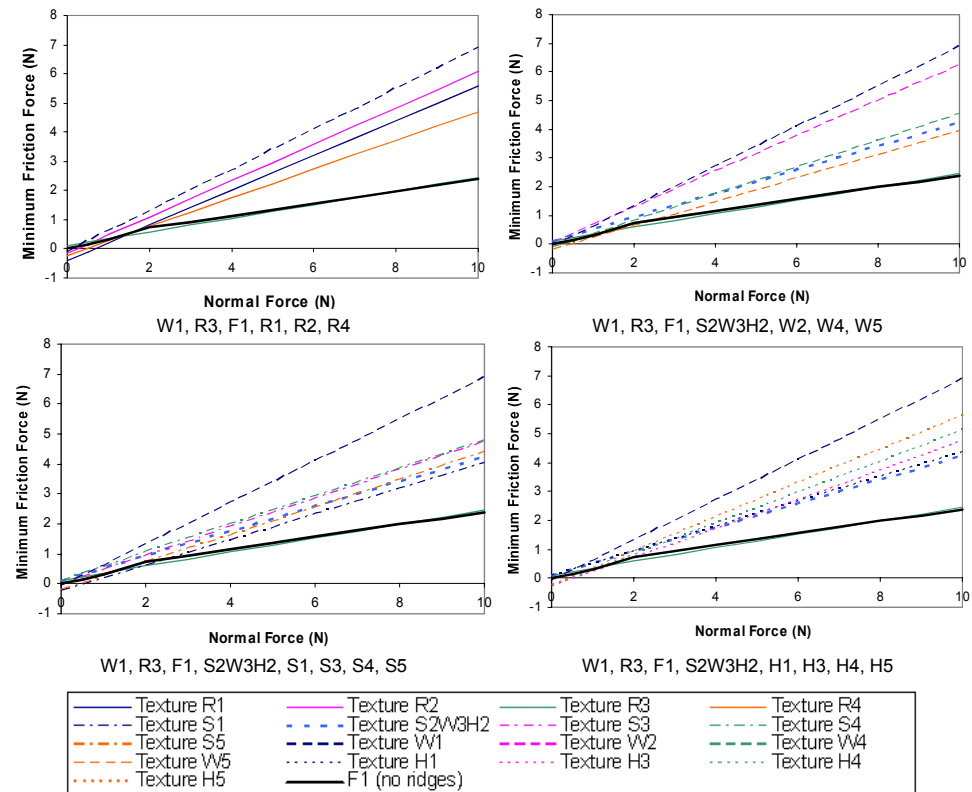


Figure 8.5 - The relationship between the minimum measured friction force (along a slide), and the corresponding normal force, for all textures tested

The friction force against normal force was also plotted for the whole of the transition from minimum to maximum friction, for a finger sliding along Texture R4. The data points were plotted using time as a colour scheme, and can be used to examine the relationship of the normal force and friction force along the slide; this is shown in Figure 8.6. This shows that there is a linear relationship between the friction force and the normal force for the transition between maximum and minimum friction, and from minimum to maximum friction.

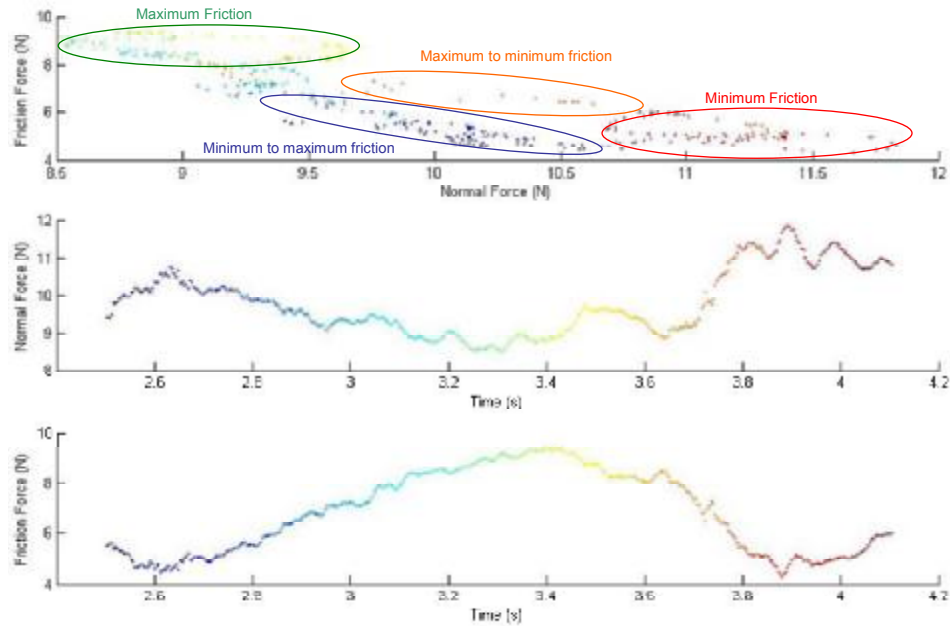
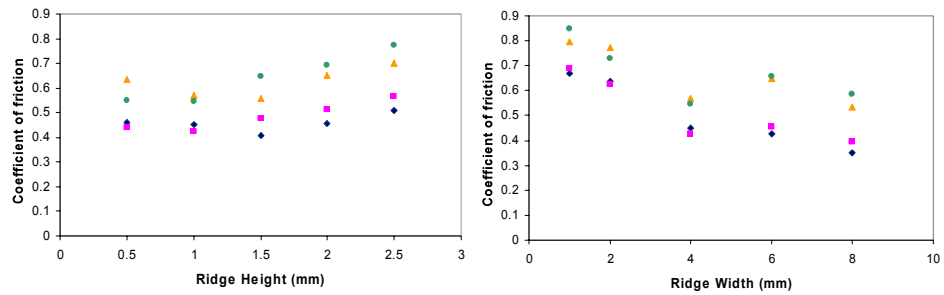


Figure 8.6 – Friction force against normal force for a finger moving across Texture R4; examining the relationship between friction force and normal force for the transition between minimum and maximum friction

Figure 8.7 shows how separately varying height, width and spacing can affect friction; the minimum and maximum coefficients of friction for loads of 3 N and 10 N are calculated from the lines of best fit, shown in Figures 8.4 and 8.5. It shows that for heights above 1 mm there is an increase in friction. There is a reduction in the coefficient of friction when the width of the ridges is increased, but then after about a width of 4 mm, the change in width has little effect on the overall friction. Increasing the spacing of the ridges increases the friction up until a ridge spacing of 10 mm, where the coefficient of friction reduces. The rate of increase also reduces between a spacing of 7 mm and 10 mm. To further understand the effect of ridge dimensions on friction, the difference between the maximum and minimum coefficients of friction, for each texture was analysed, as shown in Figure 8.8. This illustrates several points: firstly, the texture with the most consistent coefficient of friction is Texture R1; and secondly, it begins to show how much the ridge height, width and spacing contribute towards increasing friction. Figure 8.8 would initially suggest that the spacing of the ridges has

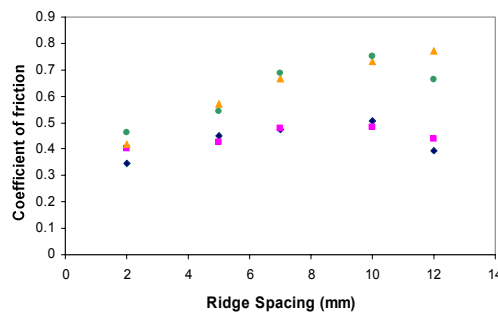
Chapter 8 Finger Friction when Contacting Large Rectangular Ridges

the largest effect on how much the friction increases, at the point of maximum friction.



a) variation in height, ridge width = 4 mm, ridge spacing = 5 mm

b) variation in width, ridge height = 1 mm, ridge spacing = 5 mm



c) variation in spacing, ridge height = 1 mm, ridge width = 4 mm



Figure 8.7 – Dependence of coefficient of friction upon dimensions of ridges

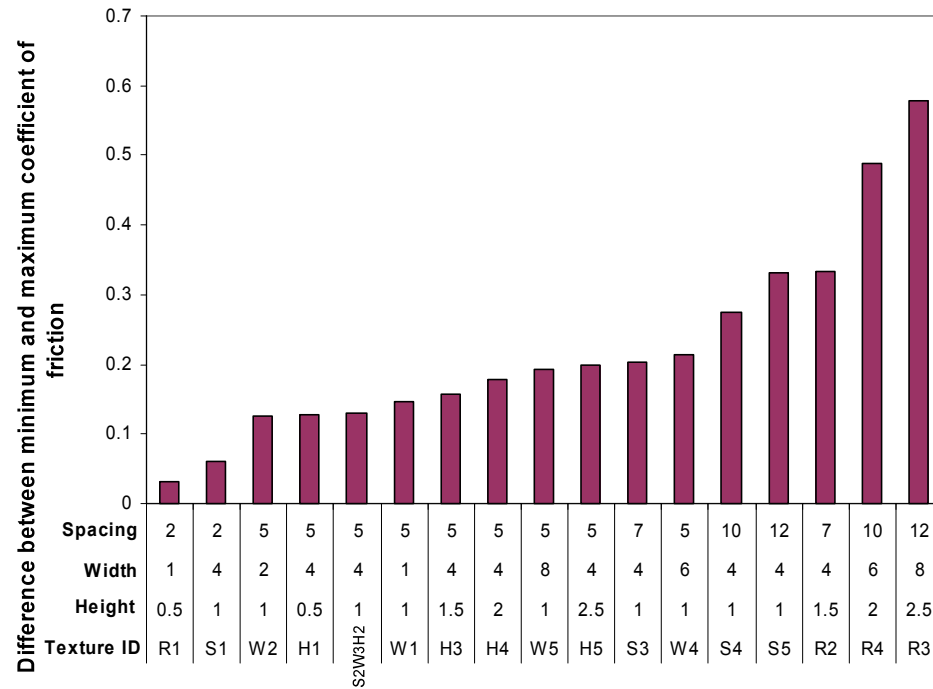


Figure 8.8 – the difference between the maximum and minimum coefficient of friction for each texture tested, averaged across all loads tested. All dimensions are in millimetres.

The friction force was found to increase at high humidity, for all textures tested. The magnitude of this increase was dependent upon the texture tested; the increase for each texture is shown in Figure 8.9. However, at first glance, there are no features highlighted as having a predominant effect on the friction increase.

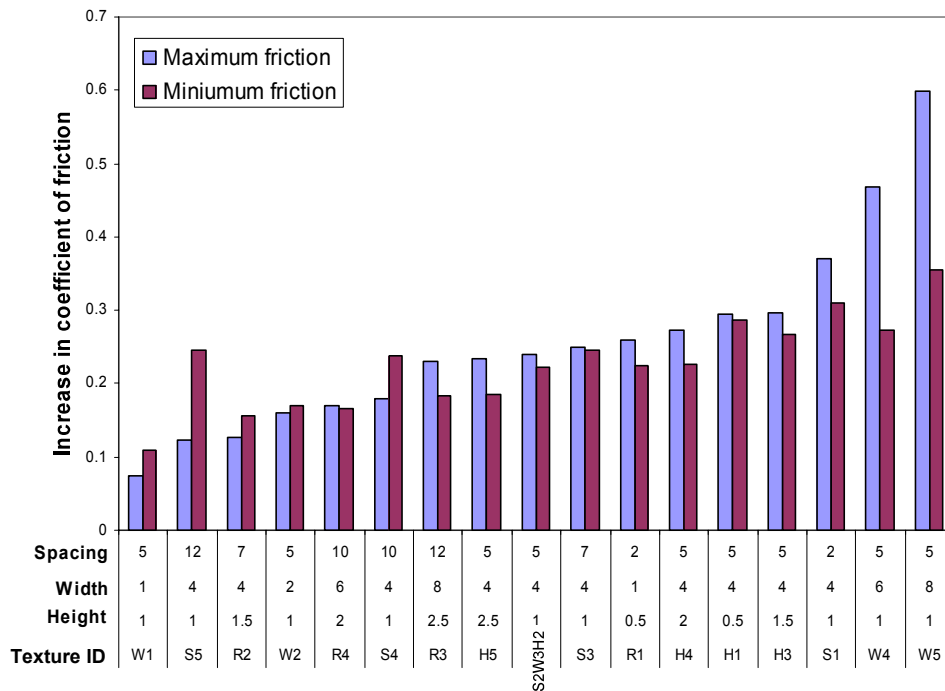


Figure 8.9 – the increase in coefficient of friction at the maximum and minimum friction points for one slide, averaged over all forces tested, for increased humidity and temperature. All dimensions are in millimetres.

8.3 Discussion

8.3.1 Friction Mechanisms

The overall friction can be understood by considering the model of friction formed in Chapter 5. However, in this case there are two more mechanisms to consider. One is ploughing friction (F_p); due to the ridges causing the skin to deform, so there is a volume of skin in front of the ridge. For the finger to move along the surface, the ridge has to move or ‘plough’ this skin out of its path. Second is the reduction in friction force (F_e) due to the energy return created when the ‘ploughed’ skin reforms to its original shape. These two mechanisms are considered separately in this case, as opposed to the previous chapter where the mechanisms were considered together as hysteresis friction. This is due to the scale of the ridges meaning that the mechanisms are operating separately, depending on where the finger is on

the texture, and the ridge dimensions. This means that the overall friction can be described using Equation 8.1.

$$F_T = F_a + F_p - F_e \tag{8.1}$$

where F_T is the total friction force and F_a is the adhesive friction

To gain a better understanding of the contributions of adhesion, ploughing friction and the reduction in friction due to the finger returning to its original shape, the positioning of the finger, related to the friction measurements was analysed; this can be seen in Figure 8.10.

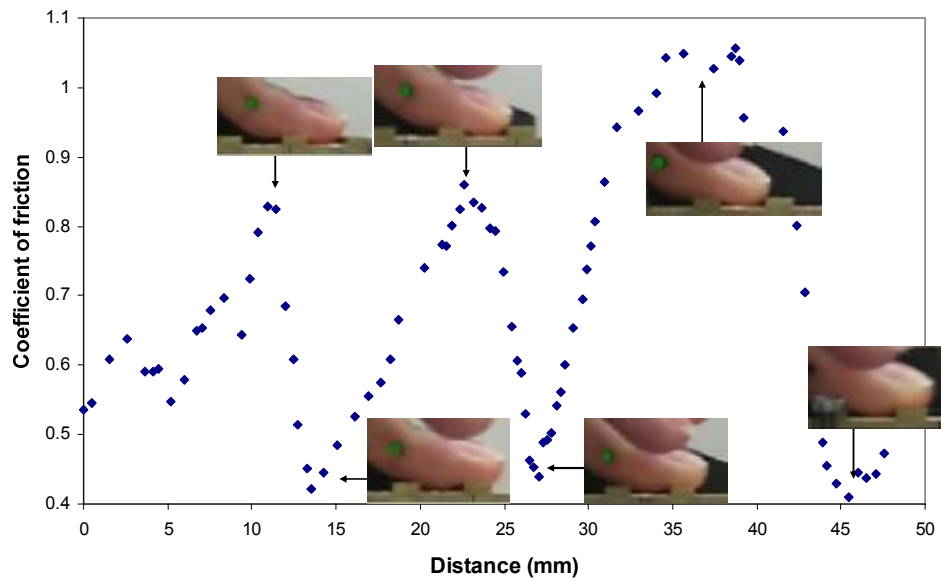


Figure 8.10 – The position of the finger at maximum and minimum friction for Texture R4

Analysis of the position of the finger along the slide enables the friction mechanisms to be better understood. The slide, along Texture R4, can be split into four sections, as illustrated in Figure 8.11. Figure 8.11 shows the deformation expected for loads above 2 N. At lower loads, the deformation

of the finger and area of contact will be less. The figure shows that at the point of maximum friction, the ploughing friction is also at a maximum, but the adhesion is at a minimum. This illustrates how ploughing friction has a large influence on the overall friction measurement; ploughing friction is also present in all stages. The reduction in friction is due to a combination of a reduction in ploughing friction and an energy return from the finger returning to its original shape. The finger then reaches a point of minimum friction, this is just before any large amount of ploughing friction is present, and is also the point of maximum adhesion. Then as the finger continues to move, ploughing friction is present, but not to the maximum degree, due to the positioning of the finger, reducing the area of skin directly contacting the front of the ridge. There is also still an energy return from the finger deforming back to its original shape, until the point of maximum friction is reached.

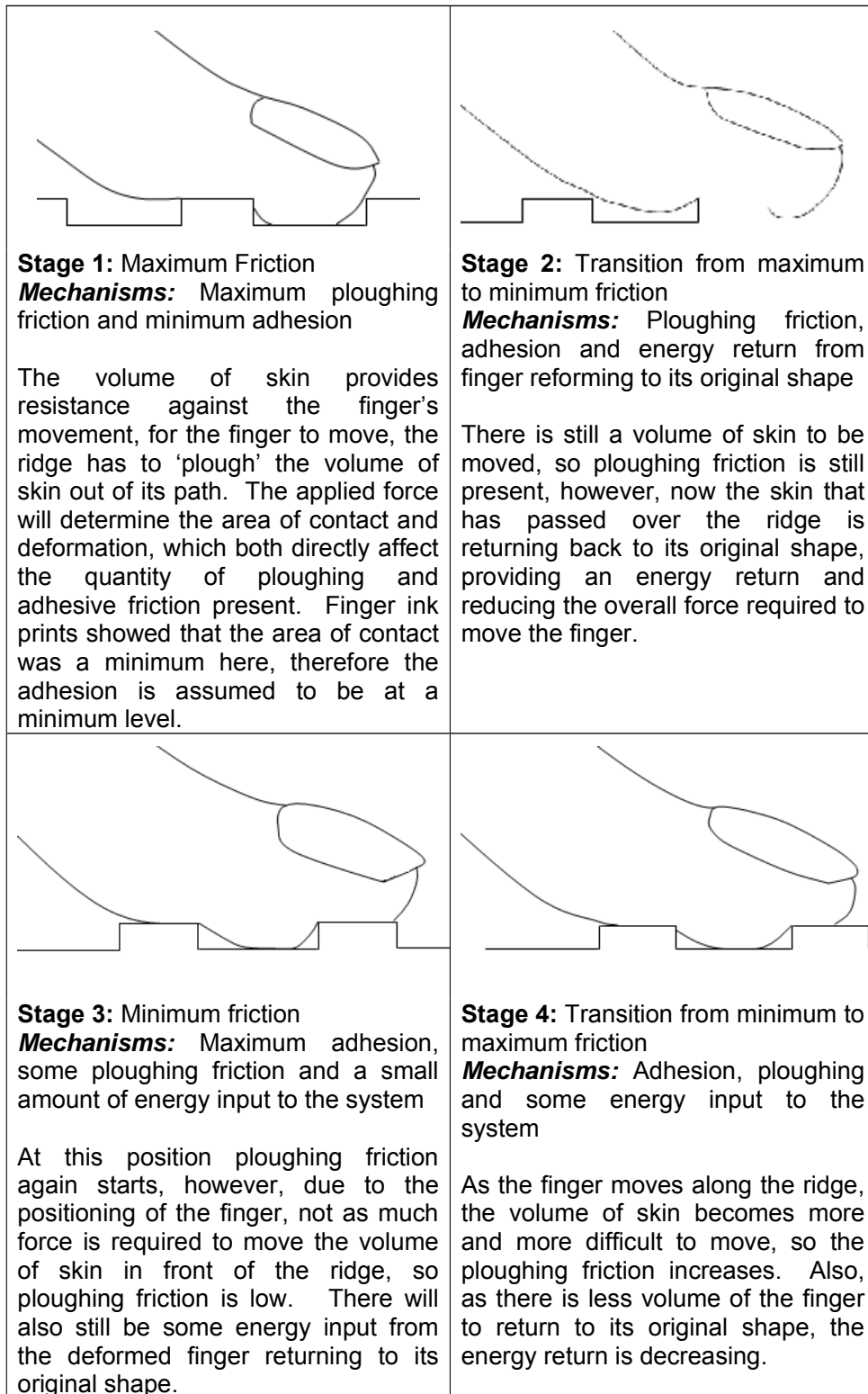


Figure 8.11 – mechanisms of friction as the finger moves over Texture R4

The amount of finger deformation, and therefore the amount of ploughing friction and adhesive friction will vary both with normal force and with the dimensions of the surface. The positioning of the finger was plotted in a similar way to in Figure 8.10, for the other textures, and the area and positioning data could be correlated to that seen for Texture R4. The position of the finger for maximum and minimum points of friction, along the same slide, at forces greater than 2 N, for the other textures, are shown in Appendix 12. However, with differing amounts of each mechanism at each stage; for example, in some cases there is always an energy return. The generalisation of this will be discussed later in this chapter. Understanding how the positioning of the finger relates to the friction force, can help to explain why in Figures 8.4 and 8.5, there is a force at which some of the surfaces start to have greater friction than some others. A change in the area of contact, and also the depth of penetration of a ridge into the finger skin, could be responsible for this observation.

Assuming that the adhesive friction can be predicted using a similar relationship as found for a flat plate, as shown in Equation 8.2 (valid for brass and loads greater than 1.6 N), the amount of adhesion can be predicted (the calculation of the equation is shown in Appendix 7, and explained in Chapter 5). Finger ink prints were used to estimate the area of contact.

$$F_a = 2337 \cdot A + 0.22 \cdot N \quad 8.2$$

where A is the real area of contact and N is the normal force

Once the adhesive friction was calculated, this could be subtracted from the total friction. The ploughing friction and energy return had to be estimated, based on some assumptions assumed from the results. It is assumed that the remaining friction results from ploughing friction, and friction reduction from an energy return. There are points on the slide when there is no energy return, so the ploughing friction could be calculated directly from the data at

these points. That is the adhesive friction was subtracted from the total friction, since at this point on the slide the only friction mechanism is assumed to be the ploughing friction, the remaining friction was said to be ploughing friction. It was assumed that in ploughing friction the finger behaves as a linear spring. This assumption is based upon the linear relationship found between the friction force and normal force both at maximum and minimum friction points along the slide. The linear relationship was calculated for the region of the slide where there was no energy return. This was then extrapolated for the rest of the slide. The energy return was then assumed to be the difference between the estimated ploughing friction and the measured friction. This allowed the different friction mechanisms to be crudely estimated for this one slide, at the applied load. The results are shown in Figure 8.12.

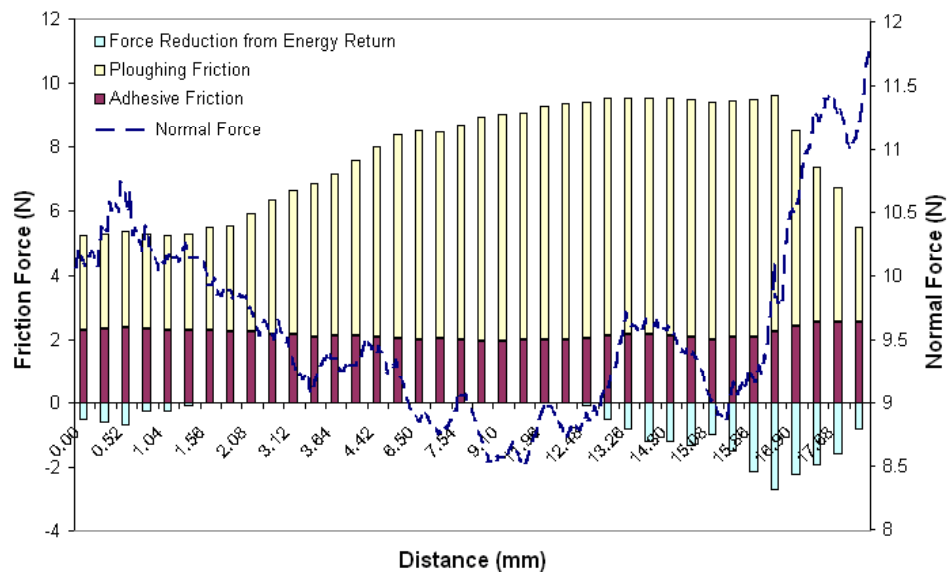


Figure 8.12 – the estimated contribution to the total friction of the different friction mechanisms, for a finger moving over part of Texture R4

Figure 8.12 shows that adhesion does alter along the slide, as the normal force and area of contact varies, however in terms of the overall friction, it is

fairly constant throughout the slide. This shows that the main contribution to the increase and decrease in normal force is the change in ploughing friction as the finger progresses along the slide. Possible methods of predicting the amount of each friction mechanism for a given texture will be discussed later in the chapter. However, the current experimental data does not provide enough information about the contact to accurately model the friction, so only the formation of the model will be discussed.

8.3.2 Friction Prediction

The tests in this study have provided information about general trends of friction related to texture dimensions, but it does not provide information on a prediction of overall friction. To enable this, further work needs to be done.

Figure 8.6 shows that the transition from maximum to minimum friction (stage 2) is linear. This indicates that the finger can be modelled as a linear spring, with the compression in the opposite direction to travel. This means that ploughing friction could be predicted using Equation 8.3. However, the spring constant (k) is a function of the volume of the finger (V) deformed in front of the ridge, which is a function of the normal force (N), width of the ridges (w), height of the ridges (h) and ridge spacing (s), as described in Equation 8.4.

$$F_p = k \cdot x \tag{8.3}$$

where x = distance travelled along the surface

$$k = f(V) \text{ and } V = f(N, w, s, h_r) \tag{8.4}$$

This means that for a prediction of ploughing friction, for any ridged texture, the amount of deformation of the finger needs to be predicted. This is not a trivial issue, since the Young's modulus of the skin is variable, and also dependent upon load, ridge width, ridge spacing and ridge height. Currently,

it is thought that the best method of modelling such deformation, or creating a prediction for such deformation, is to use a finite element model.

In each stage of the slide, excluding stage 1, there is a reduction in friction force due to energy recovery from the finger returning back to its original shape. Usually to account for this, a loss fraction is used, however, this needs to be loading specific. This data is currently not available and would need to be found experimentally. This again is not trivial, since the loading direction needs to be adhered to, but also the loading rate. The loading rate will vary depending on the ridge width and spacing. Using the model of a spring, the energy release is similar to the spring returning to its original shape. However, due to the viscoelastic nature of the finger, this is not 100 % efficient, which is where the loss fraction comes into play. The data in this experiment could be used to approximate the loss fraction, depending on the accuracy of the ploughing and adhesive friction predictions.

Prediction of adhesive friction suffers with similar problems to the prediction of ploughing friction, in that it is deformation dependent. Therefore, a finite element model would again be needed to calculate the area of contact. Depending on the accuracy of this model, the roughness could be added to the model, or the nominal area of contact could be calculated using the model and then a ratio of 0.22 for the real to nominal area of contact can be assumed [120]. The adhesive friction was predicted previously in this chapter using the assumption that Equation 8.2 is transferrable to a ridged surface. In doing this it is assumed that the pressure across the area of contact can be averaged, and therefore the shear force can be averaged. This may not be the case since the shear force is pressure dependent, as shown in Equation 8.5 [74].

$$\tau = \tau_0 + \alpha \cdot p \qquad 8.5$$

where τ is the interface shear stress, τ_0 and α are system dependent constants and p is the average contact pressure

There will be a larger pressure on top of the ridges than in the grooves. There will also be a concentration of high pressure where the edge of the ridge contacts the skin. These factors could mean that the basic prediction used previously in this chapter is not substantial enough. This needs to be investigated further.

Additional factors to consider are the positioning of the finger, which will also affect the friction, although to a lesser extent than the deformation. For example, there may be some energy input from the change in potential energy, from the finger moving from the top of the ridge back to resting in the groove.

8.3.3 Influence of Ridge Dimensions on Friction Measurements

Texture R1 was tested, since it has very similar dimensions to the textures tested by Bobjer *et al.* [64]. Bobjer *et al.* found that in dry conditions the friction decreased with the presence of ridges, this is different to what has been found in this test. For example, one of Bobjer *et al.*'s textures had ridges of 1 mm width, 1 mm spacing and 0.5 mm height, compared to Texture R1, with ridges of 1 mm width, 2 mm spacing and 0.5 mm height. Bobjer *et al.* found that at a normal force of 10 N the friction coefficient was 0.74, compared to 1.01 in the smooth surface tests. For Texture R1 in these tests, at 10 N, the minimum friction coefficient is 0.56, compared to only 0.24 for the finger on a smooth surface. It is the case for all the textures, excluding Texture R4, that in all instances, the minimum friction is greater than that for a flat surface (as illustrated in Figure 8.5). Adding a large dimensioned texture to a surface is expected to reduce the amount of adhesive friction, from the smooth case, due to the reduction in contact area,

however, ploughing friction increases the overall friction. The measurements in these tests have shown that ploughing friction contributes more greatly to the overall friction, than the adhesive friction lost due to reduced contact. Texture R4 in the minimum friction case, has a friction measurement similar to that for a smooth surface. This is because the surface has wide ridges and very wide spacing. Consequently there is very little ploughing friction and very little energy return, at the minimum level of friction, so adhesion is the main contributing mechanism to friction; hence, it is similar to the friction for the case of a smooth surface.

There are several reasons why the results may differ in this experiment compared to that of Bobjer *et al.*; the material used in Bobjer *et al.*'s tests was polycarbonate, in these tests it was brass. However, viewing the variation in friction between the metals and polymers in Chapter 4, this is not expected to have such a large effect on the general friction trend. The measured coefficients of friction on the smooth are 1.01 for the polycarbonate and 0.24 for brass, however, these are not comparable, since they were done on different people, and the tests in Chapter 4 showed that the friction force, for the same applied load varies greatly between people. The corners on Bobjer *et al.*'s textures were rounded (0.03 – 1 mm), this small amount of rounding could have a large influence on reducing ploughing friction, and also perhaps reducing adhesion, due to a reduction in the stress concentration at the ridge edge. The testing conditions cannot be compared, however they do seem to be similar; Bobjer *et al.* tested at a temperature of 20 – 22 °C, and stated that the tests were done in ambient conditions. The final difference could be related to the condition of the finger. Bobjer *et al.* tested 14 male volunteers, in this test the finger belonged to a female. There was no difference in the general friction mechanisms between people on a flat surface, but there may be some seen when a texture is added to the surface. The amount the finger deforms will greatly affect the amount of ploughing friction, if this is much less for men than women (or more for the female tested), then less ploughing friction will be present. More work needs

to be done to analyse how texture changes the friction of a finger contact, for people of different gender, age and race.

Figure 8.7 shows how the friction coefficient changes when either the height of the ridges, the width of the ridges or the spacing of the ridges is varied. The figure shows that after a height of 1 mm there is an increase in the coefficient of friction with ridge height. However, the ridges only went to a maximum height of 2.5 mm. In Chapter 7, it was found that the finger could be compressed by approximately 7 mm when using a 0.5 mm thick, rectangular indenter, whereas it could only be compressed by 4.7 mm when using a 0.85 mm thick, rectangular indenter. This indicates that depending on the width of the ridge, there will be a limit to the amount the ridge can compress the finger. The amount of compression directly affects the volume of skin in front of the ridge, therefore, at this point, it is predicted that the effect of ridge height upon the coefficient of friction will plateau, as a plateau in the amount of ploughing friction is reached.

Figure 8.7 also shows that the coefficient of friction reduced with increased ridge width, until a width of 4 mm, but then little effect was seen. Using the current data this cannot be compared, however it is predicted, that as seen with the two indenters, a narrower piece of material is able to penetrate deeper into the finger. Since the amount of ploughing friction is related to the depth of penetration of the ridge into the skin, the ploughing friction will increase with a narrower ridge.

Figure 8.7 shows that the coefficient of friction increases with ridge spacing, up until a spacing of 10 mm, at which point the coefficient of friction reduces. Again, this is mainly due to ploughing friction. As the spacing increases, there is more deformation of the finger possible, therefore there is a greater volume of finger directly in the ridge's path, and this increases the ploughing

friction. Viewing all the textures below a spacing of 10 mm, there is always more than 1 ridge in contact with the finger, however, for the 12 mm spacing, there are points where the finger is just in contact with two ridges, but the majority of the time, the finger is only in contact with one ridge. Due to the narrow width and low height of the ridges, there seems to be always be a small amount of energy return, which will be reducing the overall friction throughout the slide.

Figure 8.8 shows the difference between the maximum and minimum friction for each texture (consistency of friction along the slide). It shows that the spacing seems to have the greatest effect on the friction increase from the minimum to maximum points, therefore the amount of ploughing friction. From visual analysis of how the finger deforms on each of the surfaces, this can be attributed to the finger being able to deform more when there is large spacing. This increases the volume of the finger the ridge needs to displace, thus increasing the ploughing friction. The figure also shows that Textures R1 and S1 are the most consistent. This is because the spacing of ridges is narrow, so there is less deformation of the finger, and therefore less ploughing friction. The same follows for the least consistent textures; Textures S5 and R2, in that they have large spacing between ridges, which increases the deformation of the finger and therefore the ploughing friction.

To summarise; in designing a ridged surface for grip, the maximum friction occurs when there is maximum spacing, up to a point (10 mm in this case). This is because wider spacing allows more deformation of the finger and therefore an increase in ploughing friction. However, if consistency is required, a high level of friction has to be sacrificed, and narrow ridges used. The needs of the design will depend on the way in which the item is gripped, if no slipping is required then large ridges are useful, since the user can position their hand at the point of maximum friction. The width of the ridges had little effect, in these tests; however, narrow ridges are thought to be better, as they allow the finger to deform more. The ridge height should be as high as possible, but it is predicted that there will be a cut-off point to this,

where increasing the height may well start to decrease friction, or at the least a plateau in friction will be observed.

This analysis gives a general idea of how a ridged surface can be designed to optimise grip. However, it needs to be coupled with another study analysing comfort and perception, for each of the surfaces. The large scale of the ridges was useful to observe the different friction mechanisms at work; however, the very large ridges are probably impractical for the majority of grip designs. It is also predicted that in terms of comfort, brass is not the best material to use. A hard elastomer was used in some of the surveyed gripping applications (Appendix 8), but this may deform at certain points, and adhesion may play a much larger contribution to the overall friction, as observed for the friction tests on flat elastomers in Chapter 4. Therefore, the mechanisms may need to be re-assessed for this material category.

8.3.4 Affect of Increased Humidity on Friction

Figure 8.9 shows that there is an increase in both the maximum and minimum friction measurements for all the surfaces, when the humidity and temperature were increased from 45% and 20°C to 90% and 30°C, respectively. However, the increase is not the same for all textures, and there is no clear indication from this figure, what feature of the surface texture is causing the increased friction.

In Chapter 6, moisture addition (or a change in humidity), was found to increase friction on a flat surface by increasing the area of contact, and therefore the amount of adhesion possible. The primary mechanism for this was a reduction in the Young's modulus of the stratum corneum, when it absorbed water, and the secondary mechanism was capillary adhesion. To investigate if the increase in friction is due to a possible increase in area, the increase in coefficient of friction was plotted against the length of the top of

ridges presented to a 10 mm length contact (length illustrated in Figure 8.13); shown in Figure 8.14. There is a lot of scatter in this figure; however, the general trend is increasing coefficient of friction with increase in ridge area. This implies that an increase in adhesion is contributing to the increase in friction. To estimate whether adhesion was contributing to the total friction increase, an assumed average normal force of 6 N and Equation 8.2 were used, to equate the change in coefficient of friction to the necessary change in area. This calculation showed an increase in contact area varying from 52 to 421 mm² across all the textures. This is an extremely large increase in contact area, and considering the nominal area of contact on the flat surface, at a maximum, is only 194 mm², such a large increase is not possible. There are errors in this calculation, due to the assumption that Equation 8.2, which was calculated for a flat surface, is applicable to a ridged surface. However, it could also mean that the moisture can modify the ploughing friction mechanism. The stratum corneum was measured by Egawa et al. [124] and found to be 173 μm thick on the palm, so water absorption will not greatly affect the deformation of the whole finger, however, since there are sharp corners on the textures, an increase in the deformability of the thin but contacting stratum corneum, could serve to increase ploughing friction.

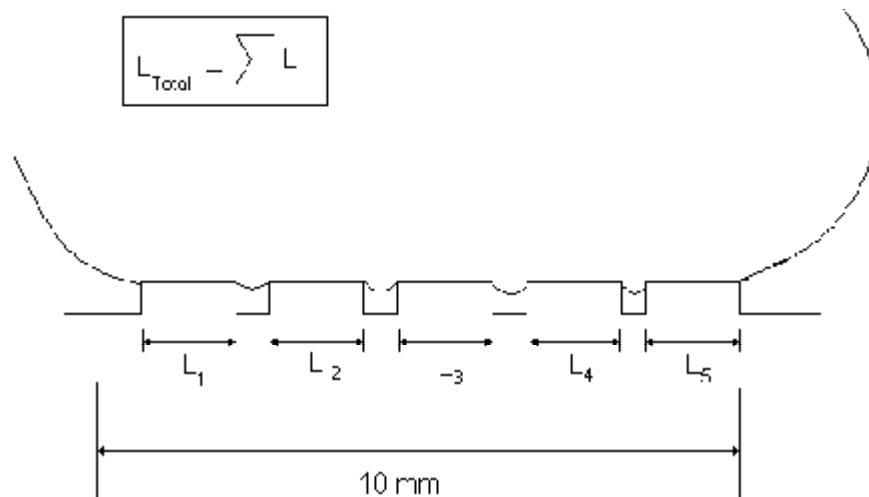


Figure 8.13 –definition of the length of the top of the ridges presented in a 10 mm contact (L_{total})

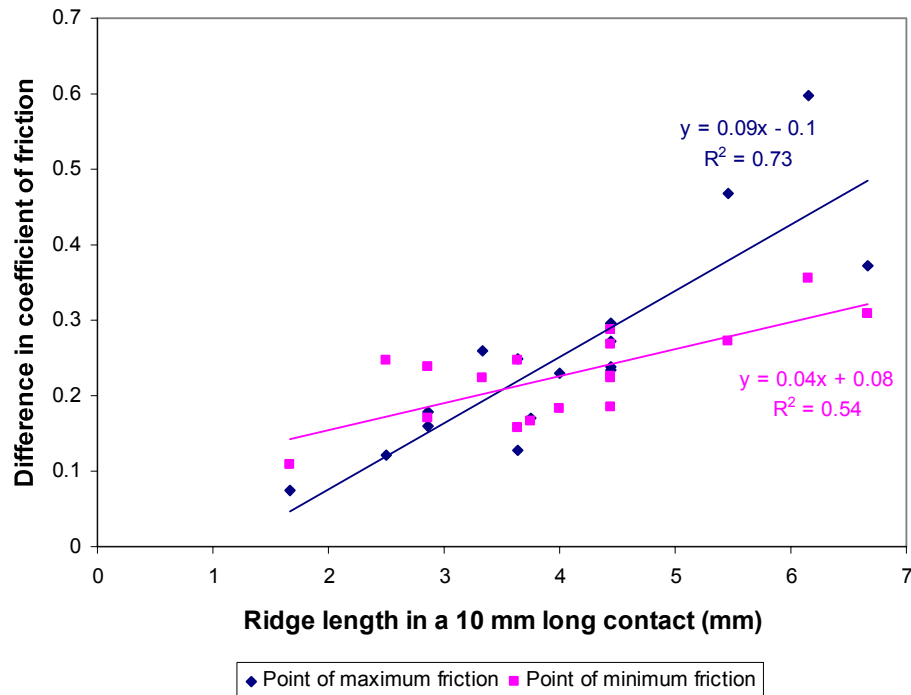


Figure 8.14 – the increase in the average coefficient to friction plotted against the length of ridge tops, along a 10 mm contact

8.4 Conclusions

The main contributions to friction for the finger moving over large rectangular ridges are from adhesion, ploughing friction and a reduction in friction due to the finger reforming back to its initial shape. The slide can be split into four stages. In stage 1, when there is a large volume of the finger in front of and contacting the ridge, the maximum friction is reached. The friction mechanisms are adhesion and ploughing friction and depending on the ridge dimensions there will sometimes be energy return. In stage 2, there is a transition between maximum and minimum friction, the total friction is due to a contribution of energy return, adhesion and ploughing friction. These three mechanisms are also present in the other two stages, where the finger is at minimum friction and then the final stage of progression from minimum to maximum friction. These mechanisms have been recognised by examining the behaviour of the finger in contact with the surfaces, however, further work

needs to be done to quantify the contributions of each friction mechanism to the overall friction, for any given ridge texture.

To design for high friction, large ridge spacing is required (at a maximum of 10 mm), and the ridges should be high and narrow. However, as explained, the friction moves between maximum and minimum points, and this type of texture will have a large difference between the maximum and minimum friction. For a more consistent friction force, the spacing should be narrow, although this will be to the sacrifice of high friction.

9 Relating Finger Friction to Rugby

This chapter addresses how finger friction measurements can be applied to the design of rugby balls. Several designs of rugby ball were compared to assess the effectiveness of the grip provided by the pimple patterns. This study verified that the method of finger friction tests used throughout this thesis is suitable for this type of application and also provided initial findings for the design of future rugby balls. Some of the testing was done alongside a fourth year undergraduate final year project, in these cases the testing was done together and we both independently analysed the results, to meet our specific research objectives. Additional test results have also been taken and re-analysed from a previous MEng thesis [83].

The contact of a finger with rugby ball surfaces is a complex problem, which draws on understanding developed in the previous chapters of this thesis. The rugby materials are elastomers; minimal deformation was found for the flat elastomers, but there may be increased deformation of the pimples (on the rugby ball surface). The surfaces are textured; having a variety of different pimple designs. The different sizes, shapes and distributions of the pimple will alter the friction, to understand how these factors affect friction, information can be drawn from the work done on ridges. There will be moisture in the contact; on a rainy day, at night time from dew, or on a sunny day when the hands are sweaty. This is an additional factor to consider, and the work done in the moisture chapter aids the understanding of this. There are also additional complexities to the problem, which have not been examined in this thesis, such as contaminants (e.g. mud and sand) and temperature.

9.1 Introduction to Rugby and the Need for Friction Tests

The International Rugby Board (IRB) rules specify the ball's size and weight along with material. However, the material specifications are very broad.

These rules state that 'The ball should be manufactured from leather or suitable synthetic material. It may be treated to make it water resistant and easier to grip.' [125]. Hence, there are many different balls on the market, made by numerous manufacturers, from a range of materials and with different surface patterns.

Since rugby is played more or less throughout the year, the ball needs to perform in a number of different weather conditions, which can all affect the handling of the ball. There are three main changes to consider under different weather conditions; the moisture level of the contact; the temperature; and the nature of and amount of any interlayer material, e.g. soil. There is currently no other work found in the literature, which has reported the changes these factors have on the grip of a rugby ball.

There are many ways in which the hands contact the ball in a game. This can be in the form of passing the ball, catching the ball, from hand kicks or running with the ball. This study concentrated on passing and catching the ball. The lateral pass is the most basic of passes and forms the fundamentals of many situations, for example, pass off the floor and pass out of a tackle. To make a lateral pass over larger distances the ball is generally spun about its long axis, travelling point first. This is known as a spin pass. The spin pass will be used in this study as it is frequently used during a game.

The testing procedure consisted of three experiments, with the aim of determining the different mechanisms for catching and throwing the ball; analysis of ball performance in a game; and comparison of ball performance in more controlled conditions.

9.2 Method of Testing Rugby Balls

9.2.1 Ball Surfaces Tested

The rugby ball surfaces used in this study were chosen to represent a range of different balls. These surfaces are shown in Figure 9.1.

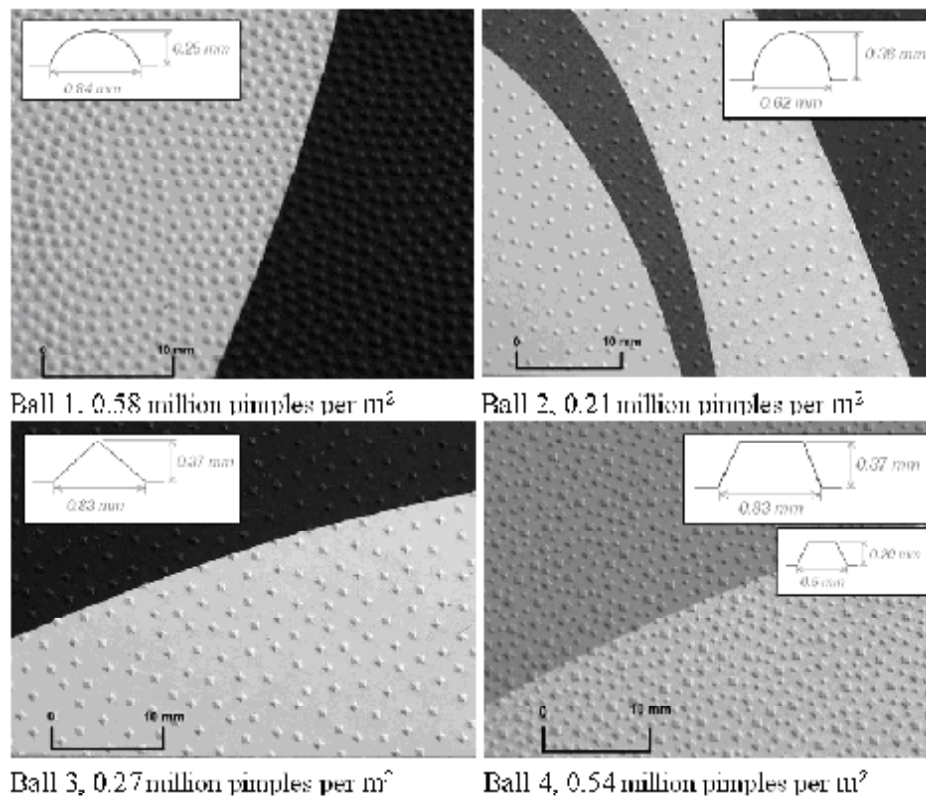


Figure 9.1 – Rugby ball surfaces used in testing.

One surface used in the tests, not pictured in Figure 9.1, is a smooth rugby ball with no pimples, this Smooth Ball is not in production, but has been used in these tests to provide a base comparison. The surfaces of Balls 1 and 2 both consist of round pimples, however, the pimples of Ball 1 are much larger and more densely populated (approximate spacing of pimples is 0.2 – 0.7 mm for Ball 1 and 0.5 – 2.2 mm for Ball 2). The pimples of Ball 3 are of a similar size and distribution to that of Ball 2 (approximate spacing of 1.1 – 2.6

mm), but they are square-based pyramids. The final surface, Ball 4, is a mixture of large ($\approx 40\%$) and small ($\approx 60\%$), square/cross shaped pimples. The distribution of the pimples is fairly random, but the small pimples do seem to intersperse the larger pimples (approximate spacing of 0.9 – 3.5 mm between large pimples, 0.3 – 2.0 mm between small pimples and 0.1 – 1.1 mm between large and small pimples).

Laboratory condition tests were done on the ball surfaces, alongside in-field friction tests, accuracy tests and high-speed video filming of ball handling. Due to the residue that can be left on the balls from the manufacturing process, all balls and surfaces were washed with washing up liquid and water prior to use. The friction tests involve using the same area of the surface repeatedly and so the consistency of the test results was assessed. This showed that Balls 1 to 4 should be used for between 30 and 70 runs, and the Smooth Ball for between 20 and 40 runs. This was incorporated into the test method, to make sure that surfaces were not over used. The surfaces were also pre-used; that is the finger was run over the new material 20 – 30 times prior to testing; again, pre-use is recommended by the ball producer, due to a residue that is left on the ball from the manufacturing process.

9.2.2 Friction Tests

In the laboratory tests, the temperature and humidity in the room varied from 19 – 24.5 °C and from 38 – 58 %, respectively. Ten participants were tested (1 female and 9 male, aged 19 – 22), against all five ball surfaces. The tests were carried out in the manner explained in Chapter 3. Each test was repeated three times per person. The surfaces were tested in a different order for each person, to average out any unwanted effects due to placing in the test sequence. For tests involving water, dry materials were always used and then the water applied.

There were three levels of water applied to the finger; Case A was a sponge wet finger, more water was applied in Case B by adding water with a fabric tea towel and in Case C the finger was fully immersed in water. In the next set of tests water was added to the material. In case I, one spray of water was added to the material, in case II, three sprays of water were added to the material and in case III, three sprays of water were added to the material and the finger was fully immersed in water before the test.

The in-field friction tests were performed alongside accuracy tests, after substitutions in a university game of rugby. These tested the friction between the middle finger of sixteen participants (male, aged 18 – 22), and four different surface-water combinations. The Smooth Ball and Ball 1 were tested wet (3 sprays of water), and Balls 1 and 3 were tested dry. The environmental conditions for these tests were a temperature of 10 °C and relative humidity of 78 %. The procedure in Chapter 3 was followed, however, participants were not asked to wash their hands prior to the test.

9.2.3 Accuracy Tests

The accuracy tests were composed of a target set up on the side of the training hut, next to the pitch, at a distance of 10 m away from the player. The target was a circle 100 mm in radius, and split into three equally spaced inner circles, shown in Figure 9.2. Each section was scored relative to the distance away from the centre of the target, with a hit in the centre scoring 8 points down to a complete miss scoring 0 points. On the day, the temperature was 10 °C, pressure was 1017 mb, relative humidity was 78%, there was no precipitation and the wind was blustery. The balls used in this test corresponded to the surfaces tested in the in-field friction tests, i.e., Ball 1 wet and dry, the Smooth Ball wet and Ball 3 dry; only one of each ball/condition were used in the tests. The balls were pressurised to a value recommended by the manufacturer (10 psi), this was checked half way through the test, and had not decreased. The water was added to the wet

balls by completely immersing them in a bucket of water and shaking the excess off, this ball was then handed to the player. There was a separate wet and dry Ball 1 to help prevent water addition to the dry ball. The players also wiped excess water from their hands after the wet tests. The balls were given to the players in rotation to counteract the effects of learning or change in condition from previous tests. Each ball was tested three times. Before the tests, the players were allowed a few practise shots with a dry control ball.

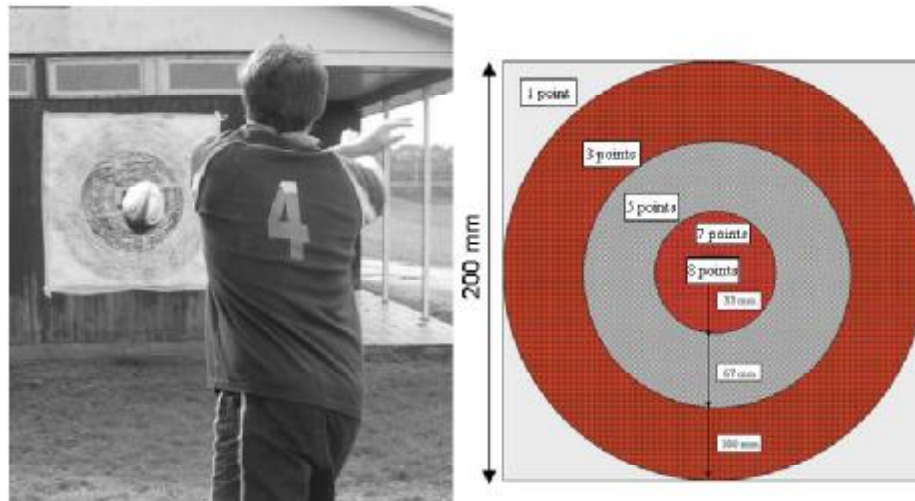


Figure 9.2– Target used in accuracy tests

9.2.4 High Speed Video Filming

To support and understand the findings from the friction and accuracy tests, high speed video filming was used. These were carried out in two separate sessions, with all filming being done indoors. Six university rugby players, aged 21 - 23, who train and play rugby regularly in the field positions of prop, second row, back row, fly half and centre, were asked to throw and catch the ball with good aim, over a distance of 10 m. The balls used in this test were the same balls as the in-field friction and accuracy tests; Ball 1 wet and dry, Ball 3 dry and the Smooth Ball wet. Again, one ball/condition was used (i.e. 1 x Ball 1 Wet, 1 x Ball 1 Dry, 1 x Smooth Ball Wet and 1 x Ball 3 Dry), these

were the same balls as used in the previous tests, for consistency. The balls were inflated to the manufacturer's recommended pressure (10 psi). Each ball was thrown 5 times by each player, in a rotated order. The speed of pass was not specified to them. High speed video recordings (Phantom v4.2) were then used to examine both the passes and catches. The cameras were set up to record the catch, throw and trajectory (filming at 200 frames per second). The recordings were saved as bitmap images and then analysed using a MATLAB® based tracking program, developed by Choppin [96].

9.3 Results from Rugby Ball Testing

The moisture tests carried out in the lab showed that when water was applied to the finger (See Figure 9.3) the quantity of water influenced the change in the coefficient of friction. Adding a small amount of water to the finger decreased the coefficient of friction, however, adding a little more water increased the coefficient of friction to a value above that measured for the dry test. Adding further water resulted in the coefficient of friction reducing once again. When ANOVA Tukey Post Hoc analysis was carried out on these data it was found that the changes were not all statistically different ($p < 0.05$). The statistical differences can be seen on Figure 9.3, where the 95% confidence interval bars do not overlap (e.g. Ball 2 test B and C). Although the differences are not all at $p < 0.05$ level, the changes in mean and comparisons between groups of all balls show recognisable trends. There are large confidence intervals shown, because the properties of the finger vary extensively from person to person.

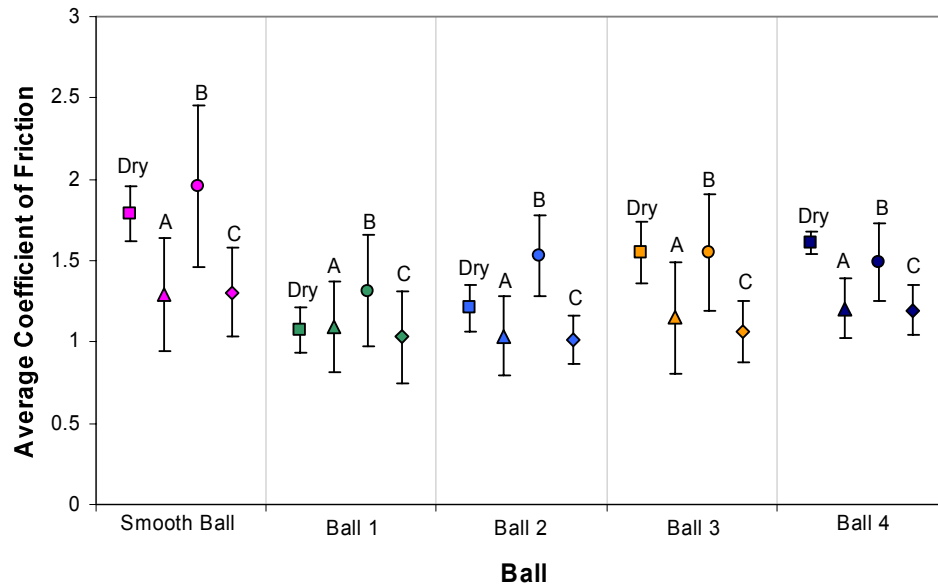


Figure 9.3 – Coefficients of friction when fingers were wet. A is a sponge wet finger, B is a towel wet finger and C is a finger that has been fully immersed in water

Figure 9.4 shows the moisture tests where water was applied to the ball surfaces. These tests show that there is little difference between the three wet conditions. The Smooth Ball, Ball 3 and Ball 4 showed a decrease in coefficient of friction when water was added to the ball, however, no large difference was seen between the dry and wet conditions for Balls 1 and 2.

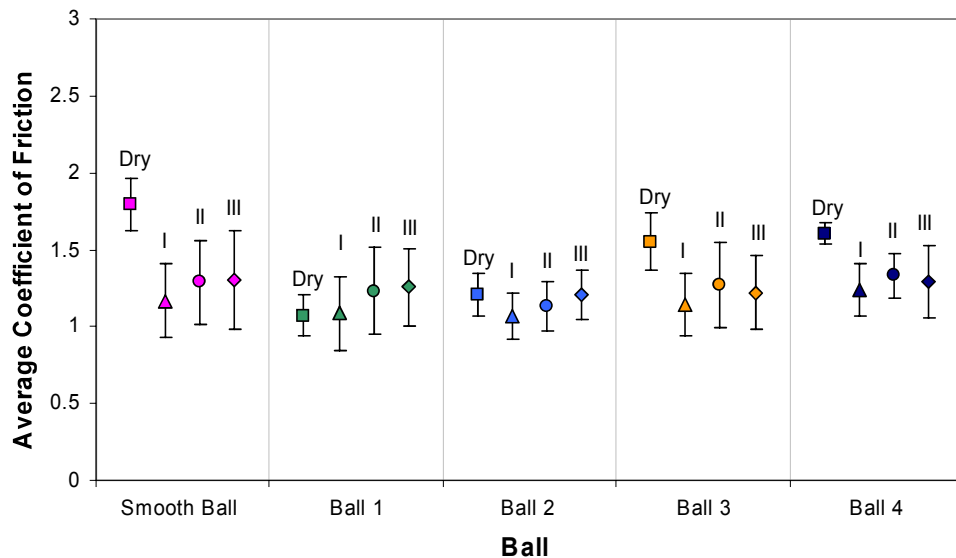


Figure 9.4 – Coefficients of friction when rugby ball material was wet. I is one spray of water on the material, II is three sprays of water on the material and III is three sprays of water on the material and a finger that has been fully immersed in water

Figures 9.3 and 9.4 also show a comparison of the 5 balls in dry conditions. ANOVA Post Hoc Tukey analysis was again carried out on these data and the cases of $p < 0.05$ can be seen by the non-overlapping 95% confidence interval bars. These show that Ball 1 and Ball 2 are not statistically different, nor are the Smooth Ball, Ball 3 and Ball 4. The coefficients of friction of Balls Smooth, 3 and 4 are statistically higher than the coefficients of friction of Balls 1 and 2.

The in-field accuracy tests indicated that the coefficient of friction (see Figure 9.5) of the two dry balls was greater than that of the two wet balls. The error in the accuracy target test is quite large, due to the very nature of the test, in that it is dependent upon player ability as well as ball properties. It therefore, cannot be conclusively said, that there is a relationship of increasing accuracy with greater coefficients of friction. The mean coefficient of friction values with 95 % confidence bars and the mean scores from the accuracy tests are shown in Figure 9.5.

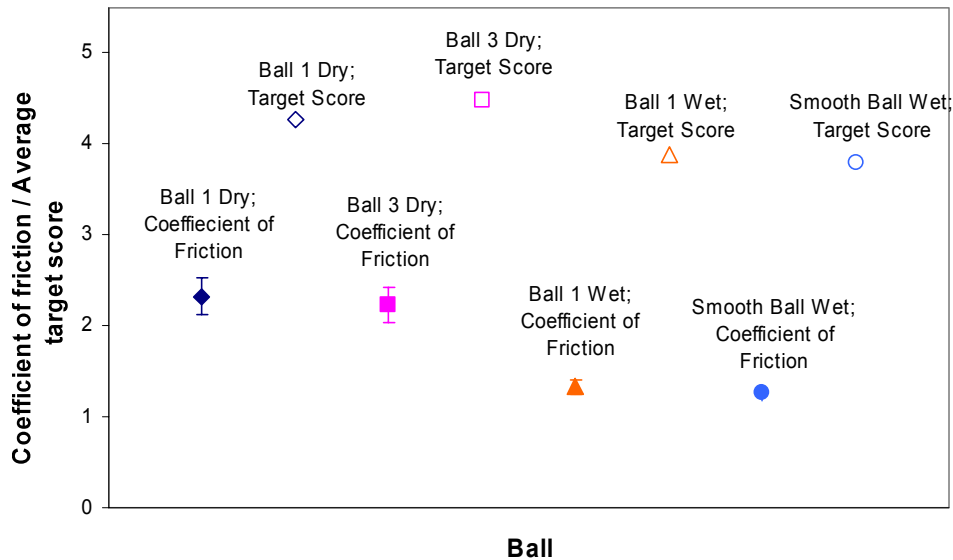


Figure 9.5 – Coefficients of friction and mean target scores

The high speed video filming identified that there was one main type of catch, with a further one seen only once. In the main catch type the top of the palm (part adjoining the fingers) was the first point of contact with the ball. This contact with the palm slows the ball down and then the fingers waver over the top of the ball until choosing a fixed position to clamp down and secure the ball. Figure 9.6 shows the change in position of the fingers, from first contact with the ball until the ball is secured. The time for the player to secure the ball from first contact was 41.5 ± 1.5 ms.

The second type of catch, seen only once, was where the fingertips contacted the ball first. The ball then seemed to slow down smoothly until the palm was in contact with the ball, unlike the more sudden deceleration with the main catching mechanism. Once in contact with the palm, the ball was then secured in the hands of the player. There are no contacting and de-contacting movements of the fingers visible in this case.

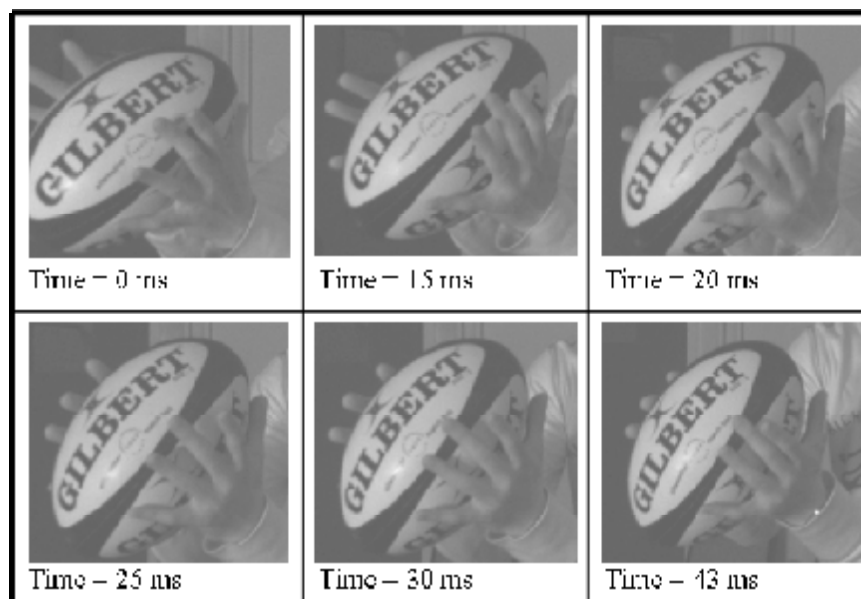


Figure 9.6 – Different stages of the ‘finger wiggle’ on the ball

To throw a ball, the right hand (of a right handed player) grips the ball with all five digits, and the left hand is simply used as support. In the process of providing spin to the ball, the fingers leave contact with the ball surface, one after another. Starting firstly with the thumb and finishing finally with the little finger; the images in Figure 9.7 illustrate this process. The average speed at which the ball was thrown was 10.7 ms^{-1} ($\pm 1.8 \text{ ms}^{-1}$) and the average spin rate was 148 rpm ($\pm 23 \text{ rpm}$). This is slightly lower than reported by Holmes [126] (13.79 ms^{-1} ($\pm 1.48 \text{ ms}^{-1}$) and 219.09 rpm ($\pm 5.26 \text{ rpm}$), however, this is reasonable since the rugby players tested by Holmes were of a professional standard.

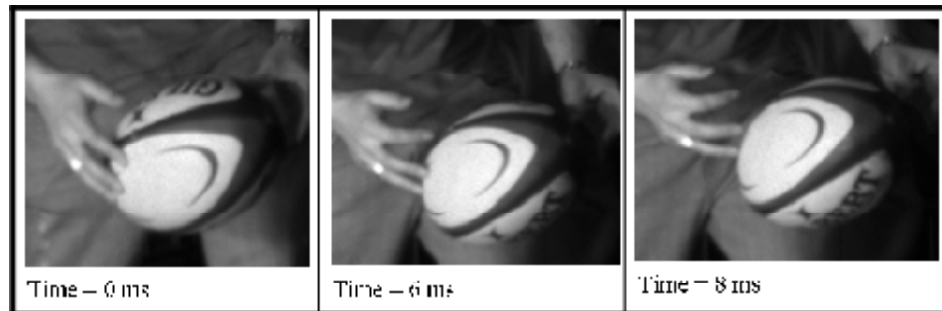


Figure 9.7 – Application of spin to the ball

The spin players were able to apply to each ball is shown in Figure 9.8. This figure shows that players are able to apply less spin to the Smooth Ball wet, compared to the other three balls tested. There was no significant difference between the spin applied to Ball 1 wet and Ball 1 dry. The spin applied to Ball 3 is not statistically different to that applied to Ball 1 wet and dry.

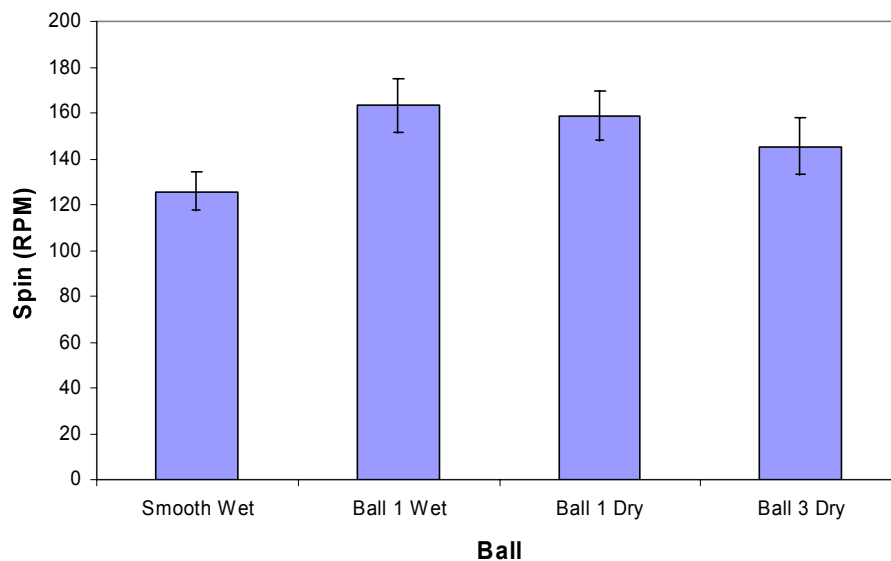


Figure 9.8 – Average spin applied to balls, displaying one standard error

9.4 Discussion of the Results from Rugby Ball Tests

9.4.1 *Mechanism for Catching a Ball*

It is known that to lift an object, the frictional properties of the finger-surface contact are perceived using receptors in the fingertips, this information is then fed to the brain [2]. The information is then used to alter the normal force, for both the tangential force and the frictional properties of the grip, by the use of controlled 'frictional slips' [8]. This total force is then distributed between the digits in a way that reduces the overall normal force, to ensure that the ratio between normal force and load is similar across all digits [8]. The greater the frictional interaction between the surface and the finger, the lower the normal force that the digits are required to apply, to secure the object [8].

There will be a similar process to this taking place when a ball is caught, however, it may be more complex due to the fact that the ball is moving. The loads on the ball were not monitored, and from the video it is not possible to quantify the deformation of the ball when contacting the hand, therefore it is not possible to fully characterise the process from these tests alone. The finger movements may be part of the surface perception process, or they may just be an involuntary act. Further experiments could determine this. These experiments would have to monitor the normal force applied by each digit, throughout the process. If the normal forces applied by the digits are known, the exact time to fully secure the ball will also be known, and it can be seen whether the force profile suggests the finger movements are part of the perception process, or an involuntary action.

The fact that the fingers are moving, and therefore sliding on the ball surface before securing it, highlight that the dynamic friction behaviour is relevant to describe how easy a ball is to catch. The fingers are also seen to move over

the surface of the ball when it is thrown, indicating that again the dynamic friction behaviour is a useful measure of how easily a ball can be handled.

9.4.2 Handling a Ball with Dry Hands

The ball with the highest measured coefficient of friction, in dry conditions was the Smooth Ball (although not at a difference level of $p < 0.05$ from all balls) (see Figures 9.3 and 9.4). The lack of pimples on this surface means that there is a larger area of contact, and therefore more adhesion present, causing it to have the largest average friction measurement.

Of the balls in current production (i.e. Balls 1 to 4), in dry conditions, Balls 3 and 4 had the higher coefficients of friction. Ball 3 has a similar pattern of pimples to that of Ball 2, however, the pimples on Ball 3 are square-based pyramids compared to the round ones of Ball 2. The significantly increased coefficient of friction for Ball 3 compared to Ball 2, implies pyramids are a more effective shape for increased friction. The previous studies in this thesis have shown that for a textured surface, hysteresis friction contributes to the overall friction. The estimated contributions for each pimple pattern were calculated, and are shown in Table 9.1. The hysteresis friction was estimated for the square based pyramids using Equation 9.1, modified from that used for the ridges in Chapter 7 (see Appendix 13). However, the contribution of adjacent pimples is neglected due to the large spacing. Equation 9.2 was used to estimate the hysteresis friction for the round pimples. This was modified from that used by Adams *et al.* [74] by multiplying the friction they calculated for a single sphere, by the number of spheres within a 200 mm^2 contact. The estimation of friction for Ball 2 will be a slight underestimate because the radius of the top of the pimple was used (0.31 mm), but the pimple has slightly elongated edges, so it has a height of 0.36 mm.

$$F_h = \beta \cdot n \cdot \frac{N_{\max}}{4} \cdot \cot \theta \quad 9.1$$

$$F_h = n \cdot \beta \cdot \left(\frac{9}{128 \cdot R} \right)^{\frac{2}{3}} \cdot \left(\frac{1 - \nu^2}{E} \right)^{\frac{1}{3}} \cdot N_{\max}^{\frac{4}{3}} \quad 9.2$$

where F_h is the hysteresis friction, β is the loss fraction for the finger (assumed to be 0.5, based on compression experiments on the finger [77]), n is the number of pimples, N_{\max} is the normal force for maximum deformation = $k \cdot h_r$, k is the spring constant for spring (1030 Nm^{-1}), h_r is the pimple height, θ is the half angle of pimple point, R is the radius of the sphere indenter, ν is the Poisson's ratio of skin (0.5), and E is the Young's modulus of skin

Table 9.1 – Estimation of percentage contribution of hysteresis friction to the total measured friction for each ball surface tested

Ball Surface	Percentage hysteresis friction (%)	Average Coefficient of Friction (Dry)
Smooth	0	1.79
Ball 1	0.28	1.07
Ball 2	0.18	1.21
Ball 3	9.6	1.55
Ball 4	6.9	1.61

Table 9.1 shows that the shape of the pyramidal pimples significantly increases the amount of hysteresis friction. There could also be interlocking friction. Since the angle of the pimple edge to the vertical (θ) is smaller (the majority of the time) for the pyramid pimple, than the round pimple, interlocking friction will be greater for the pyramid pimples than for the round pimples. Although both the rubber and the finger are viscoelastic materials, it is thought that the finger will deform around the pimples. This is because, although the Young's modulus can be variable, a comparison of two stated values of each show that skin has a Young's modulus 10^2 times smaller than that of the rugby ball material. The rubber is quoted from the manufacturer

as having a Young's modulus of 10 MPa, and the Young's modulus of the skin on the forearm, for young adults is 0.42 MPa [38].

There are two sizes of pimples for Ball 4. The work on rectangular ridges (Chapter 8) found that widely spaced, narrow and high ridges had the highest coefficient of friction, when contacting the finger. Correlating this finding to pimples; Ball 4 would be expected to have a lower coefficient of friction than Ball 3, due to the closer spacing of pimples. However, this is not the case. This could be due to the different sizes of pimples across the surface. The different sizes of pimples mean that there will be different levels of deformation, which could be altering both the hysteresis and adhesion friction mechanisms. This should be investigated further, to fully understand the mechanism.

Balls 1 and 2 have the lowest overall friction. This is because the pimples mean there is a smaller area of contact and therefore less adhesion. Also, the contribution of hysteresis to the total friction is low, as illustrated in Table 9.1, due to the shape of the pimples (hemi-spherical).

9.4.3 Handling a Ball with a Small Amount of Moisture on the Fingers

For all balls, except Ball 1, there is a decrease in coefficient of friction compared to the dry tests, with the addition of a small amount of water (Figure 9.3). This decrease does not follow the results expected following the analysis in Chapter 6. There could be several possible reasons for this, all of which would need further research. The tests were taken on different days, so the humidity could have affected the tests, if the humidity on the dry test day was higher than that on the damp finger test days, there would be a higher than expected dry coefficient of friction (humidity range in the lab is 30 – 60 %). The effect may also be temperature related. This was investigated using Digitron Infrared Non-Contact Thermometer to measure the

temperature of the surface immediately after testing; however, this did not provide enough accuracy to see a difference between tests. Therefore, the test would need to be repeated using a method such as a thermal camera or embedded thermocouples to better characterise the temperature change during each test.

In Case B (towel wet finger), where slightly more water was added to the finger, an increase in coefficient of friction was observed (for all balls except Ball 1). The increase in friction follows that expected from the work in Chapter 6, and is due to an increase in contact area from both absorption of water into the stratum corneum and capillary adhesion. The texture of the rugby ball could be increasing the capillary adhesion due to an increase in the combined surface roughness.

For Ball 1, there may be a trend of increased coefficient of friction with a small amount of water (case B); however, this is not confirmed as it is not statistically significant. This ball is unique in comparison to the other balls because it performs consistently across all the levels of water added to the finger. This ball has much wider, shorter and more densely populated pimples than the other balls. These results could therefore indicate that a close network of pimples increases consistency in the performance of the ball, but, further studies need to be carried out to confirm this. More work also needs to be done to investigate why there is not a large increase in friction with moisture. It is understandable that there could be less capillary adhesion due to a modification or reduction in liquid bridges, but absorption of moisture in the stratum corneum would still be expected to increase friction.

9.4.4 *Handling a Ball with Wet Fingers*

In all instances, except for Ball 1, the coefficient of friction was reduced compared to the dry condition and towel wet finger (case B), when the finger was fully immersed in water (case C). The coefficient of friction is low because the water is at such a level that it is separating/partly separating the finger from the surface of the ball. This means there is less ball-finger contact, therefore the friction is reduced. The measured coefficient of friction in the wet finger case was not statistically different between balls, nor was it for the other wet finger cases. The results from the wet friction tests performed in the laboratory agree well with the in-field friction tests. The similarity of these results in the different environments indicates that the water dominates the interaction. Therefore, at a certain level of moisture on the fingers, friction between the finger and ball is almost independent of the environmental or ball conditions.

9.4.5 *Handling a Wet Ball*

There was no trend of increasing and then decreasing coefficient of friction seen in the wet material tests. The level of water, in these tests, is at such a level that it dominates the interaction; showing little difference between the three balls. The water dominates the interaction because under the specific dynamic conditions of the test, a water film forms between the finger and the rugby ball surface; this causes the underlying surface to be less influential in the interaction.

The dry coefficient of friction is higher than the wet conditions for the balls, except Balls 1 and 2. The surface pattern of these balls is different, in that Ball 1 has much wider, more closely spaced pimples than Ball 2. However, in each case both pimples are round. More work needs to be done to explain why round pimples behave in this way, but it could be due to round pimples

enabling better water drainage. For surfaces where a decrease in friction was observed, the water is separating the finger from the underlying surface.

9.4.6 Handling a Ball in a Game, Compared to in the Laboratory

In wet ball conditions, the in-field friction tests, laboratory friction tests, and target tests were all in agreement. The friction tests measured the same coefficient of friction, and highlighted no difference between the Smooth Ball and Ball 1 wet. The target tests also showed no difference between the two balls. However, the high-speed video images did highlight a difference between the Smooth Ball wet and Ball 1 wet. Players were able to apply more spin to Ball 1 wet, than to the Smooth Ball wet. Application of more spin to a ball would generally imply better accuracy. However, the two balls performed equally well in the accuracy and friction tests, although the reason for this difference is not known. It could be related to the perception the participants have of how easily the ball can be handled. This hypothesis can be investigated using an in-depth perception study.

The dry in-field friction test results measured a higher average coefficient of friction than the laboratory tests. There was also no significant difference between the Smooth Ball dry and Ball 1 dry in the in-field tests, which is contrary to the laboratory test results. The reason for this is the difference in the environmental conditions. The humidity was greater for the in-field tests, the temperature was lower, and the players were in-game condition, i.e. their hands were not clean. The laboratory tests suggest that the increased humidity would increase the friction force for the Smooth Ball, but would make little difference for Ball 1. Generally, a lower temperature would be expected to reduce compliance of a viscoelastic material, and therefore a decrease in the frictional force would be expected. However, the finger is deforming much more than the rugby ball rubber, and the body regulates the temperature of the finger. If the pimples become more rigid, the adhesion and hysteresis mechanisms will be modified, so in this way it could alter the

friction mechanisms. These factors indicate that the mud on the hands of the players increased the coefficient of friction. The mud from the field was not analysed, and so the composition is not known. This observation, however, highlights the need for contaminants such as mud to be included in future friction measurements, on rugby ball surfaces.

9.5 Conclusions from the Rugby Ball Tests

The recorded catches showed the fingers moving over the top of the ball before it is fully secured. Further work needs to be done to investigate if this is part of the perception process or is involuntary.

The balls with the highest measured coefficient of friction were the ones with square-based pyramidal pimples and a mixture of pimple sizes. From an initial assessment of the friction mechanisms, it was found that hysteresis friction contributed to 9.6 % for the pyramid pimples, compared to only 0.18 – 0.28 % for the round pimples. From work done on the triangular ridges, in Chapter 7, there could also be some interlocking friction increasing the friction for the pyramid pimples. The full effect of pimple shape needs further investigation, in particular the effect of having different sized pimples on the same surface (such as Ball 4).

The ball which showed the best consistency in friction tests across dry and wet conditions was the ball with wider, rounded, closely spaced pimples. More work needs to be done to better understand why this is the case. The addition of large amounts of water to the hand or ball surface reduces the variability of the measured friction between the individual balls. This is because there is an increase in the amount of finger-water contact, rather than finger-ball contact.

There was an increase in measured friction for the in-field tests when contaminants, such as mud, were on the fingers, suggesting the requirement for future tests involving contaminants, such as soil and sand.

10 Conclusions and Future Work

10.1 Conclusions

The conclusions from this work, with regards the general friction mechanisms, can be summarised using the flow diagram, shown in Figure 10.1. This summarises the mechanisms of friction for each category of surface tested (flat; fine triangular ridges; large rectangular ridges; rugby ball). There were two very small contributions to friction from the finger compressing onto the surface and then the bulk of the finger moving laterally (in the opposite direction to travel), before sliding commences, and also deformation and movement of the finger ridges, however, calculations have shown these to be negligible in comparison to the other mechanisms, so they are omitted from the diagram.

Part of this study assessed the contact of a finger with a nominally flat plate, and found that there is a two part linear relationship between the friction force and the normal force. Previous work had mostly concentrated on a rigid sphere contacting the skin of the forearm; however, there are a couple of studies that examined the finger. The work in this thesis expanded these studies to look at the finger contact over a larger range of forces. The results differ to previous conclusions, which usually stated a power relationship. This power relationship is theoretically derived from Hertzian contact, of which, some of the assumptions are not valid for the finger. It was found in the previous experiments that the power is often slightly higher than the predicted 0.67, due to energy losses. In one previous study, a two part linear relationship was proposed for the palm, however, the transition was at a larger load than tested in this PhD study, and the previous work did not test at normal loads below 5 N. There is, therefore, a difference between the relationship between friction force and normal force for a rigid sphere contacting a forearm, and a finger contacting a flat, rigid surface. This is thought to be due to the difference in structure of the finger and the forearm, resulting in the finger reaching a visible compression limit at approximately 1.6 N (for the finger tested), after this, the area of contact will still increase with load, however, at a different rate to the lower load contact.

Work has also been done in this study to look at the area of contact for a finger. The majority of contact measurements use a light source reflecting through a prism and onto the finger contact, so the surface needs to be translucent. Although, a measurement of real area of contact was not achieved, an electrical method of measuring area of contact was developed, and also a method using high-speed video of a side view of the finger. This gives a measurement of nominal area of contact; it is then a case of using statistical data to calculate the real area of contact. These methods increased the understanding of the force data, by providing nominal contact data, for a finger contacting a flat surface. It was shown that a rough approximation for the nominal area of contact (taking ridges into account), is

to measure the largest radius of the finger and then use this in the Hertz equation of contact. At low loads the contact can be considered circular, but then at larger loads it becomes oval. Using the larger radius of the finger, estimates the increased contact area, due to an oval not round contact.

Previous work on the effect of moisture on the friction of human skin has concentrated mostly on the forearm, and an increase in friction is fully attributed to the absorption of water by the stratum corneum. This reduces its Young's modulus, increasing the area of contact, and therefore adhesive friction. Dinç *et al.* [57] did tests on the finger at different moisture levels and found an increase in friction at a certain level of moisture, as found in this study, they attributed this increase to liquid bridges forming and then viscous shear forces in the bridges increasing friction. However, they only stated this as a theory. In this study calculations were done to look into the possibility of this and viscous shearing was discounted from being a principle reason for the increase in friction. Capillary adhesion can significantly increase friction for soft elastomers, but previously had not been considered for the finger. This study found that although absorption of water into the stratum corneum is the most significant factor increasing the friction, in moist conditions, capillary adhesion also contributes to the increase in friction force, due to capillary forces causing an increase in contact area.

The investigations into the contact of the finger with fine triangular ridges, found that the friction increased compared to a nominally flat surface. This is thought to be due to an increase in adhesion, which includes the introduction of interlocking friction. Then for larger ridges, hysteresis friction also has an increased contribution to the friction mechanism. This work is unique in that no other work has been done to look at triangular shaped ridges contacting the finger, or other areas of the skin. A model has also been developed, based on an existing model of a conical slider contacting an elastomer. This

model can predict the hysteresis friction for a finger contacting a triangular ridged surface; a model that previously did not exist.

The investigations into the contact of the finger with large, rectangular ridges, expanded upon previous work done, on a small sample of rectangular ridged textures. However, the findings from this study are in disagreement with those from the previous study. Previously, it was found that friction decreased with the addition of ridges to the surface, and this was explained due to a reduction in adhesive friction. However, in this study, friction was found to increase with ridges due to the introduction of ploughing friction. This highlights an area for further investigations, since the previous study was done on 14 males and this one was done on one female. There may be a difference in the deformation of the finger, depending on person or gender, which is altering the amount of ploughing friction present. In this study it was found that the amount of friction fluctuated as the finger moved over the ridges. This was due to a change in the amount of ploughing friction, and also an energy return, resulting in a reduction of friction force. This study has also introduced a new understanding of the effects of height, width and spacing, which can be used as an initial starting point for surface design. It found that high, narrow, widely spaced ridges have the largest friction, but, for this case, the friction will not be consistent along the slide.

Figure 10.2 shows a scale of friction for the textures tested (applied normal force of 10 N); the humidity for each measurement is also recorded, as this has been shown to have a large impact on the friction measurement. This shows that the smooth surface has the lowest coefficient of friction, and widely spaced, high, narrow, rectangular ridges, at high humidity have the highest friction. This also shows that the large, triangular ridges have a higher coefficient of friction than the closely spaced, low height, rectangular ridges. This implies that triangular ridges are a more effective shape for high friction. This is predicted to be due the presence of interlocking friction.

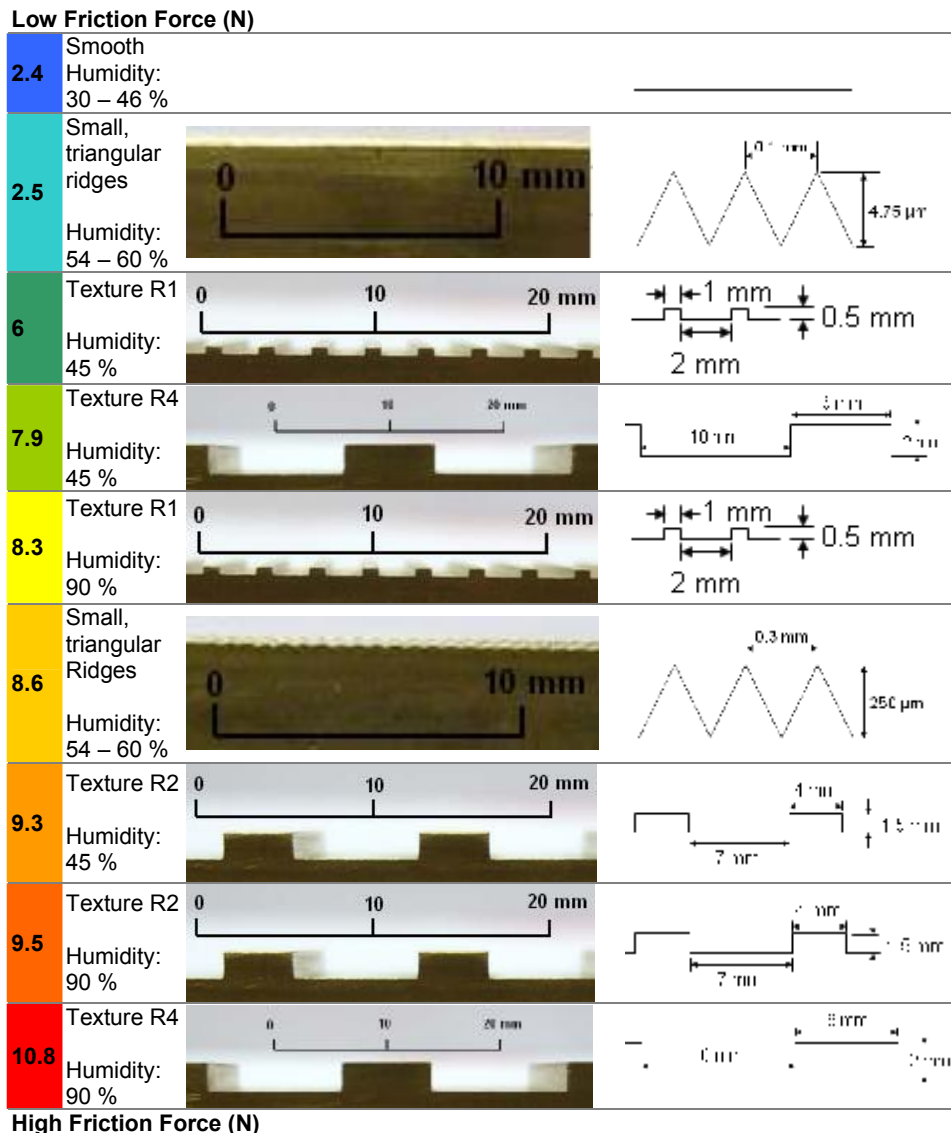


Figure 10.2 – Maximum friction force for a selection of textures tested, with an applied load of 10 N, applicable for brass, and a linear sliding velocity (perpendicular to the ridge direction) of 14 to 44 mms^{-1}

There has been no previous work examining the friction between human hands and rugby balls. Nor, has the mechanism of catching the ball been observed at high-speed, but the spin and speed of the ball have previously been recorded. This work enabled a comparison of the different surfaces in terms of grip performance, in a number of different conditions. The existing model of hysteresis friction for a sphere and a modified version for a conical

indenter were applied to explain some of the differences seen between the balls. The smooth ball had the highest coefficient of friction, due to increased adhesion. The round pimped balls both had a lower coefficient of friction than the pyramidal pimples. This was investigated and it was found that for round pimples, hysteresis friction is negligible. There is a much larger contribution for pyramidal pimples, resulting in a larger coefficient of friction.

The main aim of this study was to 'improve the understanding of friction mechanisms for finger contact'. This has been achieved for a flat surface, surfaces with triangular ridges, surfaces with rectangular ridges, and some rugby ball surfaces. This study has also improved the understanding of the effect of moisture on grip. There are of course areas for more work, which will be explained in the following section. None-the-less this study has provided conclusions that can be used in the initial stages of surface design, for products which come into contact with human hands.

10.2 Future Work

Although this study has addressed several aspects of finger friction, many questions have arisen during the course of the work, which were not covered in the scope of this study. However, they would further the understanding of finger friction considerably.

10.2.1 *Area of contact*

If a method for measuring the real area of contact, for any surfaces with different roughness could be designed, this would dramatically aid the understanding of friction in different applications, and make the calculation of adhesion substantially easier. Also, the contact calculations used Hertz theory, with an assumed radius. There is a need for this model to be modified to account for the oval shape of the contact at high loads.

10.2.2 *Moisture Tests*

Further work needs to be done to better model capillary adhesion of the finger, by experimentally gaining better estimates of the Young's modulus, for different levels of moisture. Experimentally, capillary adhesion can be investigated by establishing a method of film thickness measurement. Silicon gels with the same viscosity of water could also be used, since these have been shown not to absorb into the skin [74].

10.2.3 *Pressure Distribution of Contact*

When the finger is contacting a textured surface, there will be points of increased pressure; this will cause an increase in localised adhesion. In this study, it has been assumed that the average pressure can be used, as it is for flat contacts. However, this assumption needs further investigation and verification.

10.2.4 *Deformation of the finger*

Estimation of how much a finger deforms when on a texture, in particular the large, rectangular ridged surfaces, would enable the ploughing friction to be predicted for any given ridged surface. A suggested method is to use a finite element model.

10.2.5 *Rugby balls*

The study on rugby balls highlighted several gaps in knowledge. These included the effects of a multi-dimensional texture, such as two different sized pimples, and how the viscoelastic nature of the rugby ball material alters the overall friction. The rugby ball material does not deform to the same extent as the finger, however, there is likely to be some deformation, which may be affecting the friction mechanisms.

References

References

1. Health and Safety Executive. Health and Safety Statistics. Statistics on work-related ill-health, injuries, dangerous occurrences, enforcement and gas safety. www.hse.gov.uk; 2008.
2. Johansson RS, Westling G. Signals in tactile afferents from the fingers eliciting adaptive motor responses during precision grip, *Experimental Brain Research* 66(1) (1987) 141 - 154.
3. Liu X, Yue Z, Cai Z, Chetwynd DG, Smith ST. Quantifying touch-feel perception: tribological aspects, *Measurement Science and Technology* 19(2008) 1 - 9.
4. Sivamani RK, Goodman J, Gitis NV, Maibach HI. Coefficient of Friction: Tribological Studies in Man - An Overview, *Skin Research and Technology* 9(3) (2003) 227 - 234.
5. Yoxall A, Luxmoore J, Austin M, Canty L, Margrave KJ, Richardson CJ, Wearn J, Howard IC, Lewis R. Getting to grips with packaging: Using ethnography and computer simulation to understand hand-pack interaction, *Packaging Technology and Science* 20(3) (2007) 217 - 229.
6. Napier JR. The prehensile movements of the human hand, *The Journal of Bone and Joint Surgery* 38-B(4) (1956) 902-913.
7. Cadoret G, Smith AM. Friction not texture, dictates grip forces used during object manipulation, *Journal of Neurophysiology* 75(5) (1996) 1963-1969.
8. Burstedt MKO, Flanagan JR, Johansson RS. Control of grasp stability in humans under different frictional conditions during multidigit manipulation, *Journal of Neurophysiology* 82(1999) 2393–2405.
9. Flanagan JR, Burstedt MKO, Johansson RS. Control of fingertip forces in multidigit manipulation, *Journal of Neurophysiology* 81(4) (1999) 1706–1717.
10. Jenmalm P, Johansson RS. Visual and somatosensory information about object shape control manipulative fingertip forces, *Journal of Neuroscience* 17(11) (1997) 4486 - 4499.
11. Jenmalm P, Goodwin AW, Johansson RS. Control of grasp stability when humans lift objects with different surface curvatures. , *Journal of Neurophysiology* 79(1998) 1643 - 1653.
12. McDonnell MN, Ridding MC, Flavel SC, Miles TS. Effect of human grip strategy on force control in precision tasks, *Experimental Brain Research* 161(3) (2005) 368 - 373.

References

13. Forssberg H, Eliasson AC, Kinoshita H, Westling G, Johansson RS. Development of human precision grip. IV: Tactile adaptation of isometric finger forces to the frictional condition, *Experimental Brain Research* 104(2) (1995) 323 - 330.
14. Cole KJ, Rotella DL, Harper JG. Mechanisms for age-related changes of fingertip forces during precision gripping and lifting in adults, *The Journal of Neuroscience* 19(8) (1999) 3238–3247.
15. Cua AB, Wilhelm KP, Maibach HI. Frictional properties of human skin: relation to age, sex and anatomical region, stratum corneum hydration and transepidermal water loss, *British Journal of Dermatology* 123(4) (1990) 473 - 479.
16. Sivamani RK, Wu GC, Gitis NV, Maibach HI. Tribological testing of skin products: gender, age and ethnicity on the volar forearm, *Skin Research and Technology* 9(4) (2003) 299 - 305.
17. Asserin J, Zahouani H, Humbert P, Couturaud V, Mougín D. Measurement of the friction coefficient of the human skin in vivo. Quantification of the cutaneous smoothness, *Colloids and Surfaces B: Biointerfaces* 19(2000) 1-12.
18. Vivier Ad. *Atlas of Clinical Dermatology*. Third ed Churchill Livingstone, 2002 .
19. Wheat HE, Salo LM, Goodwin AW. Human ability to scale and discriminate forces typical of those occurring during grasp and manipulation, *The Journal of Neuroscience* 24(13) (2004) 3394 - 3401.
20. Boyer G, Zahouani H, Bot AL, Laquieze L. In vivo characterization of viscoelastic properties of human skin using dynamic micro indentation. Proceedings of the 29th Annual International Conference of the IEEE EMBS Lyon, France: IEEE Engineering and Biology Society; 2007, 4584 - 4587.
21. Gent AN. Rubber Elasticity: Basic Concepts and Behavior. In: Mark JE, Erman B, Eirich FR, eds. *Science and Technology of Rubber*. Academic Press; 1994:1 - 21.
22. Lindner M, Kröger M, Popp K, Blume H. Experimental and analytical investigation of rubber friction. Proceedings of XXI International Congress of Theoretical and Applied Mechanics. Warsaw, Poland; 2004.
23. Moore DF. *The Friction and lubrication of elastomers*. Vol. 9 Pergamon Press, 1972 International Series of Monographs on Materials Science and Technology.
24. Persson BNJ, Volokitin AI. Theory of rubber friction: Nonstationary sliding, *Physical Review B* 65(13) (2002) 134106 - 134116.

References

25. Williams JA. *Engineering Tribology* Oxford Science Publications, 1994.
26. Palasantzas G. Influence of self-affine roughness on the friction coefficient of rubber at high sliding velocity, *Physical Review B* 70(19) (2004) 195409.
27. Hutchings IM. *Tribology: Friction and Wear of Engineering Materials* Arnold, 1992.
28. Barquins M, Roberts AD. Rubber friction variation with rate and temperature: some new observations, *Journal of Physics D: Applied Physics* 19(1986) 547 - 563.
29. Schallamach A. The load dependence of rubber friction, *The Proceedings of the Physical Society. Section B* 65(1952) 657-660.
30. Persson BNJ, Albohr O, Tartaglino U, Volokitin AI, Tosatti E. On the nature of surface roughness with application to contact mechanics, sealing, rubber friction and adhesion, *Journal of Physics: Condensed Matter* 17(2005) R1–R62.
31. Lavrentev VV. Theory of Friction of Elastomers. In: Lee L-H, ed. *Advances in Polymer Friction and Wear*. Vol. 5B: Plenum Press; 1974.
32. Berman AD, Ducker WA, Israelachvili JN. Origin and characterization of different stick-slip friction mechanisms, *Langmuir* 12(19) (1996) 4559 - 4563.
33. Brown RP. *Physical Testing of Rubbers* Applied Science Publishers, 1979.
34. Williams AC. *Transdermal and Topical Drug Delivery*. London: Pharmaceutical Press. 2003.
35. Lennard CJ, Patterson T. Friction ridge skin. *The Thin Blue Line Information Section* 2007.
36. Tang W, Ge S, Zhu H, Cao X, Li N. The influence of normal load and sliding speed on frictional properties of skin, *Journal of Bionic Engineering* 5(1) (2008) 33 - 38.
37. Comaish S, Bottoms E. The Skin and Friction: Deviations from Amonton's Laws, and the effects of hydration and lubrication, *British Journal of Dermatology* 84(1) (1971) 37 - 43.
38. Agache PG, Monneur C, Leveque JL, Rigal JD. Mechanical properties and Young's modulus of human skin in vivo, *Dermatological Research* 269(1980) 221-232.
39. Lees C, Vincent JF, Hillerton JE. Poisson's ratio in skin, *Bio-Medical Materials and Engineering* 1(1) (1991) 19 - 23.

References

40. Sanders R. Torsional elasticity of human skin in vivo, *Pflugers Archive: European Journal of Physiology* 342(1973) 255 - 260.
41. Diridollou S, Vabre V, Berson M, Valliant L, Black D, Lagarde JM, Grégoire JM, Gall Y, Patat F. Skin ageing: changes of physical properties of human skin in vivo, *International Journal of Cosmetic Science* 23(2001) 353 - 362.
42. Waller JM, Maibach HI. Age and skin structure and function, a quantitative approach (I): blood flow, pH, thickness, and ultrasound echogenicity, *Skin Research and Technology* 11(4) (2005) 221 - 235.
43. Cua AB, Wilhelm KP, Maibach HI. Elastic properties of human skin: relation to age, sex, and anatomical region, *Archives of Dermatological Research* 282(5) (1990) 283-288.
44. Habif T. Principles of diagnosis and anatomy. In: Habif T, ed. *Clinical Dermatology* New York: Mosby; 2004:1-2.
45. Hendriks FM. (Koninklijke Philips Electronics Nat. Lab. Unclassified Report). Mechanical behaviour of human skin in vivo. 2001.
46. Hendriks FM, Brokken D, Oomens CWJ. Mechanical properties of different layers of skin. *Philips Research Laboratories, Eindhoven and Eindhoven University of Technology*.
47. Duck FA. *Physical Properties of Tissue. A Comprehensive Reference Book*. Bath: Academic Press Ltd, 1990.
48. Holt SB. Quantitative genetics of finger-print patterns, *British Medical Bulletin* 17(3) (1961) 247 - 250.
49. Verbov J. Clinical Significance and Genetics of Epidermal Ridges - A Review of Dermatoglyphics, *The Journal of Investigative Dermatology* 54(4) (1970) 261-271.
50. Stücker M, Geil M, Kyeck S, et al. Interpapillary lines - the variable part of the human fingerprint, *Journal of Forensic Sciences* 46(4) (2001).
51. Koudine AA, Barquins M, Anthoine PH, Aubert L, Lévêque JL. Frictional properties of skin: proposal of a new approach, *International Journal of Cosmetic Science* 22(1) (2000) 11 - 20.
52. Highley DR, Coomey M, DenBeste M, Wolfram LJ. Frictional Properties of Skin, *The Journal of Investigative Dermatology* 69(1977) 303-305.
53. Sivamani RK, Goodman J, Gitis NV, Maibach HI. Friction coefficient of skin in real-time, *Skin Research and Technology* 9(3) (2003) 235 - 239.

References

54. Han H-Y, Shimada A, Kawamura S. Analysis of Friction on Human Fingers and Design of Artificial Fingers. Proceedings of the 1996 IEEE International Conference on Robotics and Automation. Minneapolis, Minnesota; 1996, 3061 - 3066.
55. Srinivasan MA, Biggs SJ, Raju BI, et al. (MIT Touchlab). Role of Skin Biomechanics in Mechanoreceptor Response. 2002.
56. Gee MG, Tomlins P, Calver A, Darling RH, Rides M. A new friction measurement system for the frictional component of touch, *Wear* 259(7 - 12) (2005) 1437-1442.
57. Dinç OS, Ettles CM, Calabrese SJ, Scarton HA. Some parameters affecting tactile friction, *Journal of Tribology* 113(3) (1991) 512-517.
58. Roberts AD, Brackley CA. Friction of Surgeons' gloves, *Journal of Physics D: Applied Physics* 25(1992) A28 - A32.
59. Spurr RT. Fingertip Friction, *Wear* 39(1) (1976) 167 - 171.
60. Lewis R, Menardi C, Yoxall A, Langley J. Finger friction: grip and opening packaging, *Wear* 263(7 - 12) (2007) 1124 - 1132.
61. Zahouani H, Flament F, Vargiolu R, Bot AL, Mavon A. Acoustic Tribology of Human Skin. World Tribology Congress III Washington DC, USA; 2005.
62. Zahouani H, Vargiolu R, Boyer C, Pailler-Mattéi C, Laquière L, Mavon A. Friction Noise of Human Skin in Vivo, *Wear* 267(5 - 8) (2009) 1274 - 1280.
63. Ramalho A, Silva CL, Pais AACC, Sousa JJS. In vivo friction study of human skin: Influence of moisturizers on different anatomical sites, *Wear* 263(7 - 12) (2007) 1044 - 1049.
64. Bobjer O, Johansson S-E, Piguet S. Friction between hand and handle. Effects of oil and lard on textured and non textured surfaces; perception of discomfort, *Applied Ergonomics* 24(3) (1993) 190-202.
65. Fuss FK, Niegl G, Tan AM. Friction between hand and different surfaces under different conditions and its implication for sport climbing. The Engineering of Sport Davis, California; 2004, 269 - 275.
66. Zatsiorsky VM. *Kinetics of Human Motion* Leeds: Human Kinetics Champaign III, 2002.
67. Cutkosky MR, Jourdain JM, Wright PK. Skin materials for robotic fingers, *Proceedings of the 1987 IEEE International Conference on Robotics and Automation* 4(1987) 1649-1654.
68. Levesque V, Haywood V. Experimental evidence of lateral skin strain during tactile exploration. *Proceedings of Eurohaptics* 2003;261 - 275.

References

69. Mackenzie CL, Iberall T. The Grasping Hand. Skin: An Organ Critical for Grasp, *Advances in Physiology* 104(1994) 205 - 218.
70. Kwiatkowska M, Franklin SE, Hendriks CP, Kwiatkowski K. Friction and deformation behaviour of human skin, *Wear* 267(5 - 8) (2009) 1264 - 1273.
71. Smith AM, Cadoret G, St-Amour D. Scopolamine increases prehensile force during object manipulation by reducing palmar sweating and decreasing skin friction, *Experimental Brain Research* 114(3) (1997) 578 – 583.
72. Persson BNJ. Capillary adhesion between elastic solids with randomly rough surfaces, *Journal of Physics: Condensed Matter* 20(2008) 1 - 11.
73. Gitis N, Sivamani R. Tribometry of Skin, *Tribology Transactions* 47(4) (2004) 461 - 469.
74. Adams MJ, Briscoe BJ, Johnson SA. Friction and lubrication of human skin, *Tribology letters* 26(3) (2007) 239-253.
75. Adelman S, Taylor CR, Heglund NC. Sweating on paws and palms: what is its function?, *American Journal of Physiology* 229(5) (1975) 1400-1402.
76. Serina ER, Mockensturm E, Jr CDM, Rempel D. A structural model of the forced compression of the fingertip pulp, *Journal of Biomechanics* 31(7) (1998) 369 - 646.
77. Pataky TC, Latash ML, Zatsiorsky VM. Viscoelastic response of the finger pad to incremental tangential displacements, *Journal of Biomechanics* 38(7) (2005) 1441 - 1449.
78. Johnson KL. *Contact Mechanics* Cambridge: Cambridge University Press, 1985.
79. Johnson KL, Kendall K, Roberts AD. Surface energy and the contact of elastic solids, *Proceedings Royal Society London A: Mathematical, Physical and Engineering Sciences* 324(1558) (1971) 301 - 313.
80. Pailler-Mattéi C, Zahouani H. Analysis of adhesive behaviour of human skin in vivo by an indentation test, *Tribology International* 39(1) (2006) 12 - 21.
81. Gerhardt LC, Strässle V, Lenz A, Spencer ND, Derler S. Influence of epidermal hydration on the friction of human skin against textiles, *Journal of the Royal Society of Interface* 5(28) (2008) 1317 - 1328.
82. Smith AM, Gosselin G, Houde B. Deployment of fingertip forces in tactile exploration, *Experimental Brain Research* 147(2) (2002) 209 - 218.

References

83. Tomlinson SE. Grip on Rugby Balls [MEng]. The University of Sheffield, 2006.
84. Peebles L, Beverley N. *Adultdata : data for design safety : the handbook of adult anthropometric and strength measurements* Department of Trade and Industry, 1998.
85. Sunaga T, Ikehira H, Furukawa S, Shinkai H, Kobayashi H, Matsumoto Y, Yoshitome E, Obata T, Tanada S, Murata H, Sasaki Y. Measurement of the electrical properties of human skin and the variation among subjects with certain skin conditions, *Physics in Medicine and Biology* 47(2002) N11 - N15.
86. Murrell JN, Jenkins AD. *Properties of liquids and solutions*. Second ed Wiley & Sons, 1994.
87. André T, Lefèvre P, Thonnard J-L. A continuous measure of fingertip friction during precision grip, *Journal of Neuroscience Methods* 179(2) (2009) 224-229.
88. Courage W. Hardware and Measuring Principle: Corneometer. In: Elsner P, Berardesca E, Maibach HI, eds. *Bioengineering of the skin: Water and the stratum corneum* London: CRC Press; 1994:171 - 176.
89. Zhang S-W. *Tribology of Elastomers* Elsevier, 2004.
90. Tabor D. Elastic work involved in rolling a sphere on another surface, *British Journal of Applied Physics* 6(1955) 79 - 81.
91. Greenwood JA, Tabor D. The friction of hard sliders on lubricated rubber: The importance of deformation losses, *Proceedings of the Physical Society* 71(1958) 989 - 1001.
92. Diversified_Enterprises. Solid Surface Energies. http://www.accudynetest.com/surface_energy_materials.html. Claremont, USA; 2003.
93. DataPhysics. Solid surface energy data for common polymers. <http://surface-tension.de/solid-surface-energy/>; 2007.
94. Kinloch AJ. *Adhesion and Adhesives* Springer, 1987.
95. Bhushan B. *Principles and applications of tribology* United States of America: Wiley - Interscience, 1999.
96. Choppin S. Modelling of tennis racket impacts in 3D using elite players [PhD]. The University of Sheffield, 2008.
97. Luo X, Chung DDL. Tribology of Graphite and Concrete, Studied by Contact Electrical Resistance Measurement During Cyclic Compression, *ASME Journal of Tribology* 123(2001) 682 - 685.

References

98. Yamamoto T, Yamamoto Y. Dielectric constant and resistivity of epidermal stratum corneum, *Medical and Biological Engineering* 14(5) (1976) 494 - 500.
99. Swain ID, Wilson GR, Crook SC. Simple Method of Measuring the Electrical Resistance of the Skin, *Journal of Hand Surgery (British and European Volume)* 10(3) (1985) 319 - 323.
100. McAdams ET, Jossinet J, Lackermeier A, Risacher F. Factors affecting electrode-gel-skin interface impedance in electrical impedance tomography, *Medical and Biological Engineering and Computing* 34(6) (1996) 397 - 408.
101. Serina ER, Jr. CDM, Rempel D. Force response of the fingertip pulp to repeated compression - Effects of loading rate, loading angle and anthropometry, *Journal of Biomechanics* 30(10) (1997) 1035 - 1040.
102. Yang C, Persson BNJ. Contact mechanics: contact area and interfacial separation from small contact to full contact, *Journal of Physics: Condensed Matter* 20(2008) 1 - 13.
103. Greenwood JA, Tripp JH. The elastic contact of rough spheres, *Transactions of the ASME Journal of Applied Mechanics* 34(1967) 153 - 159.
104. Bhushan B. Contact mechanics of rough surfaces in tribology: multiple asperity contact, *Tribology letters* 4(1) (1997) 1 - 35.
105. Polonsky IA, Keer LM. A numerical method for solving rough contact problems based on the multi-level multi-summation and conjugate gradient technique, *Wear* 231(2) (1999) 206 - 219.
106. Johnson KL, Greenwood JA. An approximate JKR theory for elliptical contacts, *Journal of Physics D: Applied Physics* 38(2005) 1042 - 1046.
107. Cherry BW. *Polymer Surfaces* Cambridge University Press, 1981 Cambridge Solid State Science Series.
108. Adams MJ, McKeown R, Whall A. A micromechanical model for the confined uni-axial compression of an assembly of elastically deforming spherical particles, *Journal of Physics D: Applied Physics* 30(1996) 912 - 920.
109. Deleau F, Mazuyer D, Koenen A. Sliding friction at elastomer/glass contact: Influence of the wetting conditions and instability analysis, *Tribology International* 42(1) (2009) 149 - 159.
110. deVicente J, Stokes JR, Spikes HA. Rolling and sliding friction in compliant, lubricated contact, *Proceedings of the Institution of Mechanical Engineers, Part J: Journal of Engineering Tribology* 220(2) (2006) 55-63.

References

111. Bongaerts JHH, Fourtouni K, Stokes JR. Soft-tribology: Lubrication in a compliant PDMS-PDMS contact, *Tribology International* 40(10-12) (2007) 1531-1542.
112. deVicente J, Stokes JR, Spikes HA. Behaviour of complex fluids between highly deformable surfaces: isoviscous elastohydrodynamic lubrication. *Marie Curie Fellowship Association Annals* Vol. IV; 2005.
113. Myant C, Spikes HA, Stokes JR. Influence of load and elastic properties on the rolling and sliding friction of lubricated compliant contacts, *Tribology International* In press: doi: 10.1016/j.triboint.2009.04.034(2009).
114. DelRio FW, Dunn ML, deBoer MP. Capillary adhesion model for contacting micromachined surfaces, *Scripta Materialia* 59(9) (2008) 916 - 920.
115. Park AC, Baddiel CB. Rheology of Stratum Corneum - I: A molecular interpretation of the stress-strain curve, *Journal of Cosmetic Science* 23(1) (1972) 3 - 12.
116. Park AC, Baddiel CB. The effect of saturated salt solutions on the elastic properties of stratum corneum, *Journal of Cosmetic Science* 23(8) (1972) 471 - 479.
117. Eroschenko VP, diFiore MSH. *DiFiore's atlas of histology with functional correlations*. Eleventh ed Lippincott, Williams and Wilkins, 2007.
118. Rosen MR. *Delivery System Handbook for Personal Care and Cosmetic Products - Technology, Applications and Formulations* William Andrew Publishing, 2005.
119. Lévêque J-L. Water-keratin interactions. In: Fluhr J, Berardesca E, Elsner P, Maibach HI, eds. *Bioengineering of the Skin: Water and the Stratum Corneum* Second ed: CRC Press; 2004.
120. Persson BNJ. E-mail discussion about capillary adhesion of skin. Jülich Forschungszentrum; 2009.
121. Persson BNJ. Wet adhesion with application to tree frog adhesive toe pads and tires, *Journal of Physics: Condensed Matter* 19(2007) 1 - 16.
122. Jerrams SJ. Friction and adhesion in rigid surface indentation of nitrile rubber, *Materials and Design* 26(3) (2004) 251 - 258.
123. Adams MJ. Friction of granular non-metals. In: Singer IL, Pollock HM, eds. *Fundamentals of friction: Macroscopic and microscopic processes* Vol. 220: Springer; 1991:183 - 209.

References

124. Egawa M, Hirao T, Takahashi M. In vivo estimation of stratum corneum thickness from water concentration profiles obtained with Raman spectroscopy, *Acta dermato-venereologica* 87(1) (2007) 4 - 8.
125. International Rugby board. (International Rugby board). Law 2 The ball, Playing Charter. 2006.
126. Holmes C, Jones R, Harland A, Petzing J. Ball Launch Characteristics for elite Rugby Union Players, *The Engineering of Sport* 6 1(2006) 211 - 216.
127. Department of Microbiology and Immunology TUoM. Hand Washing Instructions; 2001:
<http://www.microbiol.unimelb.edu.au/staff/ehs/washhands.html>.
128. Myshkin NK, Petrokovets MI, Kovalev AV. Tribology of polymers: Adhesion, friction, wear, and mass-transfer, *Tribology International* 38(11-12) (2005) 910 - 921.

Appendix 1 – Publications

S. E. Tomlinson, R. Lewis and M. J. Carré. The effect of normal force and roughness on friction in human finger contact, *Wear*, 2009, 267 (5-8), 1311 – 1318

S. E. Tomlinson, R. Lewis and M. J. Carré. Understanding the effect of finger-ball friction on the handling performance of rugby balls, *Sports Engineering*, 2009, 11 (3), 109 - 118

S. E. Tomlinson, R. Lewis and M. J. Carré. Friction between players' hands and sports equipment. In: M. Estivalet, P. Brisson, eds. *The Engineering of Sport 7*: Springer, Paris; 2008, 1, 27 - 34

S. E. Tomlinson, R. Lewis and M. J. Carré. Friction between players' hands and sports equipment. Extended abstract in *Mission of Tribology Research* 16, 5 December 2007

S. E. Tomlinson, R. Lewis and M. J. Carré. Review of the frictional properties of finger-object contact when gripping. *Proceedings of the IMechE Part J. Journal of Engineering Tribology*. 2007, 221(J8), 841-850

S. E. Tomlinson, R. Lewis and M. J. Carré. Improving the understanding of grip. In: F. K. Fuss, A. Subic, S. Ujihashi, eds. *The Impact of Technology on Sport II*: Taylor and Francis Group, London; 2007, 129-134

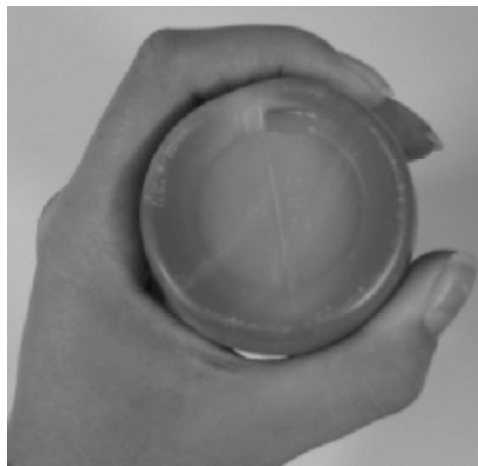
Appendix 2 – Grip Classifications



Box grip



Flipped cylindrical grip



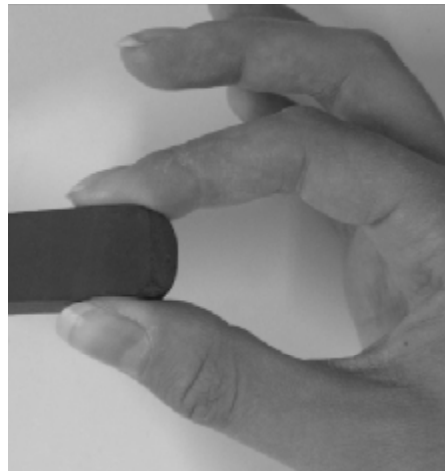
Cylindrical grip



Tip grip



Hook grip



Pulp/Palmer grip

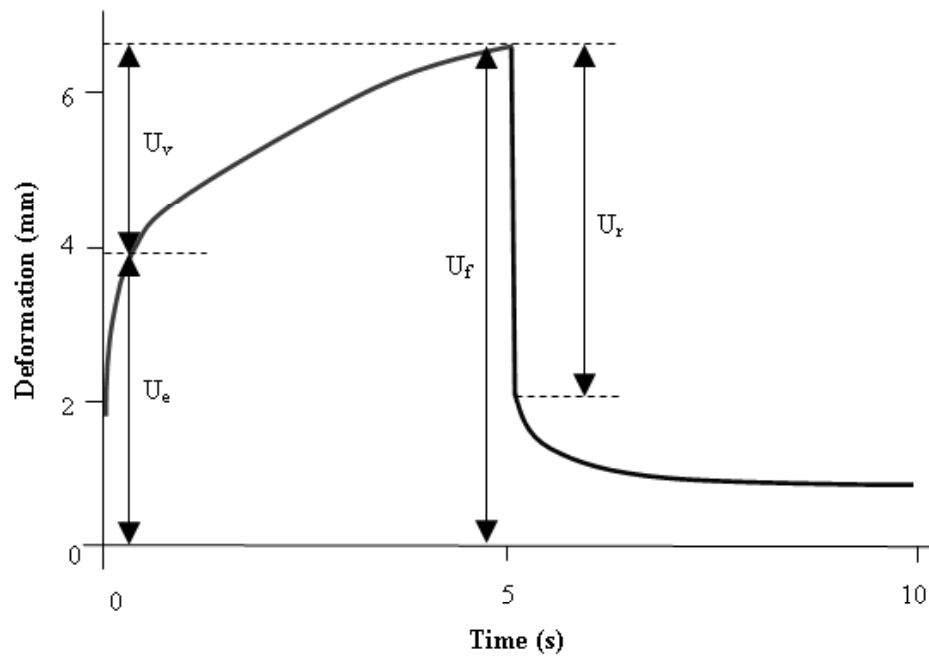


Spherical grip



Lateral grip

Appendix 3– Cutometer Measurements for Elasticity and Viscoelasticity with Respect to Immediate Distension



U_v – delayed distension

U_e – immediate distension (after 0.48 s)

U_f – final deformation

U_r – immediate retraction

Reproduced from [43]

Appendix 4– Hand Washing Procedure

The following procedure is taken from [127].

1. Wet hands in **warm** (but not hot) running water and apply soap.
2. Rub hands together to make a lather and scrub all surfaces.
3. Continue rubbing hands, in way illustrated, for 20 seconds (Sing ‘Happy Birthday’ through twice).
4. Rinse hands under running water.
5. Dry hands well with a paper towel.



1. Wet hands and wrists.
Apply soap



2. Right palm over left,
left over right



3. Palm to palm, fingers
interlaced



4. Back fingers to opposing
fingers. Interlocked.



5. Rotational rubbing of
right thumb clasped in
left palm, and vice versa.

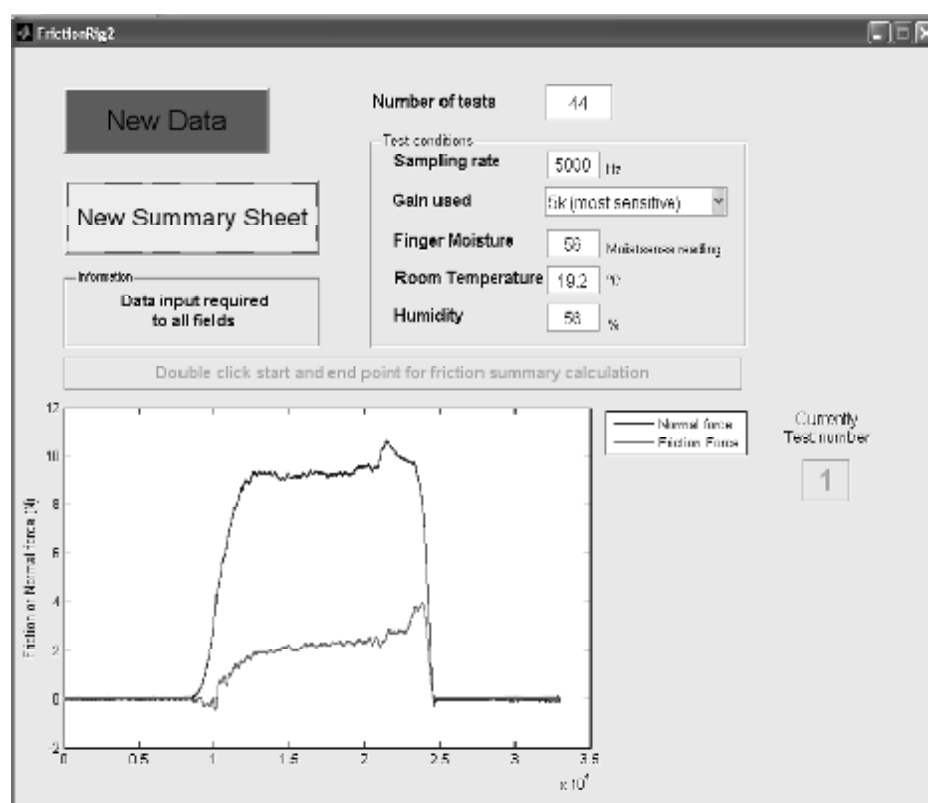


6. Rotational rubbing
backwards and forwards with
tops of fingers and thumb of
right hand in left and vice
versa.

Repeat 1 – 6 until the hands are clean

Appendix 5– Matlab® Program for Calculating Average Friction and Normal Force

User Interface:



M-File code for the 'New Data' (Databtn) and 'New Summary Sheet' (summarybtn) buttons

```
% --- Executes on button press in databtn.
function databtn_Callback(hObject, eventdata, handles)
%Opens specified number of files from the directory and then saves
these to
%the given file, a new sheet for each test
%The test data file should be saved as test1,2,3 etc sequential
order

testnumber = get(handles.testtxt,'string');
t=str2num(testnumber);
```

Appendix 5

```
directory = uigetdir('C:\Documents and Settings\Sarah T\My
Documents','Choose correct directory');
[File Path] = uigetfile('C:\Documents and Settings\Sarah T\My
Documents\*.xls','Choose Excel Data File');
FilePath = strcat(Path,File);
%Takes the test data and records the data and the calculated
friction and
%normal force to excel

%uses the gain information to select the right calibration factor
for the %normal force and friction force calculations
str = get(handles.gainpopup, 'String');
val = get(handles.gainpopup, 'Value');
switch str[128];
    case '0.5k (least sensitive)'
        calN = 46.2;
        calF = 46.4;
        gainvalue = '0.5k';
    case '1k'
        calN = 23.3;
        calF = 23.8;
        gainvalue = '1k';
    case '2.5k'
        calN = 9.3;
        calF = 9.2;
        gainvalue = '2.5k';
    case '5k (most sensitive)'
        calN = 4.9;
        calF = 4.7;
        gainvalue = '5k';
end

%loop to calculate the average friction and normal force for each
test
for i = 1:t
%selects the text data file
filename = strcat(directory,'\test',int2str(i),'.txt');
handles.data = dlmread(filename,'\t');
a = handles.data;
guidata(hObject, handles);
%separates the friction and normal force data from the text file
(note that %the normal force load cell should be in channel 2 of the
DAQ and the %friction force load cell in channel 1
F = a(:,1);
N = a(:,2);
%zeroing of the base line force
xN = N(1:1000,1);
xF = F(1:1000,1);
Nmod = N-mean(xN);
Fmod = F-mean(xF);

%calculation of the forces and then writing the data to the
specified excel %file
NormalF = Nmod.*calN;
FrictionalF = Fmod.*calF;
b = horzcat(N,F,NormalF,FrictionalF);
c = [1 1 1 1];
d = vertcat(c,b);
Title={'N readout (V)', 'F readout (V)', 'Normal Force (N)',
'Friction Force (N)'};
ForceData = d;
```

Appendix 5

```
Sheetname = strcat('Test',int2str(i));
xlswrite(FilePath,ForceData,Sheetname);
xlswrite(FilePath,Title,Sheetname,'A1');
end
%Indicates data has been added
msgbox('Data added')

% --- Executes on button press in summarybtn.
function summarybtn_Callback(hObject, eventdata, handles)
%Creates a summary sheet in the specified excel sheet of the given
number
%of tests. Summary includes test number, average and standard
deviation of
%normal and friction force
testnumber = get(handles.testtxt,'string');
t=str2num(testnumber);
directory = uigetdir('C:\Documents and Settings\Sarah T\My
Documents','Choose correct directory');
[File2 Path2] = uigetfile('C:\Documents and Settings\Sarah T\My
Documents\*.xls','Choose Excel Data File');
FilePath2 = strcat(Path2,File2);

%loop to calculate the average friction and normal force for each
test
for i = 1:t
set(handles.numinfotxt,'string',i)
filename = strcat(directory,'\test',int2str(i),'.txt');
handles.data = dlmread(filename,'\t');
a = handles.data;
guidata(hObject, handles);

%separates the friction and normal force data from the text file
(note that %the normal force load cell should be in channel 2 of the
DAQ and the %friction force load cell in channel 1
F = a(:,1);
N = a(:,2);
xN = N(1:1000,1);
xF = F(1:1000,1);
Nmod = N-mean(xN);
Fmod = F-mean(xF);

%uses the gain information to select the right calibration factor
for the %normal force and friction force calculations
str = get(handles.gainpopup, 'String');
val = get(handles.gainpopup, 'Value');
switch str[128];
    case '0.5k (least sensitive)'
        calN = 46.2;
        calF = 46.4;
        gainvalue = '0.5k';
    case '1k'
        calN = 23.3;
        calF = 23.8;
        gainvalue = '1k';
    case '2.5k'
        calN = 9.3;
        calF = 9.2;
        gainvalue = '2.5k';
    case '5k (most sensitive)'
        calN = 4.9;
        calF = 4.7;
```

Appendix 5

```
        gainvalue = '5k';
    end

%calculates the friction force and normal force

NormalF = Nmod.*calN;
FrictionalF = Fmod.*calF;

%Plots friction force and normal force
z1=1:length(NormalF);
z2=1:length(FrictionalF);
handles.outputplot=plot(z1,NormalF,z2,FrictionalF);
ylabel('Friction or Normal force (N)');
s=legend('Normal force','Friction Force',-1);
set(handles.datatxt, 'string', 'Double click start and end point for
friction summary calculation')
%Select the start and end points for the average force calculations
handles.spt=getpts;
handles.fpt=getpts;
normG=NormalF(handles.spt:handles.fpt);
fricG=FrictionalF(handles.spt:handles.fpt);
%Average and standard deviation calculations
AveN = mean(normG);
AveF = mean(fricG);
stdevN = std(normG);
stdevF = std(fricG);

%Calculation of speed, based on a slide of 6.5 cm, however this
value needs %to be altered depending on the test
set(handles.datatxt, 'string', 'Double click start and end point for
speed calculation')
start = getpts;
finish = getpts;
X1 = start(1,1);
X2 = finish(1,1);
amount = X2 - X1;
rate = str2num(get(handles.ratetxt, 'string'));
time = amount/rate;
speed = 0.065/time;

%Add data to the summary sheet
M = get(handles.moisturetxt, 'string');
T = get(handles.temperaturetxt, 'string');
H = get(handles.humiditytxt, 'string');

Title2={'TestID', 'Average N (N)', 'Stddev N', 'Average F
(N)', 'stddev F', 'Speed (m/s)', 'Moisture (Moistsense)',
'Temperature (°C)', 'Humidity (%)' };
xlswrite(FilePath2,Title2,'Summary','A1');
d=i+1;
e=int2str(d);
p=strcat('A',e);
q={i,AveN,stdevN,AveF,stdevF,speed,M,T,H};
xlswrite(FilePath2,q,'Summary',p);

end
%Indicates data has been added

msgbox('Data added')
```

Appendix 6

Appendix 6– Results from tests with 32 volunteers examining the effect of normal force on friction force

Test ID	Gender	Age	Finger Area (mm ²)	Steel			Glass			Rugby ball rubber		
				Slope	Intercept	R ² Value	Slope	Intercept	R ² Value	Slope	Intercept	R ² Value
F1	Female	27	266	0.69	0.67	0.95	0.73	2.74	0.96	2.30	-0.03	0.98
F2	Female	26	228	0.51	3.70	0.85	0.92	3.28	0.98	0.67	6.04	0.58
F3	Male	24	436	0.52	0.82	0.99	0.41	2.77	0.83	2.50	-1.12	1.00
F4	Male	25	322	0.89	2.69	0.98	0.98	7.43	0.93	2.58	3.02	0.99
F5	Male	29	274	0.85	0.68	0.97	0.86	7.84	0.71	2.84	0.23	0.98
F6	Male	23	205	0.95	2.05	0.97	0.57	11.03	0.78	2.46	-0.79	1.00
F7	Female	22	267	0.72	1.99	0.93	1.17	1.76	0.97	2.08	-0.09	0.99
F8	Male	21	300	1.23	2.09	0.98	1.31	1.29	0.99	2.35	0.34	0.98
F9	Female	34	245	1.04	2.13	0.97	1.64	1.05	0.96	1.67	1.38	0.99
F10	Male	33	273	0.40	1.37	0.98	0.51	5.21	0.97	1.66	5.78	0.94
F11	Male	29	316	0.78	3.11	0.96	0.92	4.59	0.95	0.88	3.65	0.97
F12	Male	27	293	0.76	2.35	0.92	1.70	0.88	1.00	2.40	-0.91	1.00
F13	Male	23	317	0.94	5.05	0.97	0.45	3.95	0.96	1.55	8.37	0.86
F14	Male	49	493	0.64	1.58	0.96	0.99	-5.83	1.00	2.34	-1.69	1.00
F15	Male	22	284	0.77	1.48	0.97	1.59	-11.67	0.95	2.44	0.26	0.98
F16	Male	24	377	1.24	3.43	0.99	1.21	2.74	0.94	1.79	2.84	0.95

Appendix 6

F17	Male	27	392	0.72	4.69	0.96	1.46	-4.84	0.97	1.11	9.63	0.88
F18	Male	24	281	0.81	-0.26	0.97	0.85	-3.78	0.99	1.41	4.19	0.97
F19	Male	23	285	0.90	1.89	0.95	1.30	-7.49	0.97	2.08	-0.54	0.99
F20	Male	47	351	0.39	10.69	0.79	0.98	1.16	0.95	2.64	-4.29	0.89
F21	Male	30	257	0.84	1.94	0.94	1.01	-0.54	0.85	1.13	1.74	0.97
F22	Male	32	261	0.80	3.39	0.97	1.36	-3.73	0.99	0.61	10.29	0.89
F23	Female	37	283	0.40	0.82	0.98	0.71	-2.40	0.84	1.60	1.53	0.95
F24	Male	31	380	0.77	2.64	0.93	1.43	-7.22	0.82	2.35	-0.89	0.94
F25	Male	26	330	1.00	2.02	0.99	1.01	0.65	0.96	1.12	9.51	0.97
F26	Male	23	345	0.50	3.73	0.94	0.77	-1.37	0.99	0.67	5.61	0.77
F27	Male	39	252	0.37	1.24	1.00	0.43	-0.51	0.97	2.13	0.36	0.98
F28	Male	27	222	0.98	-0.65	1.00	0.92	-4.83	0.97	0.99	2.93	0.94
F29	Male	23	307	0.84	2.24	0.70	0.58	1.94	0.77	1.94	-0.80	0.97
F30	Female	31	217	1.31	0.17	0.96	0.59	-0.80	0.60	1.49	3.99	0.73
F31	Male	30	303	0.96	1.98	0.93	1.42	-9.65	0.98	1.88	3.96	0.94
F32	Male	22	189	0.92	0.51	0.98	0.71	-2.69	0.96	0.86	2.33	0.82

Appendix 7 - Sample calculation of the adhesive friction, for brass

Figure A5.1.1 shows a plot of the shear stress against applied pressure. These were calculated by taking the ratio of the friction and normal force to contact area (respectively). The gradient of the graph then provides the value α and the intercept is τ_0 , for use in Equation 5.11. These values can also be calculated numerically using the equations provided in [108].

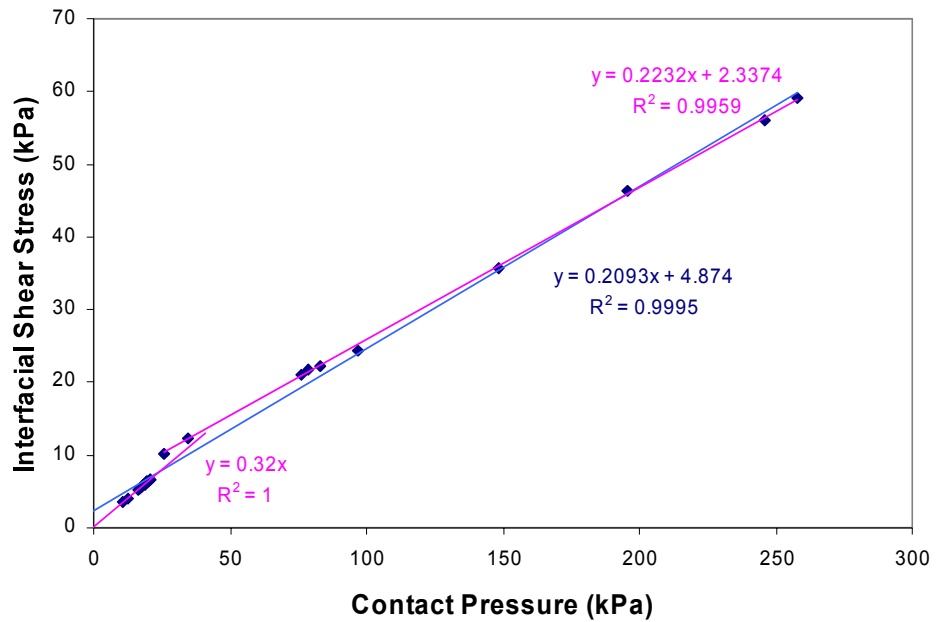


Figure A5.1.1 – Plot of interfacial shear stress against contact pressure, for a finger sliding on brass

Appendix 8

Appendix 8 – Summary of surveyed textures

ID	Tool	Use	Type of grip	Grip dimensions (mm)	Material	Pattern description line	Shape of pattern
1	High speed dental hand piece	Dental drilling	Lateral	11.9 - 17.4	Metal - Stainless Steel?	Oval indented pattern	Dimples
2	Dental tweezers	Hold flesh out of the way whilst carrying out work on teeth	Lateral	10.3 - 15	Metal - Stainless Steel?	Ridges, made from elongated ovals	Ridges
3	Right angle bur	Cutting	Lateral	8	Metal - Stainless Steel?	Thin criss-crossed ridges forming a pattern of diamonds	Grooves
4	Dental tweezers	Hold flesh out of the way whilst carrying out work on teeth	Lateral	6.9 - 11.4	Metal - Stainless Steel?	Thin criss-crossed ridges forming a pattern of diamonds	Grooves
5	Probe	Inspect the teeth. E.g.: pocket depths around the teeth	Lateral	5	Metal - Stainless Steel?	Ridges	ridges
6	?	Dentistry	Lateral	3.9	Metal -Brass?	Round ridges specific for the index finger and thumb grip	Ridges

Appendix 8

7	Probe	Inspect the teeth. E.g.: pocket depths around the teeth	Lateral	5.6	Metal - Stainless Steel?	Ridges, but on each ridge there is a criss-cross of thin ridges to form a diamond pattern	Ridges
8	Right angle bur	Cutting	Lateral	8.3	Metal - Stainless Steel?	Thin criss-crossed ridges forming a pattern of diamonds	Grooves
9	Filling holder	Turn wheel to tighten up the space to put the filling material	Tip	10	Metal - Stainless Steel?	Ridges	Ridges
10	Ultrasonic tool	Held next to teeth and the ultrasonic breaks up the plaque	Lateral	9.5	Hard polymer	Ridges	Ridges
11	High speed dental hand piece	Dental drilling	Lateral	12.3 - 15.7	Metal - Stainless Steel?	Pattern of elongated hexagons with a ridge running through the centre of the hexagons, the width of the sides.	Pimples
12	Ultrasonic tool	Held next to teeth and the ultrasonic breaks up the plaque	Lateral	12.4	Polymer	Round, sparsely populated dimples	Dimples
13	Mirror	Held to see things out of view	Lateral	11	Soft polymer	Round, sparsely populated pimples	Pimples
14	Mirror	Held to see things out of view	Lateral	6.42	Metal - Stainless Steel?	Very fine criss-cross of ridges	Grooves

Appendix 8

15	Precision work tool	Small tool used for very fine and intricate work	Tip	3.1 - 3.6	Hard polymer	Widely spaced ridges	Ridges
16	Precision work tool	Small tool used for very fine and intricate work	Tip		Soft polymer	Vertical slits (x4) in the direction of the finger	Dimples
17	Dental tweezers	Hold flesh out of the way whilst carrying out work on teeth	Lateral	8.5 - 15.8	Metal - Aluminium?	circular grooves to produce thin ridges	Ridges
18a	?	Used to hold gum etc away from the area worked on	Lateral		Metal - Stainless Steel?	No pattern - indentation for fingers to rest on	None
18b	Dental Pliers	Used to put objects in place	Cylindrical		Metal - Stainless Steel?	Smooth - no pattern	None
18c	Dental Pliers	Used to put objects in place	Cylindrical		Metal - Stainless Steel?	Smooth - no pattern	None
19	Top for a putty gun	Turn the top to click into place on the gun	Lateral	14.6	Plastic	Ridges	Ridges
20	Bottle	Turn the lid to open the bottle	Lateral	16.6	Plastic	Ridges	Ridges

Appendix 8

21	Bottle	Turn the lid to open the bottle	Lateral	21	Plastic	Ridges, sequence of 5 close together and then a large gap	Ridges
22	Bottle	Turn the lid to open the bottle	Lateral	32.8	Plastic	Ridges	Ridges
23	Bottle	Turn the lid to open the bottle	Lateral	20.9	Plastic	Ridges	Ridges
24	Casing of needle for syringe (bottom)	The top is twisted off and that end of the needle place in the syringe, the bottom can then be removed to expose the needle to go in the skin	Lateral	7.5	Plastic	Ridges	Ridges
25	Casing of needle for syringe (top)	The top is twisted off and that end of the needle place in the syringe, the bottom can then be removed to expose the needle to go in the skin	Lateral	9	Plastic	Ridges	Ridges

Appendix 8

26	Caplet for a silver filling	The top and bottom are twisted in opposing directions to mix the two metal compounds, to form the silver filling	Lateral	12.8	Plastic	Ridges	Ridges
27	Caplet for a silver filling (top)	The top and bottom are twisted in opposing directions to mix the two metal compounds, to form the silver filling	Lateral	11.9	Plastic	Ridges	Ridges
28	Caplet for a silver filling (bottom)	The top and bottom are twisted in opposing directions to mix the two metal compounds, to form the silver filling	Lateral	15.2	Plastic	Ridges	Ridges
29	Top for a precision instrument	Turned to fix in place on the instrument	Lateral	5.6	Plastic	Widely spaced ridges	Ridges
30	Caplet for a silver filling	Two parts pushed together and then shaken to allow the compounds to mix	tip	-	Polymer, quite soft but not flexible	none	None

Appendix 8

31	Cap for tools	Tool top is pulled off when the tool is to be used. This can often be difficult as it has no texture on the surface	tip	-	Plastic - hard	none	None
32	Bike handle	Holding on when riding a bike	Cylindrical	32	Elastomer	Raised ovals, with hollow centre	Pimples
33	Bike handle	Holding on when riding a bike	Cylindrical	27	Elastomer	Raised rectangles	Pimples
34	Bike handle	Holding on when riding a bike	Cylindrical	32 to 28 (thicker on outside of handle)	Elastomer	Rough surface. On top of this are 8 raised ovals which contain 3 grooves	Pimples
35	Toddler's bike handle	Holding on when riding a bike	Cylindrical	27	Elastomer	Lines of dimples	Dimples
36	Bike handle	Holding on when riding a bike	Cylindrical	30	Elastomer	Criss-crossed grooves to make diamonds. Occasional hexagon shapes and diamonds/hexagons with 3 layers	Ridges
37	Bike handle	Holding on when riding a bike	Cylindrical	29	Elastomer	Small criss-crossed grooves to make diamonds	Grooves

Appendix 8

38	Bike handle	Holding on when riding a bike	Cylindrical	34	Elastomer	Lines of dimples. There are 6 raised ridges along the length of the handle with no dimples (every 5 lines of dimples)	Dimples
39	Basket ball	Passing, catching, dribbling	Spherical	n/a	Elastomer	Irregular, roundish pimples	Pimples
40	Basket ball	Passing, catching, dribbling	Spherical	n/a	Elastomer	Resembles a repeated tyre track	Pimples
41	Basket ball	Passing, catching, dribbling	Spherical	n/a	Synthetic leather	Flat top pimple pattern of irregular shapes	Pimples
42	Hockey stick	Textured part is where the main holding hand is positioned	Cylindrical	27	Polymer tape	Series of arches	Pimples
43	Hockey stick	Textured part is where the main holding hand is positioned	Cylindrical	29	Polymer tape	7 lines of dimples per wrap	Dimples
44	Hockey stick	Textured part is where the main holding hand is positioned	Cylindrical	29	Polymer tape	Series of shaped grooves	Grooves
45	Hockey stick	Textured part is where the main holding hand is positioned	Cylindrical	29	Polymer tape	Squares containing opposing directions of grooves (3 grooves per square)	Pimples
46	Hockey stick	Textured part is where the main holding hand is positioned	Cylindrical	29	Polymer tape	Large round dimples	Dimples

Appendix 8

47	Hockey stick	Textured part is where the main holding hand is positioned	Cylindrical	29	Polymer tape	Criss-crossed pattern of grooves	Grooves
48	Hockey stick	Textured part is where the main holding hand is positioned	Cylindrical	29	Polymer tape	Curved ridges	Ridges
49	Racing bike handles		Cylindrical		Velvet feel wrap	No texture	None
50	Resistance tube	A tube with a handle at each end, used to increase intensity of certain exercises	Cylindrical		Soft cushioned	Micro textured material	Roughness
51	Medicine ball	Used to add resistance to exercises	Spherical		Polymer	Irregular micro roughness	Roughness
52	Weight bars and dumbbells	Exercising muscles	Cylindrical	31	Metal	Criss-crossed grooves	Grooves
53	Rackets	Table tennis/ badminton/ tennis	Cylindrical		Either have a polymer wrap or a wood/polymer handle	No added texture	None
54	Golf club	Held with 2 hands (clubs were woods, drivers or irons)	Cylindrical	28 to 19 (largest diameter at top of club)	Elastomer	Hexagons with a central groove	Pimples

Appendix 8

55	Golf club	Held with 2 hands (clubs were woods, drivers or irons)	Cylindrical	28 to 19 (largest diameter at top of club)	Elastomer	V-shapes with a central groove	Pimples
56	Golf club	Held with 2 hands (clubs were woods, drivers or irons)	Cylindrical	28 to 19 (largest diameter at top of club)	Elastomer	Crosses cut out with a larger vertical body than the horizontal part of the cross	Dimples
57	Fishing rod		Cylindrical		Polymer	Micro textured material	Roughness
58	Walking frame	Used as a walking aid	Cylindrical	37	Elastomer	Irregular raised roughness	Roughness
59	Walking trolley	Used as a walking aid, but also has trays for carrying items (it is on wheels)	Cylindrical	Shaped handle	Elastomer	Irregular raised roughness	Roughness
60	Tripod cane with broad base	Walking aid	Cylindrical	Shaped handle Approx. 35	Hard polymer	Criss-crossed grooves	Grooves
61	Electric wheelchair front handles	Stability safety handles for when the wheel chair is in motion	Cylindrical	39	Elastomer	Irregular raised roughness	Roughness
62	Electric wheelchair front handles	Stability safety handles for when the wheel chair is in motion	Cylindrical	30	Elastomer	4 raised panels with criss-crossed grooves to form diamonds	Grooves

Appendix 8

63	Electric wheelchair front handles	Stability safety handles for when the wheelchair is in motion	Cylindrical	The handles are rounded as opposed to the just straight ones	Uses very soft elastomer, with no texture	none	None
64	Wheelchair push handles	Used to push the wheelchair	Cylindrical	31	Elastomer	Irregular micro roughness	Roughness
65	Wheelchair push handles	Used to push the wheelchair	Cylindrical	30	Foam	No added texture	None
66	Wheelchair push handles	Used to push the wheelchair	Cylindrical	27	Hard polymer	High ridges on the top of the handle, but no ridges on the bottom	Ridges
67	Wheelchair push handles	Used to push the wheelchair	Cylindrical	28	Soft polymer	V-shapes of flexible ridges, on the top of the handle	Ridges
68	Walking sticks and crouches	Used as a stability aid when walking	Cylindrical			Same variety of materials and textures as seen for walking frame and tripod. No textures used on crouches	None
69	2 litre milk bottle top	Keep the bottle sealed	Lateral	43	Plastic	Arches of closely spaced ridges	Ridges
70	2 litre squash bottle top	Keep the bottle sealed	Lateral	40 - 42 (Widest at the bottom of lid)	Plastic	Widely spaced high ridges	Ridges

Appendix 8

71	4 pint milk bottle top	Keep the bottle sealed	Lateral	39	Plastic	Widely spaced high ridges, every other has a small short ridge either side, which merge into the lid at the top	Ridges
72	75cl wine bottle screw top	Keep the bottle sealed	Lateral	30	Thin metal (aluminium?)	Ridges only on bottom part of lid. 3 circumferential ridges on the top of the lid.	Ridges
73	Screw top on bottle of olive oil	Keep the bottle sealed	Lateral	32	Thin metal	Series of ridges at the top of the lid. 3 circumferential ridges on the bottom of the lid.	Ridges
74	Milkshake mix carton lid	Keep the carton sealed	Spherical	88	Plastic	Ridges	Ridges
75	Hot chocolate carton lid	Keep the carton sealed	Spherical	78.3	Plastic	Ridges on bottom part (to over half way) which then merge into the smooth top half of the lid	Ridges
76	Lid on bottle of milkshake	Keep the carton sealed	Lateral	36	Plastic	Ridges	Ridges
77	Kitchen utensils, grip section	Found on large spoons, pie slice and potato masher, section there to stop the hand slipping on the otherwise smooth surface	Lateral / Cylindrical	Oval, 23.2 mm wide and 15 mm high	Elastomer	Small circumferential ridges and then on the front of the utensil there are 3 rectangles	Ridges

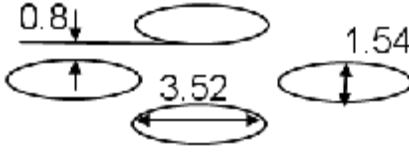
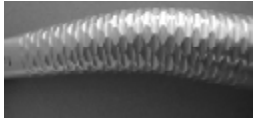
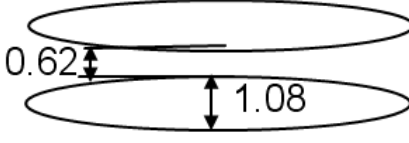
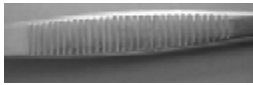
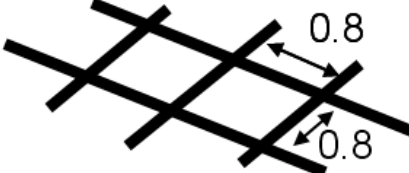
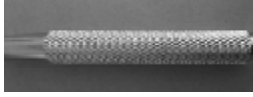
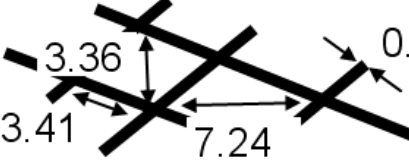


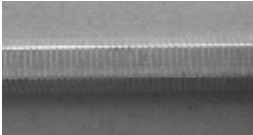
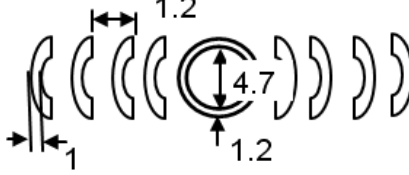

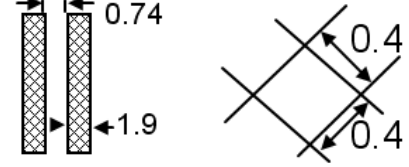

Appendix 8

78	Iron	Used to iron clothes	Cylindrical	Oval, 41.5 mm wide and 28 mm high	Elastomer grip, but a plastic handle	Large area of un-patterned elastomer. At the end of this there are 2 curved ridges.	Ridges
79	Hair straighteners	Used to style hair	Cylindrical	38 - 56	Hard polymer	Criss-crossed grooves to make diamonds.	Grooves
80	Twist top deodorant, aerosol can	Top of can twisted so that it moves down, exposing the aerosol mechanism to spray the deodorant	Cylindrical	51.5	Plastic	Ridges	Ridges
81	Electric toothbrush	Brushing teeth	Cylindrical	27	Elastomer	Round pimples	Pimples
82	Electric toothbrush	Brushing teeth	Cylindrical	30	Elastomer	Closely spaced ridges at the brush end, which get more widely spaced away from the brush	Ridges
83	Men's disposable razor	Shaving face	Lateral	Rectangular, 9.9 mm high and 9.9 mm wide	Plastic	Ridges	Ridges
84	Women's disposable razor	Shaving areas other than the face, so the razor may not only be held on the sides but also sometimes a supporting finger on the top e.g.: for when shaving legs	Lateral / pulp grip	Square, 10 mm	Elastomer (hard)	Ridges on the sides and oval dimples on the top	Ridges

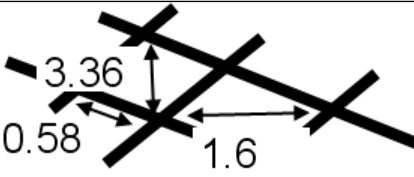
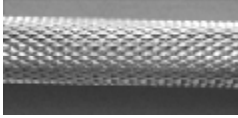
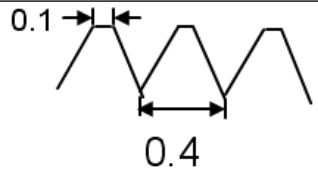

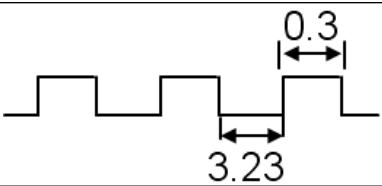

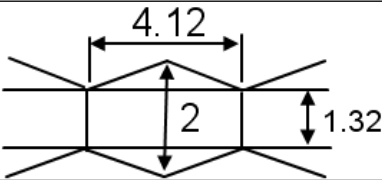

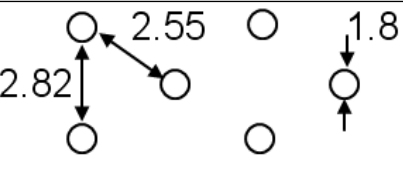
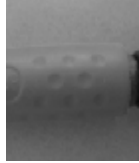
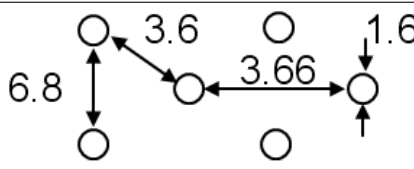
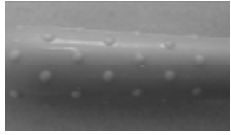

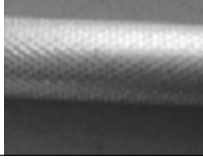
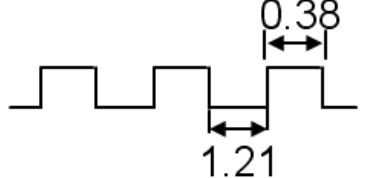

Appendix 8

85	Tweezers	Plucking hairs	Lateral	6.5 - 13.4	Metal (Steel?)	Ridges	Ridges
86	Women's anti-clog roll on deodorant twist body	Twist the body to remove the lid (which is at the bottom of the container), then hold the body to roll on the deodorant.	Lateral / Cylindrical	44.5	Plastic	Round dimples	Dimples
87	hair brush	Styling hair	Cylindrical	Oval, 28.4 mm wide and 20 mm high	Elastomer (hard)	Ridges	Ridges
88	Rugby ball	Kicking, throwing, catching and holding	Spherical	n/a	Elastomer	Round pimples, wide and spaced closely together	Pimples
89	Rugby ball	Kicking, throwing, catching and holding	Spherical	n/a	Elastomer	Round pimples, small diameter, fairly high and widely spaced	Pimples
90	Rugby ball	Kicking, throwing, catching and holding	Spherical	n/a	Elastomer	Square pimples, fairly high and widely spaced	Pimples
91	Rugby ball	Kicking, throwing, catching and holding	Spherical	n/a	Elastomer	Mixture of large and small square pimples	Pimples

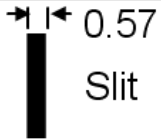

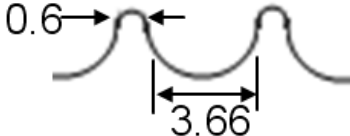
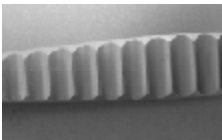
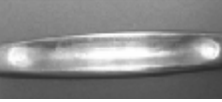
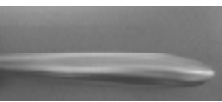
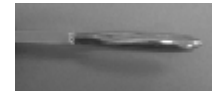
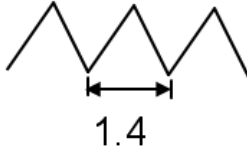
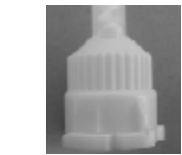
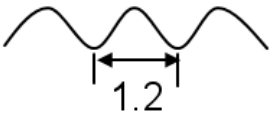

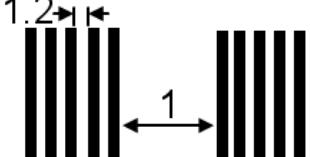

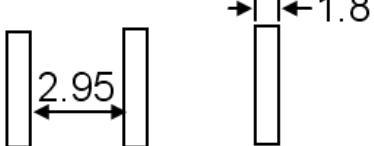
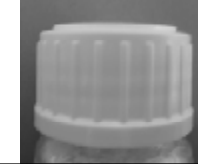
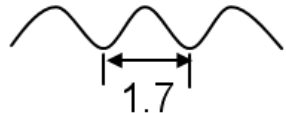

Appendix 8

ID	Pattern Size and Spacing	Height of pattern	Photo
1		Varies, at it's largest it is 0.9 mm	
2		0.2	
3		Can't measure height	
4		0.22	
5		Can't measure height	
6		0.36	
7		0.225	


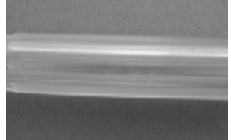
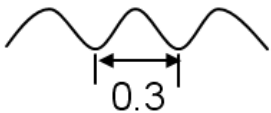

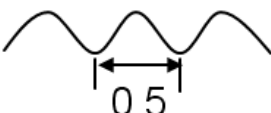

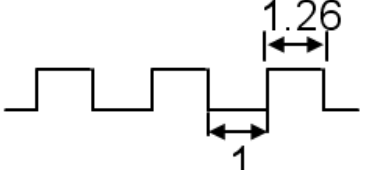



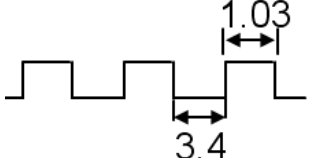



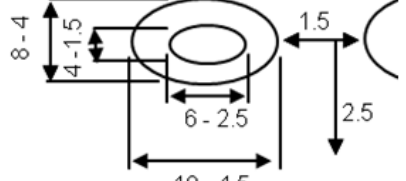

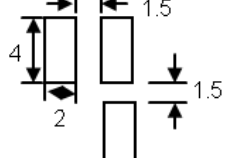
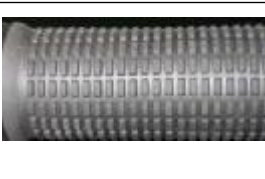
Appendix 8

8		Can't measure height	
9		Can't measure height	
10		0.2	
11		Can't measure height	
12		Can't measure height	
13		Can't measure height	
14		Can't measure height	
15		0.11	

Appendix 8

16	 <p>0.57 Slit</p>	N/A	
17	 <p>0.6 3.66</p>	0.8	
18a		n/a	
18b		n/a	
18c		n/a	
19	 <p>1.4</p>	Can't measure height	
20	 <p>1.2</p>	Can't measure height	
21	 <p>1.2 1</p>	Can't measure height	
22	 <p>2.95 1.8</p>	0.48	
23	 <p>1.7</p>	Can't measure height	



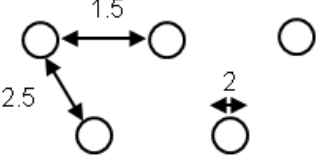

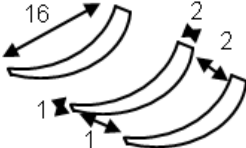
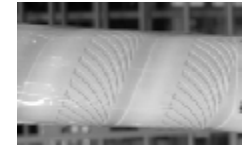
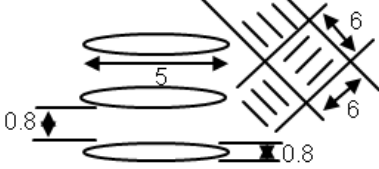

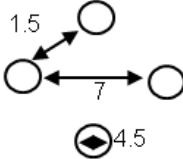

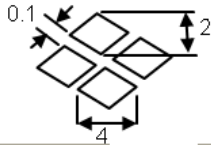

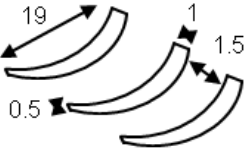



Appendix 8

24		0.39	
25		Can't measure height	
26		Can't measure height	
27		Can't measure height	
28		Can't measure height	
29		0.45	
30		n/a	
31		n/a	
32		1.5	
33		0.5	


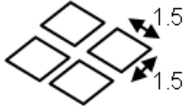


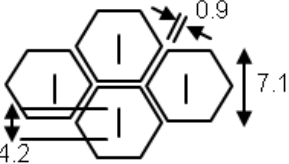

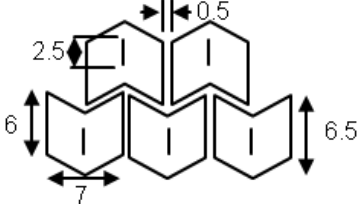

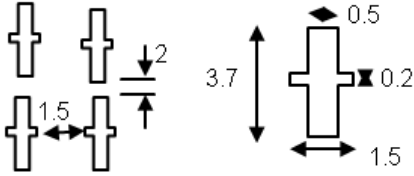
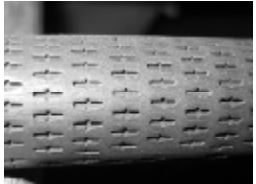


Appendix 8

34		0.3	
35		approx. 1.5 (Couldn't measure)	
36		0.5	
37		approx. 0.5	
38		approx. 0.5 (Couldn't measure)	
39		Approx. 0.2	
40		0.5	
41		Less than 0.1 (Couldn't measure)	

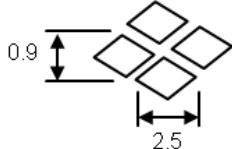


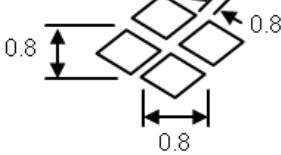







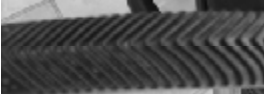
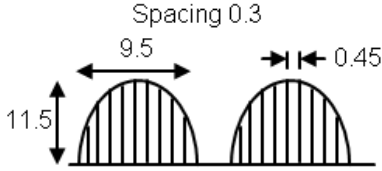
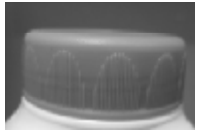
Appendix 8

42	<p>width = 1.5</p> 	Approx. 0.2mm (Couldn't measure)	
43		Approx. 0.3 (Couldn't measure)	
44		Approx. 0.3 (Couldn't measure)	
45		Approx. 0.1 (Couldn't measure)	
46		Approx. 0.2-0.3 (Couldn't measure)	
47		Approx. 0.1-0.2 (Couldn't measure)	
48		Approx. 0.1 (Couldn't measure)	
49			
50			

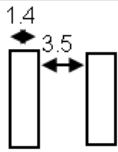
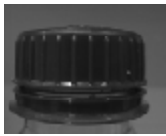
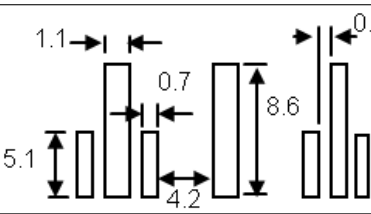

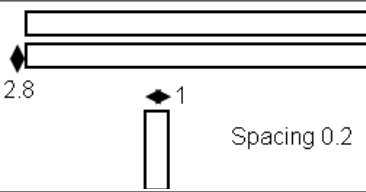

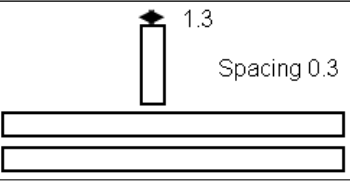

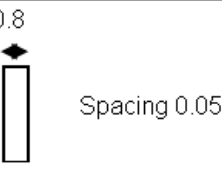
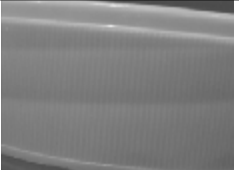
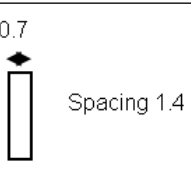


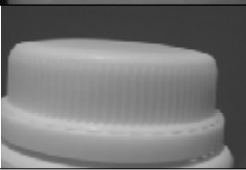
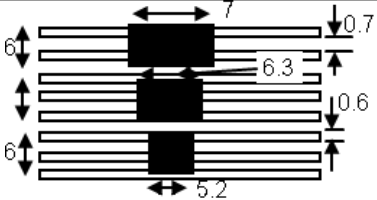

Appendix 8

51			
52		Approx. 0.1-0.2 (Couldn't measure)	
53			
54		Approx. 0.3	
55		0.5	
56		Approx. 0.4	
57			
58			
59			

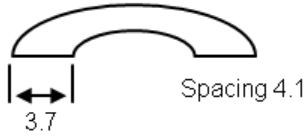
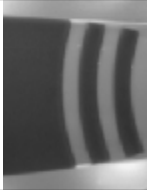
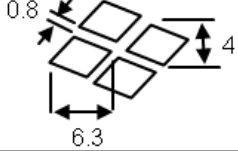

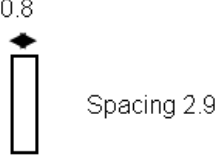

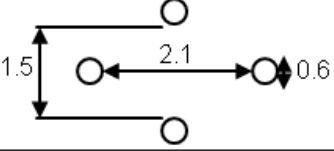

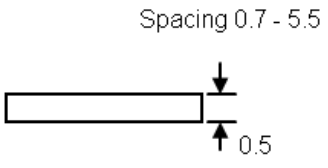



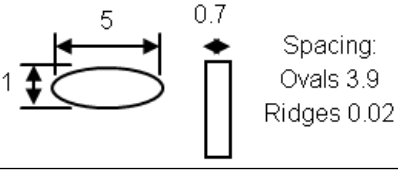

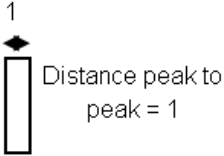
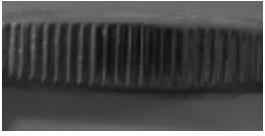
Appendix 8

60		Approx. 0.1 (Couldn't measure)	
61			
62		Approx. 0.1 (Couldn't measure)	
63			
64			
65			
66		5	
67			
68			
69		0.3	

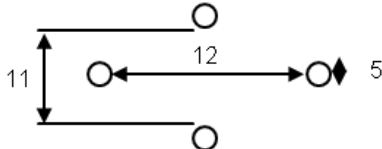
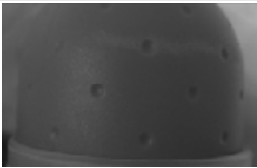







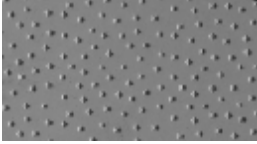
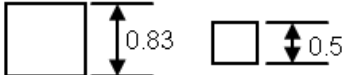
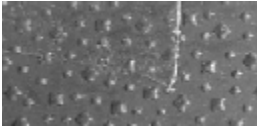
Appendix 8

70		0.5	
71		0.8	
72		Approx. 0.1 - 0.2 (Couldn't measure)	
73		Approx. 0.2 (Couldn't measure)	
74		Approx. 0.1 (Couldn't measure)	
75		Approx. 0.1 (Couldn't measure)	
76		Approx. 0.1 - 0.2 (Couldn't measure)	
77		Approx. 0.2 (Couldn't measure)	

Appendix 8

78	 <p>Spacing 4.1</p>	Approx. 0.1 (Couldn't measure)	
79		Approx. 0.2 (Couldn't measure)	
80	 <p>Spacing 2.9</p>	Approx. 0.1 (Couldn't measure)	
81		Approx. 0.1 (Couldn't measure)	
82	 <p>Spacing 0.7 - 5.5</p>	Approx. 0.2 (Couldn't measure)	
83		Approx. 0.3 (Couldn't measure)	
84	 <p>Spacing: Ovals 3.9 Ridges 0.02</p>	Oval - 0.4 Ridges - approx. 0.3 (Couldn't measure ridge height)	
85	 <p>Distance peak to peak = 1</p>	Approx. 0.05 (Couldn't measure)	

Appendix 8

86		Approx. 0.1 - 0.2 (Couldn't measure)	
87		0 - 3 (Arched profile)	
88	<p>Spacing 0.1 - 0.7</p> 	0.26	
89	<p>Spacing 0.8 - 2.6</p> 	0.36	
90	<p>Spacing 1 - 3.2</p> 	0.37	
91	<p>Spacing 0.1 - 1.2</p> 	0.37 0.20	

Appendix 9 – Spring Constant of an Uncompressed Finger

A finger was loaded with a brass indenter, of thickness 0.58 mm, and depth greater than that of the finger. The deflection of the finger was recorded, by tracking the bottom corner (facing edge) of the brass indenter. The results are shown in Figure A7.2.1. This shows that under this loading condition the spring is non-linear, contrary to the loading of the finger on a flat plate, where the spring constant was linear (Chapter 5).

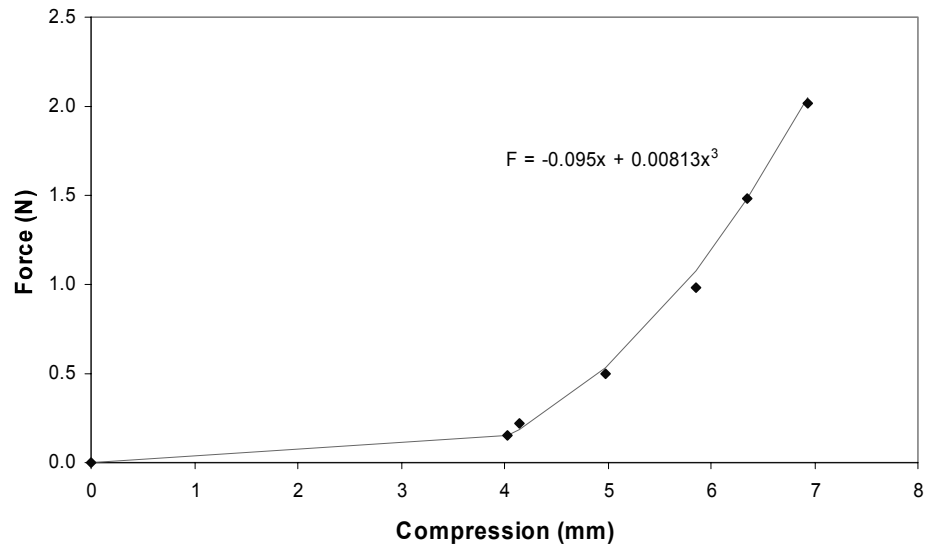
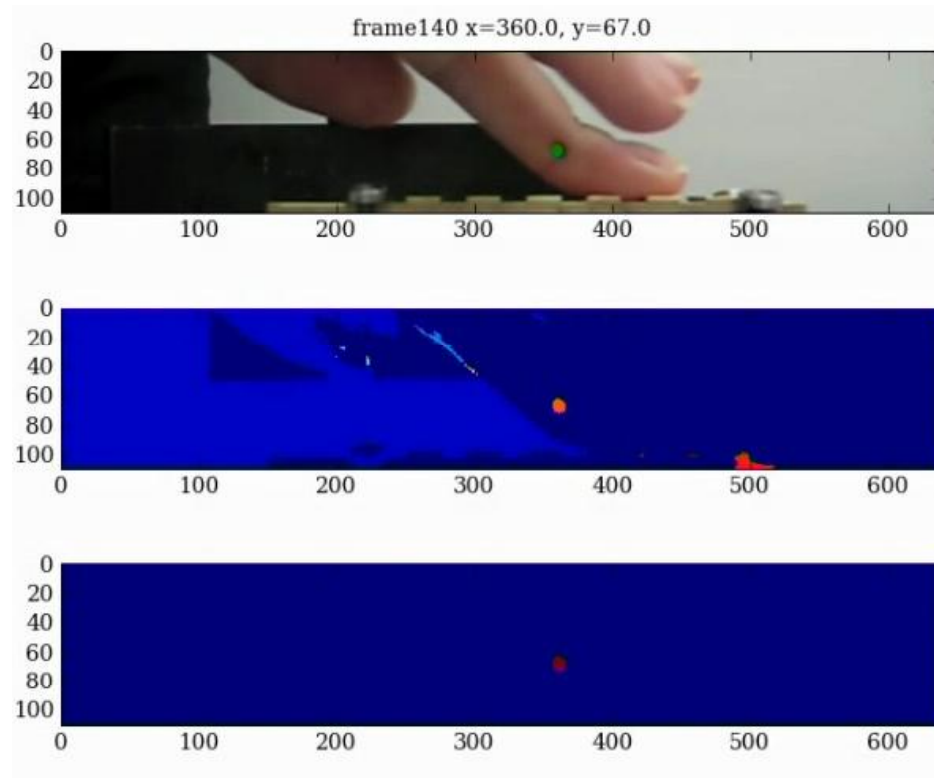


Figure A7.2.1 – the force vs. compression data for a brass knife edge loaded onto a finger pad






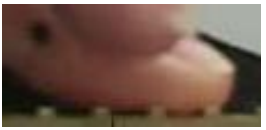












Appendix 10 – Tracking of Finger, Video Output

















Appendix 11 – The Equations for the Lines of Best Fit Relating the Normal Force to the Maximum and Minimum Friction Force

Texture	Max. Friction			Min. Friction		
	Gradient	Intercept	R-squared	Gradient	Intercept	R-squared
1	0.64	-0.39	0.94	0.60	-0.39	0.95
2	0.93	-0.04	0.92	0.62	-0.15	0.95
3	0.71	0.19	0.97	0.62	0.06	0.97
4	0.78	0.15	0.95	0.23	0.12	0.77
5	0.71	0.76	0.89	0.49	-0.22	0.95
6	0.47	-0.04	0.95	0.41	-0.02	0.96
7	0.53	0.11	0.96	0.41	0.11	0.94
8	0.70	-0.09	0.95	0.48	-0.01	0.93
9	0.76	-0.08	0.94	0.47	0.11	0.91
10	0.62	0.47	0.92	0.46	-0.20	0.95
11	0.87	-0.21	0.97	0.70	-0.09	0.97
14	0.66	-0.03	0.93	0.47	-0.12	0.94
15	0.61	-0.22	0.92	0.41	-0.19	0.96
16	0.51	0.37	0.90	0.43	0.09	0.93
18	0.69	-0.38	0.93	0.50	-0.30	0.95
19	0.71	-0.18	0.93	0.54	-0.23	0.95
20	0.80	-0.31	0.93	0.59	-0.24	0.95

Appendix 12 - Positioning of the Finger at Maximum and Minimum Points of Friction, During the Same Slide

Texture ID	Position of Finger	
	Maximum Friction	Minimum Friction
R1		
R2		
W2		
R4		
S1		
S2W3H2		
S3		
S4		
S5		

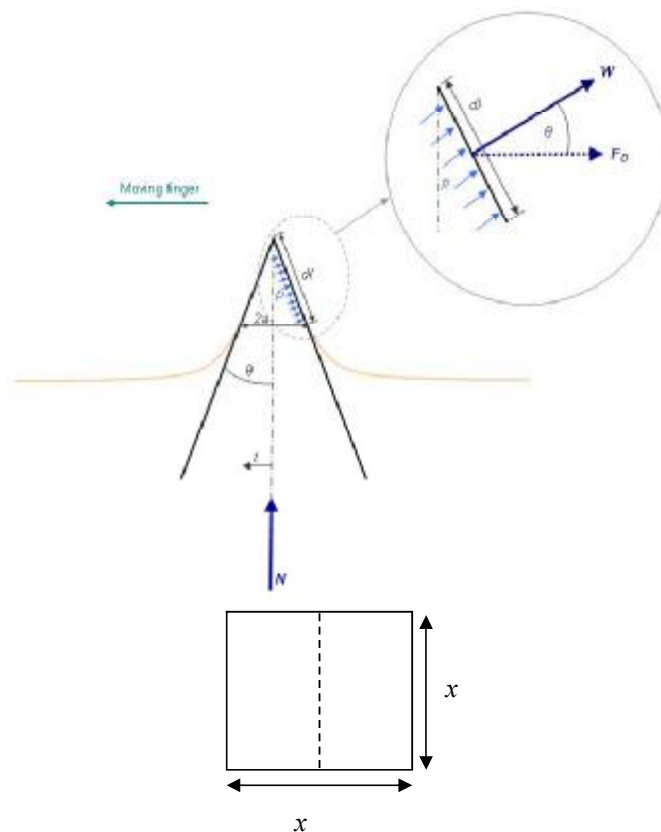
Appendix 12

W1		
W4		
W5		
H1		
H3		
H4		
H5		

Appendix 13 – Derivation of Hysteresis Friction, for Pyramid Pimples

Assumptions:

- Frictionless contact. In assuming this, it is assumed that the pressure acts perpendicular to the pimple edge. This is obviously not the case in reality, so could alter the overall hysteresis contribution to friction.
- All pimples are aligned perpendicular to the direction of the finger slide. Again, this is a simplification, since the pimples are in a multitude of directions along the surface.
- Indenter does not deform. The pimple is made from rubber. This has a lower Young's modulus than the finger, so compared to the finger, it will not deform. However, there may be some deformation, which ultimately will affect the hysteresis friction.



Appendix 13

Since the deformation force (F_D), is the force on only the approaching side of the pimple, it can be described as:

$$F_D = \int p \cdot x \cdot dl \cdot \cos \theta = \int_0^a p \cdot x \cdot dt \cdot \frac{\cos \theta}{\sin \theta}$$

The normal force (N) is applied to the whole of the pimple, therefore it is described by:

$$N = \int 4 \cdot x \cdot p \cdot dl \cdot \sin \theta = 4 \cdot \int_0^a p \cdot x \cdot dt$$

This means the deformation force is:

$$F = \frac{N}{4} \cdot \cot \theta$$

Taking the hysteresis of the material into account, and also the multiple pimples in the contact, the friction due to hysteresis F_h is:

$$F_h = \beta \cdot n \cdot \frac{N}{4} \cdot \cot \theta$$

where β is the loss fraction and n is the number of pimples.